Exploring Open Channel Block of the NMDA Receptor

David W. McClymont B.Sc M.Res

Thesis submitted to the University of Nottingham for the degree of Doctor of Philosophy, October, 2010

Abstract

The GluN3 subunits of the NMDA receptor are thought to reduce the Ca^{2+} permeability and Mg^{2+} sensitivity of NMDA receptors. cRNA for rat NMDA receptor subunits were injected into Xenopus oocytes and responses were recorded using two electrode voltage clamp at -100, -75 and -50 mV. GluN1-1a/2A, GluN1-1a/2A/3A and GluN1-1a/2A/3B containing receptors were characterised using Mg^{2+}, memantine, philanthotoxin-343, methoctramine and MK-801. IC_{50} values were calculated and generally showed significant increases between those containing GluN1-1a/2A/3 subunits and GluN1-1a/2A, while those with GluN3B were found to be significantly higher than GluN3A. Activity was also typically shown to be partially restored with mutations at the N and N+1 site asparagines of GluN3A. As the IC_{50} was only partially restored the changes cannot be attributed to the loss of the N-site alone. Further differences may be due to a constricted threonine ring within the M3 vestibule region, or due to continued reduced flux through the channel. Another possibility is that to restore block it may require both the double N and N+1 mutation at the N-site.

Multi-target-directed ligands combine two pharmacophores to produce drugs which retain the properties of the constituents. Memantine has been approved for use in Alzheimer's disease and there is a search for drugs that have similar actions. A range of multi-target compounds were tested to determine if NMDA receptor blockade activity was obtained. The pharmacophores explored were tacrine, donepezil, lipoic acid carvedilol and dimebon. The most promising compounds were carbacrine(3) (tacrine and carvedilol) and lipocrine (lipoic acid and tacrine), and it was found that the former was equipotent and the latter more potent than memantine. Potency was likely due to the

tacrine moiety. These compounds should be further categorised to determine if they retain the kinetics that gives memantine its favourable side effect profile.

Publications

ROSINI, M., SIMONI, E., BARTOLINI, M., CAVALLI, A., CECCARINI, L., PASCU, N., MCCLYMONT, D. W., TAROZZI, A., BOLOGNESI, M. L., MINARINI, A., TUMIATTI, V., ANDRISANO, V., MELLOR, I. R. & MELCHIORRE, C. 2008. Inhibition of acetylcholinesterase, beta-amyloid aggregation, and NMDA receptors in Alzheimer's disease: a promising direction for the multi-target-directed ligands gold rush. J Med Chem, 51, 4381-4.

Acknowledgements

I would like to thank my supervisor Ian Mellor for his excellent supervision throughout my PhD. I would also like to thank Tim Smith, Declan Brady and Tina Schwabe for teaching me many further techniques required to carry out my work. I would also like to thank the Medical Research Council and the University of Nottingham for investing in me by funding this project. Lastly, I would also like to thank my parents for their continued support.

Contents

Abbreviations

Aβ	β-amyloid protein
AC	Adenyl cyclase
AChE	Acetylcholine esterase
AChEI	Anticholinesterase inhibitor
AD	Alzheimer's disease
ADAM	'a disintegrin and metalloproteinase domain'
ADAS-cog	Alzheimer's disease assessment scale-cognitive subscale
AQ	Anthraquinone
APOE	Apolipoprotein E
APP	Amyloid precursor protein
BuChE	Butyrylcholinesterase
CaMKII	Calmodulin dependent protein kinase II
CREB	cAMP response element binding
CSF	Cerebrospinal fluid
DAOA	D-amino acid oxidase activator
EC_{50}	Half-maximal effective concentration
EDTA	Ethylene-diamine-tetraacetic acid
ER	Endoplasmic reticulum
GAPDH	S-nityrosylated glyceraldehyde-3-phosphate dehydrogenase
GFP	Green fluorescent protein
GRIN1	Glutamate receptor ionotropic
hERG	Human ether-à-go-go related gene
IDE	Insulin degrading enzyme
HA	Hemagglutinin-tagged
IC_{50}	Half-maximal inhibitory concentration
LB	Luria-Bertani
LTD	Long term depression
LTP	Long term potentiation
MAP	Microtubule associated protein
MAPK	Mitogen-activated protein kinase
MMPs	Matrix metalloproteinases
MMSE	Mini-mental state examination
MTDL	Multi-target directed ligands
nAChR	Nicotinic acetylcholine receptors
NEP	Neprilysin
NTD	N-terminal domain
PDZ	Post synaptic density
PhTX	Philanthotoxin
PKA	Protein kinase A
PKC	Protein kinase c
PICALM	Phosphatidylinositol-binding clathrin assembly protein
PLC	Phospholipase C
PP2B	Protein phosphotase 2B
PTK	Protein tyrosine kinase
qGluR	Quisqualate-sensitive glutamate receptors
REDOX	Reduction-oxidation reaction
SNARE	*N*-ethylmaleimide-sensitive factor attachment protein receptor
SNP	Single nucleotide polymorphisms
SOC	Super Optimal broth with Catabolite repression

TAE	Tris-acetate-EDTA
TMEM16A	Transmembrane proteins with unknown function 16A
TRPV1	Transient receptor potential cation channel, subfamily V, member 1
UHDRS	Unified Huntington's disease rating scale
VAMP2	Vesicle-associated membrane protein 2
VIP	Vasoactive intestinal peptide
WT	Wild-type

1

Introduction

Glutamate is the main excitatory transmitter in the nervous system and two classes of receptor activated by it are known, ionotropic (ion channel) and metabotropic (G-protein coupled). The ionotropic receptors can be split into three classes N-methyl-D-aspartic acid (NMDA), α-amino-3-hydroxy-5-methylisoxazole-4-propionic acid (AMPA) and kainate, and are termed according to the synthetic agonist that preferentially activates them (Rang et al., 2007). The NMDA receptor family is further split into subtypes, GluN1 which has eight spice variants; GluN2, which has four subtypes A-D and GluN3 (formerly NMDAR-L or x^{-1} and x^{-2}) which has two subtypes A and B (see Paoletti and Neyton, 2006). Four subunits come together to form a functional receptor that are mainly comprised of two pairs of GluN1/2 dimers in a 1/2/1/2 formation creating a pore that is highly Ca^{2+} permeable (Sobolevsky et al., 2009). It is thought that the GluN3 subunit is rapidly incorporated into receptor assemblies, but its stoichometry is unknown (Tong et al., 2007).

The GluN3 subunits of the NMDA receptor are the most recently discovered and what effect its presence has on the ion channel is currently unknown, although due to amino acid changes in the pore it is thought to reduce Mg^{2+} sensitivity and Ca^{2+} permeability (see Paoletti and Neyton, 2006). With these changing properties and the fact that expression peaks during development it has led to the suggestion that the GluN3 subunits protect neurones from excitotoxicity, or help produce mature synapses (see Henson et al. 2010). Another suggestion has been that the GluN3 subunit tags receptors for removal as they have been shown to allow rapid endocytosis from the membrane (Perez-Otano et al., 2006). Although the expression patterns in rat seem to suggest a link

to development, *in situ* hybridisation studies in human show expression of GluN3A and GluN3B throughout adulthood (Nilsson et al., 2007, Henson et al., 2008, Bendel et al., 2005, Chatterton et al., 2002, Wee et al., 2008). Further complicating any interpretation of function has been the reports of NMDA receptors that consisted only of GluN1 and GluN3 subunits where the GluN2 was not present which could be gated by glycine alone, although there has been little evidence to support their existence *in vivo* (Das et al., 1998, Chatterton et al., 2002, Tong et al., 2007). Without having fully established the properties of open channel block (endogenous or exogenous) and identifying the residues involved, together with the glycine-gated complications, it has been difficult for researchers to conclusively state what effect the subunit has on activity of NMDA receptors, and what function the subunit has.

As the GluN3 subunit has a G instead of an R at the Mg^{2+} binding site potency should be lost when the subunit is present (Wollmuth et al., 1998a, Wollmuth et al., 1998b). Although the effect of Mg^{2+} has been explored in some transgenic neuronal cultures, it has not been fully tested in recombinant expression systems and a full study will be carried out (Sasaki et al., 2002, Tong et al., 2007). Residues involved in the binding of memantine and MK-801 have been located in the pore region of GluN1/2 NMDA receptors (Kashiwagi et al., 2002, Chen and Lipton, 2005). Therefore, these compounds can be tested at GluN3 containing receptors, and if their activity is impaired, residues that have already been implicated may help identify regions where the structure of the pore is altered. Furthermore, polyamine open-channel blockers such as the philanthotoxin (PhTX) group derived from the wasp *Philanthus triangulum* have been shown to block the AMPA ionotropic glutamate receptor, and are of interest to our group. Philanthotoxins show reduced block if there is an R residue at the equivalent of the NMDA receptor N-site within the pore of the AMPA receptor (Andersen et al., 2006). GluN1/2 NMDA

receptors have an N at this position, but the GluN3 subunits have a G then an R, therefore the PhTX compounds may have the ability to selectively antagonise NMDA receptors that do not contain a GluN3 subunit.

The current study aimed to address some of the issues outlined by carrying out a comprehensive categorisation of the activity of open-channel blockers at GluN3 containing receptors. Such information will be useful in determining what changes occur in the pore region, and can be used to interpret what possible function the subunit may have *in vivo*. There was also the possibility that PhTX compounds may be subunit selective for GluN1/2 over GluN3 receptors similar to the effect of the R residue on the GluA2 subunit of the AMPA receptor, and if such a molecule is discovered it would be useful pharmacological tool.

The second part of the study exploited the mechanism of block by memantine to test new multi-target directed ligands (MTDL) for the treatment of Alzheimer's disease. In collaboration with the University of Bologna these new compounds were designed to have multiple targets and the study determined their ability to block the NMDA receptor. Compounds based on the acetylcholine esterases tacrine and donepezil where combined with compounds that had anti-oxidant activity lipocrine and the β-blocker carvedilol to create new pharmacological entities. Furthermore, compounds based on dimebon a potential Alzheimer's disease drug, were explored to determine their NMDA receptor activity. Although this group of multi-target compounds were not specifically designed to be active at NMDA receptors tacrine, donepezil and dimebon have previously been shown to have this property (Wang et al., 1999, Wu et al., 2008). The ability to block NMDA receptors would be in any case useful in an Alzheimer's disease compound as that is the mechanism by which memantine has been approved for use in the disease. The

study aimed to determine if such an effect was retained by tacrine, donepezil and dimebon within the MTDL compound structure.

1.1 Glutamate Receptor Classes

The first indication that glutamate acted as a transmitter in the central nervous system was when its injection into the motor cortex of dogs was shown to cause convulsions (Hayashi, 1954). Later, ionophoretic delivery of glutamate to the spinal cord of the cat was found to produce similar effects (Curtis et al., 1959). Even though glutamate was found in very high concentrations, it was not thought that an amino acid could have a major role in the nervous system. It was known that other amino acids such as aspartate had similar effects when delivered in the same manner to the spinal cord, and it was thought that a non-specific amino acid receptor was involved.

Modifications to the structure of glutamate allowed stereoselective evidence to be obtained that led to a specific receptor being identified (see Watkins and Jane, 2006) (Table 1). Glutamate did not show stereoselectivity so bulky substitutions of other amino acids were made to engineer this. NMDA, an aspartate analogue, was found to be a more potent agonist compared to the L enantiomer of the aspartate analogue providing evidence for the existence of a specific membrane receptor. Other glutamatergic receptors were also identified using chemical means. AMPA, a modification of ibotenic acid, was generated in the search for a more stable glutamate agonist (Krogsgaard-Larsen et al., 1980). Kainic acid, a glutamate analogue, was isolated from *digenea simplex,* a marine red alga and was found to potentiate L-glutamate induced depolarisation of the crayfish opener neuromuscular junction (Shinozaki and Shibuya, 1974b). These same researchers showed that quisqualic acid from the seeds of *Quisqualis indica* activated the same areas of the crayfish opener muscle as L-glutamate (Shinozaki and Shibuya, 1974a).

Structure	Name
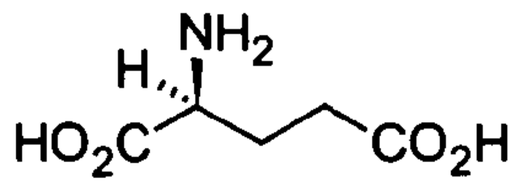	L-glutamate
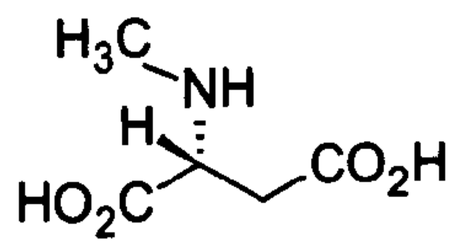	NMDA
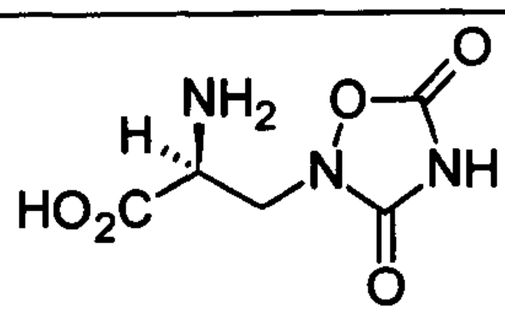	Quisqualate
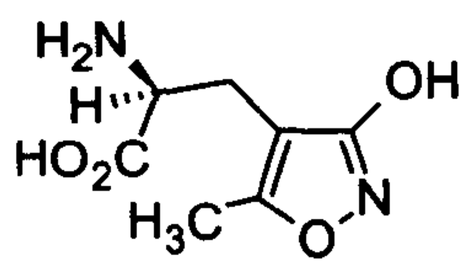	AMPA
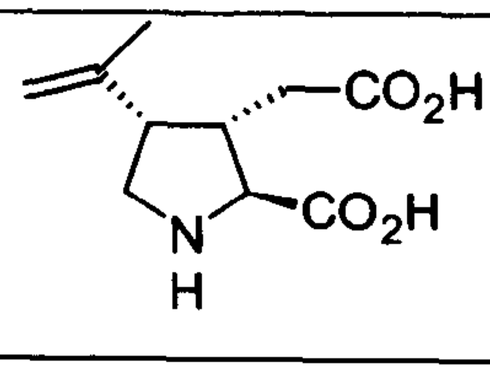	Kainate

Table 1: Agonists of the glutamate receptors. Shown are the endogenous agonist glutamate and the synthetic agonists which were selective between the receptor types NMDA, AMPA and Kainate. Quisqualate was originally used instead of AMPA until the latter proved more selective. Adapted from Watkins and Jane, (2006).

When these compounds were tested in various experimental preparations differing patterns of activity were found. For instance, it was found that kainate and NMDA had different effects on spinal interneurones and Renshaw cells (McCulloch et al., 1974). It was also shown in recordings from frog spinal cord that only responses elicited by NMDA were inhibited by Mg^{2+}, but not those of AMPA or kainate (Evans et al., 1979). In addition, a subpopulation in spinal cord preparations was found to respond more to kainate than AMPA or NMDA (Evans et al., 1982). Such evidence suggested that there

were different subtypes of glutamate receptor, with differing regional expression and differing properties.

Although classifying the receptors based on their agonist profiles proved useful, there was still a subset of glutamatergic responses that were not activated by any of the agonists shown in table 1. When DNA sequencing became available this shed light on two separate classes of glutamate receptor. The first, ion channels, were found to be the class that responded to the synthetic agonists, and the second class were found to be G-protein coupled receptors (Figure 1). Those that responded to AMPA were found to be the subset that mediated fast excitatory transmission in the central nervous system (Boulter et al., 1990, Cull-Candy et al., 2006). They are constructed from four subunits GluA1-4 which are encoded by the genes *GRIA1-4*. AMPA receptors come together as a group of four subunits and those that lack the GluA2 subunit are permeable to Ca^{2+} (see Isaac et al., 2007). Ion selectivity is mediated by the RNA editing of glutamine to arginine (the Q/R switch, equivalent to the NMDA receptor N-site) in the pore region causing receptors containing the subunit to be impermeable to Ca^{2+}. The predominant form of the AMPA receptor contains the GluA2 subunit while the GluA2 lacking form is though to be expressed mainly through development possibly mediating plasticity (see Isaac et al., 2007).

The receptors that responded to kainate were found using low stringency hybridisation probes to the AMPA sequence, and subunits in this class are termed GluK1-5 (see Pinheiro and Mulle, 2006). GluK1, GluK2 and GluK3 can form functional homomeric channels that are termed low affinity subunits due to their low affinity to kainate. GluK4 and GluK5 show a high affinity but cannot form functional channels alone. They show less than 40% homology to the AMPA receptor subunits, and do not form channels with

GluA1-4. GluK1 and GluK2 also contain the Q/R switch that is found in AMPA receptors to reduce Ca^{2+} permeability (see Pinheiro and Mulle, 2006). GluK2 has two further amino acid substitutions in the first transmembrane region, isoleucine/valine (I/V) and a tyrosine/cysteine (Y/C), also leading to a reduction in Ca^{2+} permeability. No regions of RNA editing have been found for the GluK4 and GluK5 subtypes.

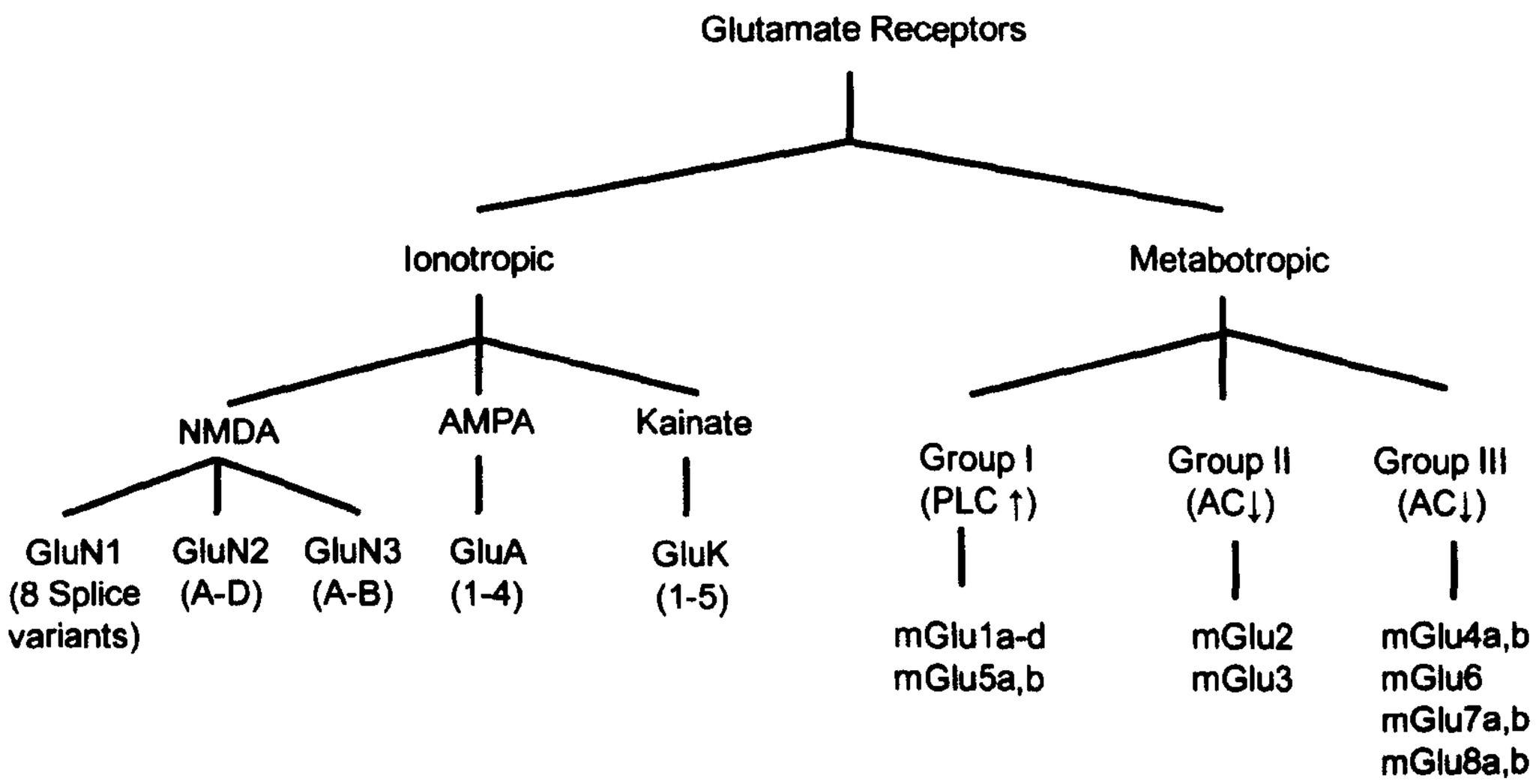

Figure 1: Glutamate receptors and their subtypes. The left branch shows the ionotropic glutamate receptors, followed by their agonist then the subunits. The right branch shows the metabotropic receptors followed by their effects on phospholipase C (PLC) and adenyl cyclase (AC) with the last branch showing the subunits that are involved. Adapted from Watkins and Jane, 2006.

The NMDA receptor is the ionotropic glutamate receptor whose agonist is the compound from which it takes its name. As well as glutamate binding to the GluN2 subunit, NMDA receptors also require the co-agonist glycine to bind to the GluN1 subunit for activation (Kleckner and Dingledine, 1988). In addition, at resting membrane potentials, there is an endogenous voltage-dependent block by Mg^{2+} of the NMDA receptor (Evans et al., 1979). Depolarisation of the membrane removes block allowing the channel to open. These features makes the NMDA receptor unique amongst the ionotropic glutamate receptors as they only respond when glutamate is present, glycine is

present and if the membrane is depolarised to a level which removes Mg^{2+} block. This means that the receptor acts as a coincidence detector which reduces temporal jitter, spontaneous activity and integrates the status of the input events (see Dingledine et. al. 1999). The NMDA receptor is highly permeable to Ca^{2+} and may help trigger evens such as LTP (Mayer and Westbrook, 1987, Malenka and Bear, 2004). The GluN3 subunits are gated by glycine and there are two subtypes GluN3A and GluN3B (Yao and Mayer, 2006). The presence of a GluN3 subunit is thought to act in a dominant-negative manner, reducing the amplitude of inward currents, reducing Ca^{2+} entry and decreasing Mg^{2+} sensitivity (Yamakura et al., 2005, Tong et al., 2007).

1.2 Receptor Structure

1.2.1 AMPA Receptor

The complete crystal structure for the AMPA receptor has been reported and is closely related to the NMDA receptor (Sobolevsky et al., 2009). The AMPA receptor is shaped like a capital Y with the N-terminal domain at the top and the ion channel at the bottom. The ligand binding domain is at the intersection of the lines of the Y, positioned like a block over the ion channel, occluding it when closed. The extracellular region has a two-fold rotational symmetry vertically down its centre with the N-terminal domain rotated ~24° and the ligand binding domain rotated ~19° from this axis. AMPA receptors come together in a dimer of dimers that are lettered A-D (Figure 2A). Dimer A/B comes together with dimer C/D giving an orientation that terms A/C proximal and B/D distal to the axis of two-fold symmetry, although referring to dimer pairs is less descriptive as they swap pairings across domains. At the N-terminal domain subunit A and B form a dimer pair; however, at the ligand binding the domains swap over so that subunit A forms a dimer pair with dimer C and *vice versa.* A/C also has extensive contacts between

the N-terminal domain and the ligand binding domain which are not present in the B/D dimer.

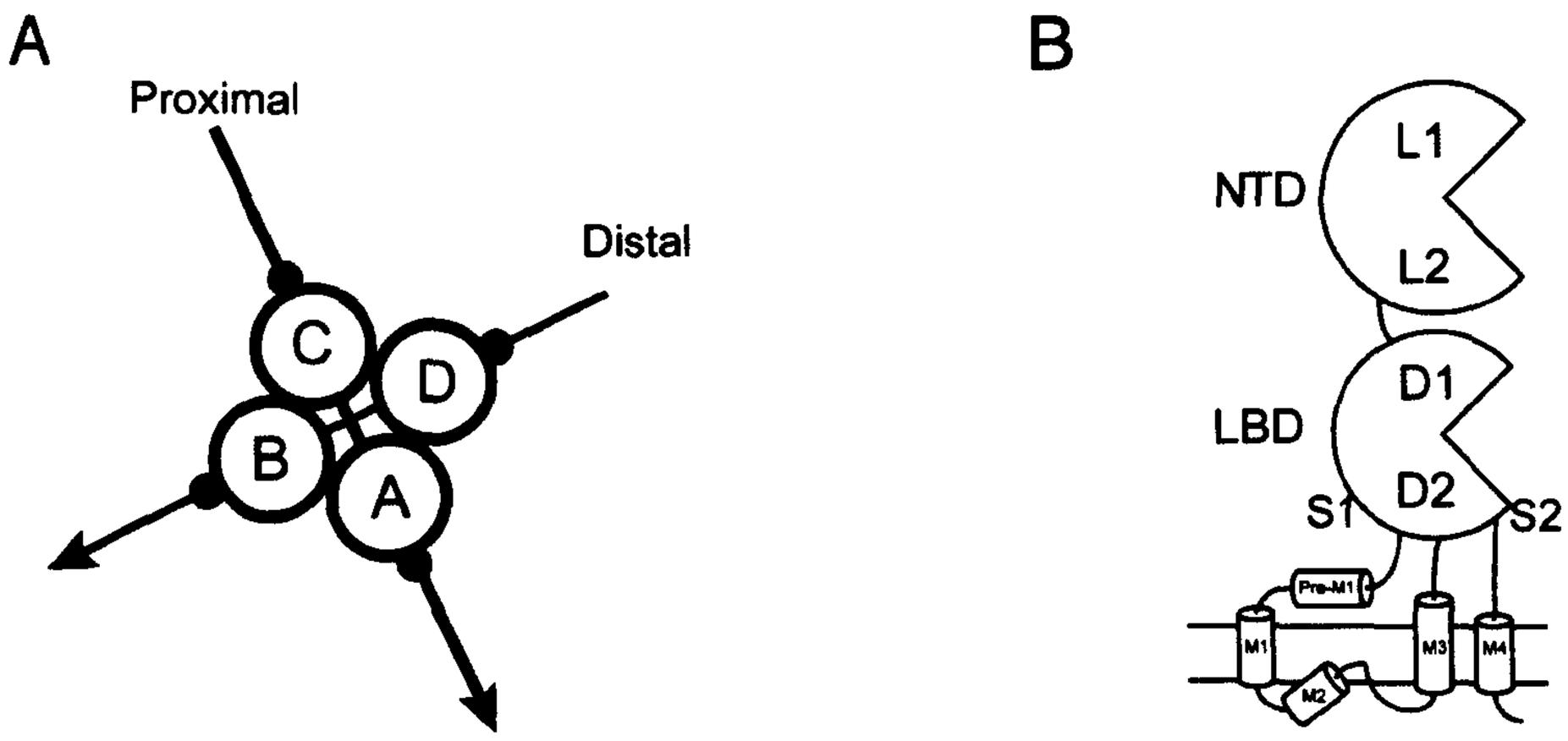

Figure 2: AMPA receptor composition. (A) Stoichometry of subunits. A/C are termed proximal, and B/D are termed the distal, to the overall two-fold axis of symmetry. (B) Cartoon representation of a subunit of the AMPA receptor. Adapted from Sobolevsky et al., (2009).

At the N-terminal domain is a bilobar clamshell with the upper lobe termed L1 and the lower L2, the latter of which has extensive contacts across the distal subunits B and D (Sobolevsky et al., 2009) (Figure 2A). The contacts between the dimers A/B and C/D, as well as crossover contacts between the distal subunits B/D, contribute to the stability in N-terminal domain. At the ligand binding domain the majority of connections exist diagonally across the receptor structure so that the local dimer pairs would be considered A/C and B/D, proximal and distal to the origin of four-fold rotational symmetry. Again, the ligand binding domain is a clamshell structure which has an upper domain D1 and the lower domain D2. The AMPA receptor was crystallised in the presence of the AMPA receptor competitive antagonist ZK 200775 and was shown to bind within this region, indicating antagonism occurs within a subunit unlike, for example, the acetylcholine receptor (Czajkowski and Karlin, 1995, Sobolevsky et al., 2009).

At the transmembrane domain the four AMPA receptor subunits come together to form a pore with four-fold rotational symmetry (Sobolevsky et al., 2009). There are the four transmembrane segments M1, M3 and M4 and the M2 pore region which contains a pore lining loop. Starting at the S1 region of the ligand binding domain, pre-M1 extends and turns 90° so it runs parallel to the membrane (Figure 2B). Pre-M1 region has contacts with the amino and carboxyl end of M3 and M4 and forms a collar around the ligand binding domain linker regions to the membrane regions and may be involved channel opening.

The M1 region lies outside the ion channel while the M2 region forms the pore that has a central cavity above where the Q/R site is located (Sobolevsky et al., 2009). This site is the Q/R switch in AMPA receptors, the 'N-site' of GluN1 and the N+1 site of GluN2 (Wollmuth et al., 1998a, Wollmuth et al., 1998b, Sobolevsky et al., 2009). The M3 regions are crossed over at the level of pre-M1 at the conserved SYTANLAAF motif when the channel is closed, and forms the ion channel gate (Sobolevsky et al., 2009) (Figure 3 and Figure 4). The M3 α-helix was also shown to be longer in the A/C subunits than the B/D subunit. There is also further occlusion of the ion channel by M629 of the A/C subunits which resides above the SYTANLAAF glutamatergic ion channel conserved motif and may be involved in desensitisation. M3 then returns to form part of the ABD which then returns to the pore to start M4. It lies outside the ion channel and has significant interactions between adjacent subunits contributing to overall structure and function. From here this region leads to the C-terminus.

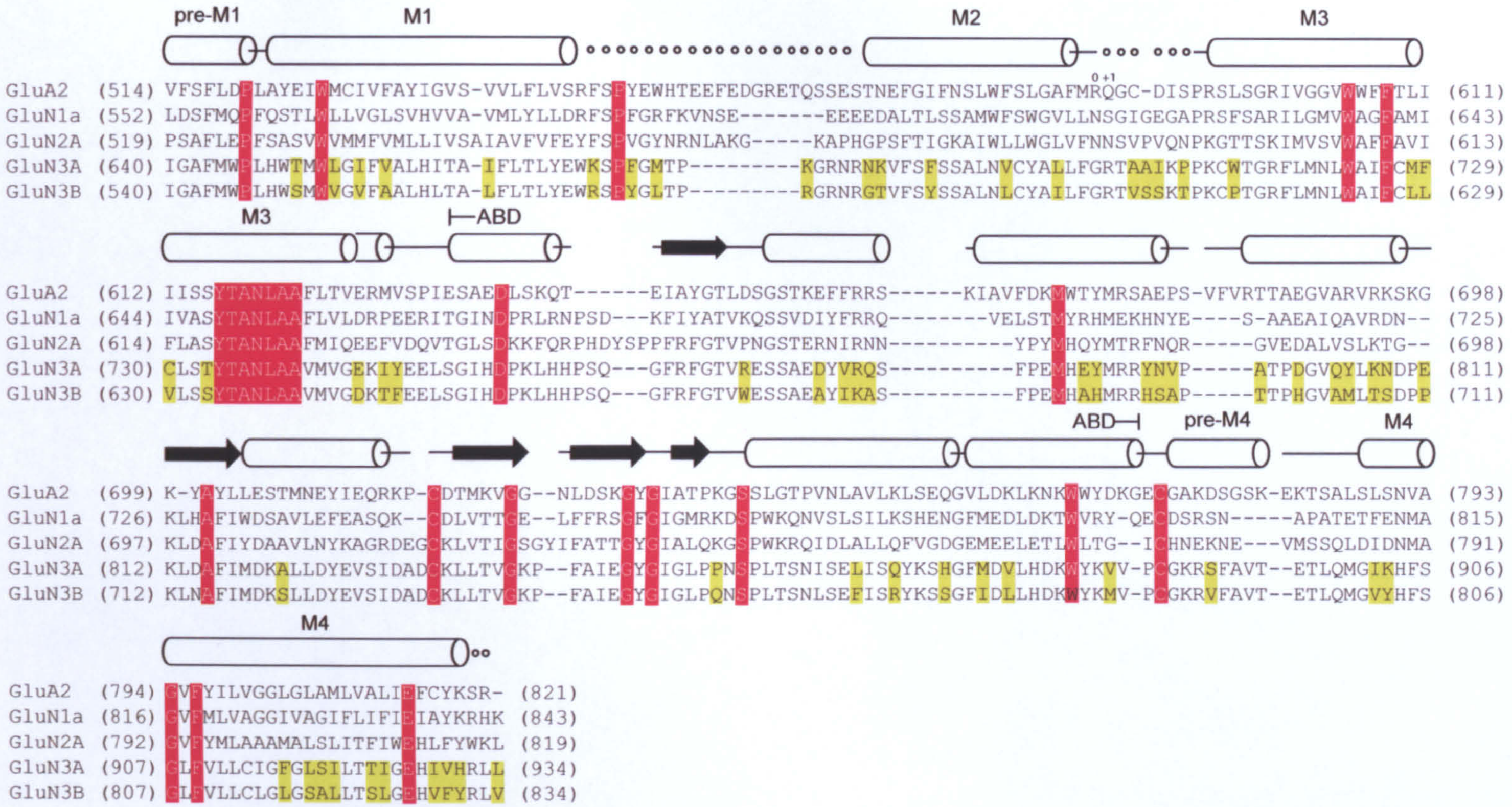

Figure 3: Amino acid sequence of the pore region of the GluA2 subunit and the subunits of the NMDA receptor. Highlighted in yellow are nonhomologous residues between GluN3A and GluN3B. Highlighted in red are the conserved residues between AMPA and NMDA subunits. Denoted by 0 is the Q/R/N site. Secondary structure elements for the GluA2 crystal are shown where α-helices are cylinders, β-strands are arrows and loops represented by lines. The extra M3 c-terminal section indicates the longer helix of the A/C subunits. Disordered regions with no clear density are shown by the dotted lines. Adapted from Chatterton et al., 2002. and Sobolevsky et al., 2009.

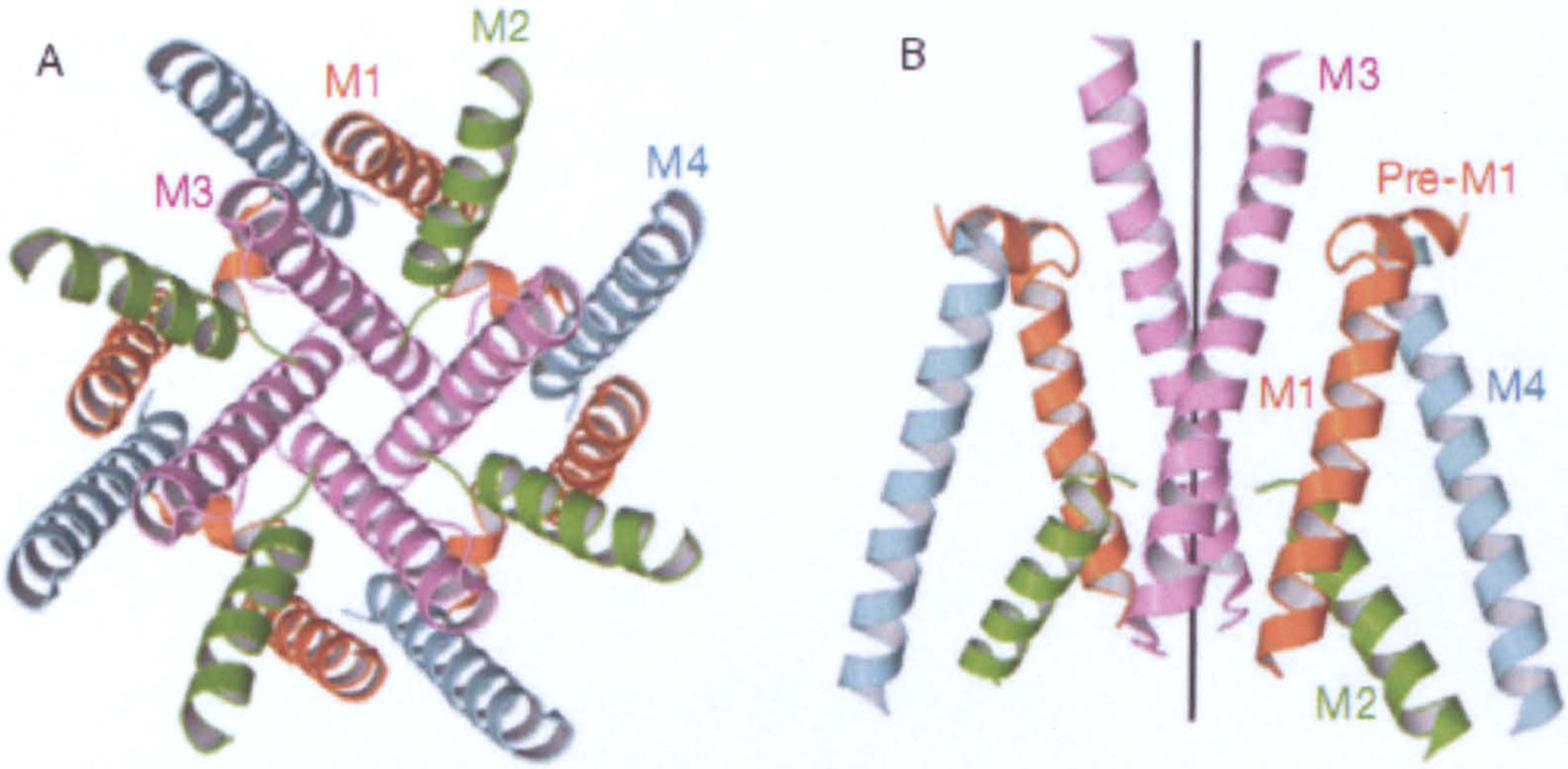

Figure 4: Transmembrane domain of the AMPA receptor. M1 is orange, M2 is green, M3 is purple and M4 is blue. (A) is viewed above the axis of four-fold symmetry and (B) is viewed parallel to the membrane (Sobolevsky et al., 2009).

By superimposing the crystal structure of a desensitised mutant (S729C) onto the AMPA receptor crystal structure a model of channel gating can be proposed (Sobolevsky et al., 2009). Agonist binds to the ligand binding domain clamshell pushing D2 toward D1 by a ~25° rotation while competitive antagonists keep it open. Binding separates the transmembrane domains by ~20 Å pulling apart the M3 region which opens the channel. The M3-S2 linker in the proximal A/C dimer moves less than the distal subunits B/D; therefore, the proximal subunits may play a lesser role in gating. To examine desensitisation, the D2 lobes of the ligand binding domain of a desensitised-like mutant receptor with bound glutamate was superimposed on antagonist bound AMPA receptor crystal and showed few differences in structure (Sobolevsky et al., 2009). Therefore, it is thought that for the desensitised receptor, the ligand binding domains twist back around into the position they took in the closed state, but while glutamate is still bound.

1.2.2 NMDA Receptor

The NMDA receptor also consists of a large extracellular N-terminal domain, a ligand binding domain, transmembrane regions containing a re-entrant pore loop and a intracellular C-terminus (see Paoletti and Neyton, 2006). The N-terminal domain has a

more important role in NMDA receptors binding allosteric modulators such as Zn^{2+} and polyamines. It is bilobar, similar to a leucine/isoleucine/valine binding protein, and it oscillates spontaneously between open and closed states affecting open probability of the channel (Gielen et al., 2009). Chimeras of the NTD have also been shown to transfer glutamate potency which is higher at GluN2D than at GluN2A (Yuan et al., 2009). Receptors containing chimeric GluN2D-(GluN2A NTD) subunits decreased glutamate potency toward GluN2A compared with GluN2D wild-type. The same study showed that the GluN2A-(GluN2D NTD) chimera increased potency toward the levels of GluN2D wild-type. The crystal structure of the N-terminal region has also been reported, confirming Zn^{2+} binding in the cleft between the two lobes promoting the closed conformation (Karakas et al., 2009). The structure also showed that the lobes are twisted ~45° to 54° degrees away from each other compared with the AMPA and kainate receptor subunits. The same study showed that this region had Na^{+} and Cl^{-} binding sites although their physiological role is unclear.

The second extracellular domain is the ligand binding domain which is formed by the pre-transmembrane M1 region and M3-4 loop (Mayer, 2006). The ligand binding domain shows homology with bacterial periplasmic proteins, but with a substructure that is increased in size and complexity. GluN1 and GluN3 binds glycine and GluN2 binds glutamate. The glutamate binding region of the GluN2 subunit consists of an S1 region which is N terminal to the M1 domain and the S2 region, which occurs between M3 and M4 (Furukawa et al., 2005). Selectivity for NMDA over AMPA and kainate is due to an aspartate residue in the binding pocket which is shorter than the glutamate found in the other ionotropic glutamate receptors. It is suggested that the changed residue leaves space for the N-methyl group of NMDA to enter. After agonist has bound there is rotation of the ligand binding domain region leading to channel opening (Furukawa et al.,

2005). As it is the movement of the ligand binding domain lobes that allow the channel to open, it is thought that the partial agonist homoquinolinate may mediate its effects by reducing stability for the closed conformation due to increased motion in the binding pocket, or through conformational changes that occur after binding (Erreger et al., 2005b).

The glycine binding domain of GluN1 has a similar bilobar clamshell structure to the glutamate binding domain of GluN2, and the agonist binding residues were in the same position when they were superimposed over GluN2 (Furukawa and Gouaux, 2003). However, GluN1 may exclude glutamate through steric effects as well as through a local hydrophobic environment meaning only glycine can enter. Similar to GluN2, the presence of an agonist keeps the lobes of the binding domain in the open configuration. GluN3 subunits have been shown to have a higher affinity for glycine than GluN1 even though they have similar binding residues, positions and domain rotation after binding (Yao et al., 2008). There may be a different hydrogen bonding network in GluN3 which increases the stability of the closed state by producing more constrained amino acid interactions. Such a mechanism would be the opposite to how homoquinolinate reduces stability of the closed conformation. In the binding pocket there is also the loss of a T731 which is M in GluN3A and GluN3B. This residue has been shown to interact with the Cl^- of 5,7-DCKA, as 5-DCKA showed no difference in affinity between GluN3A and GluN3B (Yao and Mayer, 2006).

Similar to the AMPA receptor, agonist binding to the NMDA receptor is thought to result in the ligand binding domain closing disrupting the linkers to the transmembrane region which opens the channel (Mayer, 2006). M1, M3 and M4 are directly linked to the ligand binding domains and it is known that the M3 region plays the most important role

in gating (Sobolevsky et al., 2009). Like AMPA receptors, NMDA receptors also have a conserved region with the sequence SYTANLAAF in the M3 region and the crossing over between subunits of this area is thought to be the channel gate (Figure 3). Supporting this is the evidence that mutations between S645 and I655 of M3 resulted in constitutively open channels (Chang and Kuo, 2008). It is thought that open channel blockers such as MK-801 may bind in a manner with high affinity that they can become trapped when the channel is closed (Qian and Johnson, 2002). Substituted cysteines accessibility showed that of those residues mutated from the M3 to the M2 loop where the N-site resides were accessible, with or without glutamate binding, meaning the M3 region may be exposed to the extracellular region in NMDA receptors even in the closed state, questioning the location of the gate (Sobolevsky et al., 2002a). The M3 segments from the GluN1 and GluN2B and GluN2C subunits were shown to be staggered relative to each other in the vertical axis probably indicating a differential role in gating (Sobolevsky et al., 2002b, Kashiwagi et al., 2007).

In GluN1, C-terminal to the M3 region is an amino acid sequence DRPEER in the ligand binding domain/transmembrane domain linker (Figure 3) (Watanabe et al., 2002). The study showed that mutations of the DRPEER motif, as well as those in the conserved asparagine of the M3 region, resulted in reduced Ca^{2+} current. It is thought that it increases current by binding Ca^{2+} and excluding monovalent ions from the pore. The DRPEER sequence is not present in GluN3, which may account for the reduction in Ca^{2+} current when the subunit is present (Figure 3). However, the DRPEER sequence is not present in the GluN2, and may not account completely for the reduction in Ca^{2+} permeability seen with GluN3 unless a GluN1 subunit is replaced.

GluN1/GluN2A receptors expressed in HEK-293 cells showed a shift in the reversal potential in the presence of 1 mM and 10 mM Ca^{2+} of -11.5 mV (Perez-Otano et al., 2001). With the addition of GluN3A, together with GluN1/GluN2A, there was a reduction of the shift to -5.93 mV indicating reduced Ca^{2+} permeability of the channel. In hippocampal neurones from transgenic mice overexpressing GluN3A it was shown that there was a three-fold reduction in Ca^{2+} permeability compared with wild-type controls (Tong et al., 2007). Expressing GluN3B together with GluN1/GluN2A in HEK-293 cells, but using 1 mM and 20 mM external Ca^{2+} concentrations, showed a two-fold reduction in calcium permeability compared with controls (Matsuda et al., 2002). Expression of the GluN3B subunit in cultured mouse hippocampal neurones led to a four-fold reduction in Ca^{2+} permeability (Matsuda et al., 2003).

The intracellular C-terminal end of the NMDA receptors contains sites that can be phosphorylated by PKA, PKC, protein tyrosine kinase (PTK) and CaMKII (Chen and Roche, 2007). Interactions with these proteins can affect signalling, trafficking and gating properties. GluN3A has a molecular weight of ~125 kDa indicating that it is the most heavily glycosylated of the NMDA receptor subunits, affecting the gating properties of the receptor (Ciabarra and Sevarino, 1997). GluN3A also has also been shown to interact with PACSIN1/syndapin1 which is involved in mediating endocytosis of the receptor (Perez-Otano et al., 2006).

1.3 Subunit Stoichiometry

Unravelling the subunit stoichiometry of the NMDA receptor has produced competing studies showing differing arrangements around the pore. Truncation of the GluN1 and GluN2 subunits before M4 was shown to form functional channels when expressed together with a separate M4 region (Schorge and Colquhoun, 2003). Doing this

supposedly allowed the N and C-terminals to reside on the same side of the membrane and these could be linked together to form subunit tandems. The subunits present and their orientation could be constrained depending on the truncated subunits that were linked together. Those tandems which forced an alternating orientation around the pore were either non-functional or showed rapid desensitisation. Those tandems which forced a 1-1-2-2 orientation produced functional channels with similar properties to wild-type, indicating it was the preferred orientation.

The structural data from the AMPA receptor crystal was used to determine the stoichometry of the NMDA receptor as cysteine substitutions in the ligand binding domain were made to determine regions that were in close proximity, as they would cross-link (Sobolevsky et al., 2009). These showed that only one residue of the ligand binding domain of GluN1 was required to link the NMDA receptor subunits, E699. It was deduced that the only way E699 could orientate around the NMDA receptor is by forming a diagonal pair around the pore with the GluN1 subunit in the proximal position and the GluN2 subunit in the distal position. The AMPA receptor structure was also used to explore the pore of the NMDA receptor. Cysteine mutations in the M3 region at M629 in AMPA led to cross-linking due to the proximity of these amino acids (Sobolevsky et al., 2009). In the NMDA receptor if there is an alternating subunit arrangement around the pore then the equivalent mutations in M3 of GluN1(P661) would be close enough to show cross-linking with cysteine mutations, but those of GluN2 (P631) would not, which is what was found (Figure 5). GluN2 and GluN3A dimers were shown to only form functional receptors when a GluN1 subunit was present, and GluN3 could not form a dimer with another GluN3 subunit (Furukawa et al., 2005, Schuler et al., 2008, Yao et al., 2008). Therefore, how a GluN3 containing triheteromeric assembly is formed still remains unknown.

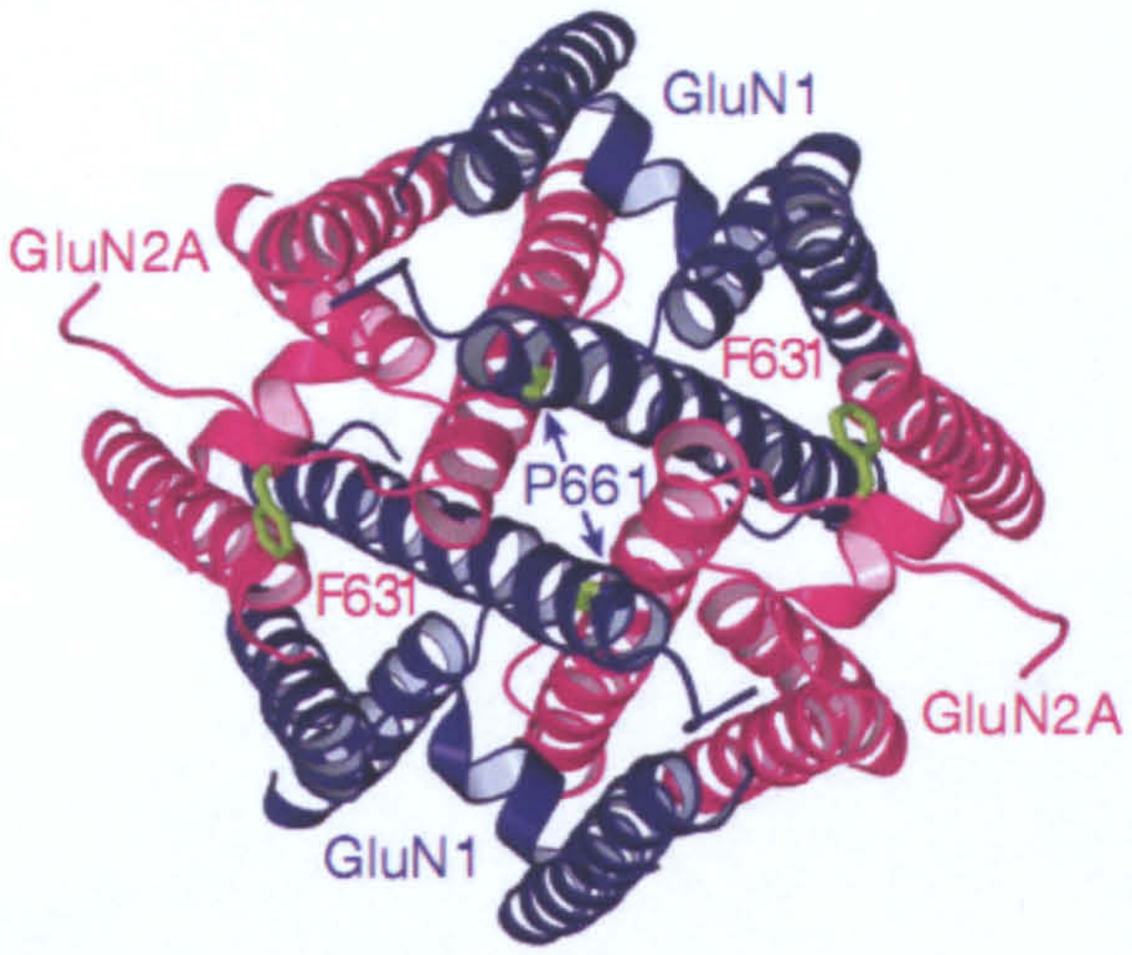

Figure 5: Subunit arrangement of the pore region of the NMDA receptor. Shown are the positions of the cysteine substitutions at P661 and F631 (Sobolevsky et al. 2009).

1.4 NMDA Receptor Subunits

1.4.1 GluN1

The GluN1 subunit was cloned in 1991 and was shown to require glycine as an agonist, confirmed later by mutagenesis of the binding site (Moriyoshi et al., 1991, Kuryatov et al., 1994). A screen of a rat forebrain library with probes for the transmembrane region of GluN1 found multiple genes with similar sequences (Hollmann et al., 1993). Eight different GluN1 splice variants were identified and these were arranged into four categories depending on the splice cassettes present (Figure 6). In rats, the gene for GluN1 *Grin1* is located at 3p13, contains 22 exons and has eight functional splice variants of pre mRNA from two regions of alternative splicing (Figure 6). The splice cassette at the 5' end it termed the N1 cassette (exon 5, 63 basepairs (bp)) and occurs at position 516 if it is present. At the 3' end there are C1 (exon 21, 111bp, between positions 2536 and 2646) and C2 (exon 22, 356bp, between positions 2647 and 3002) cassettes (Hollmann et al., 1993, Dingledine et al., 1999, Zarain-Herzberg et al., 2005, Del Valle-Pinero et al., 2007). The C2 cassette is followed by a C2' cassette, but is only translated

when C2 is not present. This removes the original stop codon allowing expression of a 22 amino acid C2' region which has its own alternative stop codon. There is one further splice acceptor site in exon 3 which is a 150 nucleotide open reading frame containing an alternative stop codon, but is not thought to be functional (Sugihara et al., 1992).

A

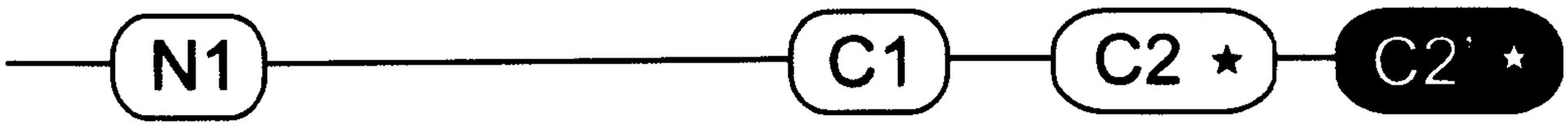

B

Splice Variant	Exons	Alternative stop codon?	EBML
GluN1-1a	C1, C2	No	U08261
GluN1-1b	N1, C1, C2	No	U08263
GluN1-2a	C2	No	U08262
GluN1-2b	N1, C2	No	U08264
GluN1-3a	C1	Yes	U08265
GluN1-3b	N1, C1	Yes	U08266
GluN1-4a	n/a	Yes	U08267
GluN1-4b	N1	Yes	U08268

Figure 6: Alternative splicing of the GluN1 receptor. (A) White boxes represent exons of the sequence which are alternatively spliced: the N1 cassette (exon 5), C1 (exon 21) and C2 (exon 22). The black box represents the C2' region with an alternative stop codon. ★represents stop codons in the sequence. (B) Combinations of splice cassettes that make up the GluN1 receptors adapted from Hollmann et al., (1993) and Yamakura and Shimoji, (1999).

The GluN1 subunits are classed 1 'a' and 'b' to 4 'a' and 'b'. The 'a' form does not contain the N1 cassette, and the increasing number indicates differing combinations of the C1 and C2 cassettes (Figure 6). The C1 cassette contains an endoplasmic reticulum (ER) retention signal meaning that the '1' and '3' forms have reduced expression in Xenopus oocytes (Cavara et al., 2009). For the 3 form, it may be less important as the C2' region contains a post synaptic density protein (PDZ) domain. The gene encoding human GluN1, glutamate receptor ionotropic (*GRIN1),* is located at 9q34.3 and comprises of 21 exons (exon 3 from the rat is not present) of which exons 4 (N1), 20

(C1) and 21 (C2) are alternatively spliced and these have the same sequence as those in the rat (Zimmer et al., 1995).

1.4.2 GluN2

The GluN2 subunit was also cloned in the early 90's and has four subtypes A-D which bind glutamate (Table 2) (Moriyoshi et al., 1991, Cull-Candy et al., 2001). Rat GluN2C (*Grin2C*) can be alternatively spliced resulting in truncation after the first transmembrane region (M1) or M3 region (Rafiki et al., 2000). GluN2D (*Grin2D*) also has a region of alternative splicing at the c-terminus which consists of a 33 amino acid insert in rats that either has a deletion (GluN2D-1) or does not (GluN2D-2) (Monyer et al., 1994). However, it is unclear if there are any functional characteristics associated with these splice variants.

	Human		Rat
Subunit	**Chromosome**	**Accession Number**	**Accession Number**
GluN2A	16p13	U09002	D13211
GluN2B	12p12	U88963	U11419
GluN2C	17q25	BC031077	U08259
GluN2D	19q13.1-qter	U77783	U08260

Table 2: GluN2 subunits and their locus positions in humans. Shown are the chromosome positions on human, human accession numbers and rat accession numbers for GluN2A-2D. Adapted from Dingledine et al., (1999), Schmidt and Hollmann, (2008) and Collingridge et al., (2009).

1.4.3 GluN3

GluN3 has two subtypes GluN3A and GluN3B (formerly NMDAR-L or x^{-1} and 3B x^{-2}) which are activated by glycine (Table 3) (see Cull-Candy et al., 2001, Yao and Mayer, 2006). GluN3A was cloned in 1995 and consists of 1115 amino acids in the rat (*Grin3A*) (Ciabarra et al., 1995, Sucher et al., 1995). There is also a splice-variant in rat that results

in a 60 bp insert at the C-terminal termed GluN3A-l (Sun et al., 1998, Cull-Candy et al., 2001). Human GluN3A (*GRIN3A*) has 9 exons and is located on chromosome 9 (Eriksson et al., 2002). It consists of 3345 bases translating to 1115 amino acids. The mature peptide contains 1089 amino acids leaving a signal peptide of 26 amino acids. There is no evidence of alternative splicing of *GRIN3A* in humans.

Rat GluN3B (*Grin3B*) contains 1003 amino acids and shares 62% nucleotide homology to GluN3A (Matsuda et al., 2002). The human GluN3B (*GRIN3B*) gene has an open reading frame of 3129 bases which translates to 1043 amino acids and contains 9 exons and exon 9 is elongated at the carboxyl end in humans (Bendel et al., 2005). It has also been described as having 2703 bases translating to 901 amino acids (Andersson et al., 2001). Human GluN3B is polymorphic with 10% of the European/American population homozygous for a 4bp insertion in exon 3 (Niemann et al., 2007). The protein is truncated causing the removal of its membrane binding domains and is a null mutant.

The C-terminal region of GluN3B contains an ER retention signal which must be masked before receptors can be trafficked to the surface (Matsuda et al., 2003). Deletion of amino acids in the C-terminal region of GluN3B distal to amino acids 914, and distal to 953, led to no surface expression when co-expressed with GluN1-1a. Deletions distal to position 986 led to normal cell surface expression. The amino acids between 952 and 985 may mask the GluN1-1a ER retention signal. However, a recent study has found the opposite, with the removal of this region in GluN3B reducing cell-surface expression (Wee et al., 2010).

	Human		Rat
Subunit	**Chromosome**	**Accession Number**	**Accession Number**
GluN3A	9q31.1	BC132866	U29873 L34938
GluN3A-I	-	-	AF061945 AF073379.1
GluN3B	19p13.3	AY507107.1	AF440691

Table 3: GluN3 subunits and their locus positions in humans. Shown are the chromosome positions on human, human accession numbers and rat accession numbers for GluN3A-3B. Only the accession number for rat GluN3-I is shown as a human variant has not been described. Adapted from Adapted from Dingledine et al., (1999), Schmidt and Hollmann, (2008) and Collingridge et al., (2009).

1.5 NMDA Receptor Single Channels

Like most ion channels the NMDA receptor has multiple conductance states, but this differs with the GluN2 subunit that is expressed in the tetramer. GluN2A and GluN2B are similar, having a main 50 pS opening with a brief 40 pS sublevel (Stern et al., 1992). GluN2C has a 36 pS and 19 pS conductance which both occur with similar brief durations. GluN2D has similar conductance levels to GluN2C, but they differ in the transitions between the states, and the mean open time for the low conductance state is longer (Wyllie et al., 1996). Single channel open probability is also altered according to the GluN2 subunit that is expressed. Within an 'activation' GluN2A has a higher open probability (0.5) than GluN2B (0.12) (Erreger et al., 2005a). GluN2C has a lower open probability (0.011) than GluN2B, and GluN2D has an open probability of 0.04 (Wyllie et al., 1998, Dravid et al., 2008). These differences are controlled by the closing of the N-terminal domain, and its linker to the ligand binding domain, leading to a lower open probability (Gielen et al., 2009, Yuan et al., 2009).

Single channel studies in HEK-293 cells expressing GluN1, GluN2A and GluN3A had one conductance level of 47 pS similar to GluN1/GluN2A receptor, and another conductance of 29 pS (Perez-Otano et al., 2001). The latter was not a subconductance

state as there were no direct transitions. Single channels studies from Xenopus oocytes injected with GluN1/2A/3A also showed two conductance states of 75 pS and 35 pS (Sasaki et al., 2002). It was shown that only the larger conduction state was blocked by Mg^{2+}. The abundance of the lower state depended on the ratio of GluN3A injected. Again, no direct transitions were observed between states and may suggest two different populations of channel. However, if there is a subpopulation of GluN1-1a/2A receptors then there would be at a minimum two sublevels, one of which would have a direct transition, which was not found. Outside-out patches from disassociated P8 cerebrocortical neurones also showed two conductances with no direct transitions (Das et al., 1998). The lower conductance may be attributed to the GluN3 subunit as it was not present in GluN3A$^{-/-}$ mice. However, with two populations, superimpositions could be expected to be found, and there was no mention of this in any of the studies outlined.

1.6 Agonists and Competitive Antagonism

1.6.1 Glutamate

The half-maximal effective concentration (EC_{50}) for L-glutamate alters depending on the GluN2 subunit that is expressed. GluN2A has the highest EC_{50} (~3 μM) and GluN2D has the lowest (~0.5 μM) (Erreger et al., 2007). GluN2B (EC_{50} ~2.86 μM) and GluN2C (EC_{50} ~1.68 μM) have intermediate potencies between these two extremes. The EC_{50} for the D-glutamate enantiomer has a 100-fold higher EC_{50} and shows the same pattern with differing GluN2 subunits. It also shows a small increase in efficacy at GluN2B, 2C and 2D receptors. NMDA is less potent overall than L-glutamate (Figure 7). It has the highest EC_{50} at GluN2A (EC_{50} ~ 94 μM) and the lowest at GluN2D (EC_{50} ~ 7.30 μM) (Erreger et al., 2007). GluN2B (EC_{50} ~ 29 μM) and GluN2C (EC_{50} ~ 21 μM) again have intermediate potencies. NMDA shows reduced efficacy at the differing GluN2 NMDA

receptor subunit combination compared with glutamate. GluN2B has the lowest efficacy (78%) and increases for GluN2C (86%), GluN2D (92%) and GluN2D (93%).

Structure	Name
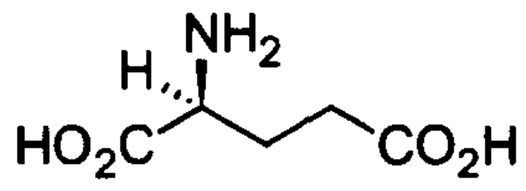	Glutamate
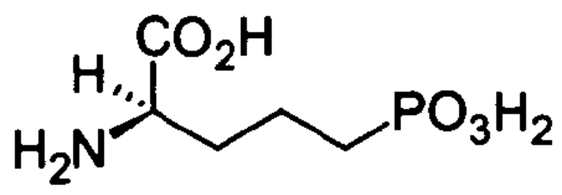	R-AP5
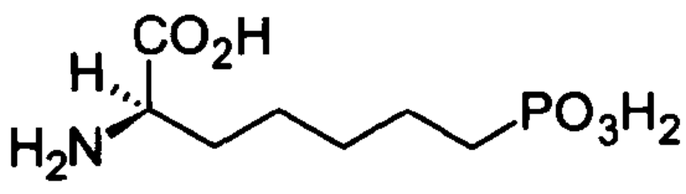	R-AP7
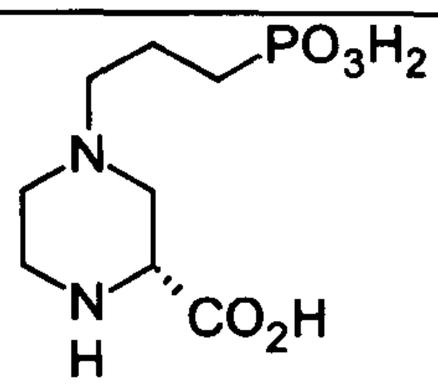	CPP
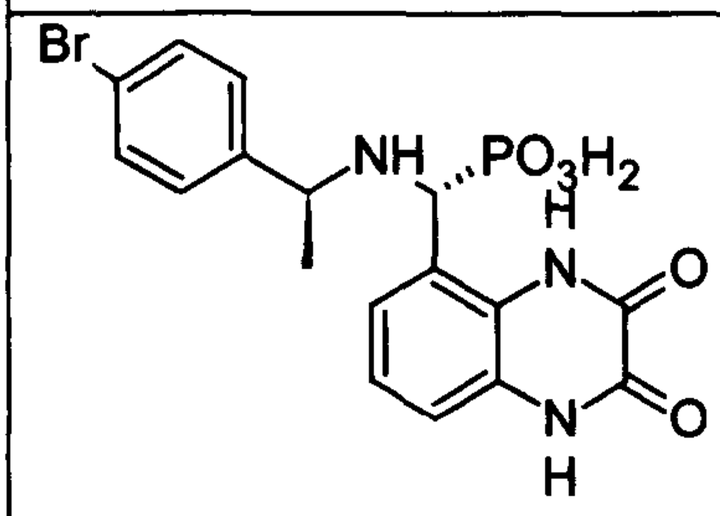	NVP-AAM077

Figure 7: Competitive antagonists for the GluN2 subunit of the NMDA receptor. Shown are glutamate and how the extended backbone and the phosphate group led to competitive antagonists in the case of R-AP5 and R-AP7 (see Monaghan and Jane, 2009). Modifications that added a piperazine ring led to the antagonists CPP. Lastly shown the compound NVP-AAM077 which was shown not to be the GluN2A specific agonist that it was thought to be (Neyton and Paoletti, 2006).

Competitive antagonists at the ligand binding domains of the GluN2 subunits were originally produced by extension of the glutamate backbone (see Monaghan and Jane, 2009). Increased potency was found with R-AP5 which was produced by extending and adding a ω-phosphonic group (Figure 7). Increasing the alkyl chain by one decreased

potency, but increasing one more to seven restored it (D-AP7). Incorporating the AP7 structure into a piperazine ring produced the compound CPP which is a potent (K_i= 0.04 μM) competitive antagonist at the NMDA receptor (Figure 7). These compounds show some selectivity between the GluN2 subunits, but not for them to be considered selective antagonists (see Paoletti and Neyton, 2006).

There was hope that the quinoxaline-2,3-dione based antagonist NVP-AAM077 was a selective antagonist for GluN2A containing receptors (Figure 7). The half-maximal inhibitory concentration (IC_{50}) for NVP-AAM077 was found to be 14 nM at GluN2A receptors, and 1800 nM at GluN2B receptors (Liu et al., 2004). However, the glutamate concentration was not varied in order to reflect the true EC_{50} value at the differing GluN2 subunits, which would be required when exploring competitive antagonism (Neyton and Paoletti, 2006). Therefore, when the glutamate concentration was adjusted to the true EC_{50} values it was found that the compound was not selective. Although it remained quite a potent compound at GluN2A receptors (K_i=0.006 μM) there was only around a 10-fold difference between the other GluN2 subunits.

1.6.2 Glycine

Similar to glutamate, the potency of glycine at GluN1 depends on the GluN2 subunit that is co-expressed. Glycine has a lower EC_{50} at GluN1 with GluN2D (EC_{50} ~ 0.13 μM) than GluN2A (EC_{50} ~ 1.31 μM), with GluN2B and GluN2C having intermediate glycine potencies (Chen et al., 2008). The same study showed that this was mediated by the S2 region of the ligand binding domain, as the mutation of L719 and T735 in the S2 region of GluN2A to that of GluN2D transferred the EC_{50} of glycine. As well as glycine, D-alanine is an agonist at GluN1, as is D-serine, the latter being more potent in GluN2A containing receptors (Chen et al., 2008). The same study has shown that the L-

enantiomer of these amino acids have a 100-fold increase in EC_{50} with a similar pattern across the GluN2 subunits. Chimeras of the GluN2 N-terminal domain and their linker domains may also transfer the differences in glycine EC_{50}, but has not been explored. The absence of the C-terminal cassettes has been shown to increase the potency of glycine, but the N1 cassette had no influence (Schmidt and Hollmann, 2009).

Kynurenic acid was the first GluN1 glycine site antagonist to be found (see Monaghan and Jane, 2009). It was modified mainly by the addition of Cl to produce compounds such as 5,7-dichlorokynurenic acid, L-683344, L-689560, L-701324 and MDL-299591 which had increased potency (Figure 8) (Leeson et al., 1991, Leeson et al., 1992, Kulagowski et al., 1994, Salituro et al., 1992). The AMPA receptor antagonists CNQX and DNQX were also found to be active here, but modifications carried out to increase potency were not water soluble and hence had limited use as therapeutics (Cai et al., 1997). Spermine has also been shown to decrease glycine dissociation leading to a 3-fold increase in affinity, and is termed glycine dependent potentiation (Benveniste and Mayer, 1993). It is only found when GluN1 is expressed with GluN2A and GluN2B, but not GluN2C and GluN2D, and is not affected by the differing GluN1 splice variants (Williams, 1997).

Structure	Name
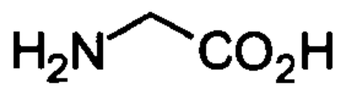	Glycine
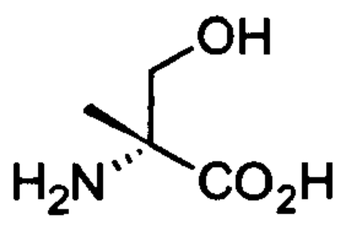	D-serine
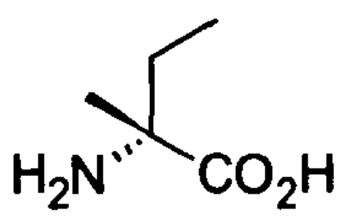	D-alanine
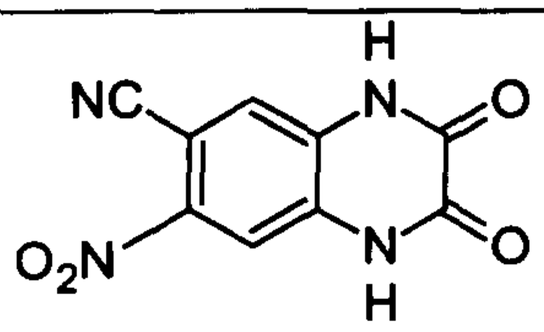	CNQX
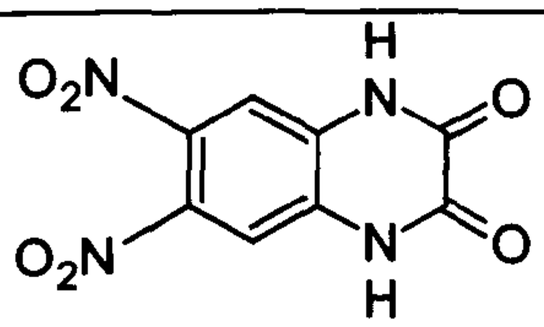	DNQX
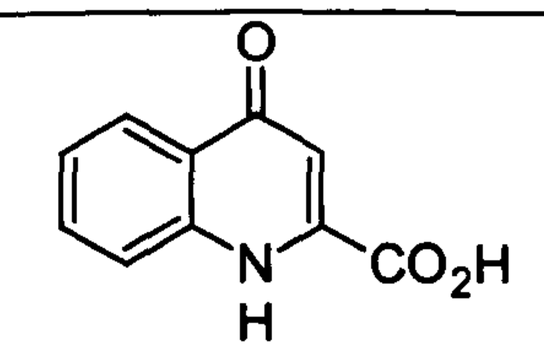	Kynurenic Acid
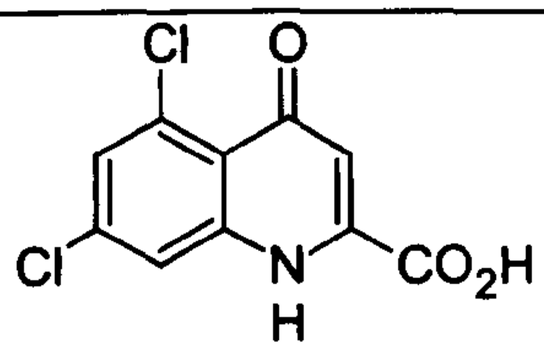	5,7-Dichlorokynurenic Acid
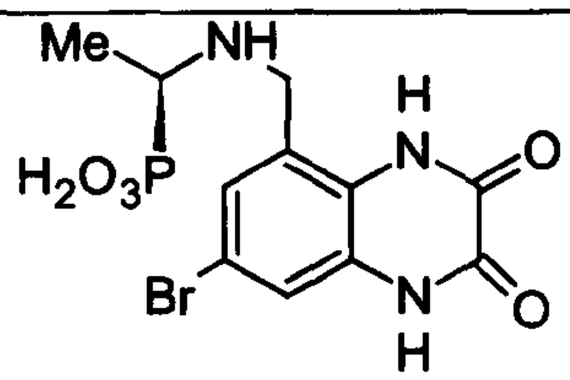	CGP-78608
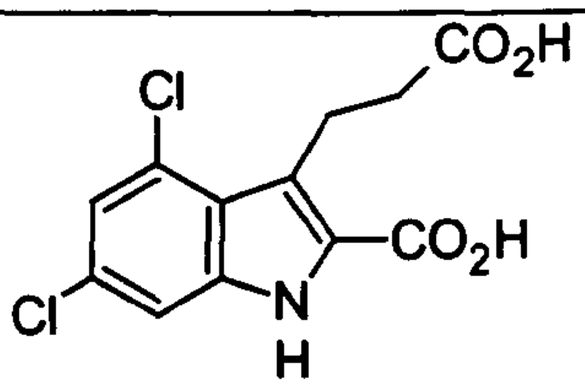	MDL-29951

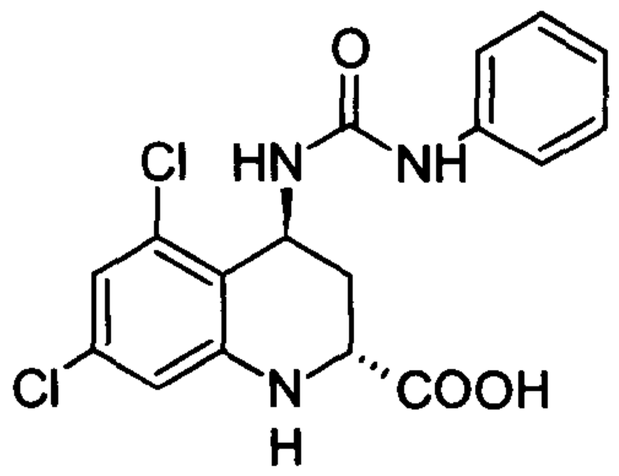	L-689560
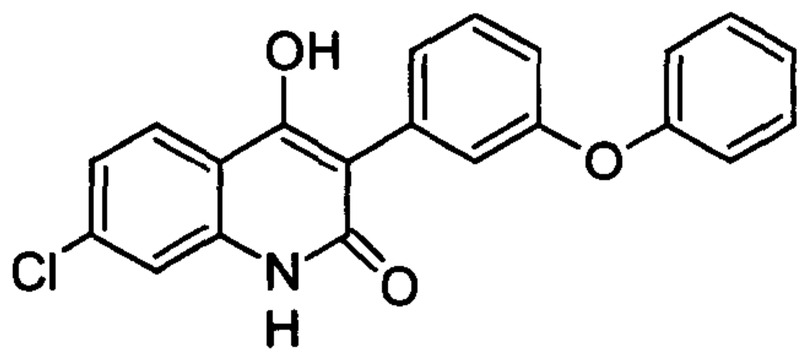	L-701324

Figure 8: Glycine site agonists, partial agonists and antagonists. Shown are the amino acid agonists glycine D-serine and D-analine for the GluN1 subunit of the NMDA receptor (Chen et al., 2008). CNQX and DNQX were AMPA receptor antagonists that were also shown to be active here (see Monaghan and Jane, 2009). Kynurenic Acid was the fist glycine site antagonist to be found and this was modified to produce the compounds with similar modes of action 5,7-dichlorokynurenic acid, L-683344, L-689560, L-701324 and MDL-299591 (see Monaghan and Jane, 2009).

Both GluN1 and GluN3 bind glycine; however, the ligand binding domains of the GluN3 subunits have different properties. Glycine binds to GluN3A with a high affinity, having a 650-fold lower K_D than GluN1, as well as binding glutamate with a low affinity (Yao and Mayer, 2006, Neyton and Paoletti, 2006). The partial agonist ACBC has a 65-fold higher affinity at GluN3A than GluN1 (Yao et al., 2008). For the antagonists, CNQX has a similar dissociation constant at GluN1 and GluN3A; however, CGP-78608, 5,7-DCKA, L-689560 and L-701324 show selectivity for GluN1 over GluN3A (Figure 8) (Yao and Mayer, 2006). L689560 and 5,7-DCKA can be considered the best selective compounds for this purpose as they have affinities in the nM range for GluN1 and 100 μM range for GluN3A.

1.7 Modulation of the NMDA Receptor

Zn^{2+} is released at many glutamatergic synapses and it may act as an endogenous allosteric modulator (see Frederickson et al., 2000). It binds to the cleft of the N-terminal domain of GluN2 subunits promoting closure, which then interferes with the ligand binding domain through its linkers causing desensitisation (Gielen et al., 2009). Zn^{2+} inhibits NMDA receptor currents in a manner that is 100-fold more selective for receptors containing GluN2A (IC_{50} ~ 15 nM) than GluN2B (IC_{50} ~ 1 μM) while having a low affinity for GluN2C (IC_{50} ~ 20 μM) and GluN2D (IC_{50} ~ 10 μM) (see Mony et al., 2009a, Rachline et al., 2005). GluN1 alternative splicing has also been shown to influence Zn^{2+} inhibition, such that those that contained N1 and the full length C2 were shown to have a 3-fold and 10-fold increase in IC_{50} at GluN2A and GluN2B containing receptors respectively (Traynelis et al., 1998). Zn^{2+} has been shown to mediate its effects by reducing mean open time open probability (Erreger and Traynelis, 2008).

Ifenprodil also acts at the N-terminal domain producing selective inhibition of the GluN2B subunit (Williams, 1993, Williams, 1995) (Figure 9). It is 1000-fold more potent here than at the GluN2A subunit, and shows little affinity to GluN2C and GluN2D (Williams, 1993). Its binding has also been shown to be competitive with Zn^{2+} indicating that it binds at the same site (Perin-Dureau et al., 2002, Rachline et al., 2005). Ifenprodil is thought to bind to both lobes of the N-terminal domain encouraging its closure hence reducing open probability in a similar manner to Zn^{2+} (Gielen et al., 2009, Mony et al., 2009b). A large range of compounds similar to ifenprodil have been produced to increase selectivity and potency. Ro 25,6981 and CP 101,606 (traxoprodil) are around 10-fold more potent than ifenprodil, and have a similar structure and similar binding sites (Figure 9) (see Gogas, 2006).

Structure	Name
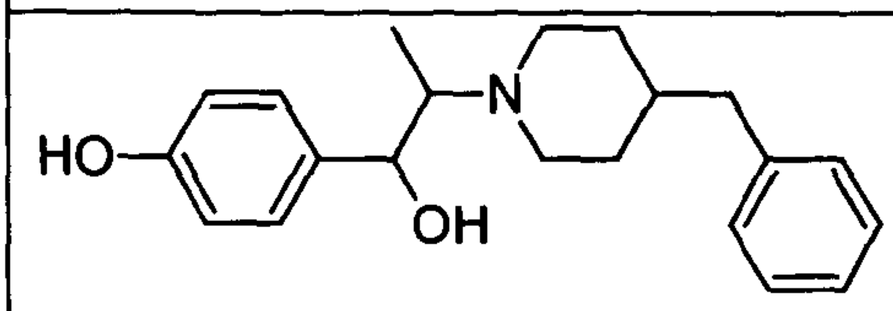	Ifenprodil
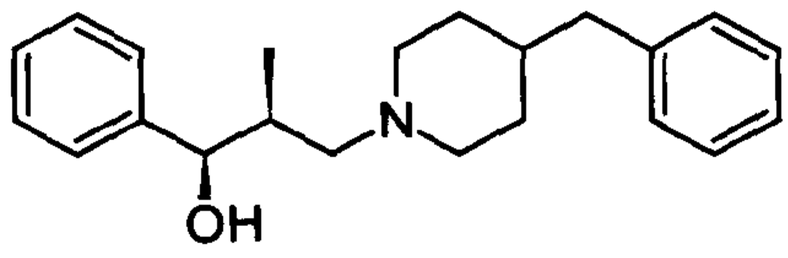	Ro 25,6981
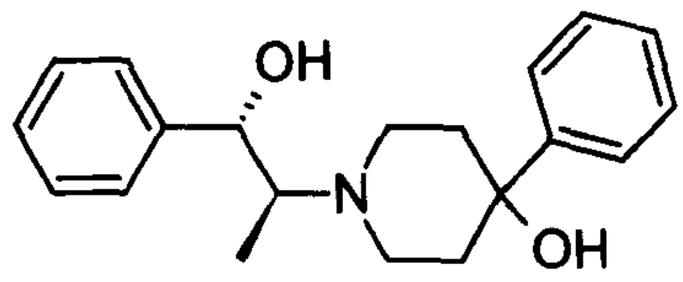	CP-101-606

Figure 9: Ifenprodil and related compounds. These compounds block at the N-terminal domain of the GluN2B subunit similar to where Zn^{2+} binds (see Gogas, 2006).

Sensitivity to Zn^{2+} and ifenprodil can alter in tri-heteromeric NMDA receptor assemblies.

GluN1/2A/2B receptors have been found in the cortex and hippocampus with GluN1/2A/2C (or 2D) in the cerebellum (Cull-Candy and Leszkiewicz, 2004). In tri-heteromeric receptors, even though GluN2A and GluN2B can be present, it was found that there was reduced efficacy of ifenprodil although affinity remained the same (Hatton and Paoletti, 2005). The GluN2C subunit also was also shown to have a similar high affinity with low efficacy. Therefore, the absence of GluN2B does not always follow from a lack of activity of ifenprodil; however, such a claim could be made if Zn^{2+} inhibition was also low. There was no loss in ifenprodil efficacy with GluN1-1a/2B/3A receptors, therefore the triheteromeric properties are related to GluN2 subunit expression (Smothers and Woodward, 2003).

NMDA receptors are inhibited by protons in a non-competitive voltage-independent manner. Inhibition is dependent on the GluN2 subunit expressed, with GluN2B and GluN2D being the most sensitive with an IC_{50} ~ pH 7.4 and GluN2C having the lowest

pH IC_{50} at ~ pH 6.5 (Low et al., 2003). GluN1-1a/GluN2A receptors show intermediate inhibition with an IC_{50} of ~ pH 6.9. GluN2B and GluN2D are therefore inhibited by 50% at physiological pH, highlighting an important role for protons in the gating of NMDA receptors. GluN1 alternative splicing has also been shown to affect proton sensitivity. Inclusion of the N1 cassette in GluN1-1b together with GluN2A or GluN2B was shown reduce the IC_{50} to ~ pH 6.7 (Traynelis et al., 1995).

The exact site of proton inhibition is unknown; however, mutations in the linkers between M2, M3 and the S2 region leading to the ligand binding domain were shown to reduce pH sensitivity in the GluN1 subunit (Low et al., 2003). For GluN2A, the same study found that mutations in the S2 to M4 linker domain also led to a reduction in pH sensitivity, and that a combination of S2-M3 in both GluN1 and GluN2A led to a 145-fold decrease in the IC_{50}. In addition, mutations that lead to open channels in the conserved SYTANLAAF motif of M3 have also been shown to influence proton sensitivity (Low et al., 2003). The results of these mutations indicate a close relationship between channel gating and protons, possibly promoting the shut conformation of the channel as shown by increased shut times in single channel studies (Banke et al., 2005). Modulation of the NMDA receptor by N-terminal may therefore mediate their effects by shifting the pKa of the putative proton sensor.

As well as inhibition of NMDA receptors, modulation of the N-terminal domain can potentiate responses. Spermine could potentiate currents, but was limited to the GluN2B subunit (see Mony et al., 2009a). It has an EC_{50} ~ 150 μM at pH 7.3 and can potentiate responses up to a maximum of 3-fold (Benveniste and Mayer, 1993). Two mechanisms of potentiation by spermine have been proposed, as many mutations across the extracellular domain of GluN1 and GluN2B inhibit the potentiation (see Mony et al., 2009a). The first

proposes that spermine binds at the ligand binding domain across a dimer pair keeping the region in the open conformation and inhibiting disruption of the N-terminal domain. Supporting this is evidence that has shown that spermine and spermidine bind to the S1S2 regions of the ABD (Stoll et al., 2007). A second model proposes binding occurs in the N-terminal domain, but rather than holding the N-terminal domain open by binding at the cleft where ifenprodil binds, spermine binds together the bottom lobes of the dimer pair. Ifenprodil and spermine have been shown to bind at distinct sites in a negative allosteric manner, hence a modified model is required (Han et al., 2008).

1.8 Open Channel Block

Mg^{2+} is the endogenous open channel blocker of the NMDA receptor. It occludes the channel pore region after opening and acts in a voltage-dependent manner (Mayer et al., 1984, Nowak et al., 1984). A single mutation at the 'N-site' asparagine site at the tip of the pore loop of the GluN1 subunit was found to reduce Mg^{2+} sensitivity (Sakurada et al., 1993). The N-site of the GluN1 is the binding site for intracellular Mg^{2+} (Wollmuth et al., 1998b). Similarly, the N-site and the adjacent asparagine (N+1 site) in GluN2A was shown to bind extracellular Mg^{2+} (Wollmuth et al., 1998a). The sensitivity to Mg^{2+} is altered according to the GluN2 subunit that is expressed. The biggest difference is between GluN2A and GluN2B, which have the lowest IC_{50} values and GluN2C and GluN2D containing receptors which have the highest (Kuner and Schoepfer, 1996, Wrighton et al., 2007). The largest difference in Mg^{2+} sensitivity is found between GluN2A and GluN2D (34 and 91 μM respectively). Chimeras where the M1, M2 and M3 regions from GluN2D were transferred to GluN2A showed a 10-fold increase in the IC_{50} for Mg^{2+} compared with wild-type GluN2A, and a 3-fold higher IC_{50} than GluN2D containing receptors (Wrighton et al., 2007). The same study showed that the chimera of the S1S2 domain of GluN2D transferred to GluN2A had an IC_{50} for Mg^{2+} that was lower

than wild-type GluN2A. The study showed that the transmembrane regions, and the S1S2 region of the ligand binding domain, play differing roles in mediating Mg^{2+} sensitivity.

The GluN3A and GluN3B subunits are thought to reduce Mg^{2+} sensitivity as the 'N-site' residue which has been shown to bind the ion is G in these subunits (Wollmuth et al., 1998a). Some review articles made this claim, but evidence was weak as no full study had been carried out on the activity of Mg^{2+} (Petrenko et al., 2003, Paoletti and Neyton, 2006). Inhibition by Mg^{2+} was not significantly different when GluN3B was present in GluN1/2A and GluN1/2B receptors expressed in Xenopus oocytes (Yamakura et al., 2005). The same study showed that mutations at the N-site and N+1 site in GluN3B did not alter Mg^{2+} sensitivity. However, the authors only applied two concentrations of Mg^{2+} at -75 mV and compared percent inhibition with a t-test. This is not a valid comparison as percentage data must be arcsin transformed to normalise the error distribution. The percentage must be divided by 100, then the square root taken and then the inverse sin is taken to get a value in degrees. The value can then be analysed using parametric statistics.

Expression of GluN3B has also been shown to have no effect on Mg^{2+} sensitivity when expressed with GluN1/2A in HEK-293 cells (Nishi et al., 2001). The authors tested 1 mM Mg^{2+}, producing an I/V curve that showed inhibition by Mg^{2+} at voltages less than -50 mV, and it was not altered by the presence of GluN3B. However, the converse has also been shown, with GluN1/2B/3A receptors expressed in HEK-293 resistant to block by 1 mM and 10 mM Mg^{2+} at negative voltages (Sasaki et al., 2002). The sensitivity of Mg^{2+} was tested in hippocampal neurones from transgenic mice overexpressing GluN3A and the IC_{50} for Mg^{2+} in wild-type (WT) neurones was found to be 9.9 μM, and was significantly increased to 133.8 μM (Tong et al., 2007). These results suggest that the loss

of Mg^{2+} sensitivity in the presence of GluN3 subunits may not be as dramatic as that suggested by the N-site changes.

Memantine (1-amino-3,5-dimethyl-adamantane) is a highly selective open-channel blocker of the NMDA receptor (Chen et al., 1992, Chen and Lipton, 1997). It is a derivative of amantadine, an anti-influenza drug, which was serendipitously found to be effective against the symptoms of Parkinson's disease. The two methyl side groups of memantine help prolong dwell time compared with amantadine which slows the off-rate and increases affinity for to the channel (Figure 10). It has a higher affinity and slower off-rate than Mg^{2+}, as well as showing less voltage-dependence (Danysz and Parsons, 2003). Memantine has a k_{on} that depends on memantine concentration, but a k_{off} that is independent, giving the compound the same off-rate at clinically relevant concentrations (Chen and Lipton, 1997). It was shown to bind preferentially to the GluN1 Mg^{2+} site (the 'intracellular' Mg^{2+} binding site) and showed electrostatic interactions at the N and N+1 on GluN2 (Chen and Lipton, 2005). The same study located a second more superficial, low affinity, less voltage-dependent binding site at L651 of the M3 region of GluN1. It is similar to where hexamethonium, the acetylcholine receptor blocker, was shown to bind (Chen and Lipton, 2005). It is thought that the superficial site is where memantine can unbind without agonist being present, contributing towards its 'partial trapping' property (see below) (Kotermanski et al., 2009). Further residues involved in memantine binding are found on the M1, M2 and M3 regions and these are shown in (Figure 11).

Structure	Name
	Amantadine
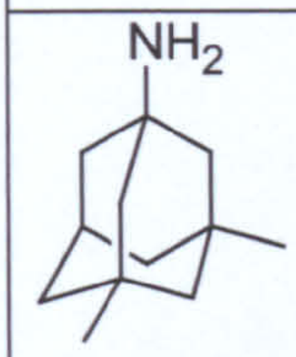	Memantine

Figure 10: Structure of amantadine and memantine. Amantadine was an influenza drug that was modified with the amino group to produce the more potent compound memantine (Chen et al., 1992).

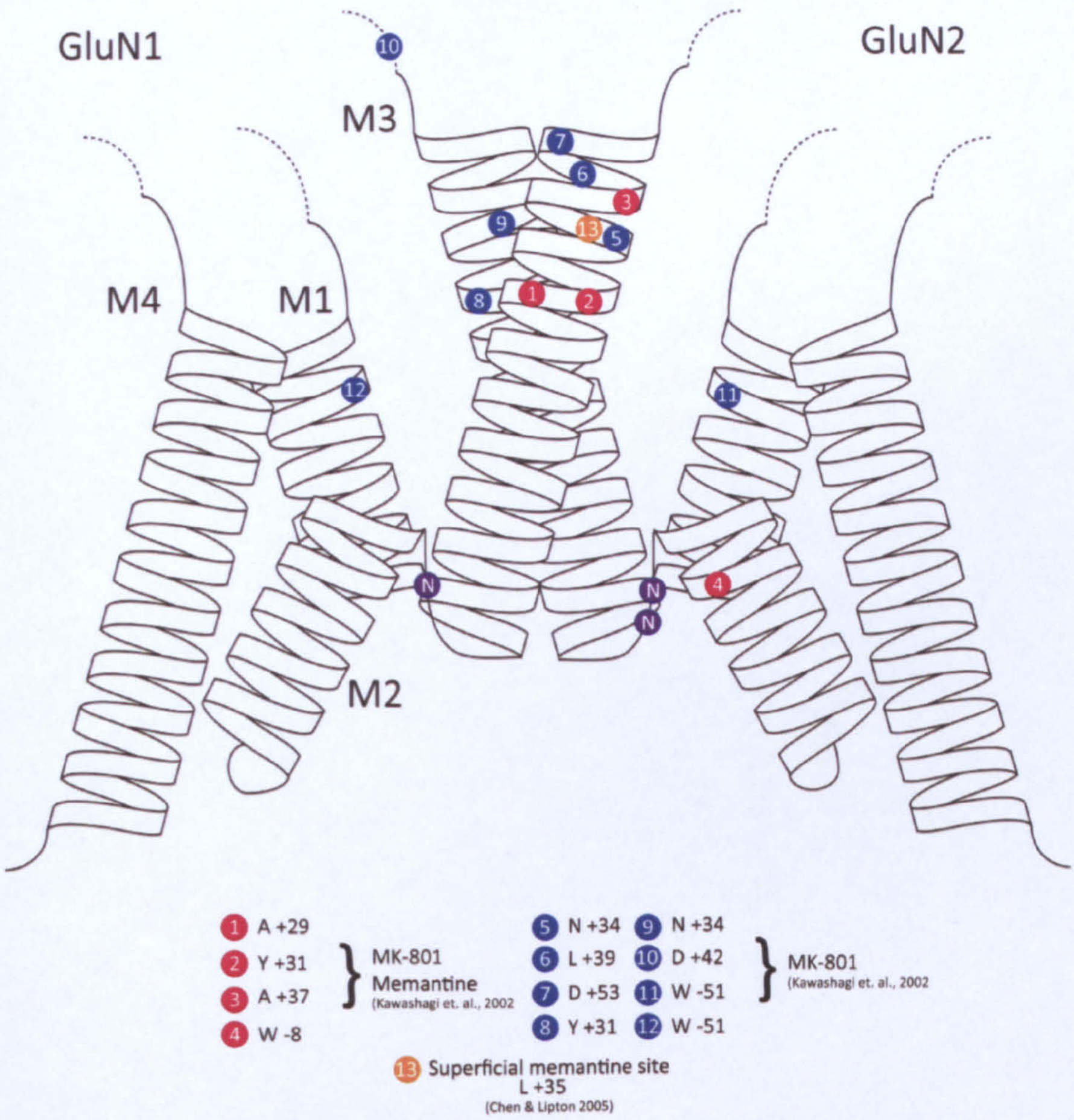

Figure 11: Binding sites of the pore region of the NMDA receptor. N shows the N site of GluN1 and GluN2, as well as the N+1 site of GluN2. Circles 1-4 show residues involved in MK-801 and memantine binding, with the circles 5-12 showing further residues involved in binding MK-801 (Kashiwagi et al., 2002). Circle 13 shows the superficial memantine binding site (Chen and Lipton, 2005). Quaternary structure adapted from AMPA crystal in the closed configuration (Sobolevsky et al., 2009). Amino acid positions should be considered diagrammatic.

Memantine is considered a 'partial trapping' compound as a proportion of agonist-induced response can be recovered immediately after a quick wash out, an effect which is not found present in fully trapping compounds such as ketamine and MK-801 (Blanpied et al., 1997, Kotermanski et al., 2009). One possible mechanism is that memantine escapes up and out of the channel when it closes, but as memantine unbinding is slower than agonist unbinding then it would have to hold the channel open by a foot-in-the-door type mechanism. If this was the case, then there should be a related tail current when memantine was released, but this was not found (Benveniste and Mayer, 1995, Blanpied et al., 1997). As the off-rate of memantine increases with membrane depolarisation, if the compound is escaping up and out the open channel then a depolarisation jump after application of agonist is stopped should leave an increased proportion of NMDA current with a second application of agonist (Blanpied et al., 1997). However, no significant differences were found in the proportion of inward current after the second application of agonist, providing further evidence that memantine does not escape out of open channels (Kotermanski et al., 2009).

It has been suggested that the deep and superficial memantine binding sites are competitive. As the superficial site is less voltage-dependent, depolarisation would push binding toward it rather than the deep site. This would be shown by increased proportional recovery after a second agonist application and this was found to be the case (Kotermanski et al., 2009). Furthermore, a mutation at the 'N-site' in GluN2A significantly increased fractional recovery after a second agonist application, indicating that the mutation in the deep binding site may have pushed memantine binding toward the superficial site. Unlike Mg^{2+}, memantine is more potent at GluN2D (0.29 μM) containing NMDA receptors than GluN2A (0.86 μM), but chimeras transferring the M1,

M2 and M3 regions from GluN2D to GluN2A did not alter memantine potency (Wrighton et al., 2007).

Memantine (ebixia) is currently the only clinically approved drug that targets glutamatergic transmission (Chen and Lipton, 2006). A tolerated NMDA receptor antagonist has to block excessive activity of the NMDA receptor without blocking normal signalling. Memantine was found to block only around 15% of the late component of synaptic transmission (which is mediated by NMDA receptors), whereas MK-801 completely blocked this (Chen et al., 1992). Memantine has been shown to block LTP in the CA1 region of the hippocampus but did not inhibit memory as measured by the Morris water maze task (Chen et al., 1998). This showed that normal functions were unaffected. Memantine was also shown to be an ineffectual blocker when low concentrations of NMDA are used, but if the agonist concentration was increased it was shown to become more effective (Chen et al., 1992). Therefore, memantine could be considered *more* useful with excessive glutamate levels, providing a further property that which spares normal glutamatergic transmission.

MK-801, PCP and ketamine (Figure 12) are not as useful as memantine as they have high affinity and can become trapped within the channel which seem to produce symptoms similar to schizophrenia and are also thought to cause acute pathomorphological changes termed Olney's lesions (Olney et al., 1989, Krystal et al., 2003). MK-801 (dizocilpine) is a high-affinity open channel blocker of the NMDA receptor that is considered fully trapping (Dingledine et al., 1999). It has a large dwell time due to its high affinity, and the N-site mutations on GluN1 and GluN2B as well as N+1 on the latter showed reduced affinity for MK-801 highlighting a potential binding site in this region (Kashiwagi et al., 2002). MK-801 is also considered fully trapping meaning that the M3 region can close

and due to its high affinity it becomes trapped in the pore. Further residues involved in MK-801 binding are found on the M1, M2 and M3 regions and these are shown in Figure 11. The dissociative anaesthetics ketamine and phencyclidine are also considered fully trapping blockers of the NMDA receptor (Figure 12). These act in a similar manner to MK-801 producing schizophrenia-like effects that limit their use as therapeutics (Mealing et al., 1999, Krystal et al., 2003).

Structure	Name
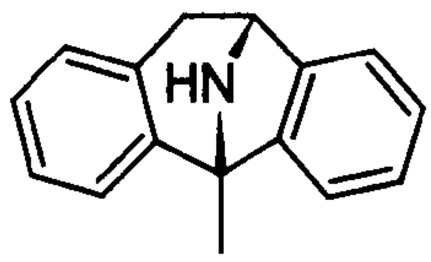	MK-801
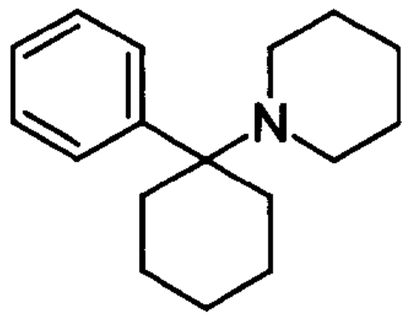	Phencyclidine
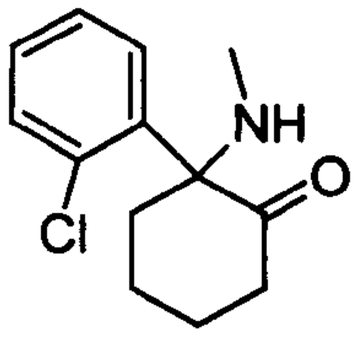	Ketamine

Figure 12: Structure of fully trapping blockers of the NMDA receptor. MK-801, phencyclidine (PCP) and ketamine are all though to be fully trapping compounds, meaning that they remain in the channel after the gate has closed due to their high affinity (Krystal et al., 2003).

1.9 Polyamines as Open channel Blockers

Endogenous polyamines such as spermine, spermidine and putrescine (Figure 13) are present in most living cells and have a wide variety of essential functions (Childs et al., 2003). They are involved in processes such as regulating nucleic acid packaging, DNA and RNA synthesis, apoptosis, transcription and translation. They can also act as electrostatic bridges between phosphate groups on nucleic acids, as well as interacting with other chain like molecules such as actin and microtubules. It has also been shown that polyamines can interact with ion channels such as inwardly rectifying potassium channels and ionotropic glutamate receptors (see Williams, 1997).

As well as potentiation of the NMDA receptor, intracellular spermine can block the outward rectification of Ca^{2+} permeable (without edited GluA2) AMPA receptors in a voltage-dependent manner that is prevented by the positively charged R at the Q/R site (Bowie and Mayer, 1995). Therefore receptors without GluA2 are inwardly rectifying due block by endogenous polyamines. As well as potentiating NMDA channels, extracellular spermine has also been shown to block them in a voltage-dependent manner suggesting open-channel block (Benveniste and Mayer, 1993). It is more potent at GluN2A and GluN2B than GluN2C and GluN2D, similar to Mg^{2+} (Williams et al., 1994, Williams, 1995). Mutations at the N-site were shown to reduce the voltage-dependent block by spermine (Kashiwagi et al., 1997). At potentials less than -60 mV spermine can dissociate from its blocking site and permeate through the channel (Araneda et al., 1999). As spermine was a weak blocker of the NMDA receptor pore, improvements in potency were made by adding a bulky headgroup as seen in N^1-Dansylspermine, (Chao et al., 1997) (Figure 13).

Structure	Name
	Spermidine
	Spermine
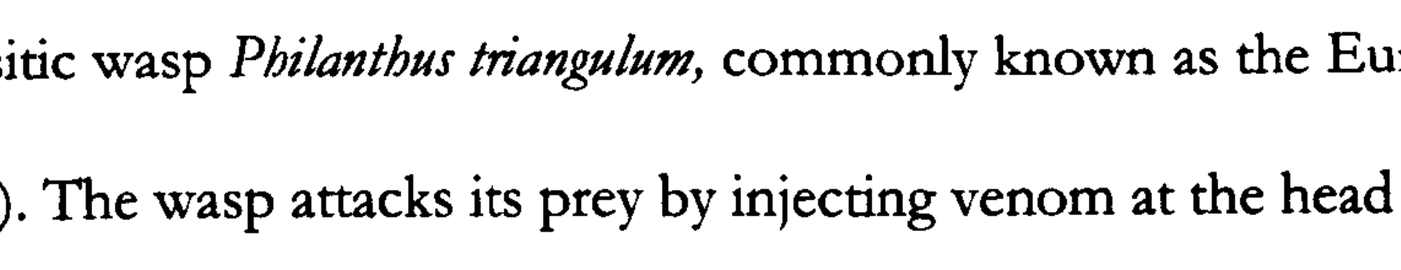	N^1-Dansylspermine

Figure 13: Spermine and related compounds. The endogenous polyamines spermidine and spermine were modified to produce the more potent glutamate receptor blocking compound N1-Dansylspermine (Bowie and Mayer, 1995, Chao et al., 1997).

1.9.1 PhTX

Polyamine toxins with a similar structure to spermine are found in the venom of the parasitic wasp *Philanthus triangulum,* commonly known as the European beewolf (Piek, 1986). The wasp attacks its prey by injecting venom at the head and the thorax causing paralysis. Although adults feed mainly on nectar and pollen, the female hunts honey bees to feed its larvae. The venom from *Philanthus triangulum* belongs to a group of related compounds known as the polyamine toxins. It was first shown to be active at quisqualate-sensitive glutamate receptors (qGluR) in the locust (May and Piek, 1979). Its most active constituent is Philanthotoxin-433 (PhTX-433) and its structure consists of a tyrosine head group with a butyryl side chain attached to a thermospermine moiety (Figure 14) (Williams, 1997). It is numbered according to the number of methylene groups between the amine groups on the polyamine chain. PhTX-433 was synthesised in

conjunction with the isomers PhTX-334 and PhTX-343 which were easier to produce (Eldefrawi et al., 1988).

At muscle type nicotinic acetylcholine receptors (nAChR) in TE671 cells, PhTX-343 was shown to inhibit responses in a voltage-dependent manner (Mellor et al., 2003). PhTX-343 was shown to cause a large reduction in mean open time at nAChR and this, coupled with its voltage-dependence, indicated that it acted as an open channel blocker (Brier et al., 2003). Also, the same study showed that pre-application of PhTX-343 gave a voltage-independent block that may have been due to binding to the closed conformation of the channel, thereby enhancing desensitisation after agonist is bound. PhTX-343 has also been shown to block neuronal nAChR in a voltage-dependent manner when measured in PC12 cells (Liu et al., 1997). Adding an ether group into the polyamine chain also increased potency at nAChR and was optimal with 4-oxa-PhTX-83 (Figure 14). The potency of the PhTX compounds was also dependent on the length of the polyamine chain, as when it was reduced, potency decreased. Replacing amines with methylene groups increased potency and of these new structures PhTX-12 (Figure 14), which had 12 methylene groups between the head group and the terminal amine, was the most potent (Brier et al., 2003). However, as it showed little voltage-dependence a second more superficial binding site was implicated. There is the possibility that the polyamine group folds back on itself when the polyamine amines were removed, causing the tail to bind to the head group (Tikhonov et al., 2004). Such a shape may stop the molecule entering the pore, possibly pushing it toward a more superficial binding site.

Structure	Name
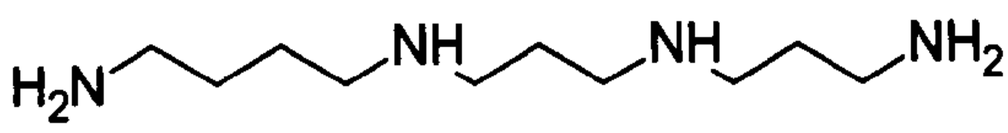	Thermospermine
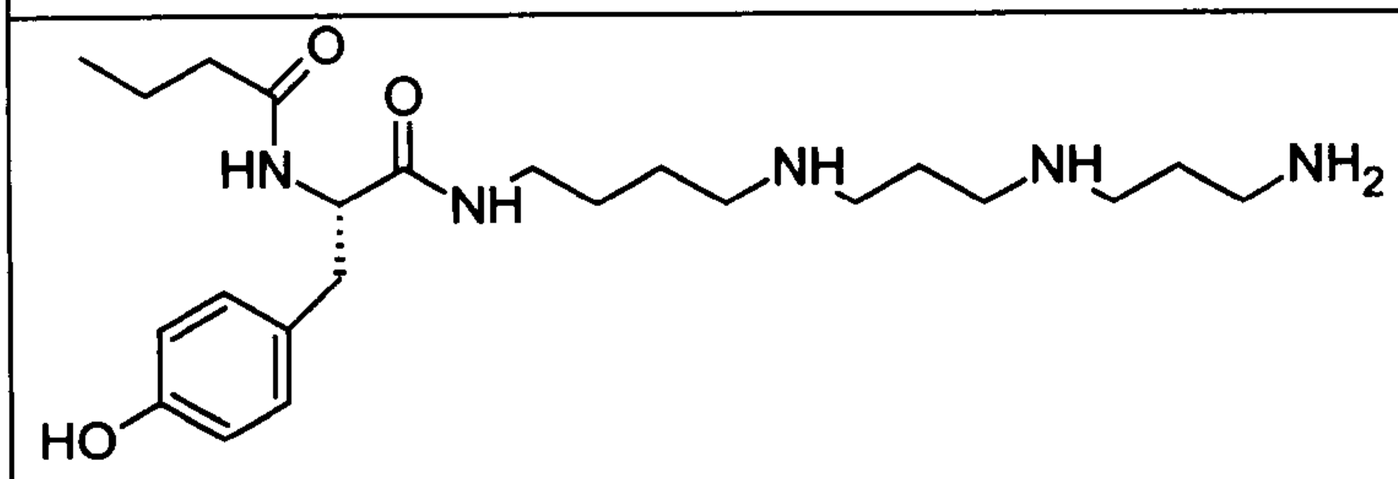	PhTX-433
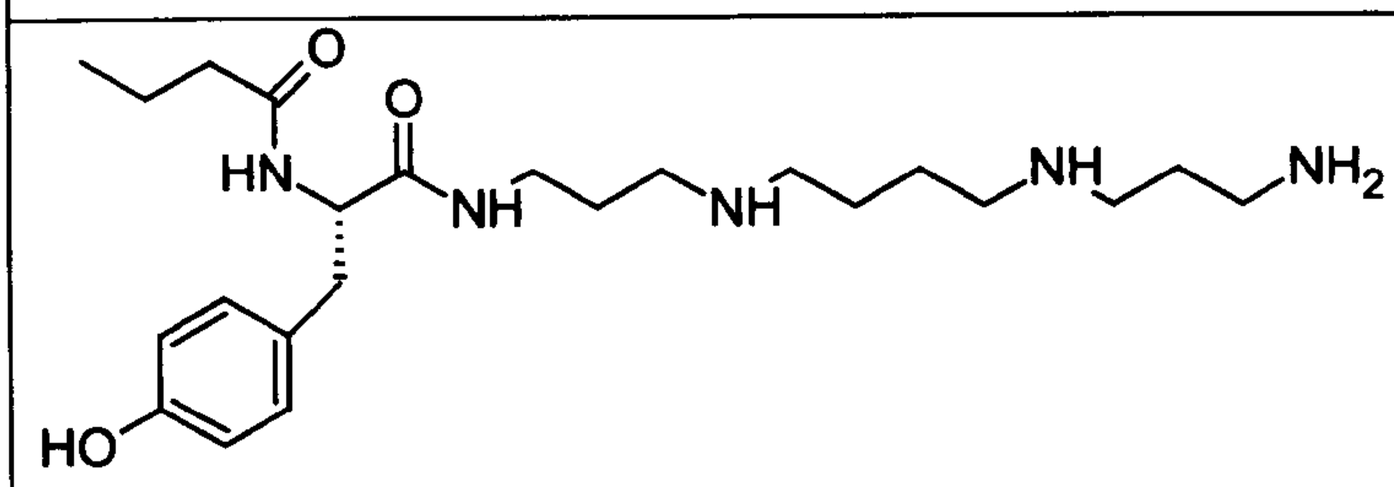	PhTX-343
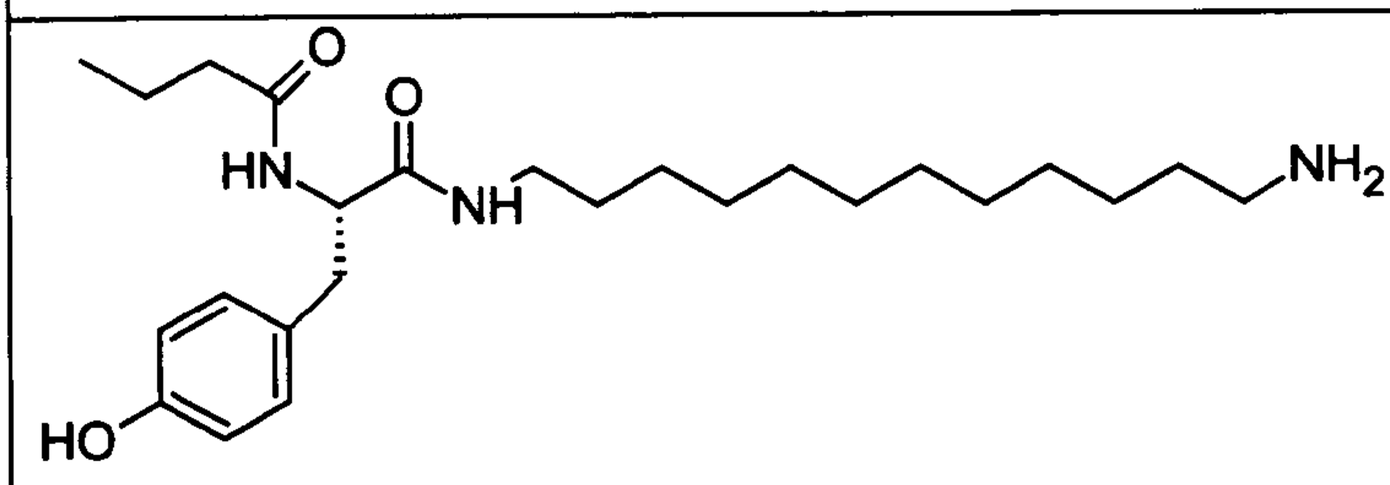	PhTX-12
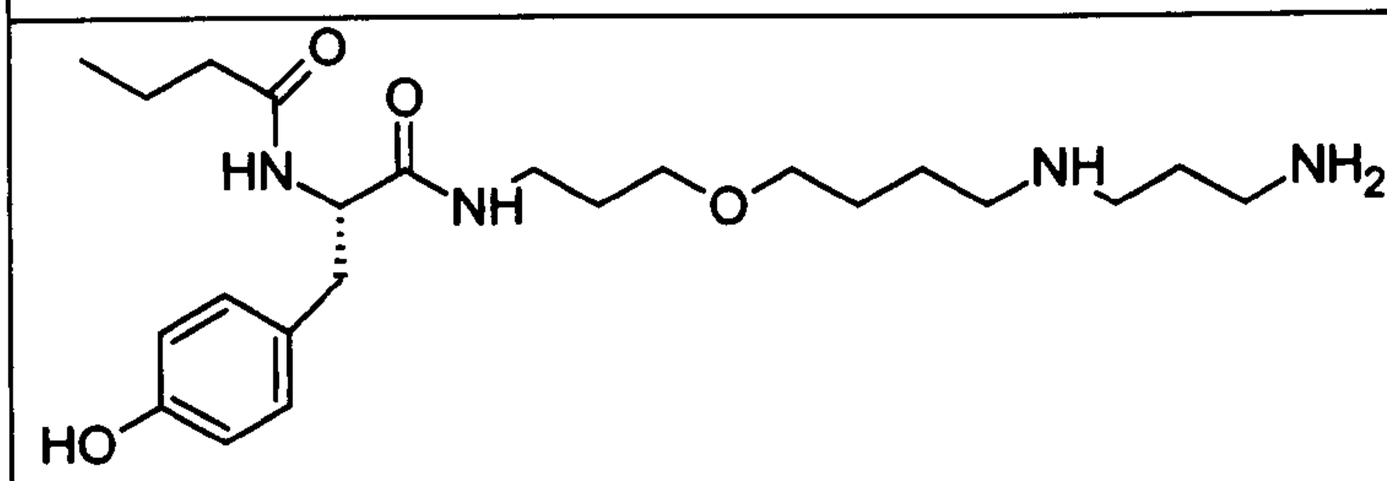	4-oxa-PhTX-83
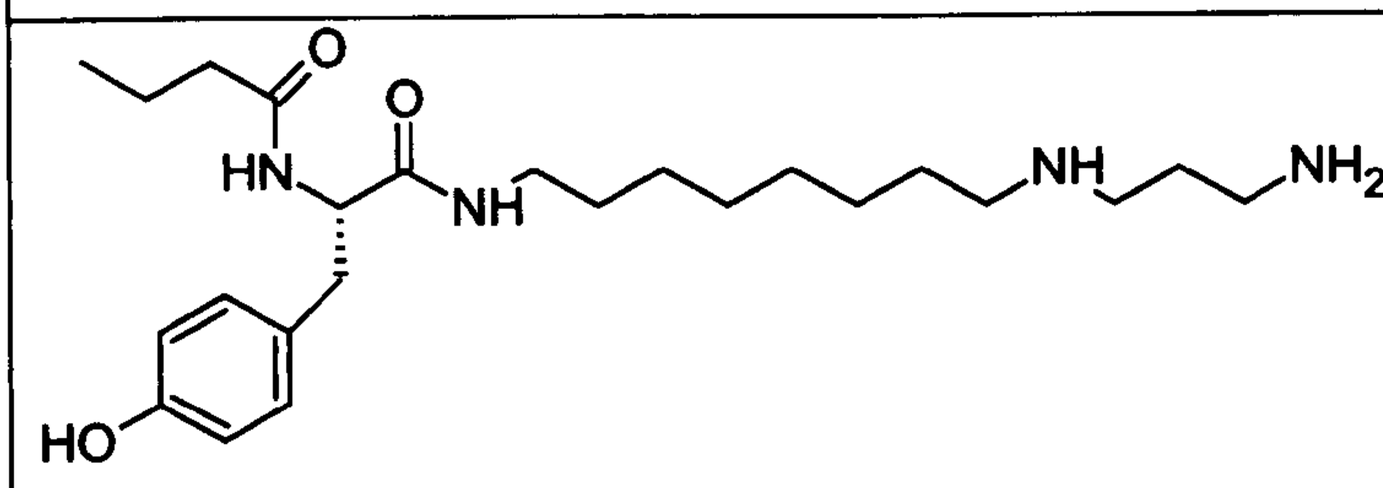	PhTX-83

Figure 14: The naturally occurring PhTX-433 and synthetic analogues. PhTX-433 was the most active constituent of the toxin from the wasp *Philanthus triangulum*, but the synthetic agonists based on their structure were easier to produce starting with the thermospermine moiety (Williams, 1997). The further modifications are shown and these show differing patterns of activity at nAChR, AMPA and NMDA receptor (Mellor and Usherwood, 2004).

Similar to endogenous polyamines, GluA2 lacking Ca^{2+} permeable AMPA receptors are also blocked by PhTX-343 (Mellor et al., 2003, Andersen et al., 2006). Truncation of the polyamine chain reduced potency and reducing the number of amines to one (PhTX-12) impaired potency, but on the other hand leaving two amines (PhTX-83) produced an Ca^{2+} permeable AMPA receptor selective antagonist that was 100-fold more potent at these receptors than at NMDA and nACh receptors (Figure 14) (Mellor et al., 2003).

PhTX-74 is another isomer that could be a selective for Ca^{2+} impermeable AMPA receptors as it has been shown to be selective for GluA1/A2 channels but not GluA2/A3 receptors (Nilsen and England, 2007). However, the concentrations used (100 and 500 μM) were high, and compared with the low IC_{50} values found with GluA2 lacking AMPA receptors it is not useful *in vivo* (Mellor et al., 2003). Furthermore, a recent poster presentation has indicated that the claims made in Nilsen and England (2007) were wrong, and that PhTX-74 may only preferentially blocked homomeric GluA1 receptors, which is what could have been expected (Poulsen et al., 2010).

A model of PhTX binding to the AMPA receptor states that two amine groups must pass beyond the selectivity filter so one amine can bind to the Q/R/N site and another to the exposed main chain oxygen at G+2 (Tikhonov et al., 2002, Andersen et al., 2006). The head group can then make multiple hydrogen bonds in the M3 segment of the channel. PhTX modifications have shown that at least a hexyl spacer is required between the charged amines to bind at both sites, as a larger chain reduced potency (Andersen et al., 2006). When the amines were pushed toward the tail, as long as the chain length was 12, the potency could be restored. It may be that both amines were able to interact with the exposed oxygen of G+2 in this case.

NMDA responses from whole rat brain RNA expressed in Xenopus Oocytes have been shown to be inhibited by PhTX-343 (Mellor et al., 2003). It was less potent than at AMPA receptors, but more potent than at muscle nAChR. Unlike inhibition of recombinant AMPA receptors methylene substitutions that reduced the number of positive charges to two or one reduced potency, indicating at least three amine groups were required for optimal activity. Ether substitutions failed to produce a compound with more potency than PhTX-343 which may be because the negative charges in the pore region of the NMDA receptor could not accommodate the oxygen (Figure 14) (Bolshakov et al., 2000). For GluN3 subunits of the NMDA receptor, there is a glycine at the N-site and a positively charged R at the N+1 site which may mean that these receptors are not blocked by PhTX-343 in a similar manner to GluA2 containing AMPA receptors which have the R at the Q/R site.

1.9.2 Anthraquinone

Anthraquinone (AQ) polyamines (Figure 15) are a group of open-channel blockers that have been shown to block the NMDA receptor (Kashiwagi et al., 2007). They are similar in structure to PhTX, with a polyamine tail group numbered in the same manner but with a different aromatic head group. Potency at the NMDA receptor is dependent on the number of positive charges on the chain, with the truncated AQ33 (IC_{50} 5.6 μM) and AQ34 (IC_{50} 7.1 μM) which had two positive charges showing reduced potency compared with AQ343 (IC_{50} 0.39 μM) and AQ444 (IC_{50} 0.57 μM) which had three charges (Kashiwagi et al., 2007). Some subunit selectivity was also found for AQ343 and AQ444 as they had the lowest potency at GluN1/2C receptors (Jin et al., 2007).

Structure	Name
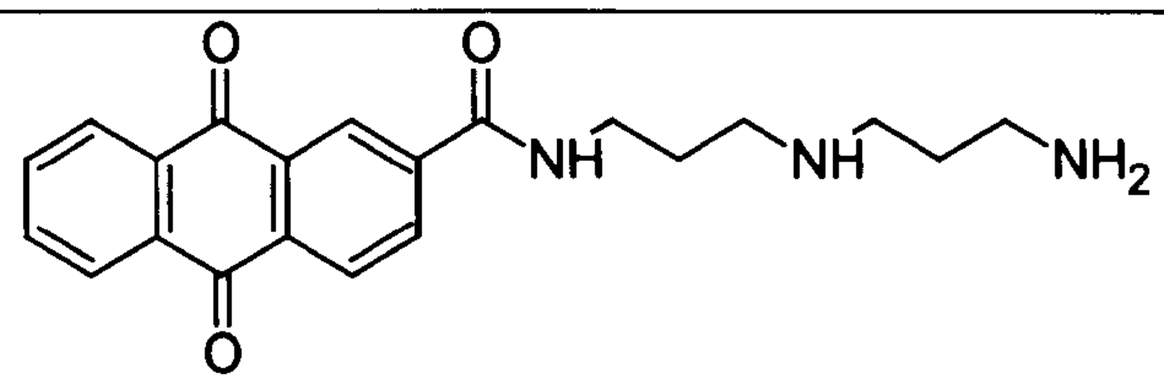	AQ33
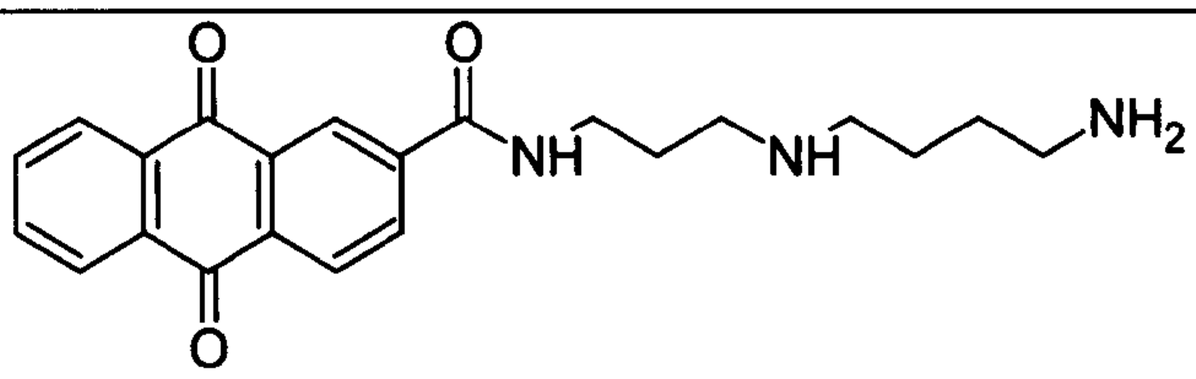	AQ34
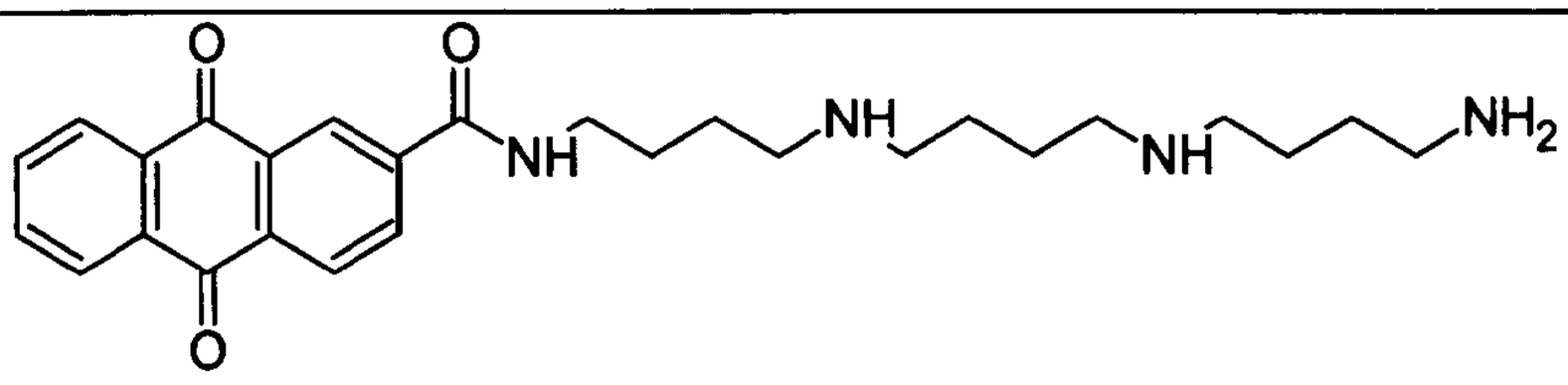	AQ444
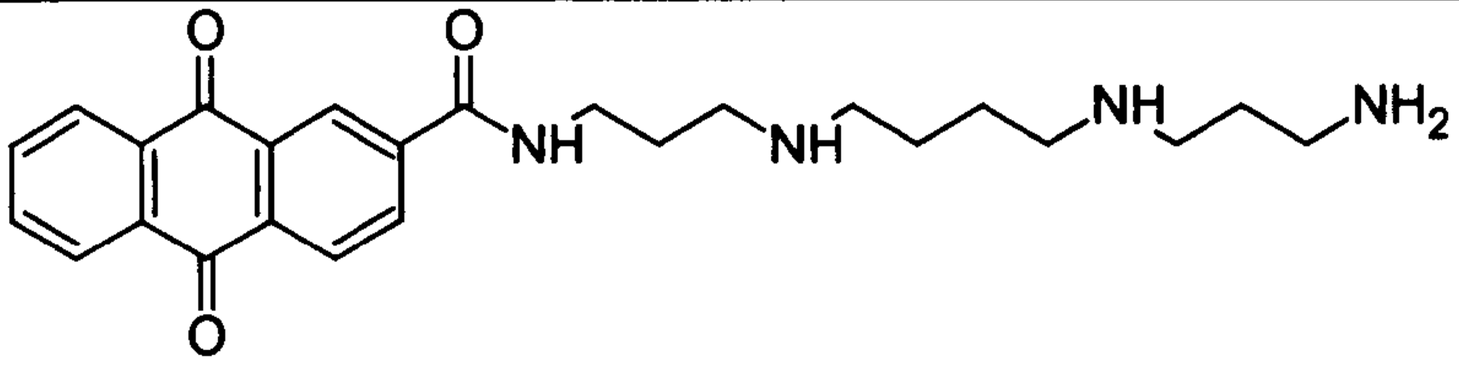	AQ343

Figure 15: Structure of anthraquinone polyamines AQ343 and AQ444. These polyamines have a similar structure to the PhTX compounds and activity at NMDA receptors (Kashiwagi et al., 2007).

Mutational studies have shown that the M3 region in GluN1 is important for the potency of anthraquinone polyamines and may be involved in compound recognition (Kashiwagi et al., 2002). Mutations which widened the vestibule increased the potency of AQ343. The difference may be due to steric effects as AQ343 has a width of 8.3 Å and AQ444 has one of 6.5 Å, with the latter possibly having a longer and more flattened tail group accounting for its smaller size. When the pore was widened AQ343 had the same potency. These compounds have also been shown to bind at the N-site of GluN1, as a mutation to Q reduced the potency of AQ343 and AQ444 but G had no effect (Kashiwagi et al., 2002). At the same site in GluN2B, the Q mutation resulted in a loss of activity but the G mutation increased block by AQ343 (Kashiwagi et al., 2007). On GluN1 the Q mutation may have inhibited the polyamine tail from entering the pore,

whereas expansion of the pore by G may have increased potency of AQ343 by no longer causing a steric hindrance. Beyond the level of the N-site a mutation in GluN1 at E621 which is five amino acids more intracellular reduced the potency of these compounds, showing that the tail group entered the pore (Kashiwagi et al., 2007).

1.9.3 Argiotoxin

Argiotoxin 636 (Arg636, Figure 16) is a toxin from the orb-web spider *Argiope lobata* and is active at insect and vertebrate ionotropic glutamate receptors (Mellor and Usherwood, 2004). Unlike other polyamine compounds it is numbered according to its molecular weight. It is a voltage-dependent open channel blocker of the NMDA receptor, and is more potent at GluN1/2A (IC_{50} 9.45 nM) and GluN1/2B (IC_{50} 4.5 nM) than at GluN1/2C (IC_{50} 460 nM) and binds in competition with Mg^{2+} and MK-801 (Raditsch et al., 1993, Raditsch et al., 1996). Mutations at the N-site to Q increased the potency of Arg636 ~10-fold at GluN2A and GluN2C indicating steric effects. Structural modifications have shown that at least three positive charges were required for optimal NMDA receptor antagonism similar to other polyamine compounds (Moe et al., 1998, Nelson et al., 2009).

Arg636 has a similar potency at AMPA receptors and modifying the amine groups in the centre of the chain to methylene produced compounds that were selective between AMPA and NMDA receptors (Nelson et al., 2009). Modifying the central amine that resides toward the terminal guanidine group to methylene resulted in an 84-fold reduction in potency at NMDA, but no change at AMPA receptors; while altering the central amine group at the head end gave a ~100-fold reduction in potency at AMPA, with no change at NMDA receptors. The same study proposed a binding model where an amine hydrogen bonds with the N-site in NMDA but not AMPA receptors, therefore

the loss of this group affects NMDA receptor potency. AMPA receptor potency is dependent on the terminal amine binding to the G+2 site deep in the pore (Nelson et al., 2009).

Structure	Name
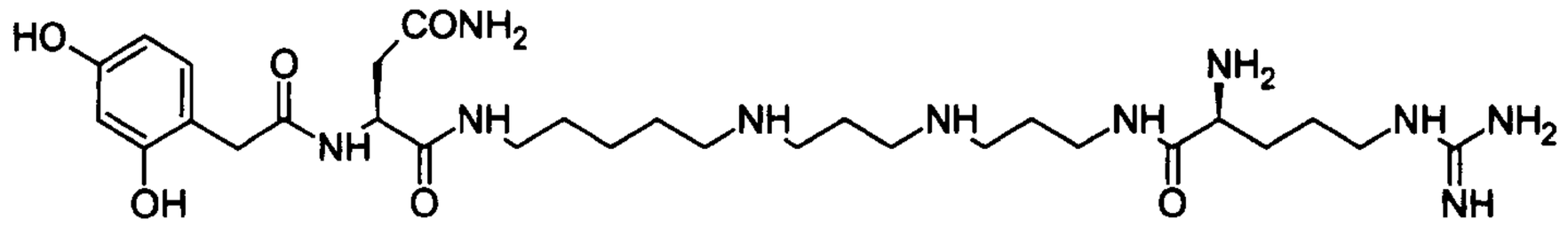	Arg636
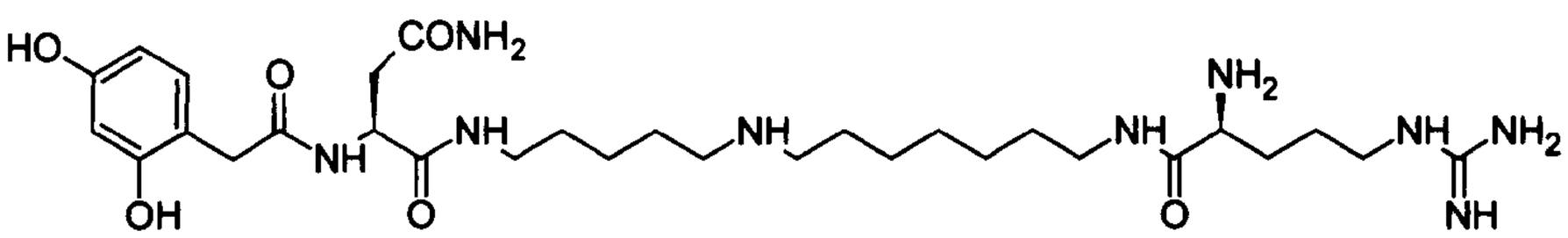	AMPA Selective
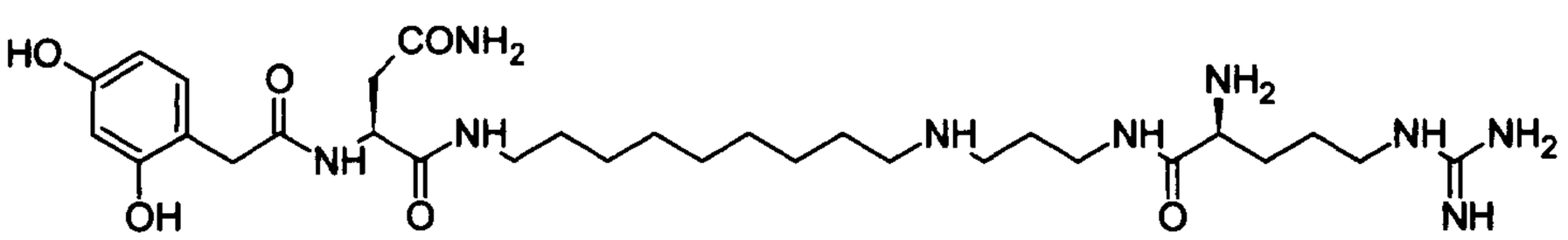	NMDA Selective

Figure 16: Argiotoxin and related compounds. These compounds were isolated from the orb-web spider *argiope lobata* and depending on the number of amines were shown to be selective for AMPA over NMDA receptors or *vice versa* (Mellor and Usherwood, 2004).

1.9.4 Methoctramine

Methoctramine (Figure 17) is a symmetrical polyamine type molecule with a 2-methoxy benzyl head group at each end. It has a 686 methylene spacing between amine groups and a fully protonated charge of +4. It can selectively block muscarinic acetylcholine M_2 and M_4 receptors and has a low affinity at M_3 receptors, leaving M_1 receptors with an intermediate affinity (Melchiorre et al., 2003). It has an IC_{50} around 4.2 μM at nAChR's and increasing the number of methylenes between the inner amines increased potency (Bixel et al., 2000). Modifications to the compound that removed an amine, or replaced an amine with amide or ether, reduced potency at muscarinic, as well as nicotinic acetylcholine receptors. It is thought that the head group at each end of the chain binds

to different subunits of the nAChR with folding occurring resulting in a V-shaped chain whose point can bind deep in the pore (Rosini et al., 2002). Methoctramine can also inhibit the transient receptor potential cation channel, subfamily V, member 1 (TRPV1) in a non-competitive voltage dependent manner indicating open channel block (Mellor et al., 2004, Rosini et al., 1999).

Structure	Name
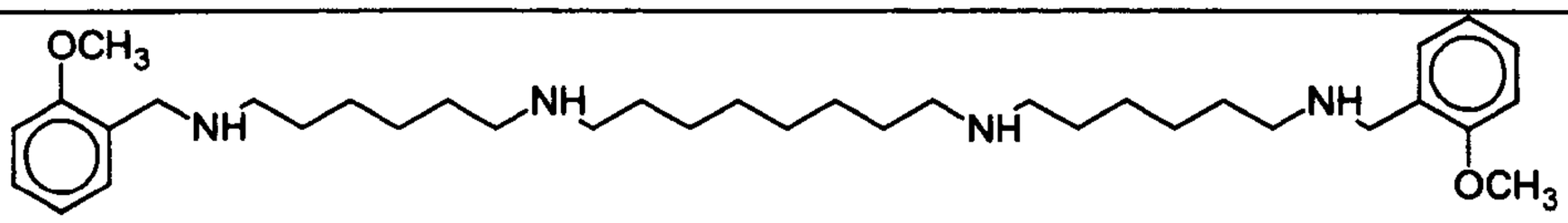	Methoctramine

Figure 17: The structure of methoctramine. Shown is the structure of methoctramine whose activity at recombinant NMDA receptors is currently unknown.

1.10 Glycine-gated NMDA Receptors

GluN1 has been shown to form functional receptors in combination with GluN3A or GluN3B producing channels that did not respond to glutamate or NMDA, but were instead glycine gated (Chatterton et al., 2002). They desensitise over 10s, with GluN1/GluN3B receptors showing a rebound of increased current after glycine application was stopped (Madry et al., 2007). In Xenopus oocytes these channels are relatively insensitive to Mg^{2+}, MK-801, memantine and APV compared with GluN1/2 receptors. Also, D-serine did not activate GluN1/3A receptors and only a small response was found for GluN1/3B (Chatterton et al., 2002). Mutations in the glycine binding domain of GluN1 potentiated currents in response to glycine, but those in the GluN3 glycine binding site reduced responses (Madry et al., 2007). The same study showed that the GluN1 glycine site antagonist MDL-29951 potentiated glycine responses from GluN1/3A and GluN1/3B receptors. Furthermore, null mutations of the GluN1 glycine binding site led to receptors that were opened by glycine binding to GluN3 alone

(Awobuluyi et al., 2007). Taken together, it may be that glycine binds to GluN3 subunits causing channel to open, and that binding to GluN1 results in desensitisation.

Zn^{2+} has been shown to potentiate glycine-gated currents in GluN1/3A receptors expressed in Xenopus oocytes (Madry et al., 2008). It occurred up to a maximum of 10-fold with 50 μM Zn^{2+} and 100 μM glycine. At concentrations greater than 100 μM, Zn^{2+} was found to activate these receptors alone. In GluN2 subunits the N-terminal domain binds Zn^{2+} as an allosteric modulator, but GluN1/3A glycine activated receptors with no N-terminal domain did not have altered potentiation by Zn^{2+} (Madry et al., 2008). The same study showed that a GluN3A mutation which abolished the glycine binding site led to no glycine induced current or potentiation of glycine induced current by Zn^{2+}. A similar point mutation in GluN1 abolished Zn^{2+} potentiation.

It has been shown that GluN1/3A and GluN1/3B receptors have a reversal potential around -10 mV (Madry et al., 2010). The study also showed that, whilst GluN1/3B receptors had a linear I/V relationship, GluN1/3A showed block of inward current at potentials lower than -30 mV which was reversed by MDL-29951 and Zn^{2+}. At -90 mV the effect of MDL-29951 on 3A (8-fold) was significantly more than GluN1/3B (2-fold), but no difference was found at +30 mV. The I/V curve also became linear with the null mutation of the GluN1 glycine binding site indicating a link to desensitisation caused by this subunit. Furthermore, it was shown that removal of 1.8 mM Ca^{2+} from the extracellular solution restored the linearity of the GluN1/3A I/V curve and that 20 mM Ca^{2+} blocked the GluN1/3A and GluN1/3B mediated current that was potentiated by Zn^{2+}. Taken together, the authors claim that under physiological conditions GluN1/3A receptors are held under a Ca^{2+} block in a similar manner to Mg^{2+} block of GluN1/2 receptors.

Using fluorescence tagged NMDA receptor subunits it has been shown that injection of GluN1, GluN2 and GluN3 into Xenopus oocytes may lead to separate populations of GluN1/2 and GluN1/3 glycine activated NMDA receptors (Ulbrich and Isacoff, 2008). The same study also found that when GluN1, GluN3A and GluN3B were injected GluN1/3A/3B receptors were preferentially formed over separate populations of GluN1/GluN3A and GluN1/GluN3B. However, it was not tested if functional channels were produced and may represent the detection of dimer pairs. Co-immunoprecipitation of GluN1/3A and GluN2B/3A was found in COS-7 cells, showing that these pairings can assemble together (Sasaki et al., 2002). In HEK-293 cells both GluN1-1a and GluN2A subunits were co-immunoprecipitated with hemagglutinin-tagged (HA) GluN3B (Matsuda et al., 2002). Hippocampal neurones transfected with GluN3B using the sindbis virus vector produced cell lysates after 24 hours that, when co-immunoprecipitated with anti-GluN1 and anti-GluN2A, were associated with GluN3B (Matsuda et al., 2003). Brain membrane fractions also showed that Glu1-1a and GluN2A were co-immunoprecipitated with GluN3A (Das et al., 1998). It has also been shown that rat GluN3A can associate with GluN1 and GluN2A separately in the endoplasmic reticulum of HEK-293 cells; but only when the receptor became a heteromer containing GluN1 was it trafficked to the membrane (Perez-Otano et al., 2001). The same study showed that GluN1/3 dimers could leave the ER, but required GluN2A to produce functional channels.

Glycine activated receptors similar to those found in Xenopus oocytes are not found in HEK-293 cells (Nishi et al., 2001, Perez-Otano et al., 2001). Instead, to produce similar channels it requires the expression of both GluN3 subunits together with GluN1 (Smothers and Woodward, 2007). These GluN1/3A/3B receptors do not show a voltage dependent Mg^{2+} block, are not inhibited by APV, ifenprodil, memantine, MK-801 but are activated by D-serine (Chatterton et al., 2002, Smothers and Woodward, 2007).

Expression is dependent on the GluN1 splice variant, as when it was changed more robust responses could be produced (Smothers and Woodward, 2009). Glycine activated currents were small with GluN1-1a; but those with GluN1-2a, GluN1-3a and GluN1-4a produced large currents indicating a role for the C-terminal in mediating surface expression of these channels. Differing expression dependent on splice variant dependent change was not found in Xenopus oocytes (Cavara et al., 2009).

Despite the above *in vitro* findings, there is little evidence to support the existence of these channels *in vivo*. Glycine-gated currents were not found in hippocampal slices from wild-type or transgenic mice overexpressing GluN3A (Tong et al., 2007). Single channel study of the same material found two distinct conductance states, 61 pS and 40 pS. These states had no direct transitions which may indicate two different types of receptor. As glycine alone did not elicit any state these may be populations of GluN1-1a/2A and GluN1-1a/2A/3A. Glycine-gated currents were also not found in hippocampal cells that were transfected with GluN3B (Matsuda et al., 2003). Single channel studies in parieto-occipital cortical neurones of eight day old mice had 56 and 26 pS conductances to NMDA/glycine, with no direct transitions, possibly indicating two receptor populations were present (Sasaki et al., 2002). Mg^{2+} did not block the lower conductance, possibly indicating a glycine activated component, but glycine alone as agonist was not tested. Cultured cerebrocortical neurones were tested in the presence of strychnine (to block glycine receptors) and excitatory glycine responses that were blocked by D-serine have been found (Chatterton et al., 2002). However, these currents have also been shown to be present in neurones cultured from GluN1 k/o mice, which is generally required for surface expression of NMDA receptors (Matsuda et al., 2003).

The evidence for GluN1/2/3 receptors *in vivo* is slightly more convincing. The transfection of GluN3B into hippocampal neurones resulted in the subunit being incorporated into receptors that were already present (Matsuda et al., 2003). Neurones from GluN3A overexpressing transgenic mice were less sensitive to Mg^{2+} and were less permeable to Ca^{2+}, while no glycine activated component was found (Tong et al., 2007).

1.11 NMDA Receptor Distribution

The GluN1 subunit is required for expression of functional NMDA receptors (Okabe et al., 1999, Perez-Otano et al., 2001). In the rat, GluN2B and GluN2D are the most abundant in the neonate nervous system but as development progresses this shifts to GluN2A and GluN2C subunits being in the majority (Figure 18) (see Henson et al., 2008). In the rat, GluN3A expression follows a similar pattern to GluN2B and GluN2D, peaking at P8 and decreasing from P12 onward (Al-Hallaq et al., 2002, Wong et al., 2002). In adult rats GluN3B expression starts low and increases throughout development becoming ubiquitous throughout the nervous system, particularly motoneurones of the spinal cord and brainstem (Chatterton et al., 2002, Wee et al., 2008). However in humans, although expression peaks during maturation, GluN3A expression is found in all regions of the cerebral cortex, the subcortical forebrain, midbrain and hindbrain, with low levels in the spinal cord (Nilsson et al., 2007, Henson et al., 2010). Similarly *In situ* hybridisation of human adult brain slices revealed GluN3B expression in the neuronal layers of the hippocampus, dentate gyrus and layer 5 of the cortex (Bendel et al., 2005).

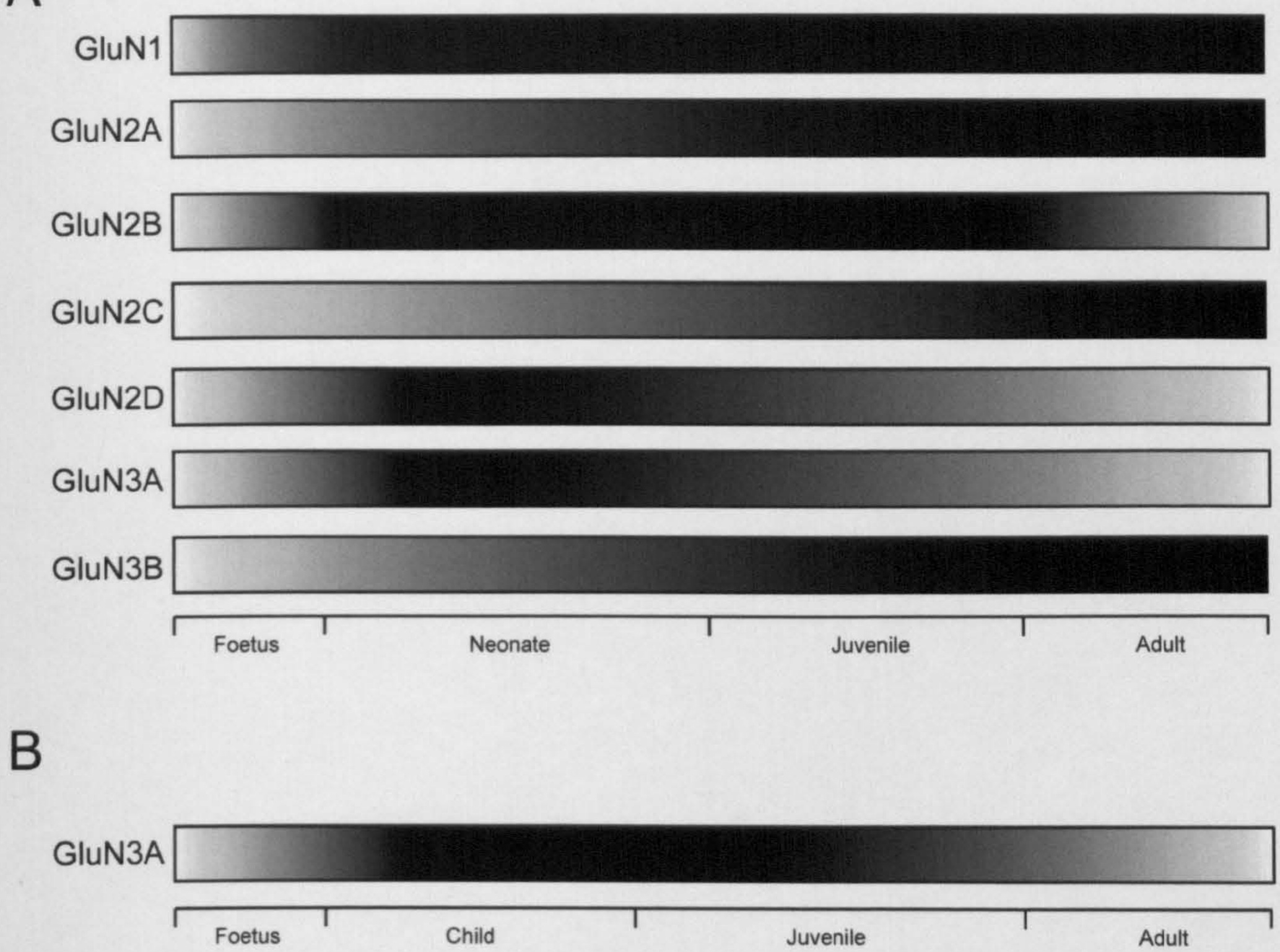

Figure 18: Expression levels of NMDA receptor subunits (A) rat (B) human. Black indicates high levels of expression. Adapted from Henson et al., (2010).

Although GluN3 containing receptors can be localised to the postsynaptic density, there seems to be more present at perisynaptic and extrasynaptic locations (Perez-Otano et al., 2006). These regions are active endocytotic sites and GluN3A can be internalised by a PACSIN1/sydapin1 complex which is involved in clathrin-coated vesicle detachment (Kessels and Qualmann, 2002). GFP tagged GluN3A was visualised moving from the postsynaptic region in a manner that increased with agonist application and was decreased by blocking voltage-gated sodium channels (Perez-Otano et al., 2006). Such movement may represent transportation to a site where receptors are removed from the synapse ready for endocytosis, leading to the hypothesis that GluN3 subunits tag synapses ready for removal (see Henson et al., 2010). Excessive activity may lead to the receptors being replaced by mature synapses and those with limited activity could be removed by the PACSIN1/sydapin1 process. Supporting this is evidence that spine

elimination is related to *takusan* (Japanese adjective 'many') proteins and the activity of these were up-regulated in GluN3A$^{-/-}$ mice (Tu et al., 2007). It has been shown that when GluN3A expression was forced to continue beyond its normal decay phase in the developing nervous system there was a reduction in plasticity, memory and the formation of mature synapses (Roberts et al., 2009). The impairment of development was reversible when the transgene system was removed, indicating that the removal of GluN3A was the trigger for producing mature synapses. Another hypothesis is that the presence of GluN3 during development increases threshold for synaptic activity to reduce excitotoxicity through reduced Ca^{2+} permeability (see Henson et al., 2010). Once the mature synapses have been produced, there then may again be endocytosis allowing them to be replaced by mature receptors by the PACSIN1/sydapin1 process.

1.12 Alzheimer's Disease and the NMDA Receptor

1.12.1 Symptoms and Potential Causes

It is estimated that worldwide 24.3 million people suffer from Alzheimer's disease (AD) and that around 4.6 million cases will be added every year (Ferri et al., 2005). It was first described by Alois Alzheimer whose patient Auguste Deter showed symptoms that included progressive cognitive impairment, confusion, mood swings, hallucinations, delusions and impaired memory. Post-mortem examination identified amyloid plaques, neurofibril tangles and arteriosclerotic changes that were later confirmed as being the cause of the disease that takes its discoverers' name. As Deter was 51 at the time of her disease her symptoms are now classified as pre-senile early onset AD (Goedert and Ghetti, 2007).

The plaques discovered by Alzheimer were found to be caused by aggregation of β-amyloid protein (Aβ) leading to the loss of mainly cholinergic neurones in the forebrain, cortex and hippocampus (Bowen et al., 1976, Glenner and Wong, 1984). Amyloid precursor protein (APP) is located in the plasma membrane and is processed by two different pathways, an amyloidogenic and a non-amyloidogenic pathway, by a family of secretase enzymes containing α, β and γ subtypes (Figure 19) (LaFerla et al., 2007). In functional neurones non-toxic $A\beta_{1-40}$ is degraded by insulin degrading enzyme (IDE) and neprilysin (NEP), and an impairment in the balance between production and clearance may lead to an abnormal build-up (Vepsalainen et al., 2008). Alzheimer also described 'dense bundles of fibrils' which were found to be tau, a microtubule associated protein (MAP) that shows an abnormal increase in phosphorylation (Grundke-Iqbal et al., 1986). Under normal conditions it promotes the stable assembly of microtubules and regulates axonal transport (Konzack et al., 2007). Phosphorylation is increased 3-4 fold in AD which leads to reduced affinity of tau to microtubules impairing cellular transport (Bramblett et al., 1993).

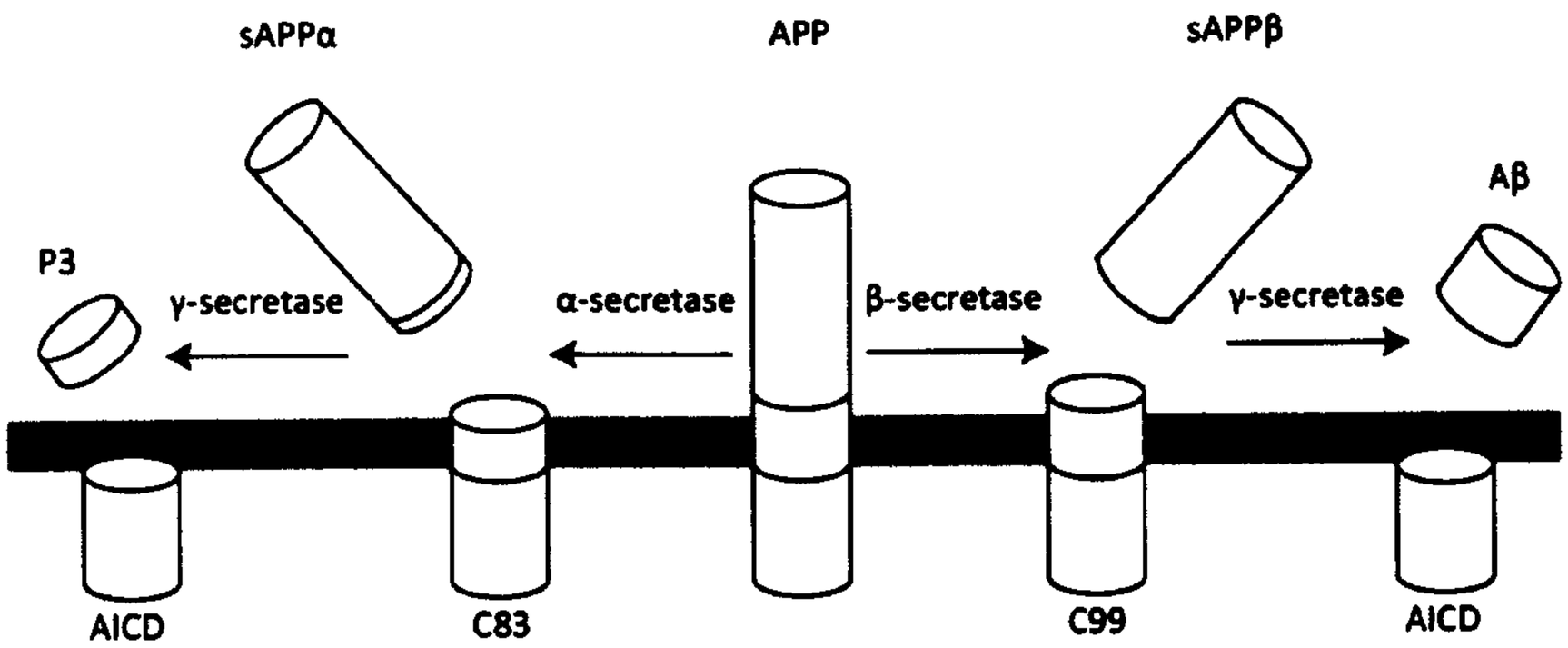

Figure 19: Amyloidogenic (right) and non-amyloidogenic (left) pathways for APP processing. The amyloidogenic pathway takes APP which is cleaved by an α secretase to produce the membrane fragment C83 while releasing sAPPα. The remaining membrane fragment is then cleaved by γ secretase releasing the fragment P3 and AICD. The non-amyloidogenic pathway on the right cleaves APP by β-secretase which leaves the membrane fragment C99 and releases sAPPβ. The membrane fragment is then cleaved by γ-secretase to leave the membrane bound fragment AICD and releasing Aβ. Adapted from LaFerla et al., (2007).

Familial AD is usually early onset and can be caused by mutations in the amyloid precursor protein gene on chromosome 21. Mutations or repetitions (such as Down's syndrome) can lead to an increase in the levels of $A\beta_{1-42}$ leading to a change in the $A\beta_{1-40}$: $A\beta_{1-42}$ ratio, with the latter thought to be more toxic, as well as increasing Aβ generation and aggregation (see Tanzi and Bertram, 2005). A recent large scale genome wide study of AD brain tissue found a link to Apolipoprotein E (APOE), which is involved in lipid metabolism, and also found a link to another apolipoprotein, clusterin (Harold et al., 2009). These proteins are also found at the blood brain barrier and may be the clearance mechanism for Aβ out of the CNS (Zlokovic et al., 1994). Harold et al. (2009) also found a link to phosphatidylinositol-binding clathrin assembly protein (PICALM). It is expressed in all cells mediating clathrin endocytosis, and is required for intracellular trafficking. In AD PICALM may lead to endocytosis of APP, increasing Aβ release possibly through a link to soluble *N*-ethylmaleimide-sensitive factor attachment protein receptor (SNARE) proteins (Yao et al., 2005, Harel et al., 2008). There is also a massive loss of cholinergic neurones and synapses in AD (Coyle et al., 1983). In the cortex it has been shown to lead to the loss of α4β2, but not α7 homomeric acetylcholine receptors (AChR) (Court et al., 2001).

There is evidence to suggest that oxidative damage plays a role in AD. It has been shown to occur at the greatest levels before the appearance of plaques; reducing as the disease progresses in human AD tissue and APP transgenic mice (Nunomura et al., 2001, Pratico et al., 2001). Furthermore, the binding of Cu^{2+} and Fe^{3+} to Aβ reduced these metals producing the reactive oxygen species H_2O_2 by double electron transfer (Opazo et al., 2002). H_2O_2 has also been shown to increase the levels of $A\beta_{1-42}$ in foetal guinea pig neurones (Ohyagi et al., 2000). Free radicals can also open mitochondrial permeability

transition pores (mtPTP) which normally transport Ca^{2+} and proteins up to 1.5 kDa leading to 'energy failure' (Sas et al., 2007).

Single nucleotide polymorphisms (SNP) in GluN3A have been linked to Alzheimer's disease in a Taiwanese cohort study (Liu et al., 2009). It was found that AD patients have a significantly higher occurrence of G compared with controls which had A at position 3723. The residue is located in exon 9 which is C-terminal to M4 region and may interact with intracellular signalling proteins. A SNP in the G72/D-amino acid oxidase activator (DAOA) gene was also linked to AD (Di Maria et al., 2009). G72 activates DAOA increasing D-serine levels, and mutations would indirectly influence NMDA receptors at their glycine binding sites. SNP's in the promoter region for *GRIN2B* in a north Han Chinese cohort were also linked to AD (Jiang and Jia, 2009).

1.12.2 The NMDA Receptor

NMDA receptors have been shown to be implicated in AD. $A\beta_{1-40}$ has been shown to induce inward current, cause increased intracellular Ca^{2+} levels and cause cell death by activating NMDA and AMPA receptors (Alberdi et al., 2010). Aβ has been shown to reduce cell surface expression of NMDA receptors by promoting endocytosis of synaptic receptors in cortical neurones (Snyder et al., 2005). Injection of $A\beta_{1-40}$ and $A\beta_{25-35}$ into cultured pyramidal neurones has been shown to downregulate expression of the GluN1 subunit (Johansson et al., 2006). A separate study has shown that pre-treatment with $A\beta_{1-42}$ also significantly reduced GluN1 surface expression (Goto et al., 2006). These effects additionally suggest the involvement of the α7 nicotinic acetylcholine receptor (ACh) as the selective blockers α-bungarotoxin and methyllycaconitine were shown to block the reduction in cell surface expression (Snyder et al., 2005). Finally, Aβ has been shown to

directly enter neurones through NMDA receptors, as APV has been shown to block internalisation (Bi et al., 2002).

200 nM $A\beta_{1-40}$ was shown to inhibit NMDA responses in hippocampal neurones within minutes of activation (Raymond et al., 2003). The same study showed that $A\beta_{1-40}$ blocked LTP, but concentrations of MK-801 that inhibited NMDA currents by the same magnitude did not. It may be due to Aβ having further actions downstream rather than directly inhibiting the channel itself. $A\beta_{1-42}$ has been shown to inhibit phosphorylation of cAMP response element binding (CREB) signalling through NMDA receptor activation, which is linked to the regulation of genes involved in neuronal survival, synapse formation and memory (Snyder et al., 2005). The fragment $A\beta_{25-35}$ has been shown to displace radiolabelled glutamate and glycine in rat cortical membranes (Cowburn et al., 1997). However, binding could have occurred at any glutamate receptor as selective agonists were not used.

NMDA receptors mediate the activity of APP cleaving enzymes. Application of NMDA caused a shift from α-secretase to β-secretase activity, producing 'neuronal Kunitz protease inhibitory domain-APP' via a Ca^{2+} dependent process (Lesne et al., 2005). Double k/o mice for the presenelins PS1 and PS2 also caused a significant increase in GluN2A expression (Aoki et al., 2009). NMDA receptor activation may promote the non-amyloidogenic pathway as it led to increases in C83 formation by α-secretase, with an attenuation of $A\beta_{1-40}$ production in cortical neurones (Hoey et al., 2009). Activation of NMDA receptors increased membrane trafficking of the α-secretase 'a disintegrin and metalloproteinase domain', (ADAM) 10 (Marcello et al., 2007).

1.12.3 Excitotoxicity

Even though glutamate it is the main excitatory transmitter in the nervous system, excess levels can be toxic to neurones (Lucas and Newhouse, 1957, Olney and Ho, 1970). There is 10 mM glutamate in the brain, with 0.00006 mM estimated to be extracellular (Lipton and Rosenberg, 1994). If the concentration increases to between 2-5 μM, damage can occur. Excitotoxicity can be a result of cerebral ischemia induced by stroke or cell death in disease states (see Hazell, 2007). There is a reduction in glutamate uptake into astrocytes due to the lack of blood flow because of 'energy failure.' The excess extracellular glutamate leads to increased levels of intracellular Ca^{2+} through NMDA receptors resulting in apoptosis (Chen and Lipton, 2006). Extracellular glutamate is removed quickly by high affinity amino acid transporters which can be found presynaptically, postsynaptically and in astrocytes (Danbolt, 2001). In glial cells glutamine synthase converts glutamate to glutamine, which is not toxic, and is taken up by neurones and converted back into glutamate - termed the glutamate-glutamine shuffle (Danbolt, 2001). The levels of excitatory amino acid transporters in the hippocampus and gyrus frontalis medialis in brain tissue from AD patients is reduced, and these correlated to areas that contained amyloid plaques (Jacob et al., 2007).

1.12.4 Treatment

Memantine (Ebixa) is the only clinically tolerated NMDA antagonist approved for use in dementia. It fits the requirement of an antagonist that only blocks overactivity, leaving normal signalling intact. Memantine is a non-competitive low affinity open channel blocker with a fast off-rate, therefore it does not accumulate in the channel in the same manner as MK-801. The phase III clinical trial found that 20 mg memantine per day slowed the onset of AD, leading to its approval (Reisberg et al., 2003).

The established cholinergic role in AD led to the use of tacrine, an anticholinesterase inhibitor (AChEI), becoming the first drug approved for the treatment of AD (Figure 20) (see Rang et al., 2007). Acetylcholine esterase (AChE) is the neuronal enzyme that hydrolyses ACh, and is a member of the α/β-hydrolase fold superfamily of proteins (Bourne et al., 1999). The main active site of AChE is centrosymmetric to the subunit and is located at the bottom of a narrow gorge at the rim of which is another allosteric site, the peripheral anionic site. Tacrine led to improvements in memory and cognition for around 40% of patients; but also had cholinergic side effects such as nausea, abdominal cramps and hepatotoxicity. It had to be taken four times daily and patients had to be continually monitored for liver damage. Therefore other cholinesterase inhibitors were developed and these included donepezil, rivastigmine and galantamine (Figure 20). Donepezil is 1000-fold more selective for AChE than the peripheral choline esterase butyrylcholinesterase (BuChE) giving it a better side-effect profile (see Francis et al., 1999).

AChEI are however not particularly effective in combating the symptoms of AD. It is estimated their use saves two months per year of disease progression; however, such outcomes may not be beneficial in a disease where quality of life is more important than actual life expectancy (Trinh et al., 2003). Such thinking led to a combination therapy approach using AChEI together with memantine treatment in order to exploit the beneficial effects of both compounds (Farlow, 2004). Studies have shown that rivastigmine, when combined with memantine, improved cognitive decline in patients that did not seem to improve on AChE alone (Dantoine et al., 2006, Riepe et al., 2006). It was also shown that donepezil and memantine treatment improved cognition (Tariot et al., 2004).

Structure	Name
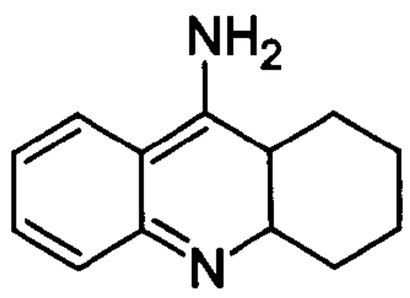	Tacrine
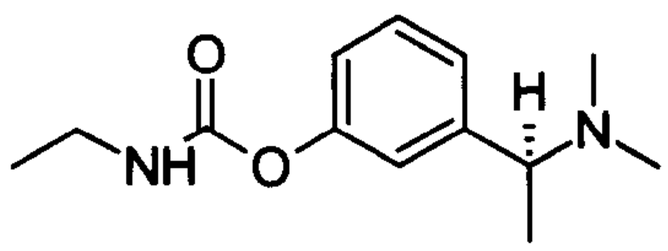	Rivastigmine
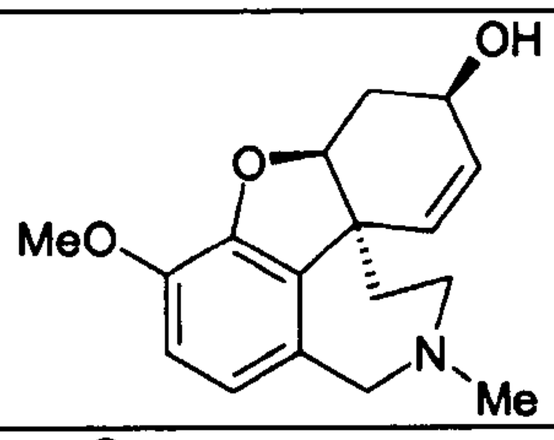	Galantamine
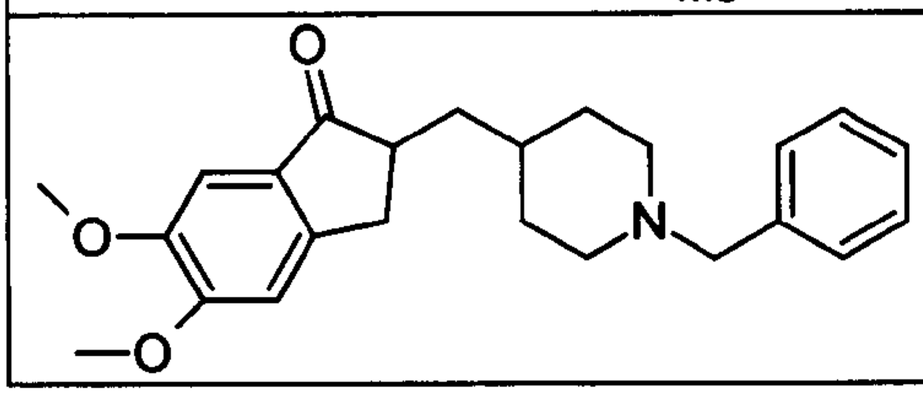	Donepezil

Figure 20: Structure of acetylcholine esterase inhibitors used clinically to treat AD. Tacrine, rivastigmine, galantamine and donepezil have all been shown to act as acetylcholine esterase inhibitors and have been used in the treatment of AD (Rang et al., 2007).

1.12.5 Multi-Target Directed Ligands

Combination therapy, although useful in a multifactorial disease such as AD, does have downsides. There can be an increase in side effects due to the multiple drugs involved, as well as unintended drug/drug interactions. Another approach would be to produce a single molecule with multiple biological properties that would reduce the difficulties such as differing pharmacokinetics/ pharmacodynamics and complex toxicological profiles. Producing a single molecule from differing drugs would limit optimisation to one compound, as toxicology is an exceedingly problematic area when moving to efficacy in man trials. There would be no drug/drug interactions and by its nature it would have a more simple treatment regime increasing compliance in patients with AD. Such an approach to drug design is termed multi-target directed ligands (MTDL).

The MTDL approach led to the production of a potential AD drug candidate memoquin (Figure 21) (Bolognesi et al., 2009a). The originator molecule caproctamine is an AChEI, and its large structure allows it to interact with both sites of the AChE enzyme. Into this backbone, the 1,4-benzoquinone radical scavenger moiety of CoQ (an antioxidant), was placed. The synthetic derivative of CoQ, idebenone, was shown in a fully randomised double-blind placebo controlled trial with 450 subjects to improve symptoms of AD over the two year study period (Gutzmann and Hadler, 1998). However, in a later similarly rigorous trial idebenone had no effect over the year of the study (Thal et al., 2003). *In vitro,* memoquin has been shown to retain its antioxidant and AChEI properties, inhibit aggregation of Aβ and inhibit the β-secretase, BACE-1 (Bolognesi et al., 2009a). Using the AD11 mouse model, memoquin was shown to prevent the loss of cholinergic neurones, inhibit Aβ accumulation, reduce tau hyperphosphorylation and restore memory in object recognition tests, hence shows promise (Bolognesi et al., 2009a).

Another MTDL, ladostigil, combined rivastigmine and rasagiline (Azilect, an MAO-B inhibitor) and is currently in phase II clinical trials (Figure 21) (Bolognesi et al., 2009b). It was shown to retain its AChE activity and retains MAO-B inhibition, but serendipitously added MAO-A activity. Inhibiting MAO reduces H_2O_2 production as well increasing monoamine levels, possibly giving the compound an antidepressant effect. It was also found to interfere with APP processing by stabilising the mitochondrial membrane potential, as well as inhibiting oxidative stress induced apoptosis (Bar-Am et al., 2009).

Structure	Name
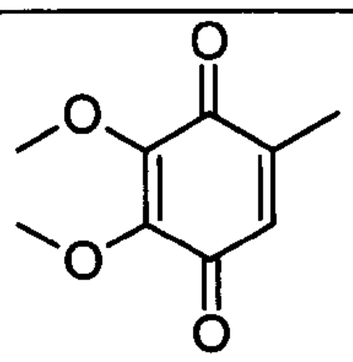	CoQ scavenger moiety
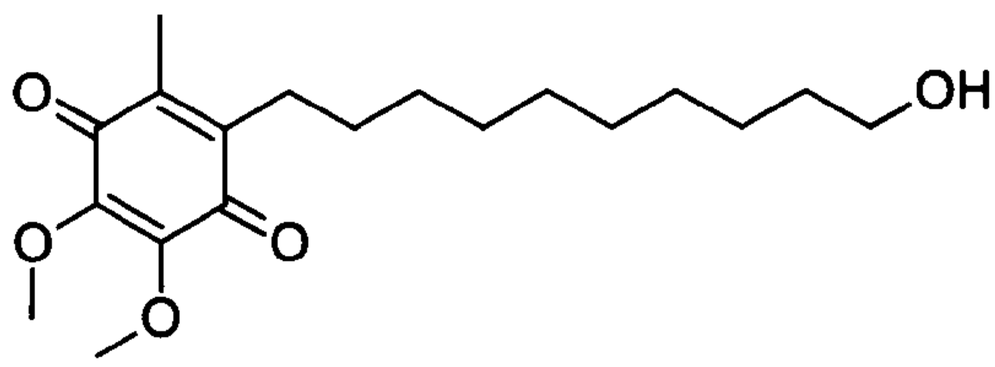	Idebenone
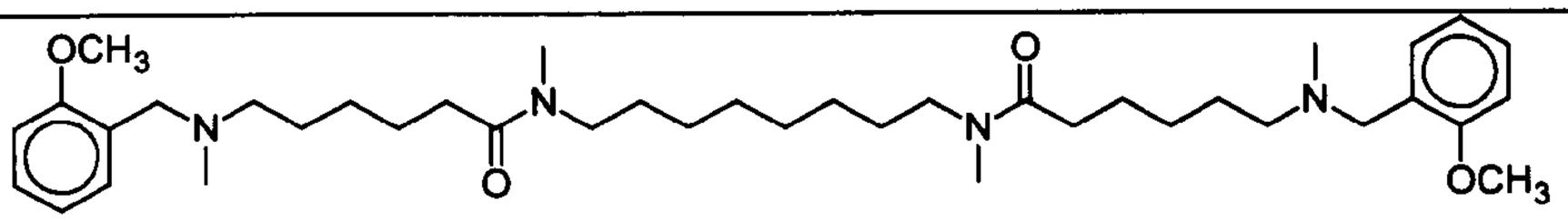	Caproctamine
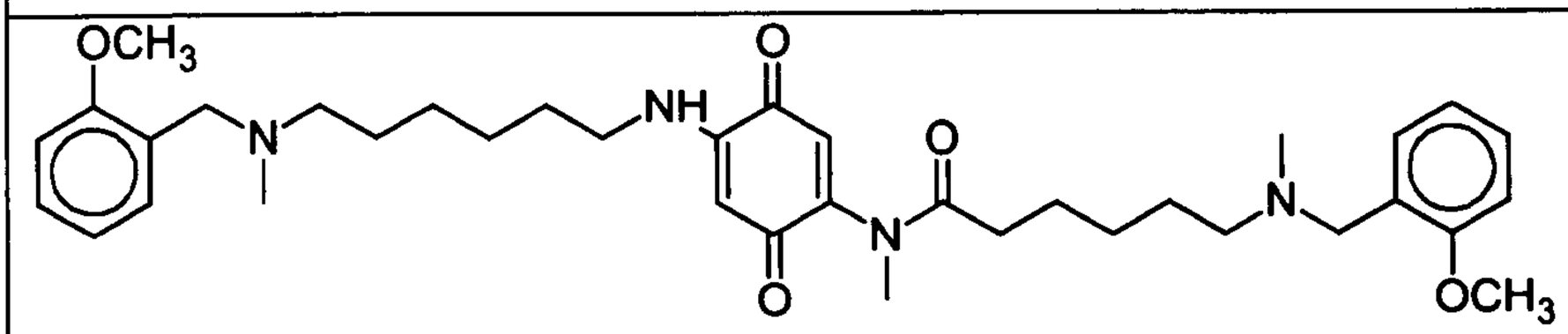	Memoqin
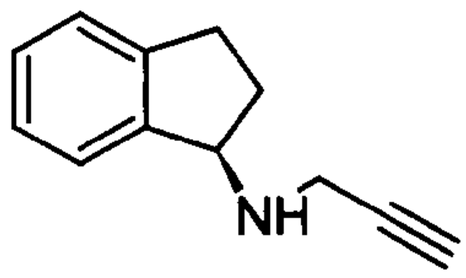	Rasagiline
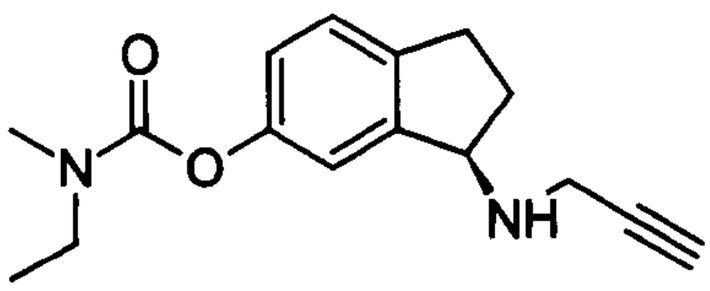	Ladostigil
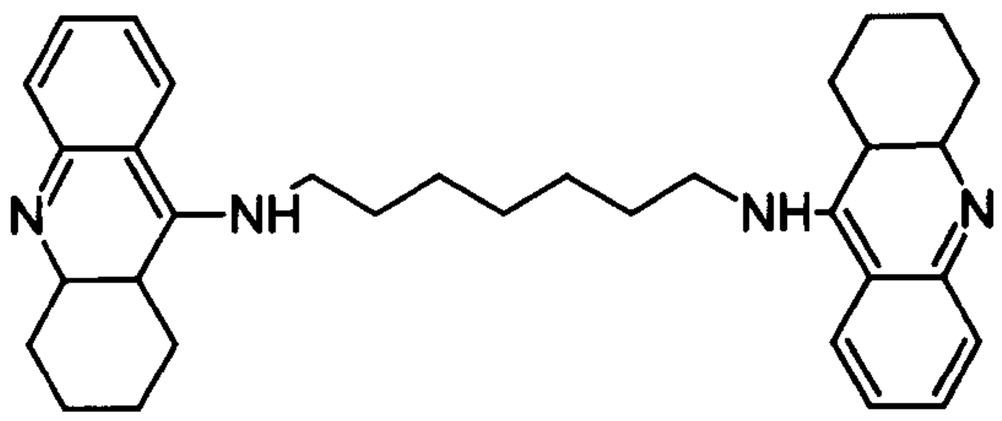	bis(7)-Tacrine

Figure 21: Structures of MTDL ligands and their originator molecules. CoQ and its synthetic derivative idebenone have been shown to act as anti-oxidants (Bolognesi et al., 2009a). Caproctamine is an AChEI that has been shown to interact with both sites of the AChE enzyme. Memoquin is the MTDL that is formed by the combination of caproctamine and CoQ. Another MTDL is ladostigil which combines rasagiline which is an MAO-B inhibitor and the AChEI rivastigmine (Bolognesi et al., 2009b). Bis(7)-Tacrine is a modification of tacrine that allows it to bind to both sites of the AChE enzyme (Liu et al., 2008).

When using a MTDL approach potential candidates have to be identified with properties that have been shown to attenuate the effects of AD. Carvedilol is a vasodilating β-blocker that acts as an antioxidant and is currently licensed for treatment of hypertension, angina and heart failure (Figure 22) (Lysko et al., 1998). In the streptozotocin-induced rat model of dementia it was shown to attenuate oxidative damage, reduce the associated increase in AChE activity and improve memory in the Morris water maze task when compared with those animals who did not receive treatment (Prakash and Kumar, 2009). It has also been shown to block $A\beta_{1\text{-}40}$ fibril formation in a fibril-dependent immunoassay (Howlett et al., 1999). Although thought to be the non-toxic form $A\beta_{1\text{-}40}$ fibrils have been shown to be toxic in PC12 cells (Okada et al., 2007). However, CNS active β–blockers (to which carvedilol belongs) do not impair cognition in normal subjects, but have been shown to impair memory retrieval in patients with AD and dementia which may limit their use as therapeutics (Gliebus and Lippa, 2007). Carvedilol may also be a neuroprotective open channel blocker of NMDA receptors as it could partially displace ^{3}[H]MK-801 binding with a K_D that was 4,800-fold less potent than MK-801 (Lysko et al., 1992). The same study showed that it could also reduce intracellular Ca^{2+} levels in cerebellar granule cells after exposure to NMDA and glycine. Carvedilol has also been shown to restore the activity of the Na^{+}/glutamate transporter and block glutamate induced excitotoxicity (Lysko et al., 1994, 1998).

Lipoic acid is another potential candidate molecule suitable for the MTDL approach (Figure 22). It is a sulphur containing compound that is synthesised in mitochondria and is a co-factor for multienzyme complexes (Biewenga et al., 1997). It can also act as an anti-inflammatory antioxidant by modulating REDOX sensitive signalling, regenerate levels of other antioxidants such as glutathione, act as a carboxyl scavenger and stimulate glucose uptake into cells increasing energy metabolism (Biewenga et al., 1997, Holmquist

et al., 2007). Intraperitoneal injection of $A\beta_{25-35}$ amyloid fibrils into mice has been shown to increase the level of reactive oxygen species, cause lipid peroxidation, decrease antioxidant levels and decrease ATPase activity in hepatocytes, splenocytes and astrocytes; effects that were inhibited by lipoic acid (Jesudason et al., 2008). Similarly $A\beta_{25-35}$-induced cell death in primary hippocampal cultures was reduced by pre-treatment with lipoic acid (Lovell et al., 2003). Twenty-four hour pre-treatment by lipoic acid inhibited glutamate induced toxicity in cultured neurones (Muller and Krieglstein, 1995). The reduced form of lipoic acid, dihydrolipoic acid, is required for the action of choline acetyl transferase and may act as a co-enzyme in the production of ACh, indicating further beneficial effects in AD (Haugaard and Levin, 2002). As lipoic acid can also act as an iron chelator and may possibly inhibit REDOX binding of metals in AD (Fonte et al., 2001). The only published clinical trial testing the effectiveness of lipoic acid found that it slowed progression of the disease (Hager et al., 2007). However, it was only a basic cohort study that was not double-blinded, placebo controlled or randomised and AD was not confirmed post mortem.

Lipoic acid has also been shown to improve memory in behavioural tasks in animal models of AD. Dietary supplementation in rats improved spatial memory performance in 24.5 month old animals, pushing performance toward levels seen in 4.5 month old rats in the Morris water maze (Liu et al., 2002). A separate study has shown that with the Tg2576 mouse model of AD, animals tested at 10 months had improved performance when lipoic acid was added to their diet over a six months period, but the levels of Aβ plaques in the brain post-mortem remained the same (Quinn et al., 2007). However, a separate study using the same model but with animals aged 6.25–11.5 months at onset, showed that 10 months chronic treatment had no effect on memory or levels of Aβ measured at endpoint (Siedlak et al., 2009).

Structure	Name
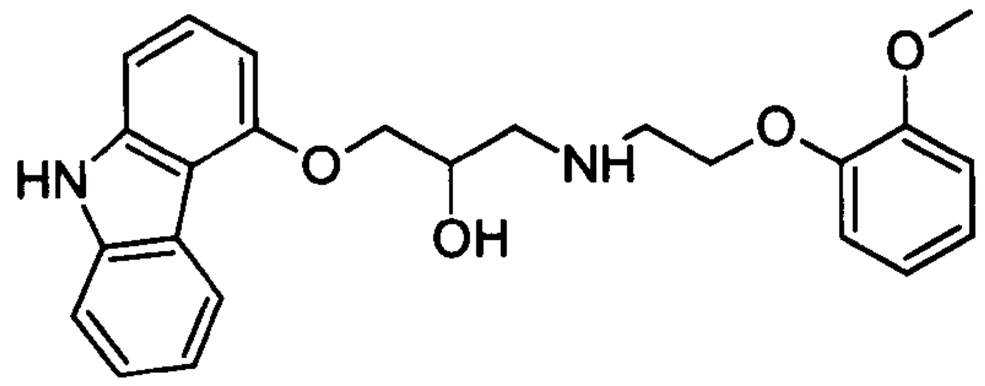	Carvedilol
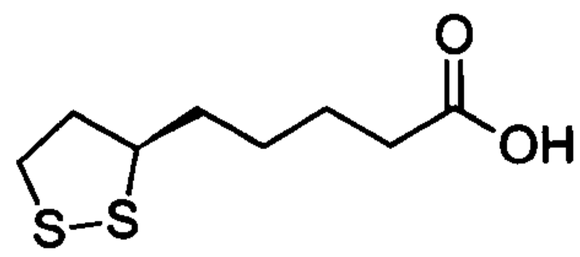	Lipoic Acid
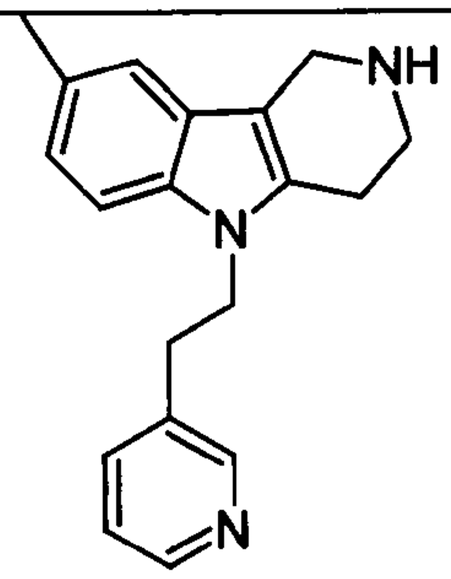	Dimebon

Figure 22: Candidate molecules for MTDL drug design approach. Shown is the β-blocker carvedilol, lipoic acid and Medivations' dimebon. These compounds were all used to produce MTDL candidate drugs in the current study.(Biewenga et al., 1997, Lysko et al., 1998).

The AChEI tacrine has displaced ^{3}[H]MK-801 indicating binding at the pore of the NMDA receptor (Wang et al., 1999). The bis(7)-tacrine (N,N'-bis-(1,2,3,4-tetrahydroacridin-9-yl)heptane-1,7-diamine) form of tacrine inhibited NMDA receptor currents with a similar potency to memantine in rat hippocampal slices (Liu et al., 2008). The same study found that it had a relatively slow onset of activity and could also reduce the efficacy of NMDA by up to 40%. Inhibition was not voltage-dependent or competitive, possibly indicating an allosteric binding site or impairment of a downstream mechanism. At the single channel level it reduced open probability and frequency of opening, but had no effect on the mean open time. Block was shown to be sensitive to changes in pH, with the IC_{50} in cultured rat hippocampal neurones shifting to the right when pH was increased from 6.8 to 9 (Luo et al., 2007). The evidence suggests that it

affects proton sensing, but at a different site to spermidine as it was shown not to alter this inhibition.

A further AChEI that may be useful for design of MTDL compounds is donepezil. As well its traditional function, it has been shown to displace ^{3}[H]MK-801 binding but was shown to be less potent at doing so than tacrine (Wang et al., 1999). The blocking effect of donepezil was shown to have differing effects with varied concentrations. Between 1 and 100 μM there was inhibition of NMDA currents in rat cortical neurones, but at higher concentrations currents were potentiated (Moriguchi et al., 2005).

Another compound that may be useful in a MTDL drug design approach is dimebon (Latrepirdine) which was originally used as an anti-histamine in Russia, but fell out of use as more selective compounds became available (Figure 22) (Matveeva, 1983). It has been shown to have an IC_{50} (although not fitted with the Hill equation) around 100 μM when inhibiting NMDA induced currents in primary striatal neurones (Wu et al., 2008). In addition, the same study showed that pre-treatment with 50 μM dimebon blocked glutamate induced excitotoxicity. The group also carried out a commercial assay that showed activity at α-adrenergic (α_{1A}, α_{1B}, α_{1D}, and α_{2A}), histamine (H_1 and H_2) and serotonin (5-HT_{2c}, 5-HT_{5A}, 5-HT_6) receptors, with greater than 90% inhibition at 10 μM. At around 70-80% inhibition, receptors blocked were dopamine (D_1, D_{2S}, D_3), imidazoline (I_2) as well as 5-HT_2 and 5-HT_{2B}. At 50 to 60% inhibition it blocked cytochrome CYP450 and 2C19 receptors, voltage-gated L-type Ca^{2+} channels, dopamine $D_{4.2}$ receptors and the 5-HT_1 receptor. Later radioligand binding studies also confirmed the compound to be a 5-HT_6 receptor antagonist (Schaffhauser et al., 2009). It has also been shown to inhibit the opening of mtPTP pores in the mitochondria providing a further possible role in AD by blocking energy failure (Bachurin et al., 2003).

The effect of dimebon has been found using two mice models of AD to be undesirable. Neuroblastoma cells from mice overexpressing the Swedish mutation of APP showed a concentration dependent increase in extracellular Aβ between 30 to 64% by dimebon (Steele et al., 2009). The same study showed that with TgCRND8 transgenic mice that had both the Swedish and Indiana mutation dimebon caused an increase in $A\beta_{1-42}$ in cortical synaptosomes. It also caused increased levels of $A\beta_{1-40}$ in the hippocampal interstitial fluid of freely moving animals. However, dimebon has been shown to improve survival of cerebellar granule cells incubated with $A\beta_{25-35}$ (Lermontova et al., 2001).

A randomised placebo controlled blinded trial for dimebon showed a significant improvement in the primary outcome measured by the Alzheimer's disease assessment scale-cognitive subscale (ADAS-cog) after 26 weeks (Doody et al., 2008). The study proved enough to get Pfizer interested in a partnership to carry out a global Phase III trial (ClinicalTrials.gov Identifier: NCT00675623). But a recent press release announced that the study failed to meet its primary and secondary outcomes. The global phase III study had the exact same protocol as the smaller study that showed promising results, and what could be leading to these differences is unclear. It may be that modifications based on its structure may lead to a more effective therapeutic.

In support of its potential clinical use, a placebo-controlled trial of dimebon in Huntington disease did meet its primary outcome of clinical tolerability (Kieburtz et al., 2010). Of the secondary outcomes, only the mini-mental state examination (MMSE) showed significant improvement, where the unified Huntington's disease rating scale (UHDRS) and ADAS-cog showed no significant differences. With such a wide range of targets, and its safe toxicological profile, it would be unwise to give up on dimebon too early.

1.13 Aims

The aim of the work presented in this thesis was to determine what effects the presence of GluN3A and GluN3B subunits in NMDA receptor assemblies had on block by the well categorised open channel blockers Mg^{2+}, memantine, and MK-801; as well as the lesser known compounds PhTX-343, PhTX-12 and methoctramine. The data was then used determine what changes in the pore region were brought about by the presence these subunits. Overall, the three main questions that were asked of the data were: was there an effect of subunit on the IC_{50} values for the blockers tested, and would this be restored by site-directed mutageneis. The second question that was asked was if block by the compounds was voltage-dependent, and if this was altered depending on the subunits that were expressed. The third main question that was asked of the data was how the potency of compounds compared to each other, and if this altered depending on the subunits tested.

Furthermore, due to the G at the N-site, and the positively charged R at the N+1 site on the GluN3 subunits, the polyamine toxin PhTX-343 was tested to determine if these amino acid changes impaired the ability to block similar to the R of the AMPA GluA2 subunit (Andersen et al., 2006). The ability for PhTX-12 to block GluN3 was also tested to see if it had any changes in potency. As PhTX-12 is not thought to interact with the N-site the loss of these residues and replacement with GR may mean that block will be impaired less than what would be expected from PhTX-343.

The N-site and N+1 site residues of the GluN3A subunit were also individually mutated back to N to determine if the IC_{50} could be restored to levels found in receptors without

the GluN3 subunit. Furthermore, a D mutation at the N+1 site was produced to determine what effect placing a negative charge at this position had on block.

The aim of second part to the study was to test the MTDL compounds provided by Dr. Michela Rosini from the University of Bologna. The activity of these determined at the GluN1-1a/2A containing NMDA receptors in order to establish their potential as therapeutics in the treatment of AD.

The carbacrine compounds took tacrine, an acetylcholinesterase inhibitor, and combined it with the vasodilating β blocker carvedilol to produce a group of compounds termed carbacrine (Lysko et al., 1998, Rang et al., 2007). The carbacrine group was also designed with increasing chain size between the pharmacophores. These compounds have a name as they have been previously described (Rosini et al., 2008). Compounds **1** and **2** were produced from donepezil, an acetylcholine esterase inhibitor, and carvedilol (Francis et al., 1999). Compounds **1** and **2** were numbered as they were unique entities described for the first time in this thesis. Compounds **3**, **4** and **5** were based on dimebon with differing linker regions between the two dimebon pharmacophores. Again these compounds were numbered as this is the first time they have been described. Lipocrine was produced from the combination of lipoic acid, an antioxidant, and tacrine, and has a name as it has been reported previously (Biewenga et al., 1997, Rosini et al., 2005). Compound **6** was derived from carvedilol and lipoic acid and takes a number as it is being first described in this thesis.

The IC_{50} for these compounds were compared with that of memantine and, if similar, would hopefully show that they had promise as drug entities. Although they did not have specifically designed NMDA blocking pharmacophores, donepezil, tacrine and carvedilol

have all been shown to have some affinity toward the receptor (Wang et al., 1999, Wu et al., 2008). Therefore, their potency was measured to determine if these pharmacophores were all that would be required to produce effects similar to memantine, while retaining their original functions.

2

Methods

2.1 Cloning

All the NMDA subunit clones used in the study were from the rat. JM109 *E. coli* were seeded in 5 ml of LB media (Sigma) and left overnight with vigorous shaking at 37.5 °C. The next day 5ml of cells was poured into 50ml of LB media and left for 2 hours under vigorous shaking at 37.5 °C in order for the cells to divide at an exponential rate. The cell suspension was spun at 10,000 G for 15 mins and the supernatant was removed. Cells were resuspended in 10ml of chilled 0.1 M CaCl, placed on ice for 10 min and spun for 15 min at 10,000 G. The supernatant was removed and cells were resuspended in 2 ml of 0.1 M CaCl and placed on ice, leaving Ca^{2+} competent cells. GluN3A and GluN3B (kindly gifted by Dr Zhang at the Burnham Institute California) were received on filter paper, extracted by adding 10 µl of DHCP water and left to soak for 5 mins. The paper was spun down to remove the liquid. Subsequently 2 µl was added to 200 µl of the competent cell suspension, then mixed and left on ice for 30 mins. The mixture was heat-shocked at 42 °C for 90 s in a water bath and placed on ice for 2 mins. To this 800µl of pre-warmed Super Optimal broth with Catabolite repression (SOC) (bacto-tryptone 20 g/L, bacto-yeast extract 5 g/L, 10 mM NaCl, 2.5 mM KCl, 20 mM $MgSO_4$) medium was added and the mixture was placed in the water bath for 45 min at 37.5 °C. 200µl of was then plated on 50 µg/ml ampicillin agar plates and left overnight in an incubator at 37 °C. The following day surviving colonies were picked and placed in 100 ml of LB media with 50 µg/ml ampicillin and left overnight at 37 °C with 200 rpm shaking.

Plasmid DNA was purified using the QIAprep Spin mini preparation kit (Qiagen) by the following protocol. Cells were resuspended in 250 µl of buffer P1 and inverted five times.

250 µl of buffer P2 was added and the microcentrifuge tube was inverted until a homogeneous blue coloured suspension was achieved. 350 µl of Buffer N3 was added and the tube was inverted until all traces of blue had disappeared. The mixture was centrifuged for 10 mins at 17,000 G. Once complete, the supernatant was transferred to the QIAprep spin column. The column was centrifuged for 60s and the flow through discarded. The column was washed with 0.5 ml Buffer PB, centrifuged for 30-60s and the flow through discarded again. The column was further washed by adding 0.75 ml buffer PE and was centrifuged for 60s. The flow through was discarded and the column was centrifuged for a further minute to remove residual wash buffer. The column was placed in a new microcentrifuge tube and the plasmid was eluted by adding 50 µl of ddH_2O to the centre of the column, left to stand for 1 min and then centrifuged for 1 min. The concentration of plasmid DNA was measured using a Nanodrop (Thermo Scientific).

2.2 Sequencing

The proposed rat GluN1-1a and GluN2A subunits did not have vector maps so sequencing had to be carried out to confirm their identity. They were known to be cloned into a 'prk7' plasmid and the sequence which was found at www.addgene.com. All DNA sequencing was carried out using a 3130 ABI PRISM Genetic Analyser at the Biopolymer Synthesis and Analysis Unit at the University of Nottingham. Sequencing was carried out for GluN1 using the primers SP6 and GluN1_1 (Table 4). Those that were not standard were designed using VectorNTI to adhere around 200 bp upstream from the sequence of interest with the correct annealing temperature (Tm 50°C - 80°C), to avoid hairpin loops and self hybridisation. GluN2A was cloned into the same plasmid so it was sequenced using SP6 and a separate primer designed upstream of the end of the insert and was named GluN2_1 (Table 4). GluN3A and GluN3B were sequenced using T7 primer and

GluN3A_1 and GluN3B_1 which annealed upstream of the end of the insert. Restriction maps were produced using MacVector (MacVector Inc.).

Primer Name	Sequence
SP6	5'-GATTTAGGTGACACTATAG-3'
T7	5'-TAATACGACTCACTATA-3'
GluN1_1	5'-TCCTGCAACCCTCACTTTTGAGAACA-3'
GluN2_1	5'-CATCATATTGCTCCAGGGACAGTCG-3'
EBV_Rev	5'-GTGGTTTGTCCAAACTCATC-3'
GluN3A_1	5'-CTCAGAGGAGAAGAGAGCTCCCTGC-3'
GluN3B_1	5'-AACCTGGGGAGGCTGGCGGAGACCG-3'

Table 4: Primers used for sequencing of the NMDA receptor subunits. SP6 and T7 are standard bacterial origin primers. GluN1_1 and GluN2_1 were designed to anneal 200 bp from the stop codon of their respective inserts. EBV_Rev was designed to anneal within the plasmid. GluN3A_1 and GluN3B_1 were both designed to anneal 200 bp from the stop codon of their respective inserts.

2.3 Restriction Digest

Restriction digests were carried out to linearise the plasmid for mRNA production.

Suitable restriction sites downstream of the gene of interest were identified by DNA sequencing and the relevant restriction enzymes were used. The total digest volume was 20 µl and was carried out using the following reagents: 1 µg DNA, 1 µl Restriction Enzyme (GluN1-1a, BamHI; GluN2A, EcoRI; GluN3A, NotI and GluN3B, XbaI), 5 µl suitable buffer, 5 µl Bovine Serum Albumin (BSA) x 10. The mixtures were incubated for 1 hour and 30 µl of ddH_2O was added then 2.5 µl of 0.5 M EDTA, 5 µl of 3 M Na acetate and 100 µl of ethanol. It was kept at -20 °C for an hour and spun at 17,000 G at

4°C for 25 min. The supernatant was removed and the microcentrifuge tube was spun at 17,000 G at 4°C for 5 mins. The supernatant was again removed and the DNA was left to air dry for 5 mins, resuspended in a suitable volume of ddH_2O and the concentration was measured using a Nanodrop (Thermo Scientific).

2.4 Agarose Gel Electrophoresis

Restriction digests were visualised using agarose gel electrophoresis to confirm the enzymes only cut once and that linearisation had occurred. 100 ml of stock 50x Tris-acetate-EDTA (TAE) buffer was produced (24.2 g Tris Base, 5.71 ml glacial acetic acid, 10 ml 0.5 M EDTA). The TAE stock solution was diluted to 1 x and to 50 ml 8 % agarose was added and heated in a microwave. 1 µl of 1% ethidium bromide was added and the mixture was poured into a mould. The gel was placed in a gel electrophoresis kit (Bio-Rad) and 1x TAE buffer was poured in until the gel was covered. 1kb plus ladder (Invitrogen) was added as well as 1 µl of the digested DNA and the gel was allowed to run at 100 V for 70 min. Bands were then visualised using Chemidoc XRS and quantity one image capture software (Bio-Rad).

2.5 mRNA synthesis

mRNA was produced using a mMESSAGE mMACHINE Kit (Ambion). The reaction assembly was the following: 10 µl NTP/CAP, 2 µl Reaction Buffer, 1 µg linear template DNA and 2 µl Enzyme Mix. This was incubated for 1 h and the RNA was recovered using lithium chloride precipitation. 30 µl of nuclease free water and 30 µl of LiCl were added and the mixture was kept at -20 °C for an hour. The RNA was spun at 17,000 G at 4°C for 15 min and the supernatant removed. The pellet was washed with 70% ethanol and spun for a further 15 min and the supernatant removed. The RNA was then

resuspended in a suitable volume of ddH_2O and the concentration determined using a Nanodrop (Thermo Scientific).

2.6 Mutations

Mutations were produced using the QuikChange mutagenesis kit (Stratagene) by mixing together 5 µl of 10 × reaction buffer, 50 ng of DNA template, 125 ng of sense primer 1, 125 ng of antisense primer 2 (Table 6), 1 µl of dNTP mix. ddH2O was added to a final volume of 50 µl, to which 1 µl of PfuTurbo DNA polymerase was then placed. The reaction was run in a thermal cycler using the settings outlined in Table 5.

Segment	Cycles	Temperature	Time
1	1	95°C	30 s
2	16	95°C	30 s
		55°C	1 min
		68°C	9 min

Table 5: Thermal cycler settings for the production of mutant DNA. The first segment contained only one denaturing step, while segment two was programmed to have one cycles as per the manufacturers instructions for one amino acid mutation. This segment contained a denaturing, annealing and extension step.

The PCR reaction was digested with DpnI restriction enzyme for 1 h at 37°C. The digested DNA was transformed into Xl1-blue *E. coli* cells by heat shock, and DNA was purified using the miniprep procedure from 2.1. Sequencing was carried out using the GluN3A_2 primer (Table 6).

Primer	Sequence
GluN3A_2	5'-TCAATACCGCACGAAGCCAG-3'
G703N_sense	5'-TCTGCTATGCCCTTCTGTTTAACAGAACAGCAGCCATCAAA-3'
G703N_antisense	3'-AGACGATACGGGAAGACAAATTGTCTTGTCGTCGGTAGTTT-5'
R704N_sense	5'-TCTGCTATGCCCTTCTGTTTGGCAATACAGCAGCCATCA-3'
R704N_antisense	3'-AGACGATACGGGAAGACAAACCGTTATGTCGTCGGTAGT-5'
R704D_sense	5'-CTATGCCCTTCTGTTTGGCGATACAGCAGCCATCAAACCCC-3'
R704D_antisense	3'-GATACGGGAAGACAAACCGCTATGTCGTCGGTAGTTTGGGG-5'

Table 6: Primers used for the production of GluN3A mutations. GluN3A_2 is the primer designed to anneal around 200 bp upstream from the mutation in the pore region. The remaining primers are the sense and antisense required to produce the mutations at position 703 and 704.

2.7 Oocyte Preparation

Adult female *Xenopus laevis* were anaesthetised with MS-222 (Sigma) and a scalpel was used to make an incision on the ventral midline to expose the oocytes. These were removed and treated with 0.2 mg/ml collagenase in Ca^{2+} free gentamicin theophylline pyruvate (GTP, 96 mM NaCl, 2 mM KCl, 1mM $MgCl_2$, 5 mM HEPES, 2.5 mM pyruvic acid, 0.5M theophylline, 5ml/l gentamicin (50 mg/L), adjusted to pH7.5 with NaOH) to remove connective tissue and follicular cells. Oocytes were rinsed and stored in GTP (96 mM NaCl, 2 mM KCl, 1.8 mM $CaCl_2$, 1 mM $MgCl_2$, 5 mM HEPES, 2.5 mM pyruvic acid, 500 mM theophylline, 5 ml/l gentamicin, adjusted to pH7.5 with NaOH) until required. Healthy oocytes were selected by eye and RNA encoding for the NMDA receptor subunits were injected using a nanolitre injector (World Precision Instruments). The RNA was injected at ratios of 1:1 for GluN1-1a/2A (in the results section this is referred to as 1-1a/2A) and 1:1:3 for GluN1-1a/2A/3A (referred to in the results section as '3A') and GluN1-1a/2A/3B (referred to in the results section as '3B'). 50 nL was injected at a minimum concentration for each subunit of 50 ng/μL. Oocytes were incubated for two days at 18°C before assaying.

2.8 Electrophysiology

Two electrode voltage clamp measurements were carried out using a voltage clamp amplifier (Gene Clamp 50, Axon) and recordings were sampled using an A/D converter (Digidata 1200) and recorded on an IBM compatible PC running WinEDR recording software (John Dempster, Strathclyde Electrophysiological Software) (Figure 23). Electrodes were produced using a P-97 Flaming Brown micropipette puller (Sutter Instruments Co) and had a resistance range of 0.5 to 3 MΩ when filled with 3M KCl. Oocytes were placed in a bath and perfused with Mg^{2+} free Xenopus Ringer solution (96 mM NaCl, 2 mM KCl, 1.8 mM $CaCl_2$, 10 mM HEPES adjusted to a pH of 7.5). Recordings were made at holding potentials of -100, -75 and -50 mV. Drugs were applied manually using a Valvelink 8 gravity perfusion system (Automatic Scientific Inc.).

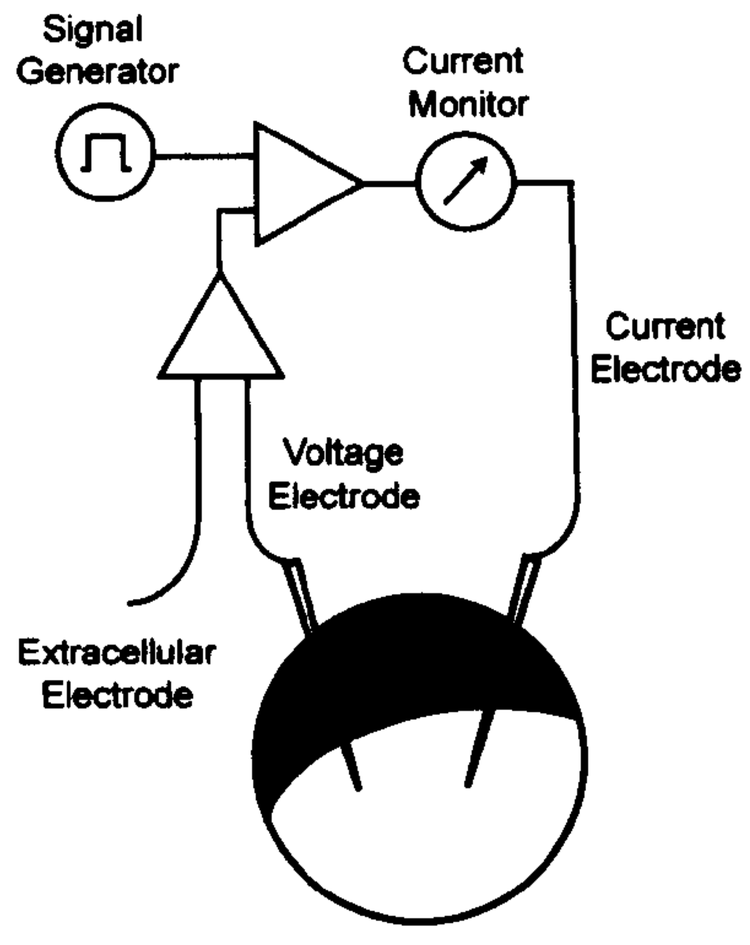

Figure 23: TEVC recording setup for Xenopus oocytes. Shown is a cartoon representation of a TEVC recording setup. The voltage electrode and extracellular electrode are connected to a pre-amp and a signal generator which passes current to the oocytes to clamp the voltage at the desired voltage.

Increasing concentrations of NMDA (0.01 μM to 1000 μM, Ascent Scientific) with 10 μM glycine, and glycine (0.01 to 100 μM, Sigma) with 100 μM NMDA were applied to establish EC_{50} values for the agonists at each receptor subtype. Mean-activation

measurements were made at each concentration of agonist as the percentage of maximum response. Agonist application also allowed saturating concentrations of agonist to be determined, and these were used when testing the open channel blockers.

Increasing concentrations (between 0.01 μM and 100 μM) of the antagonists Mg^{2+}, memantine (Sigma), PhTX-343, PhTX-12 (Both PhTX compounds gifts from Professor K Stromgaard, University of Copenhagen), methoctramine (gift from Dr Michela Rosini, University of Bologna) and MK-801 (Merck) were applied after a steady-state response to NMDA/glycine was reached. Mean-inhibition values were obtained from separate oocytes (at least three; typically six), across at least two different batches and were a percentage of the response to NMDA/glycine alone.

EC_{50} values for 50% activation and IC_{50} for 50% inhibition were calculated by fitting a four-parameter logistic equation (Hill equation) to concentration-response and concentration-inhibition plots respectively in Prism 5 (GraphPad Software Inc):

$$I = \frac{I_{max}}{\left(1 + \left(\frac{[C]}{XC_{50}}\right)^{n_H}\right)}$$

Where n_H is the Hill coefficient, I_{max} is the predicted maximum current, [C] is the concentration of agonist or blocker, and XC_{50} is the concentration of agonist or blocker that produces a half-maximum inhibition or activation.

To determine if the IC_{50} values of the blockers were significantly different to each other they were compared pairwise using the extra sum-of-squares F-test to a null hypothesis

of IC_{50} being the same for each pair (GraphPad Software Inc). Voltage-dependence was tested similarly, but as the F-test is omnibus and the results of individual pairwise comparisons were not necessary, the effect of voltage was determined by comparing the IC_{50} values for all three voltages to the null hypothesis of IC_{50} being the same at each voltage. The α level for statistical significance was set at 0.05.

The Woodhull model was used to calculate the parameter δ from the following equation (Woodhull, 1973, Ferrer-Montiel et al., 1998):

$$IC_{50}(V_h) = IC_{50}(0\,mV) \times \exp\left(\frac{z\delta V_m F}{RT}\right)$$

Where z is the valence of the blocker (+2 for Mg^{2+}, +1 for memantine, +3 for PhTX-343, +1 for PhTX-12, +4 for methoctramine and +1 for MK-801), V_h is the membrane potential (mV), R is the gas constant, T absolute temperature (K) and F is Faraday's constant (C/mol).

I-V relationships were constructed by determining current in response to NMDA/glycine at a range of holding potentials. Oocytes were voltage-clamped between −100 and 0 mV in increments of 25 mV for the generation of I-V plots. Current was normalised to that at -75 mV. Linear regression was carried out in Prism 5 (GraphPad Software Inc) between -75 and 0 mV and the x intercept was considered the reversal potential.

Peak/Plateau ratio measurements were made by dividing the peak level current with the plateau level current for each subunit at each voltage after NMDA/glycine application. These were analysed using the non-parametric Kruskal-Wallis test. Post-hoc analysis was carried out using Dunn's Multiple Comparison Test. Overall current levels produced after

NMDA/glycine application for the NMDA subunits were log transformed and compared by two-way ANOVA. Factors were 'Current' and 'voltage' and post-hoc analysis was carried out using the Bonferroni multiple comparison test. In order to test the claim of Ulbrich and Isacoff (2008) that two populations of receptor were produced in Xenopus oocytes when GluN1/2 and 3 were injected, recordings were made with application of glycine and Zn^{2+} alone.

The rise and decay of block were explored by taking steady-state current and applying IC_{50} concentrations of blocker until another steady state was achieved. The recovery phase was obtained by switching solutions back to NMDA/glycine until current returned to steady levels. Both the onset and decay phase of block were fitted well with a single exponential equation in WinWCP (John Dempster, Strathclyde Electrophysiological Software). These fits gave a time constant (τ) for the rise and recovery of block which was repeated 4-8 times per blocker (separate oocytes over two batches) at -100, -75 and -50 mV at GluN1-1a/2A, GluN1-1a/2A/3A and GluN1-1a/2A/3B containing NMDA receptors. These were log transformed and compared using two-way ANOVA in Prism 5 (GraphPad Software Inc). Factors were 'Subunit' and 'voltage' and post-hoc analysis was carried out using Bonferroni post tests.

2.9 Multi Target Directed Ligands

The study used a series of MTDLs are that are shown in Figure 24 (from Dr Michela Rosini, University of Bologna). The carbacrine compounds was tacrine, an acetylcholinesterase inhibitor, and the vasodilating β blocker carvedilol (Lysko et al., 1998, Rang et al., 2007). The differing group was designed with increasing chain size between the pharmacophores (Figure 24).Compounds group **1** and **2** were produced from donepezil, an acetylcholine esterase inhibitor, and carvedilol and are numbered

because they are unique entities described for the first time in this thesis (Francis et al., 1999). Compounds **1a** to **1e** had increased chain length, while the compound **2** group had differing position for a methoxy group, and **2a** and **2b** had differing chain lengths (Figure 24). Compounds **3**, **4** and **5** were based on dimebon with differing linker regions, while compounds **3a** – **3c** had differing chain lengths (Figure 24). Again these compounds are numbered as this is the first time they have been described. Dimebon itself was also sourced from Dr Michela Rosini. Lipocrine was from the combination of lipoic acid, an antioxidant, and tacrine and has a number as it has been reported previously (Biewenga et al., 1997, Rosini et al., 2005). Compound **6** was derived from carvedilol and lipoic acid and takes a number as it is being first described in this thesis.

Lipocrine, **1** and **2** were dissolved in a maximum of 1% DMSO. Activity was measured at V_h of -100, -80 and -50 mV, however, for **1** and **2** only -100 mV was tested due to limited availability. For the purposes of the current study -80 mV was chosen as the intermediate voltage to maintain parity with an already ongoing MTDL project (Rosini et al., 2008). The IC_{50} values, voltage-dependence and Woodhull analysis were carried out as described above.

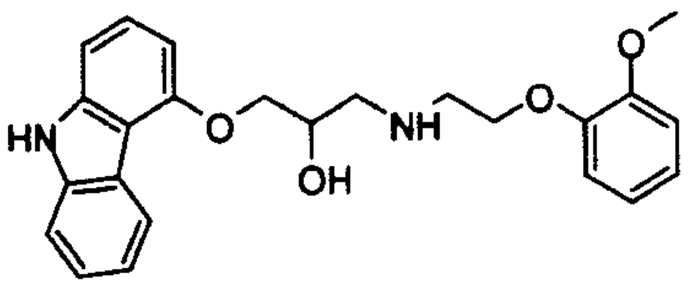

Carvedilol

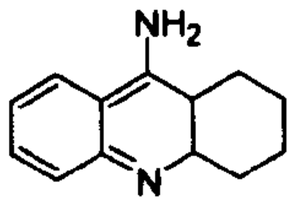

Tacrine

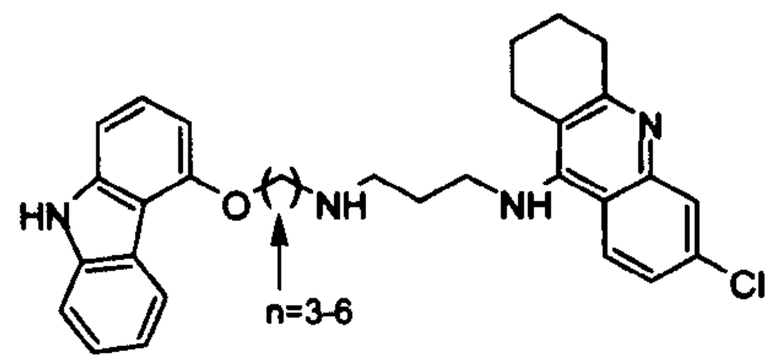

Carbacrine(n)

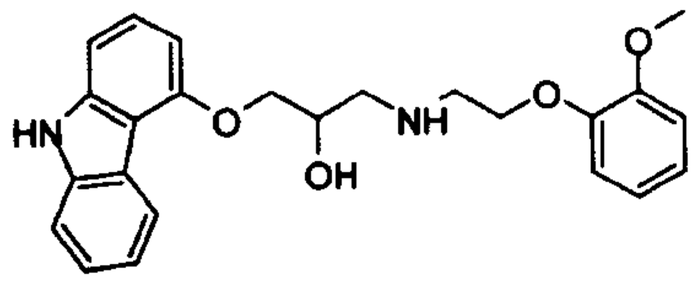

Carvedilol

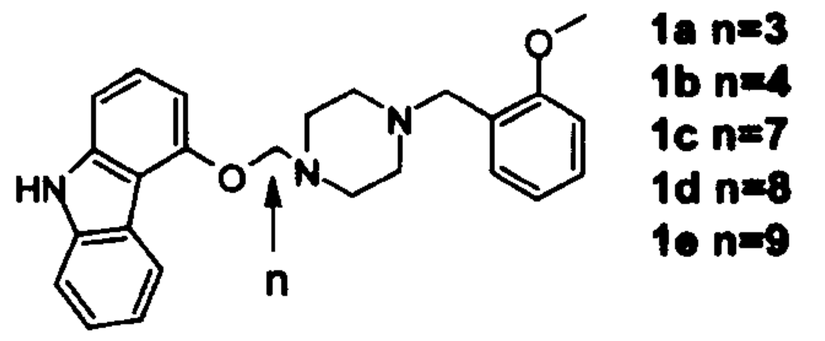

1a n=3
1b n=4
1c n=7
1d n=8
1e n=9

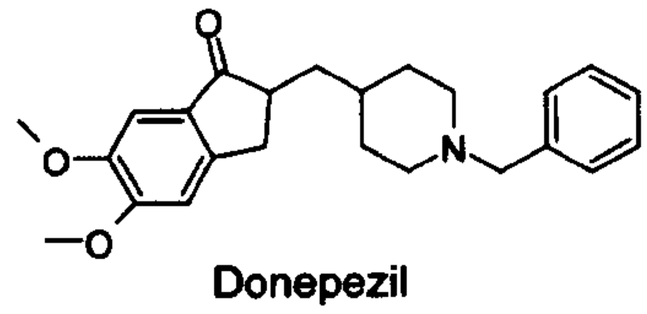

Donepezil

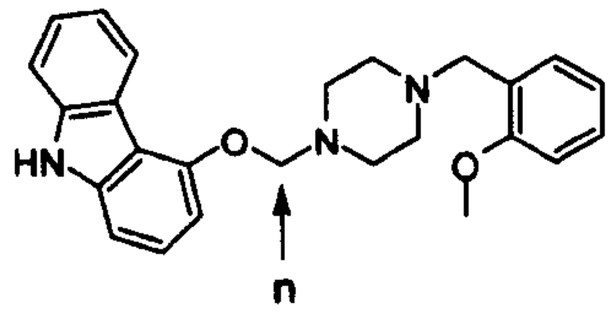

2a n=5
2b n=6

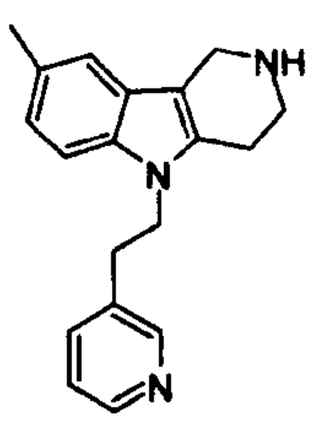

Dimebon

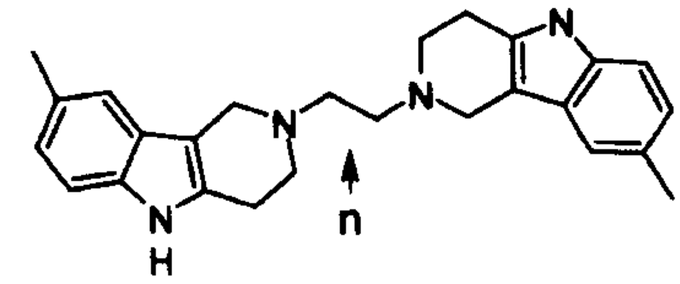

3a n=5
3b n=6
3c n=9

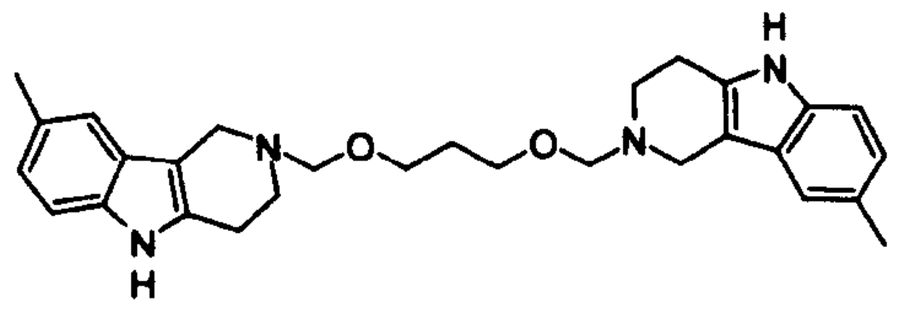

4

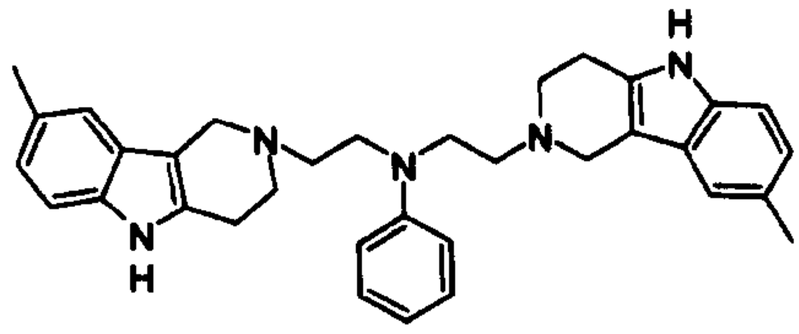

5

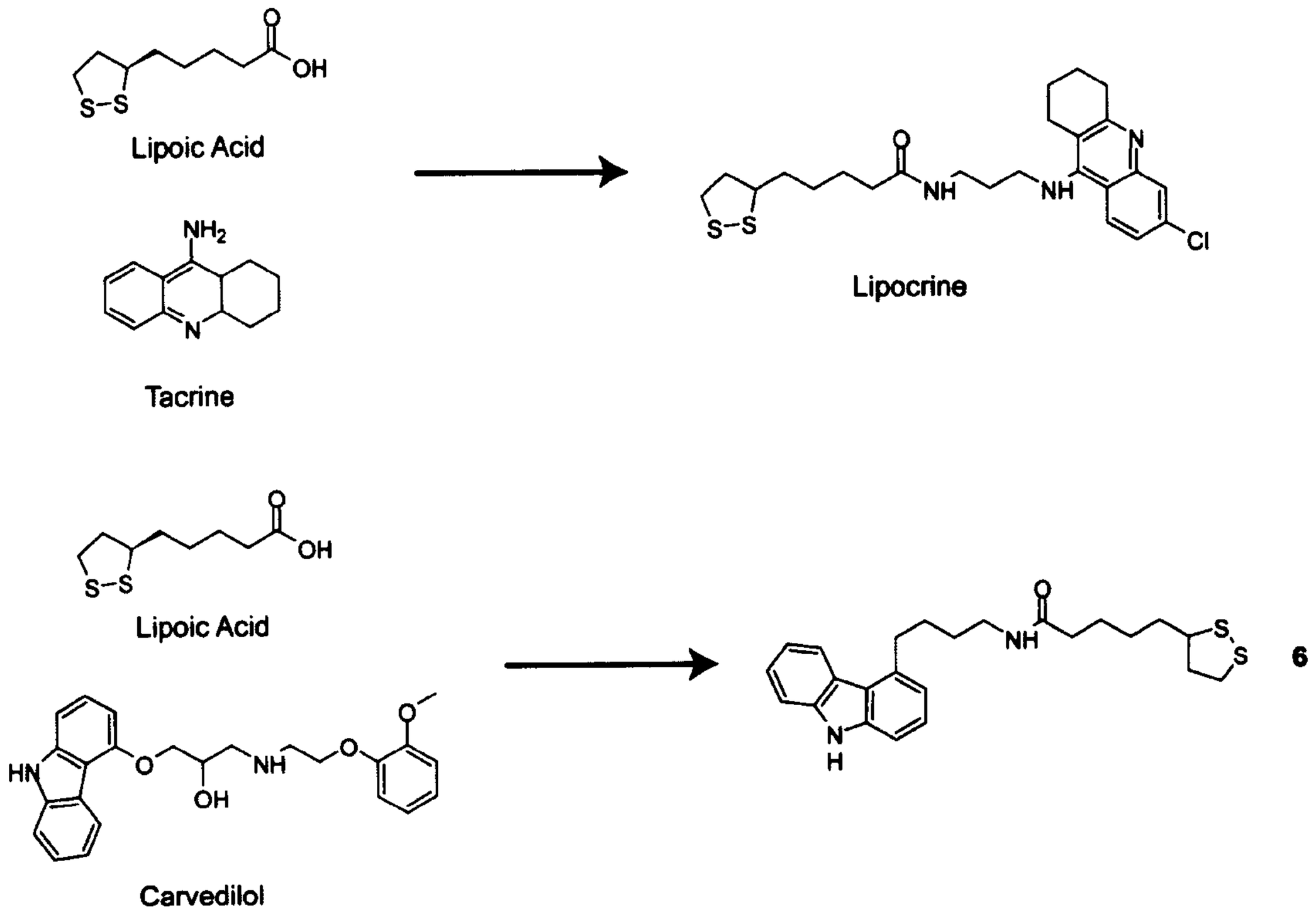

Figure 24: MTDL compounds tested at NMDA receptors. On the left is the originator molecules used to produce the MTDL compounds on the right. The values represented by n are the number of methylene groups between the positions indicated for clarity.

3

Results

3.1 Molecular Biology

The plasmids containing rat GluN1-1a and GluN2A were labelled pRK7, but the plasmid maps were not available. The pRK7 plasmid (www.addgene.com) showed that it was under the control of a SP6 promoter sequence before the multiple cloning site. GluN1-1a was sequenced using SP6 primer and the insert aligned with GluN1-1a (U08261) (Figure 25 and Figure 26). The alignment with GluN1-1b (U08263) showed that the N1 cassette was not present. The plasmid was also sequenced using the primer GluN_1 which was designed to anneal around 200bp upstream from the C1 cassette (Figure 25). Sequence was aligned with GluN1-1a and GluN1-2a (U08262) showing the C1 and C2 cassettes were present (Figure 27). Sequencing data from GluN1_1 primer also showed the presence of a BamHI restriction site downstream of GluN1-1a sequence which only appeared on the plasmid once (Figure 28).

Figure 25: Schematic representation exons that make up the splice variants of the GluN1-1a receptor. White boxes represent exons of the sequence which are alternatively spliced, the N1 cassette (exon 5), C1 (exon 21) and C2 (exon 22). ★represents the stop codon. Arrows denote primer sequencing regions and direction.

```
                1                                                                                                   100
1-1a      (1)   ATGAGCACCATGCACCTGCTGACATTCGCCCTGCTTTTTTCCTGCTCCTTCGCCCGCGCCGCCTGCGACCCCAAGATCGTCAACATCGGCGCGGTGCTGA
1-1b      (1)   ATGAGCACCATGCACCTGCTGACATTCGCCCTGCTTTTTTCCTGCTCCTTCGCCCGCGCCGCCTGCGACCCCAAGATCGTCAACATCGGCGCGGTGCTGA
sp6       (1)   ATGAGCACCATGCACCTGCTGACATTCGCCCTGCTTTTTTCCTGCTCCTTCGCCCGCGCCGCCTGCGACCCCAAGATCGTCAACATCGGCGCGGTGCTGA

                101                                                                                                 200
1-1a    (101)   GCACGCGCAAGCATGAACAGATGTTCCGCGAGGCAGTAAACCAGGCCAATAAGCGACACGGCTCTTGGAAGATACAGCTCAACGCCACTTCTGTCACCCA
1-1b    (101)   GCACGCGCAAGCATGAACAGATGTTCCGCGAGGCAGTAAACCAGGCCAATAAGCGACACGGCTCTTGGAAGATACAGCTCAACGCCACTTCTGTCACCCA
sp6     (101)   GCACGCGCAAGCATGAACAGATGTTCCGCGAGGCAGTAAACCAGGCCAATAAGCGACACGGCTCTTGGAAGATACAGCTCAACGCCACTTCTGTCACCCA

                201                                                                                                 300
1-1a    (201)   CAAGCCCAACGCCATACAGATGGCCCTGTCAGTGTGTGAGGACCTCATCTCTAGCCAGGTCTACGCTATCCTAGTTAGCCACCCGCCTACTCCCAACGAC
1-1b    (201)   CAAGCCCAACGCCATACAGATGGCCCTGTCAGTGTGTGAGGACCTCATCTCTAGCCAGGTCTACGCTATCCTAGTTAGCCACCCGCCTACTCCCAACGAC
sp6     (201)   CAAGCCCAACGCCATACAGATGGCCCTGTCAGTGTGTGAGGACCTCATCTCTAGCCAGGTCTACGCTATCCTAGTTAGCCACCCGCCTACTCCCAACGAC

                301                                                                                                 400
1-1a    (301)   CACTTCACTCCCACCCCTGTCTCCTACACAGCTGGCTTCTACAGAATCCCTGTCCTGGGACTGACTACCCGAATGTCCATCTACTCTGACAAGAGTATCC
1-1b    (301)   CACTTCACTCCCACCCCTGTCTCCTACACAGCTGGCTTCTACAGAATCCCTGTCCTGGGACTGACTACCCGAATGTCCATCTACTCTGACAAGAGTATCC
sp6     (301)   CACTTCACTCCCACCCCTGTCTCCTACACAGCTGGCTTCTACAGAATCCCTGTCCTGGGACTGACTACCCGAATGTCCATCTACTCTGACAAGAGTATCC

                401                                                                                                 500
1-1a    (401)   ACCTGAGTTTCCTTCGCACGGTGCCGCCCTACTCCCACCAGTCCAGCGTCTGGTTTGAGATGATGCGAGTCTACAACTGGAACCACATCATCCTGCTGGT
1-1b    (401)   ACCTGAGTTTCCTTCGCACGGTGCCGCCCTACTCCCACCAGTCCAGCGTCTGGTTTGAGATGATGCGAGTCTACAACTGGAACCACATCATCCTGCTGGT
sp6     (401)   ACCTGAGTTTCCTTCGCACGGTGCCGCCCTACTCCCACCAGTCCAGCGTCTGGTTTGAGATGATGCGAGTCTACAACTGGAACCACATCATCCTGCTGGT
                                                                                                      ⊢— N1
                501                                                                                                 600
1-1a    (501)   CAGCGACGACCACGAGGGACGGGCAGCGCAGAAGCGCTTGGAGACGTTGCTGGAGGAACGGGAGTCCAAG----------------------------
1-1b    (501)   CAGCGACGACCACGAGGGACGGGCAGCGCAGAAGCGCTTGGAGACGTTGCTGGAGGAACGGGAGTCCAAGAGTAAAAAAAGGAACTATGAAAACCTCGAC
sp6     (501)   CAGCGACGACCACGAGGGACGGGCAGCGCAGAAGCGCTTGGAGACGTTGCTGGAGGAACGGGAGTCCAAG----------------------------
                                  N1 —⊣
                601                                                                                                 700
1-1a    (571)   ---------------------------------GCAGAGAAGGTGCTGCAGTTTGACCCAGGAACCAAGAATGTGACGGCTCTGCTGATGGAGGCCCGGG
1-1b    (601)   CAACTGTCCTATGACAACAAGCGCGGACCCAAGGCAGAGAAGGTGCTGCAGTTTGACCCAGGAACCAAGAATGTGACGGCTCTGCTGATGGAGGCCCGGG
sp6     (571)   ---------------------------------GCAGAGAAGGTGCTGCAGTTTGACCCAGGAACCAAGAATGTGACGGCTCTGCTGATGGAGGCCCGGG

                701                                                                                                 800
1-1a    (638)   AACTGGAGGCCCGGGTCATCATCCTTTCTGCAAGCGAGGACGACGCTGCCACAGTGTACCGCGCAGCCGCAATGCTGAACATGACGGGCTCTGGGTACGT
1-1b    (701)   AACTGGAGGCCCGGGTCATCATCCTTTCTGCAAGCGAGGACGACGCTGCCACAGTGTACCGCGCAGCCGCAATGCTGAACATGACGGGCTCTGGGTACGT
sp6     (638)   AACTGGAGGCCCGGGTCATCATCCTTTCTGCAAGCGAGGACGACGCTGCCACAGTGTACCGCGCAGCCGCAATGCTGAACATGACGGGCTCTGGGTACGT

                801                                                                                                 900
1-1a    (738)   GTGGCTGGTCGGGGAACGCGAGATCTCTGGGAACGCCCTGCGCTACGCTCCTGATGGCATCATCGGACTTCAGCTCATCAATGGCAAGAATGAGTCAGCC
1-1b    (801)   GTGGCTGGTCGGGGAACGCGAGATCTCTGGGAACGCCCTGCGCTACGCTCCTGATGGCATCATCGGACTTCAGCTCATCAATGGCAAGAATGAGTCAGCC
sp6     (738)   GTGGCTGGTCGGGGAACGCGAGATCTCTGGGAACGCCCTGCGCTACGCTCCTGATGGCATCATCGGACTTCAGCTCATCAATGGCAAGAATGAGTCAGCC

                901                 921
1-1a    (838)   CACATCAGTGACGCCGTGGGC
1-1b    (901)   CACATCAGTGACGCCGTGGGC
sp6     (838)   CACATCAGTGACGCCGTGGGC
```

Figure 26: Sequence alignment for the proposed GluN1-1a (SP6), GluN1-1a and GluN1-1b. Sequenced using SP6. Nucleotides are numbered from 1 starting at the A of the first ATG start codon in NR1-1a. Shown is the N1 cassette which is only present in NR1-1b.

```
                2483                                                                                                2582
  1-1a  (2483)  TTTTCCTCATTTTCATTGAGATCGCCTACAAGCGACACAAGGATGCCCGTAGGAAGCAGATGCAGCTGGCTTTTGCAGCCGTGAACGTGTGGAGGAAGAA
  1-2a  (2483)  TTTTCCTCATTTTCATTGAGATCGCCTACAAGCGACACAAGGATGCCCGTAGGAAGCAGATGCAGCTGGCTTTTGCAGCCGTGAACGTGTGGAGGAAGAA
GluN1_1    (1)  TTTTCCTCATTTTCATTGAGATCGCCTACAAGCGACACAAGGATGCCCGTAGGAAGCAGATGCAGCTGGCTTTTGCAGCCGTGAACGTGTGGAGGAAGAA
                          ⊢— C1
                2583                                                                                                2682
  1-1a  (2583)  CCTGCAGGATAGAAAGAGTGGTAGAGCAGAGCCCGACCCTAAAAAGAAAGCCACATTTAGGGCTATCACCTCCACCCTGGCCTCCAGCTTCAAGAGACGT
  1-2a  (2583)  CCTGCAG----------------------------------------------------------------------------------------
GluN1_1    (101)  CCTGCAGGATAGAAAGAGTGGTAGAGCAGAGCCCGACCCTAAAAAGAAAGCCACATTTAGGGCTATCACCTCCACCCTGGCCTCCAGCTTCAAGAGACGT
                          C1 —⊣⊢— C2
                2683                                                                                                2782
  1-1a  (2683)  AGGTCCTCCAAAGACACGAGCACCGGGGGTGGACGCGGCGCTTTGCAAAACCAAAAAGACACAGTGCTGCCGCGACGCGCTATTGAGAGGGAGGAGGGCC
  1-2a  (2590)  ------------------AGCACCGGGGGTGGACGCGGCGCTTTGCAAAACCAAAAAGACACAGTGCTGCCGCGACGCGCTATTGAGAGGGAGGAGGGCC
GluN1_1    (201)  AGGTCCTCCAAAGACACGAGCACCGGGGGTGGACGCGGCGCTTTGCAAAACCAAAAAGACACAGTGCTGCCGCGACGCGCTATTGAGAGGGAGGAGGGCC
                                    C2 —⊣   BamHI
                2783                                                                                                2882
  1-1a  (2783)  AGCTGCAGCTGTGTTCCCGTCATAGGGAGAGCTG----------------------------------------------------------------
  1-2a  (2672)  AGCTGCAGCTGTGTTCCCGTCATAGGGAGAGCTG----------------------------------------------------------------
GluN1_1    (301)  AGCTGCAGCTGTGTTCCCGTCATAGGGAGAGCTGATAGGATCCCCAATTCAATCGATGGCCGCCATGGCCCAACTTGTTTATTGCAGCTTATAATGGTTA

                2883                                                                                                2982
  1-1a  (2818)  ----------------------------------------------------------------------------------------------------
  1-2a  (2706)  ----------------------------------------------------------------------------------------------------
GluN1_1    (401)  CAAATAAAGCAATAGCATCACAAATTTCACAAATAAAGCATTTTTTTCACTGCATTCTAGTTGTGGTTTGTCCAAACTCATCAATGTATCTTATCATGTC
```

Figure 27: Sequence alignment for the proposed GluN1-1a (GluN1_1), GluN1-1a and GluN1-2a. Proposed 1-1a sequenced using GluN1_1 primer. Nucleotides are numbered from 1 starting at the A of the first ATG start codon in 1-1a. Shown are the C1 cassette which is not present in 1-2a, the C2 cassette and the BamHI restriction site.

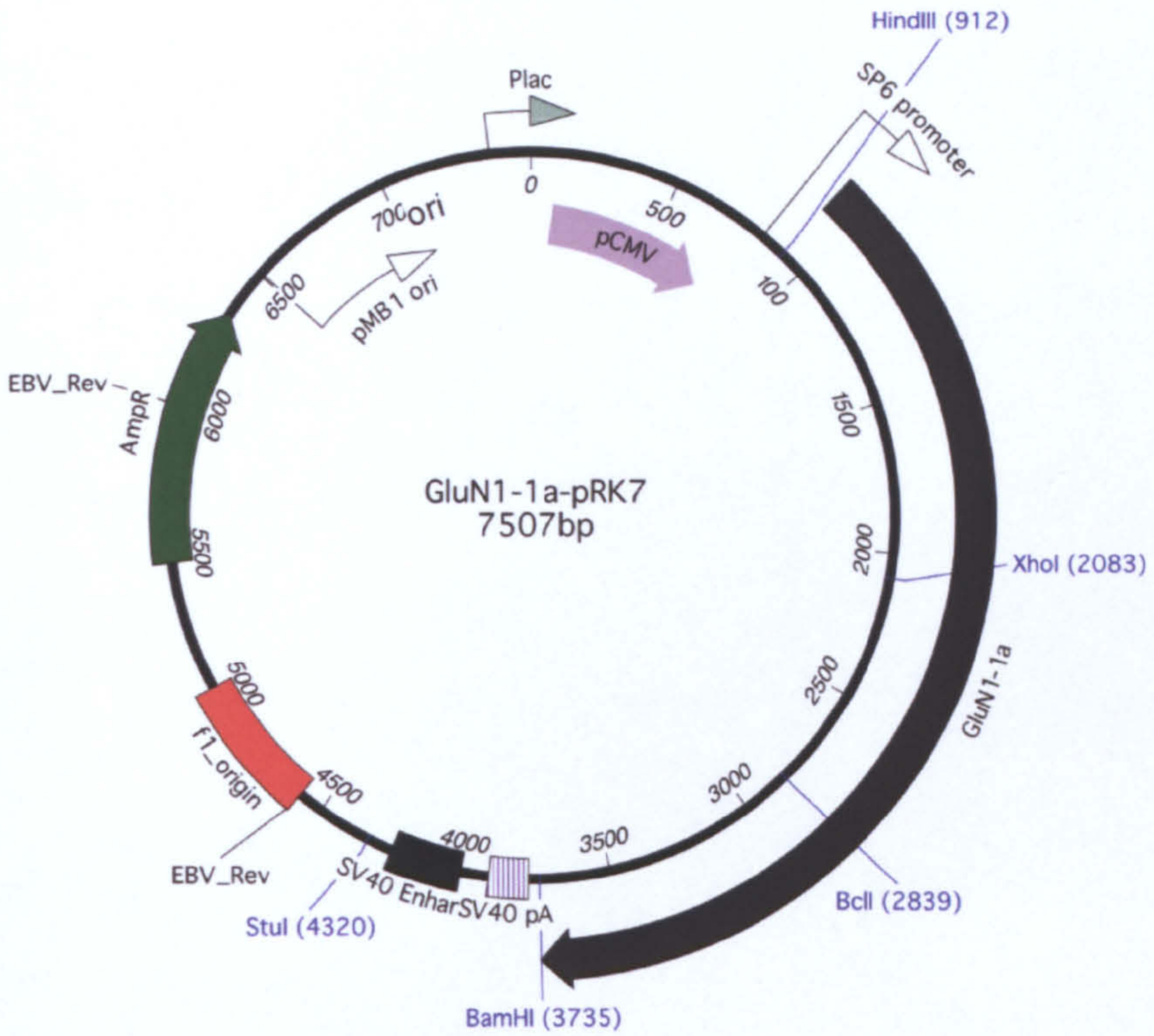

Figure 28: Vector map for GluN1-1a in pRK7. Shown are single cutter restriction enzyme sites.

Further sequencing was carried out on the pRK7 GluN2A plasmid. Sequencing data from the SP6 primer aligned with GluN2A (D13211) which confirmed the presence of the insert in the plasmid (Figure 29). The plasmid was then sequenced using the primer GluN2_1 which was designed to anneal around 200bp upstream from the end of coding sequence. Sequence was aligned with GluN2A confirming the presence of the insert, as well as the EcoRI restriction site downstream (Figure 30). The restriction map shows that EcoRI cut the plasmid once so it could be used for linearisation (Figure 31).

```
            1                                                                                                  100
2A     (1)  ----------------------------------------------------------------------------------------------------
sp6    (1)  CAACTGCACCTCGGTTCTAAGCTTCTGCAGGTCGACTCTAGAAGAGAGGCTCCTGAGGTGCTGTGCCTGAGCATGGGGCTGGATGAGGTCTGAGAGTCGC

          101                                                                                                  200
2A     (1)  ----------------------------------------------------------------------------------------------------
sp6  (101)  GGCGGCAGCAATCAGCCCTGGAGATGACCAGGGGTGGCCACTGCTGAGAACTATGTGGAGAGAGGCTGCGAGCCCTGCTGCAGAGCCTCCGGCTGGGATA

          201                                                                                                  300
2A     (1)  ----------------------------------------------------------------------------------------------------
sp6  (201)  GCCGCCCCCCGTGGGGGTGATGCGGACAGCGCGGGACAGCCAGGGGAGCGCGCGGGGGCCGCAGCATGCGGGAACCCGCTAAACCTGGTGGCTGCTGAGG

          301                                                                                                  400
2A     (1)  ----------------------------------------------------------------------ATGGGCAGATTGGGCTACTGG
sp6  (301)  CGGCCGAGATGCTCGTGCGCGCAGCACGCCCCATTGCATCCTCCACCTTCTCCGGCTACAGGGACCCTAAGTGGCGACCATGGGCAGATTGGGCTACTGG

          401                                                                                                  500
2A    (22)  ACCTTGCTGGTATTGCCGGCCCTTCTGGTCTGGCGCGATCCGGCGCAGAACGCGGCGGCGGAGAAGGGTCCTCCAGCGCTGAACATTGCGGTGCTGCTGG
sp6  (401)  ACCTTGCTGGTATTGCCGGCCCTTCTGGTCTGGCGCGATCCGGCGCAGAACGCGGCGGCGGAGAAGGGTCCTCCAGCGCTGAACATTGCGGTGCTGCTGG

          501                                                                                                  600
2A    (122)  GTCACAGCCACGACGTGACAGAACGCGAACTTCGAAATCTGTGGGGCCCAGAGCAGGCAACCGGCTTGCCCCTGGATGTGAACGTGGTGGCGTTATTGAT
sp6  (501)  GTCACAGCCACGACGTGACAGAACGCGAACTTCGAAATCTGTGGGGCCCAGAGCAGGCAACCGGCTTGCCCCTGGATGTGAACGTGGTGGCGTTATTGAT

          601                                                                                                  700
2A    (222)  GAACCGCACTGACCCTAAGAGCCTCATCACGCATGTGTGCGACCTCATGTCCGGGGCGCGCATCCACGGCTTGGTGTTTGGAGATGACACGGACCAGGAG
sp6  (601)  GAACCGCACTGACCCTAAGAGCCTCATCACGCATGTGTGCGACCTCATGTCCGGGGCGCGCATCCACGGCTTGGTGTTTGGAGATGACACGGACCAGGAG

          701                                                                                                  800
2A    (322)  GCTGTGGCCCAGATGCTGGATTTTATCTCCTCACAGACTTTTATCCCCATCTTGGGCATTCATGGGGGTGCATCTATGATCATGGCTGACAAGGATCCGA
sp6  (701)  GCTGTGGCCCAGATGCTGGATTTTATCTCCTCACAGACTTTTATCCCCATCTTGGGCATTCATGGGGGTGCATCTATGATCATGGCTGACAAGGATCCGA

          801
2A    (422)  CATCC
sp6  (801)  CATCC
```

Figure 29: Sequence alignment for the proposed GluN2A (T7) plasmid and GluN2A. GluN2A sequenced using SP6. Nucleotides are numbered from 1 starting at the A of the ATG start codon in GluN2A.

```
               4275                                                                                               4374
    2A   (4276)  AGAGCATGTTATGCCTTATGCTGCAAATAAGAATACCATGTACTCTACCCCCAGGGTTTTAAATTCCTGCAGCAATAGACGAGTGTACAAGAAAATGCCT
GluN2_1    (2)  AGAGCATGTTATGCCTTATGCTGCAAATAAGAATACCATGTACTCTACCCCCAGGGTTTTAAATTCCTGCAGCAATAGACGAGTGTACAAGAAAATGCCT

               4375                                                                                               4474
    2A   (4376)  AGTATCGAATCTGATGTTTAAGATCTTCC----------------------------------------------------------------------
GluN2_1    (102)  AGTATCGAATCTGATGTTTAAGATCTTCCATCAGTATTTATCTATAAGGAAACATATAGAATGGCCAACATTATAGAGGGTAAATGTTGGATGTCCGATA

               4475                                                                                               4574
    2A  (•4403)  ----------------------------------------------------------------------------------------------------
GluN2_1    (202)  GCACCCTACTAGGAGGAAGAGGGTACAGGGAGGTACTTTTTGTTGGCTCTTTTGCACATGGCTCCATGCCATAATCTTCCACTCAAGGAATCTTGTGAGA

               4575                                                                                               4674
    2A  (•4403)  ----------------------------------------------------------------------------------------------------
GluN2_1    (302)  TATGTGCTGAGCACAGCATATACCACGTAGGTGAATCCTTAACCAAAAACAAATAAATACACATGGGCAAGTCTCCCAGACATGGCGACTGGGCACGGCG

               4675                                                                                               4774
    2A  (•4403)  ----------------------------------------------------------------------------------------------------
GluN2_1    (402)  GCAATAATGGTGCATCAGACGGCGATGGTGACATTGTGGTTGCCTATATTCCAAATTCCATGAAGATCAATCCACCATGTAACTTCCCCCATCAGAAATG

               4775                                                                                               4874
    2A  (•4403)  ----------------------------------------------------------------------------------------------------
GluN2_1    (502)  CCTCACAGTTTCTCTAATACAGAATAAGCAATATGGTATGCATGTAAGTCTGACGCAGACAATAAGACAGTTAAGAATGCATCTGCACTGTAGTAAGATT
                                                                                                                EcoR1
               4875                                                                                               4974
    2A  (•4403)  ----------------------------------------------------------------------------------------------------
GluN2_1    (602)  GACATGTGCAAGGATTAAGAAGTTTGGCTTGTAACAGTTCTCAGATTTCTTGTTATGCCTTCCATGACAACCCTGGATCAGTCCCCCCTCGTGCCGAATT
                  -
               4975   4985
    2A  (•4403)  ----------
GluN2_1    (702)  CAATCGATGGC
```

Figure 30: Sequence alignment for the proposed GluN2A (GluN2_1) plasmid and GluN2A. Sequenced using GluN2_1. Nucleotides are numbered from 1 starting at the A of the ATG start codon in GluN2A. Also shown is the EcoRI site.

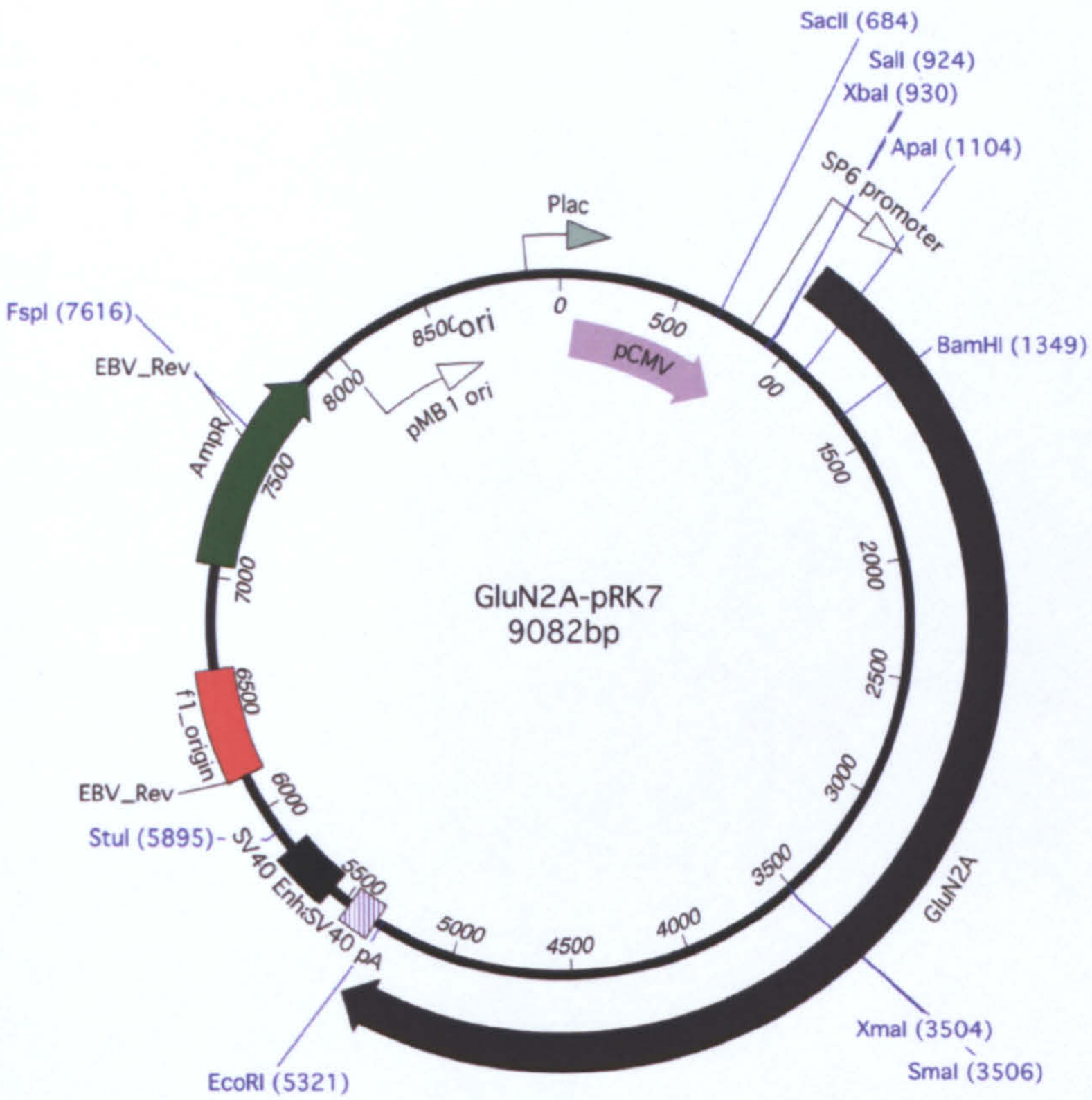

Figure 31: Vector map for GluN2A in pRK7. Shown are single cutter restriction enzyme sites

In order to confirm the GluN3A was in pcDNA3.1(+) it was sequenced using T7 primer and aligned with GluN3A (U29873) (Figure 32). It was also sequenced using the primer GluN3A_1 which was designed to anneal 200 bp upstream of the coding sequence (Figure 33). There was also a poly-(A) tail as well as a NotI restriction site downstream from the end of insert. NotI only appeared on the plasmid once as part of the multiple cloning site, and did not appear on GluN3A (Figure 34).

```
            1                                                                                                   100
3A     (1)  ------------------------------------------------------------ATGAGGAGACTGAGTTTGTGGTGGCTGCTGAGCAGGGTCT
T7     (1)  GAGCTCGGATCCCCCGGGCTGCAGGAATTCGATCGCGCTTTCTCCCAGCGGGTCTCAGTAATGAGGAGACTGAGTTTGTGGTGGCTGCTGAGCAGGGTCT

            101                                                                                                 200
3A    (41)  GTCTGCTGCTGCCGCCGCCCTGCGCACTGGTGCTGGCCGGGGTGCCCAGCTCCTCCTCGCACCCGCAACCCTGCCAGATCCTCAAGCGCATCGGACACGC
T7   (101)  GTCTGCTGCTGCCGCCGCCCTGCGCACTGGTGCTGGCCGGGGTGCCCAGCTCCTCCTCGCACCCGCAACCCTGCCAGATCCTCAAGCGCATCGGACACGC

            201                                                                                                 300
3A   (141)  GGTGAGGGTGGGCGCGGTGCACTTGCAACCCTGGACCACGGCCCCACGCGCAGCCAGTCGCGCTCAGGAAGGCGGCAGGGCGGGTGCCCAGAGGGATGAT
T7   (201)  GGTGAGGGTGGGCGCGGTGCACTTGCAACCCTGGACCACGGCCCCACGCGCAGCCAGTCGCGCTCAGGAAGGCGGCAGGGCGGGTGCCCAGAGGGATGAT

            301                                                                                                 400
3A   (241)  CCAGAGTCCGGGACGTGGCGGCCACCGGCGCCCTCGCAAGGCGCACGCTGGTTGGGGAGCGCCCTGCATGGCCGGGGTCCACCCGGCTCCCGAAAGCTCG
T7   (301)  CCAGAGTCCGGGACGTGGCGGCCACCGGCGCCCTCGCAAGGCGCACGCTGGTTGGGGAGCGCCCTGCATGGCCGGGGTCCACCCGGCTCCCGAAAGCTCG

            401                                                                                                 500
3A   (341)  GGGAGGGCGCGGGGGCCGAGACCCTGTGGCCGCGGGATGCCCTACTGTTCGCTGTGGAAAACTTGAACCGTGTGGAAGGGCTCCTACCCTACAACCTGTC
T7   (401)  GGGAGGGCGCGGGGGCCGAGACCCTGTGGCCGCGGGATGCCCTACTGTTCGCTGTGGAAAACTTGAACCGTGTGGAAGGGCTCCTACCCTACAACCTGTC

            501                                                                                                 600
3A   (441)  TTTGGAAGTAGTGATGGCCATTGAGGCGGGCCTGGGCGATCTGCCGCTTATGCCCTTCTCTTCCCCAAGCTCACCGTGGAGCAGTGACCCTTTCTCCTTT
T7   (501)  TTTGGAAGTAGTGATGGCCATTGAGGCGGGCCTGGGCGATCTGCCGCTTATGCCCTTCTCTTCCCCAAGCTCACCGTGGAGCAGTGACCCTTTCTCCTTT

            601                         628
3A   (541)  CTGCAGAGCGTGTGCCACACCGTAGTGG
T7   (601)  CTGCAGAGCGTGTGCCACACCGTAGTGG
```

Figure 32: Sequence alignment for GluN3A sequenced by T7 aligned with GluN3A. Nucleotides are numbered from 1 starting at the A of the ATG start codon in GluN3A.

```
                3187                                                                                            3286
     3A  (3188)  GGGAAAGCAGACTCCCTCAATGTAACTCGGAGCTCCGTGATTCAGGAACTCTCTGAGTTGGAGAAGCAGATCCAAGTGATCCGCCAGGAGCTGCAGTTGG
GluN3A_1   (2)  GGGAAAGCAGACTCCCTCAATGTAACTCGGAGCTCCGTGATTCAGGAACTCTCTGAGTTGGAGAAGCAGATCCAAGTGATCCGCCACGAGCTGCAGTTGG

                3287                                                                                            3386
     3A  (3288)  CTGTAAGCAGGAAGACAGAGCTGGAGGAGTATCAAAAGACAAATCGGACTTGTGAATCCTAG----------------------------------
GluN3A_1  (102)  CTGTAAGCAGGAAGACAGAGCTGGAGGAGTATCAAAAGACAAATCGGACTTGTGAATCCTAGGCTGTGTCTCCCCCCCACTTTCTCAGCCCCTGGTACTCT

                3387                                                                                            3486
     3A (•3348)  ----------------------------------------------------------------------------------------------------
GluN3A_1  (202)  GAAGCCCTTGAGACACTTTGTAAAGCCCTTTTATATTCCTTGACAAAGGTGTGGGGTCTGGCAATGAAGTGTGCTGTTCTCTGCCTATCGACCTCGAGGG

                3487                                                                                            3586
     3A (•3348)  ----------------------------------------------------------------------------------------------------
GluN3A_1  (302)  GGAGCTTGATCTGGTTACCACTAAACCAGCCTCAAGAACACCCGAATGGAGTCTCTAAGCTACATAATACCAACTTACACTTTACAAAATGTTGTCCCCC

                3587                                                                                            3686
     3A (•3348)  ----------------------------------------------------------------------------------------------------
GluN3A_1  (402)  AAAATGTAGCCATTCGTATCTGCTCCTAATAAAAAGAAAGTTTCTTCACATTCTAAAAAAAAAAAAAAAAAAAAAAAAAAAAAAACCCCCCCCCCCCC
                                        NotI
                3687                            3721
     3A (•3348)  ------------------------------------
GluN3A_1  (502)  CCCCTGCAGGATCCAGCACAGTGGCGGCCGCTCGA
```

Figure 33: Sequence alignment for GluN3A plasmid and 3A. Sequenced using GluN3A_1 and also shown is NotI restriction site.

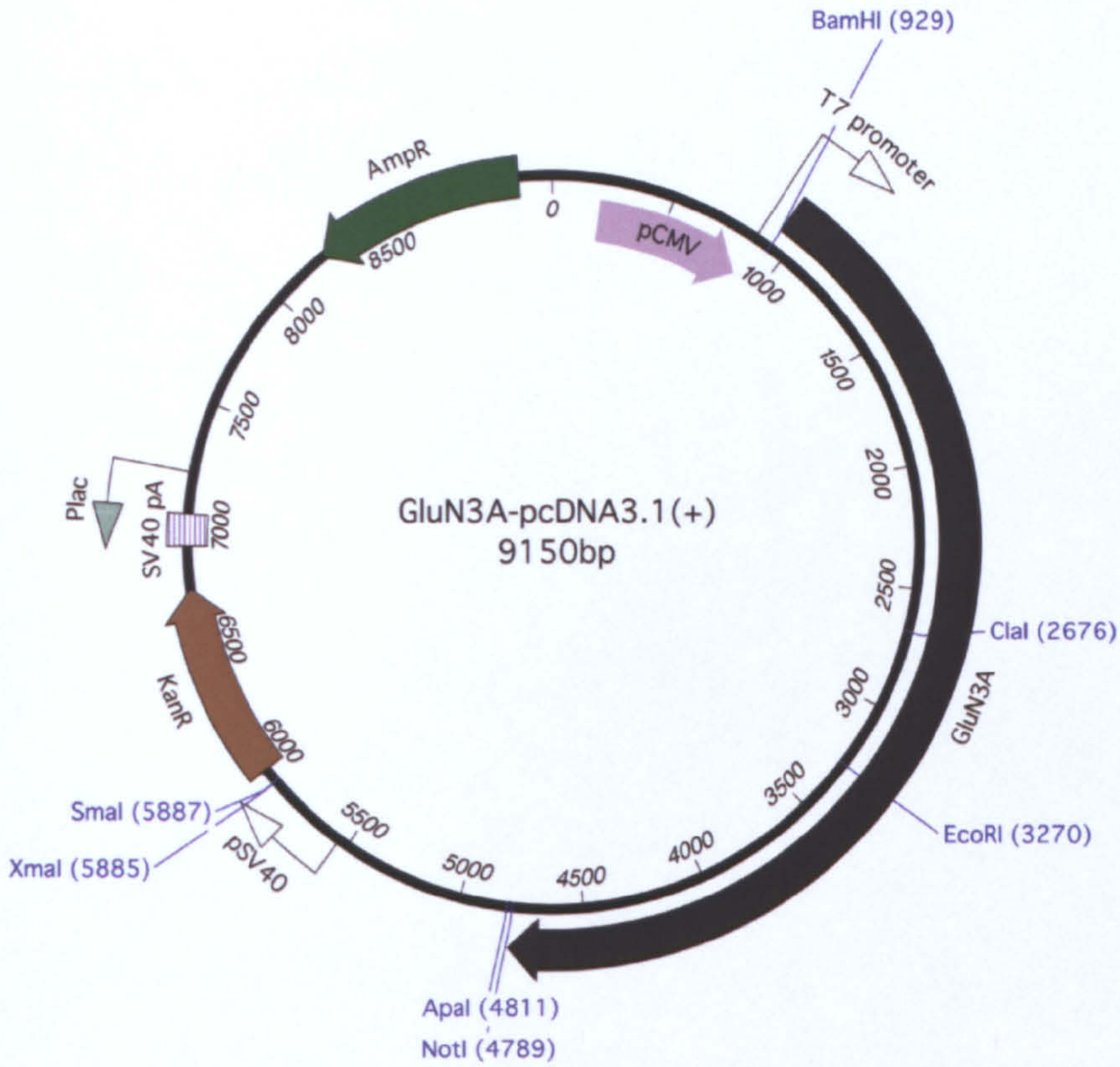

Figure 34: Vector map for GluN3A in pcDNA3.1(+). Shown are single cutter restriction enzyme sites.

GluN3B in pcDNA3.1(+) was sequenced using T7 primer and aligned with GluN3B (AF440691), confirming its presence (Figure 35). However, a consensus difference at position 556 (A/G) was found (Figure 35). A BLAST search returned GluN3B (AF440691) and no SNP was found. It was also sequenced using the primer GluN3B_1 which was designed to anneal 200bp upstream of the coding sequence where it aligned with GluN3B (Figure 36). A poly-(A) tail and XbaI restriction site were also found. XbaI only appeared on the plasmid once as part of the multiple cloning site, and did not appear on GluN3B (Figure 37).

```
                1                                                                                                   100
GluN3B    (1)   ------------------------------------ATGGAGAGTGTGCGGACGCTGTGGCTCAGCGTGGCCCTGGCGCTGGCGGTGGGGTCCCGAGTGG
  T7      (2)   ATCCACTAGTCCAGTGTGGTGGAATTCGCCGCCGCCATGGAGAGTGTGCGGACGCTGTGGCTCAGCGTGGCCCTGGCGCTGGCGGTGGGGTCCCGAGTGG

                101                                                                                                 200
GluN3B   (66)   TGCGCGGTCACCCTCAGCCCTGCCGGGTTCCCACGCGCGCTGGGGCCTCCGTGCGCCTGGCGGCGCTCCTGCCCCGGGCGCCCGCCGCCCGCGCCCGCGT
  T7    (102)   TGCGCGGTCACCCTCAGCCCTGCCGGGTTCCCACGCGCGCTGGGGCCTCCGTGCGCCTGGCGGCGCTCCTGCCCCGGGCGCCCGCCGCCCGCGCCCGCGT

                201                                                                                                 300
GluN3B   (166)   CCTAGCTGCCCTGGCCACCCCTGCGCCGCGGCTGCCGCACAACCTGAGTCTGGAACTGGTGGCCGTCGCGTCCCCGACCCGGGACCCCGCGTCGCTAGCT
  T7    (202)   CCTAGCTGCCCTGGCCACCCCTGCGCCGCGGCTGCCGCACAACCTGAGTCTGGAACTGGTGGCCGTCGCGTCCCCGACCCGGGACCCCGCGTCGCTAGCT

                301                                                                                                 400
GluN3B   (266)   CGAGGTCTGTGCCAGGTTCTGGCACCGCCTGGCGTGGTGGCCTCTATAGCCTTTCCCGAGGCGCGGCCCGAGCTGCGGCTACTGCAGTTCCTGGCAGCCG
  T7    (302)   CGAGGTCTGTGCCAGGTTCTGGCACCGCCTGGCGTGGTGGCCTCTATAGCCTTTCCCGAGGCGCGGCCCGAGCTGCGGCTACTGCAGTTCCTGGCAGCCG

                401                                                                                                 500
GluN3B   (366)   CCACAGAGACCCCAGTGGTGAGCGTCCTGCGGAGGGAGGTGCGCACGGCCCTCGGAGCCCCGACTCCGTTCCATCTGCAGCTGGACTGGGCTAGTCCCCT
  T7    (402)   CCACAGAGACCCCAGTGGTGAGCGTCCTGCGGAGGGAGGTGCGCACGGCCCTCGGAGCCCCGACTCCGTTCCATCTGCAGCTGGACTGGGCTAGTCCCCT

                501                                                                                                 600
GluN3B   (466)   GGAGACCATACTGGATGTGCTGGTGTCCCTGGTACGGGCACATGCCTGGGAGGACATTGCTCTAGTACTCTGCCGTGTCCGGGACCCTGGCAGCCTGGTG
  T7    (502)   GGAGACCATACTGGATGTGCTGGTGTCCCTGGTACGGGCACATGCCTGGGAGGACATTGCTCTAGTACTCTGCCGTGTCCGGGACCCTGGCGGCCTGGTG

                601                                                                                                 700
GluN3B   (566)   ACACTCTGGACTAACCATGCTAGCCAGGCTCCAAAGTTTGTGCTGGACCTGAGCCGGCTGGACAGCAGGAATGACAGCCTTCGGGCTGGACTGGCCCTGT
  T7    (602)   ACACTCTGGACTAACCATGCTAGCCAGGCTCCAAAGTTTGTGCTGGACCTGAGCCGGCTGGACAGCAGGAATGACAGCCTTCGGGCTGGACTGGCCCTGT

                701                                                                                                 800
GluN3B   (666)   TGGGGGCGCTGGAAGGAGGGGGAACCCCAGTGCCTGCAGCAGTCCTCCTAGGCTGCAGCACTGCCCGTGCACATGAGGTCCTAGAGGCTGCACCACCGGG
  T7    (702)   TGGGGGCGCTGGAAGGAGGGGGAACCCCAGTGCCTGCAGCAGTCCTCCTAGGCTGCAGCACTGCCCGTGCACATGAGGTCCTAGAGGCTGCACCACCGGG

                801                 823
GluN3B   (766)   TCCCCAGTGGTTGCTGGGCACAC
  T7    (802)   TCCCCAGTGGTTGCTGGGCACAC
```

Figure 35: Sequence alignment for GluN3B sequence by T7 and aligned with GluN3B. Nucleotides are numbered from 1 starting at the A of the ATG start codon in GluN3B.

```
                2856                                                                                                2955
     3B  (2857)   AGCGGAGCTGCGGGAGCTGGAGCTGCGCATTGAGGCTGCACGGGAGCGGCTGCGCAGTGCGCTGTTGCGGCGCGGGGAGCTGCGGGCCCTGCTTGGGGAT
GluN3B_1   (2)   AGCGGAGCTGCGGGAGCTGGAGCTGCGCATTGAGGCTGCACGGGAGCGGCTGCGCAGTGCGCTGTTGCGGCGCGGGGAGCTGCGGGCCCTGCTTGGGGAT

                2956                                                                                                3055
     3B  (2957)   GGCACCCGGCTCAGGCCACTGCGCCTGTTGCATGCGGCGCCTGCTGAGAGCTGA----------------------------------------------
GluN3B_1   (102)   GGCACCCGGCTCAGGCCACTGCGCCTGTTGCATGCGGCGCCTGCTGAGAGCTGAGGAACCACAAGGCCGCACTGTCCACGACAGTTTATTCTATATACAA
                                                                                  XbaI
                3056                                                                                                3155
     3B (•3009)   ----------------------------------------------------------------------------------------------------
GluN3B_1   (202)   ACACGACTCTGTACACTGCAATTAAATAGCGTGGAACGTGAAAAAAAACTCTAGAGGGCCCGTTTAAACCCGCTGATCAGCCTCGACTGTGCCTTCTAGT

                3156                                                                                                3255
     3B (•3009)   ----------------------------------------------------------------------------------------------------
GluN3B_1   (302)   TGCCAGCCATCTGTTGTTTGCCCCTCCCCCGTGCCTTCCTTGACCCTGGAAGGTGCCACTCCCACTGTCCTTTCCTAATAAAATGAGGAAATTGCATCGC

                3256                                                                                                3355
     3B (•3009)   ----------------------------------------------------------------------------------------------------
GluN3B_1   (402)   ATTGTCTGAGTAGGTGTCATTCTATTCTGGGGGGTGGGGTGGGGCAGGACAGCAAGGGGGAGGATTGGGAAGACAATAGCAGGCATGCTGGGGATGCGGT

                3356                                                                                        3438
     3B (•3009)   ------------------------------------------------------------------------------------------
GluN3B_1   (502)   GGGCTCTATGGCTTCTGAGGCGGAAAGAACCAGCTGGGGCTCTAGGGGGTATCCCCACGCGCCCTGTAGCGGCGCATTAAGCG
```

Figure 36: Sequence alignment for proposed GluN3B sequenced by GluN1_1 and aligned with GluN3B. Nucleotides are numbered from 1 starting at the A of the ATG start codon in GluN3B. Also shown is the XbaI restriction site..

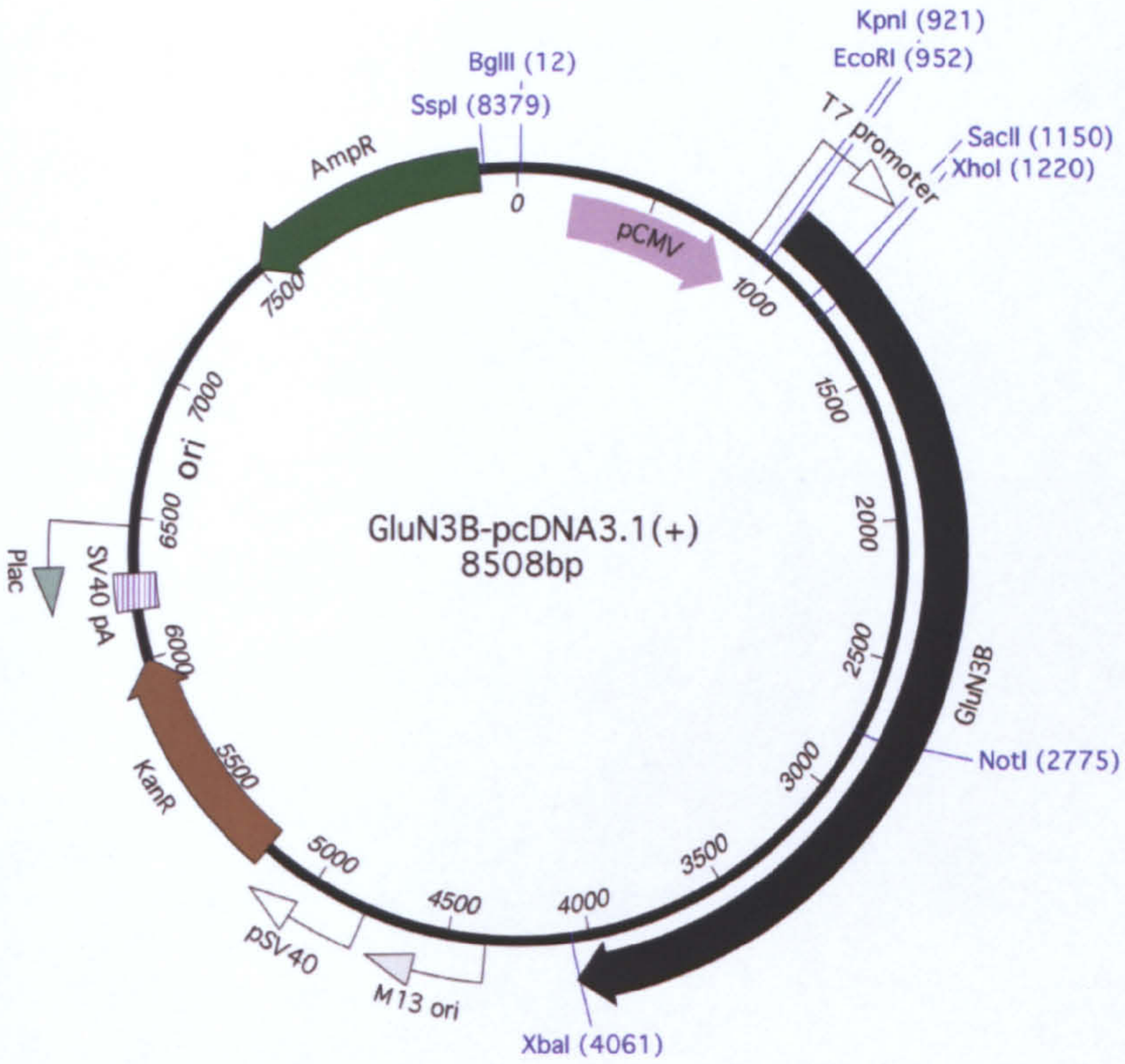

Figure 37: Vector map for GluN3B in pcDNA3.1(+). Shown are single cutter restriction enzyme sites.

The GluN3A^{G703N} mutation was confirmed using primer GluN3A_2, designed to anneal around 200 bp upstream from the N-site. The mutations G2185A and G2186A changed the codon from GGC (glycine) to AAC (asparagine) at amino acid position 703 (Figure 38). The GluN3A^{R704N} mutation produced sequence that showed that G2189A and A2190T changed the codon from AGA (arginine) to AAT (asparagine) at amino acid position 704 (Figure 39). The mutation for GluN3A^{R704D} was sequenced and it was found that mutations A2188G, G2189A and A2190T changed the codon from AGA (arginine) to GAT (aspartate) at amino acid position 704 (Figure 40).

```
                2000                                                                                                2099
      3A  (2000) GAGCCTTCATGTGGCCACTCCACTGGACCATGTGGCTGGGAATTTTCGTGGCTCTCCATATCACTGCCATTTTTCTCACTCTGTATGAATGGAAGAGCCC
GluN3A_2    (1) GAGCCTTCATGTGGCCACTCCACTGGACCATGTGGCTGGGAATTTTCGTGGCTCTCCATATCACTGCCATTTTTCTCACTCTGTATGAATGGAAGAGCCC

                2100                                                                                                2199
      3A  (2100) CTTTGGTATGACCCCTAAGGGGAGGAACAGAAACAAAGTCTTCTCCTTCTCCTCAGCTTTGAATGTCTGCTATGCCCTTCTGTTTGGCAGAACAGCAGCC
GluN3A_2  (101) CTTTGGTATGACCCCTAAGGGGAGGAACAGAAACAAAGTCTTCTCCTTCTCCTCAGCTTTGAATGTCTGCTATGCCCTTCTGTTTAACAGAACAGCAGCC

                2200                                                                                                2299
      3A  (2200) ATCAAACCCCCAAAATGCTGGACTGGAAGGTTTCTGATGAATCTTTGGGCCATTTTCTGTATGTTTTGCCTTTCTACATACACAGCGAACTTGGCTGCTG
GluN3A_2  (201) ATCAAACCCCCAAAATGCTGGACTGGAAGGTTTCTGATGAATCTTTGGGCCATTTTCTGTATGTTTTGCCTTTCTACATACACAGCGAACTTGGCTGCTG

                2300                                                                                                2399
      3A  (2300) TCATGGTAGGTGAGAAGATCTATGAAGAGCTTTCTGGAATTCATGACCCTAAGCTTCATCATCCTTCTCAAGGCTTCCGCTTTGGAACTGTCCGGGAAAG
GluN3A_2  (301) TCATGGTAGGTGAGAAGATCTATGAAGAGCTTTCTGGAATTCATGACCCTAAGCTTCATCATCCTTCTCAAGGCTTCCGCTTTGGAACTGTCCGGGAAAG

                2400                                                                                                2499
      3A  (2400) CAGTGCTGAAGACTATGTGCGCCAGAGCTTCCCAGAGATGCATGAGTACATGAGAAGGTACAACGTGCCAGCCACCCCTGATGGAGTGCAGTATCTGAAG
GluN3A_2  (401) CAGTGCTGAAGACTATGTGCGCCAGAGCTTCCCAGAGATGCATGAGTACATGAGAAGGTACAACGTGCCAGCCACCCCTGATGGAGTGCAGTATCTGAAG

                2500                                                                                                2599
      3A  (2500) AATGATCCAGAGAAACTAGACGCCTTCATCATGGACAAAGCCCTTCTGGATTATGAAGTGTCAATAGATGCTGACTGCAAGCTTCTGACCGTAGGAAAGC
GluN3A_2  (501) AATGATCCAGAGAAACTAGACGCCTTCATCATGGACAAAGCCCTTCTGGATTATGAAGTGTCAATAGATGCTGACTGCAAGCTTCTGACCGTAGGAAAGC

                2600                                                                                                2699
      3A  (2600) CATTTGCCATCGAAGGATATGGCATTGGTCTCCCTCCAAACTCTCCATTGACCTCTAATATATCTGAGCTCATCAGTCAGTACAAGTCTCACGGGTTTAT
GluN3A_2  (601) CATTTGCCATCGAAGGATATGGCATTGGTCTCCCTCCAAACTCTCCATTGACCTCTAATATATCTGAGCTCATCAGTCAGTACAAGTCTCACGGGTTTAT

                2700                                                                                        2785
      3A  (2700) GGATGTGCTCCATGACAAGTGGTACAAGGTGGTTCCCTGCGGAAAGAGAAGCTTTGCCGTCACTGAGACTTTGCAAATGGGCATCA
GluN3A_2  (701) GGATGTGCTCCATGACAAGTGGTACAAGGTGGTTCCCTGCGGAAAGAGAAGCTTTGCCGTCACTGAGACTTTGCAAATGGGCATCA
```

Figure 38: Sequence alignment for GluN3A^{G703N} with 3A$^{w/t}$ using primer GluN3A_2.
Consensus differences are highlighted in yellow.

```
                1986                                                                                                2085
      3A  (1986) AGCAGCTCCAATTGGAGCCTTCATGTGGCCACTCCACTGGACCATGTGGCTGGGAATTTTCGTGGCTCTCCATATCACTGCCATTTTTCTCACTCTGTAT
GluN3A_2     (1) AGCAGCTCCAATTGGAGCCTTCATGTGGCCACTCCACTGGACCATGTGGCTGGGAATTTTCGTGGCTCTCCATATCACTGCCATTTTTCTCACTCTGTAT

                2086                                                                                                2185
      3A  (2086) GAATGGAAGAGCCCCTTTGGTATGACCCCTAAGGGGAGGAACAGAAACAAAGTCTTCTCCTTCTCCTCAGCTTTGAATGTCTGCTATGCCCTTCTGTTTG
GluN3A_2  (101) GAATGGAAGAGCCCCTTTGGTATGACCCCTAAGGGGAGGAACAGAAACAAAGTCTTCTCCTTCTCCTCAGCTTTGAATGTCTGCTATGCCCTTCTGTTTG

                2186                                                                                                2285
      3A  (2186) GCAGAACAGCAGCCATCAAACCCCCAAAATGCTGGACTGGAAGGTTTCTGATGAATCTTTGGGCCATTTTCTGTATGTTTTGCCTTTCTACATACACAGC
GluN3A_2  (201) GCAATACAGCAGCCATCAAACCCCCAAAATGCTGGACTGGAAGGTTTCTGATGAATCTTTGGGCCATTTTCTGTATGTTTTGCCTTTCTACATACACAGC

                2286                                                                                                2385
      3A  (2286) GAACTTGGCTGCTGTCATGGTAGGTGAGAAGATCTATGAAGAGCTTTCTGGAATTCATGACCCTAAGCTTCATCATCCTTCTCAAGGCTTCCGCTTTGGA
GluN3A_2  (301) GAACTTGGCTGCTGTCATGGTAGGTGAGAAGATCTATGAAGAGCTTTCTGGAATTCATGACCCTAAGCTTCATCATCCTTCTCAAGGCTTCCGCTTTGGA

                2386                                                                                                2485
      3A  (2386) ACTGTCCGGGAAAGCAGTGCTGAAGACTATGTGCGCCAGAGCTTCCCAGAGATGCATGAGTACATGAGAAGGTACAACGTGCCAGCCACCCCTGATGGAG
GluN3A_2  (401) ACTGTCCGGGAAAGCAGTGCTGAAGACTATGTGCGCCAGAGCTTCCCAGAGATGCATGAGTACATGAGAAGGTACAACGTGCCAGCCACCCCTGATGGAG

                2486                                                                                                2585
      3A  (2486) TGCAGTATCTGAAGAATGATCCAGAGAAACTAGACGCCTTCATCATGGACAAAGCCCTTCTGGATTATGAAGTGTCAATAGATGCTGACTGCAAGCTTCT
GluN3A_2  (501) TGCAGTATCTGAAGAATGATCCAGAGAAACTAGACGCCTTCATCATGGACAAAGCCCTTCTGGATTATGAAGTGTCAATAGATGCTGACTGCAAGCTTCT

                2586                                                                        2665
      3A  (2586) GACCGTAGGAAAGCCATTTGCCATCGAAGGATATGGCATTGGTCTCCCTCCAAACTCTCCATTGACCTCTAATATATCTG
GluN3A_2  (601) GACCGTAGGAAAGCCATTTGCCATCGAAGGATATGGCATTGGTCTCCCTCCAAACTCTCCATTGACCTCTAATATATCTG
```

Figure 39: Sequence alignment for GluN3A^{R704N} with 3A$^{w/t}$ using primer GluN3A_2.
Consensus differences are highlighted in yellow.

```
                1959                                                                                                2058
      3A  (1959) GGGGATCTTAGTGAGGACTCGAGACACAGCAGCTCCAATTGGAGCCTTCATGTGGCCACTCCACTGGACCATGTGGCTGGGAATTTTCGTGGCTCTCCAT
GluN3A_2    (1) GGGGATCTTAGTGAGGACTCGAGACACAGCAGCTCCAATTGGAGCCTTCATGTGGCCACTCCACTGGACCATGTGGCTGGGAATTTTCGTGGCTCTCCAT

                2059                                                                                                2158
      3A  (2059) ATCACTGCCATTTTTCTCACTCTGTATGAATGGAAGAGCCCCTTTGGTATGACCCCTAAGGGGAGGAACAGAAACAAAGTCTTCTCCTTCTCCTCAGCTT
GluN3A_2  (101) ATCACTGCCATTTTTCTCACTCTGTATGAATGGAAGAGCCCCTTTGGTATGACCCCTAAGGGGAGGAACAGAAACAAAGTCTTCTCCTTCTCCTCAGCTT

                2159                                                                                                2258
      3A  (2159) TGAATGTCTGCTATGCCCTTCTGTTTGGCAGAACAGCAGCCATCAAACCCCCAAAATGCTGGACTGGAAGGTTTCTGATGAATCTTTGGGCCATTTTCTG
GluN3A_2  (201) TGAATGTCTGCTATGCCCTTCTGTTTGGCGATACAGCAGCCATCAAACCCCCAAAATGCTGGACTGGAAGGTTTCTGATGAATCTTTGGGCCATTTTCTG

                2259                                                                                                2358
      3A  (2259) TATGTTTTGCCTTTCTACATACACAGCGAACTTGGCTGCTGTCATGGTAGGTGAGAAGATCTATGAAGAGCTTTCTGGAATTCATGACCCTAAGCTTCAT
GluN3A_2  (301) TATGTTTTGCCTTTCTACATACACAGCGAACTTGGCTGCTGTCATGGTAGGTGAGAAGATCTATGAAGAGCTTTCTGGAATTCATTACCCTAAGCTTCAT

                2359                                                                                                2458
      3A  (2359) CATCCTTCTCAAGGCTTCCGCTTTGGAACTGTCCGGGAAAGCAGTGCTGAAGACTATGTGCGCCAGAGCTTCCCAGAGATGCATGAGTACATGAGAAGGT
GluN3A_2  (401) CATCCTTCTCAAGGCTTCCGCTTTGGAACTGTCCGGGAAAGCAGTGCTGAAGACTATGTGCGCCAGAGCTTCCCAGAGATGCATGAGTACATGAGAAGGT

                2459                                                                                                2558
      3A  (2459) ACAACGTGCCAGCCACCCCTGATGGAGTGCAGTATCTGAAGAATGATCCAGAGAAACTAGACGCCTTCATCATGGACAAAGCCCTTCTGGATTATGAAGT
GluN3A_2  (501) ACAACGTGCCAGCCACCCCTGATGGAGTGCAGTATCTGAAGAATGATCCAGAGAAACTAGACGCCTTCATCATGGACAAAGCCCTTCTGGATTATGAAGT

                2559                                                                                                2658
      3A  (2559) GTCAATAGATGCTGACTGCAAGCTTCTGACCGTAGGAAAGCCATTTGCCATCGAAGGATATGGCATTGGTCTCCCTCCAAACTCTCCATTGACCTCTAAT
GluN3A_2  (601) GTCAATAGATGCTGACTGCAAGCTTCTGACCGTAGGAAAGCCATTTGCCATCGAAGGATATGGCATTGGTCTCCCTCCAAACTCTCCATTGACCTCTAAT

                2659                          2691
      3A  (2659) ATATCTGAGCTCATCAGTCAGTACAAGTCTCAC
GluN3A_2  (701) ATATCTGAGCTCATCAGTCAGTACAAGTCTCAC
```

Figure 40: Sequence alignment for GluN3A^{R704D} with 3A$^{w/t}$ using primer GluN3A_2. Consensus differences are highlighted in yellow.

3.2 cRNA Synthesis

In order to confirm if the restriction sites identified by bioinformatic analysis for linearisation of the plasmid cut only once, agarose gel electrophoresis was carried out. The subunits GluN1-1a, GluN2A, GluN3A and GluN3B were cut with the appropriate enzymes and all produced single bands (Figure 41). The RNA was then visualised and the bands that were produced were of the correct size (Figure 41).

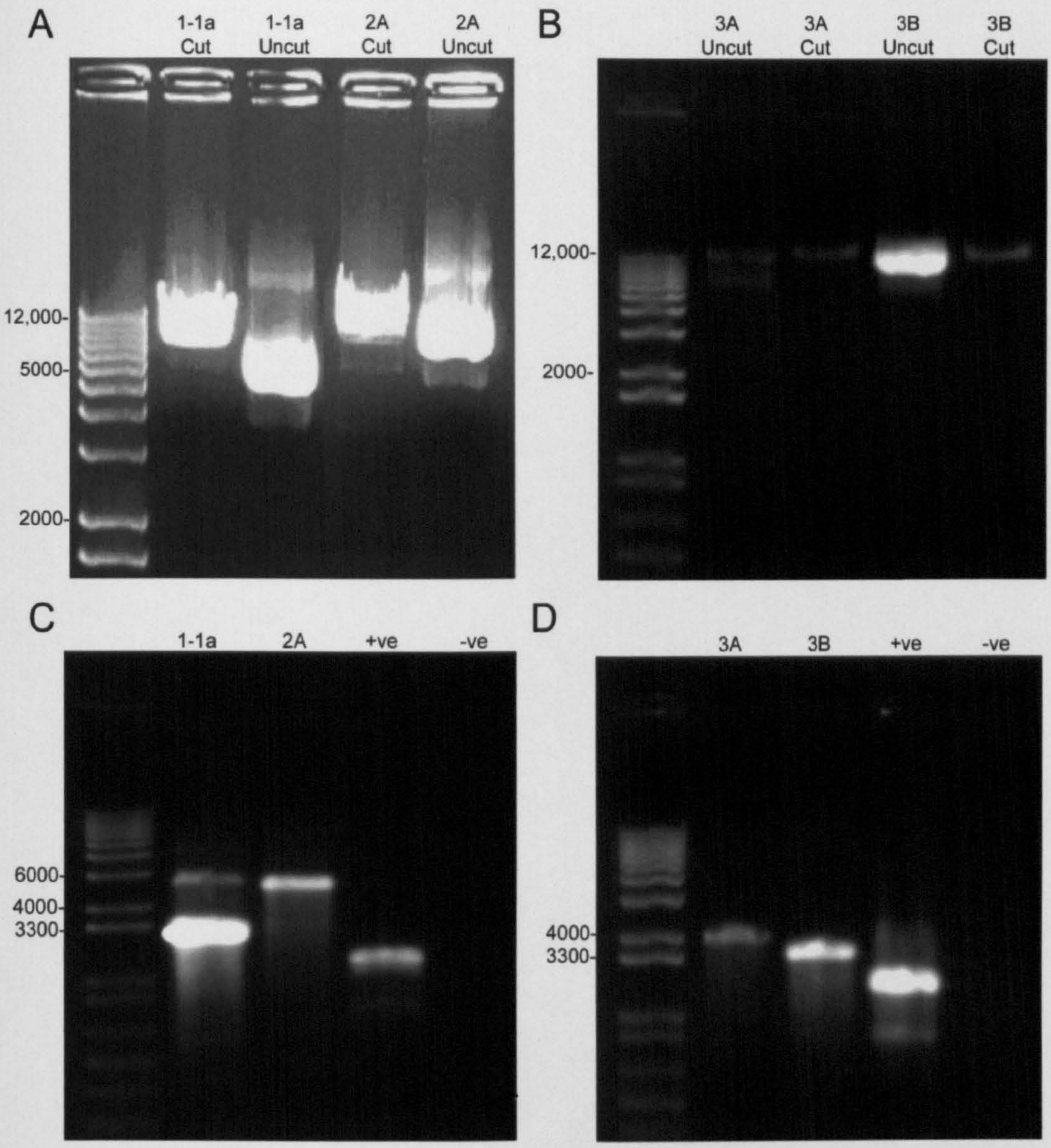

Figure 41: Agarose gel electrophoresis of NMDA receptor subunits. (A) GluN1 and GluN2 DNA single digest. Lanes show ladder, GluN1-1a cut with BamHI, GluN1-1a uncut plasmid, GluN2A cut with EcoRI and GluN2A uncut plasmid. (B) GluN3A and GluN3B DNA single digest. Lanes show 1kbplus ladder, GluN3A uncut, GluN3A cut with NotI, GluN3B uncut and GluN3B cut with XbaI. (C) GluN1 and GluN2 RNA. Lanes showing 1kb plus DNA ladder and cRNA from GluN1-1a, 2A, +ve and –ve controls. (D) GluN3A and GluN3B RNA. Lanes showing 1kb plus DNA ladder and cRNA from 1-1a, 2A, +ve and –ve controls.

3.3 Agonist

Concentration-response data for NMDA, using 10 μM glycine as a co-agonist, were used to estimate EC_{50} at 1-1a/2A, 3A and 3B receptors (Figure 42, Figure 43, Table 7). The EC_{50} for NMDA was not significantly different at all subunit combinations tested (between 5 and 10 μM). The EC_{50} for glycine was determined using 100 μM NMDA (Figure 43, Table 7). The presence of 3A and 3B produced EC_{50} values for glycine that were not significantly different to each other, but were now significantly lower than 1-1a/2A. At 10 μM glycine and 100 μM NMDA the maximum response was elicited, while at concentrations above this efficacy was reduced. Therefore, 10 μM glycine and 100 μM NMDA were considered maximal and were used to elicit responses for the remainder of the study.

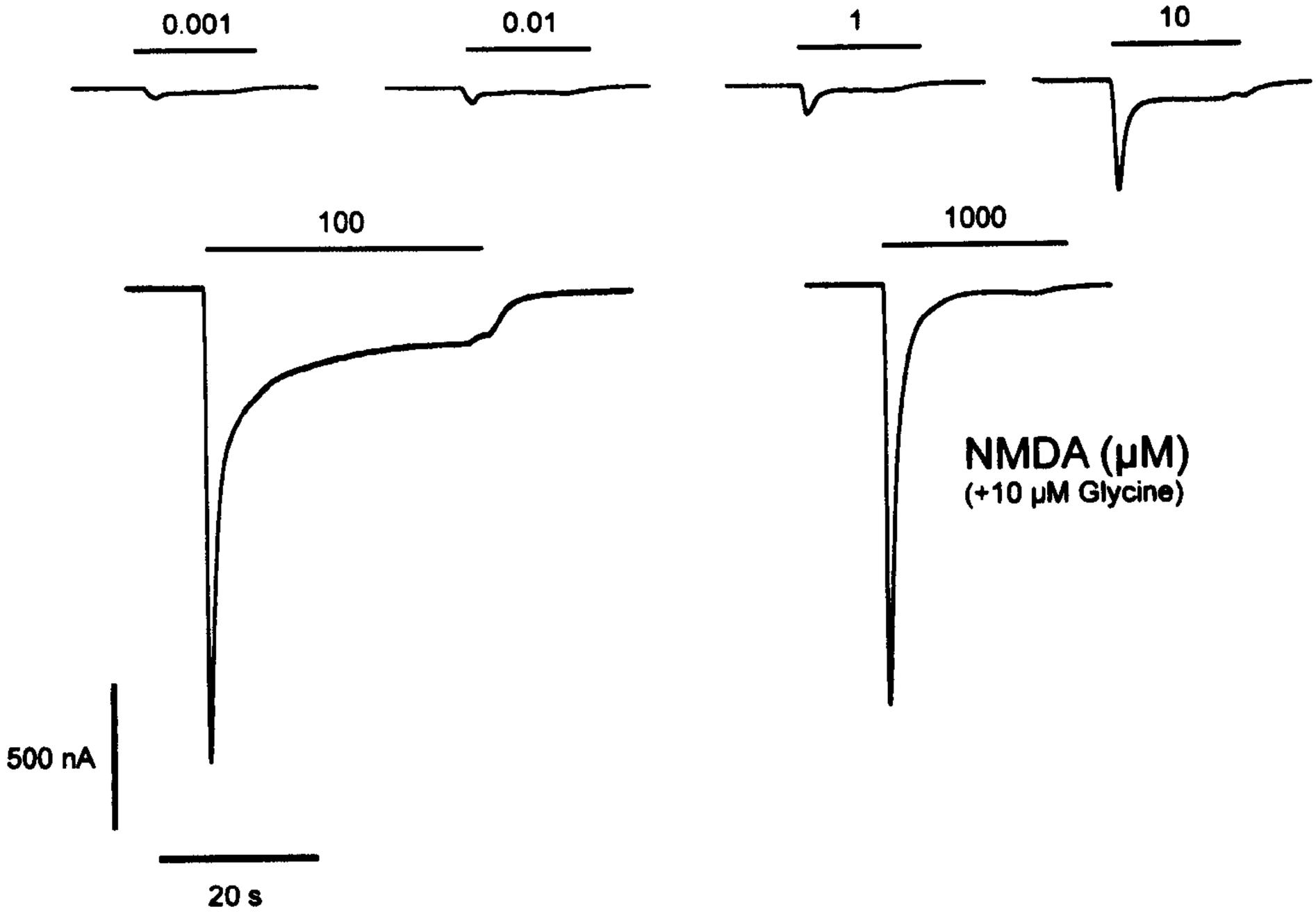

Figure 42: TEVC current recording of increasing concentrations of NMDA currents mediated by 1-1a/2A containing NMDA receptors at -50 mV. Shown are responses to increasing concentrations of NMDA in the presence of 10 μM Glycine.

Subunit	Agonist EC_{50} (95% CI) µM	
	NMDA	Glycine
1-1a/2A	**8.46** 4.90 to 14.60	**1.27** 0.67 to 2.39
3A	**10.58** 6.65 to 16.82 *P=0.3118	**0.37** 0.24 to 0.58 ***P<0.001**
3B	**5.66** 2.34 to 13.72 *P=0.458 †P=0.225	**0.44** 0.19 to 0.99 ***P<0.001** †P=0.654

Table 7: EC_{50} (95% CI) values for NMDA and glycine at 1-1a/2A, 3A and 3B containing NMDA receptors. * denotes statistical significance against 1-1a/2A and † denotes significance against 3A.

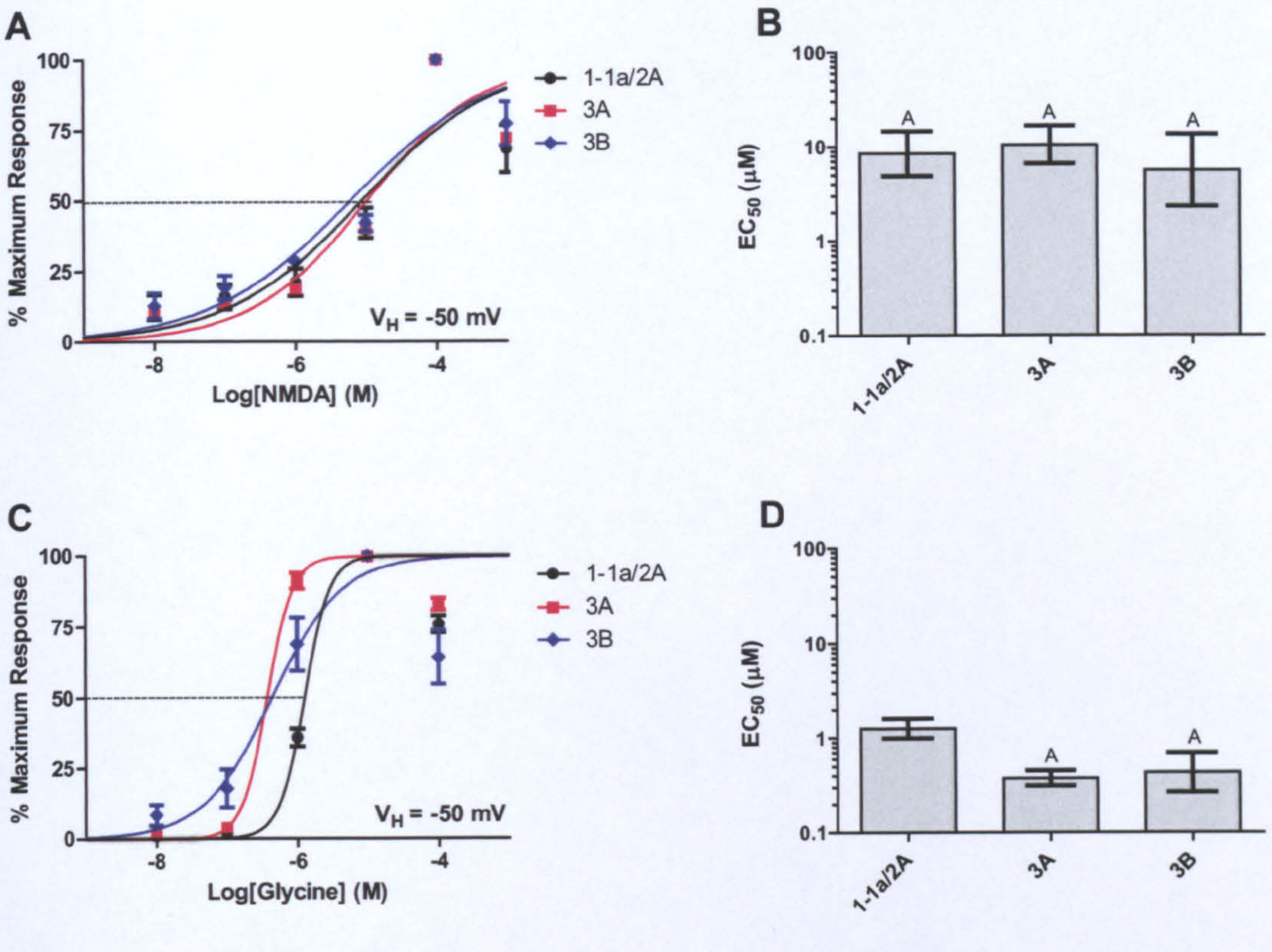

Figure 43: Concentration response relationship for NMDA and glycine in 1-1a/2A, 3A and 3B containing NMDA receptors at -50 mV. % control response (mean ± S.E.M, n=3-8) values were plotted and fitted with the Hill equation (A, C to give estimates of EC_{50} (B, D). NMDA EC_{50} was calculated using 10 µM glycine, while the glycine EC_{50} was calculated using 100 µM NMDA. Bars show EC_{50} (95% CI) µM. Groups that do not share a letter are statistically significant.

3.4 Wild-type

3.4.1 I/V Relationship

I/V relationships were produced from voltage steps between -125 and -0 mV (Figure 44). These were then used to produce the mean at each voltage and were fitted with a linear equation to give the reversal potential (Figure 45). For 1-1a/2A in 2 mM Ca^{2+} V_R = 12.15 (95% CI -19.37 to 43.68) mV and was reduced with 3A containing receptors to V_R = -2.646 (95% CI -16.89 to 11.60) mV.

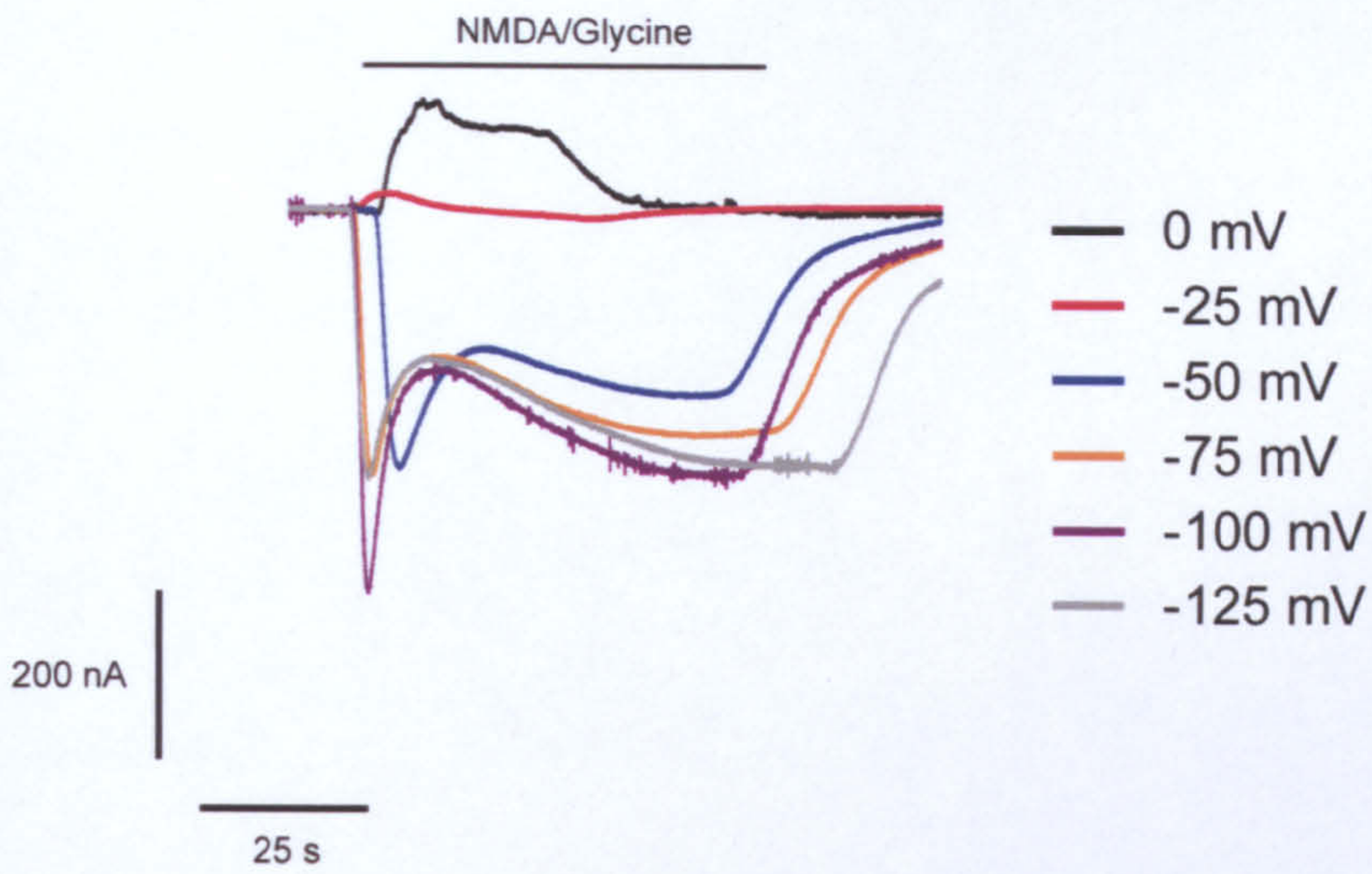

Figure 44: TEVC current recording of NMDA/glycine currents mediated by 1-1a/2A containing NMDA receptors at 0 to -125 mV. Recordings were made from one individual oocyte.

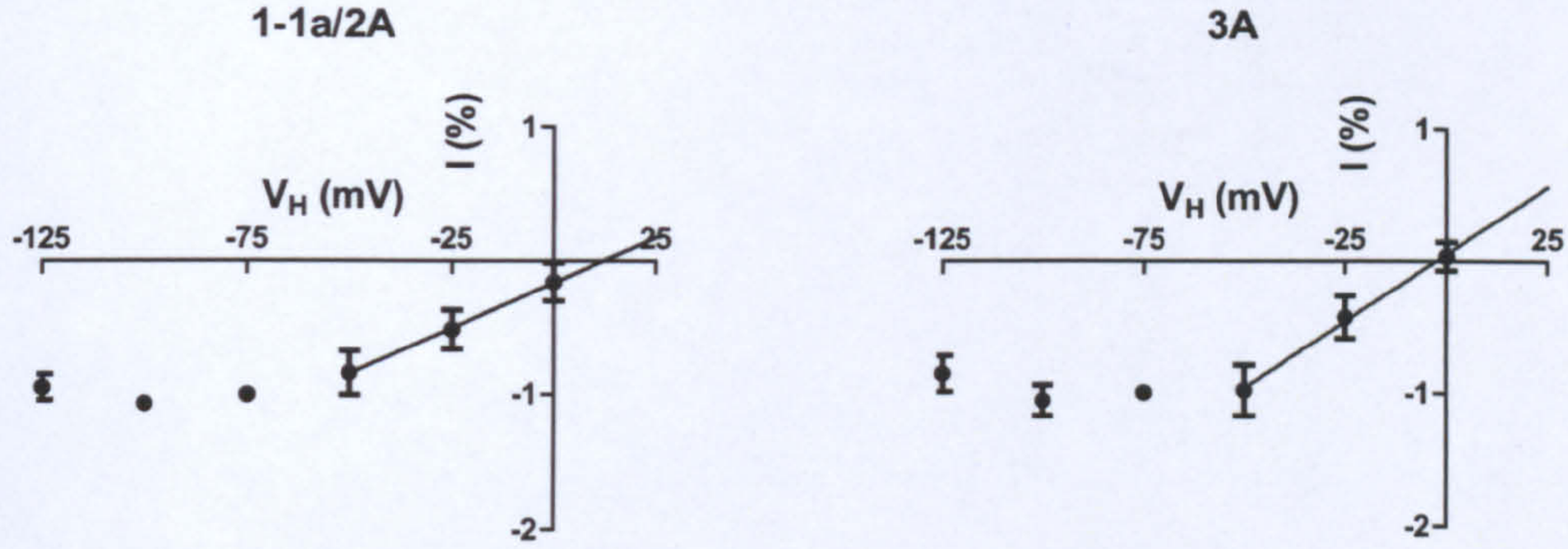

Figure 45: I/V relationship 1-1a/2A and 3A receptors. Discrete voltage steps between -100 and 0 mV normalised to current at -75 mV (mean ± S.E.M., n=4-8).

3.4.2 Steady-State Current

The steady state current for each oocytes response was established for each oocyte (Figure 46). In order to determine if the presence of the GluN3 subunits had any effect on inward current, two-way ANOVA was carried out (Figure 47). Post-hoc analysis using the Bonferroni test for multiple comparisons revealed that there was a significant reduction in current for 3A ($P<0.001$) and 3B ($P<0.001$) compared with 1-1a/2A, and no difference between the GluN3 subunits at all voltages tested.

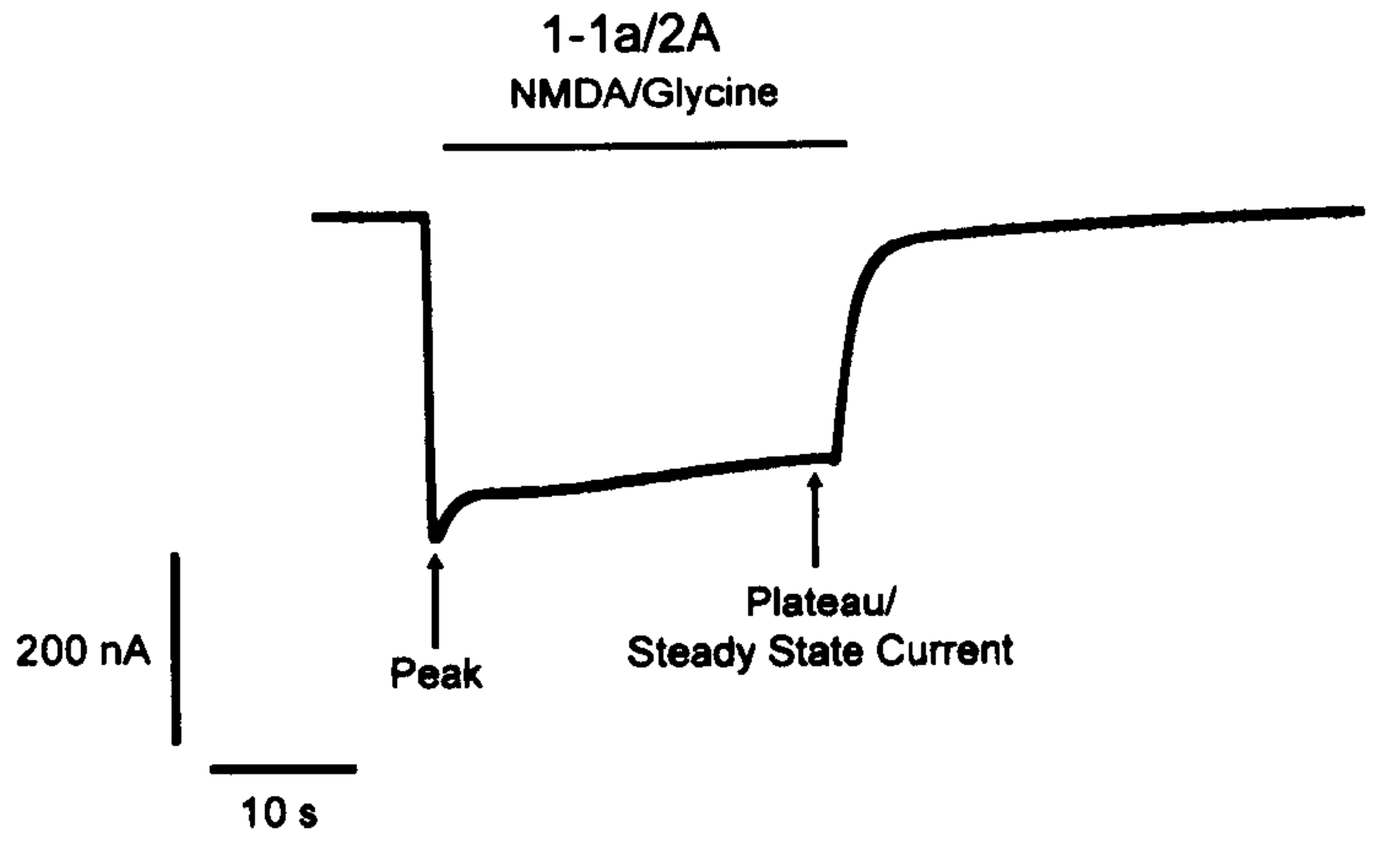

Figure 46: Location on recording trace where peak and plateau measurements were taken. Response from Xenopus oocytes expressing 1-1a/2A NMDA receptors in response to NMDA/glycine. Steady state current is highlighted and is the level at which current was compared between subunits. The peak current level was used to calculate the peak/plateau ratio for section 3.4.3.

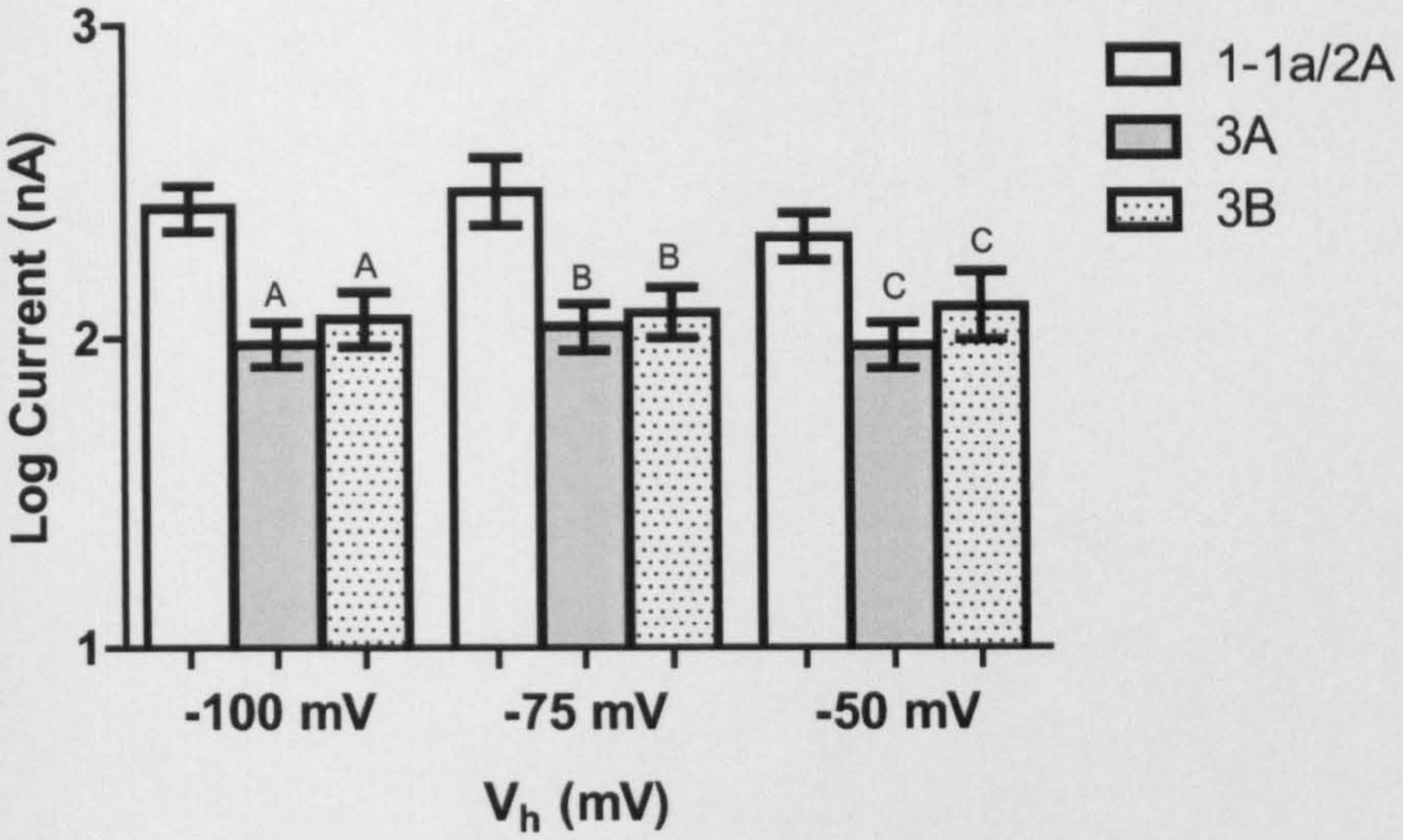

Figure 47: Effect of subunit and voltage on steady-state current recorded for 1-1a/2A, 3A and 3B NMDA receptors. Bars represent mean (95% CI, n=40-85) log current (nA). Two-way ANOVA subunit (P<0.001), voltage (P=0.198) subunit x voltage interaction (P=0.353). Within a voltage, bars that do not share a letter are significantly different (Bonferroni P<0.05).

3.4.3 Peak/Plateau Ratio

The ratio of peak current to steady state response was measured for 1-1a/2A, 3A and 3B containing receptors at -100, -75 and -50 mV (Figure 48). Numbers tending toward one indicate no difference between the peak and plateau levels. At -100 mV the Kruskal-Wallis test showed a significant effect of subunit on ratio (P<0.001). Post hoc testing using Dunn's Multiple Comparison Test found that the ratio at 3A and 3B were not significantly different to each other, but there was a significant reduction in the ratio for 3A and 3B (both P<0.001) compared with 1-1a/2A at -100 mV. At -75 mV there was a significant effect of subunit (P<0.001) and post-hoc testing found again that 3A and 3B (both P<0.001) significantly reduced the ratio compared with 1-1a/2A. However, it was found that at this voltage 3A was significantly lower than 3B (P<0.01). At -50 mV the same pattern was found as -100 mV.

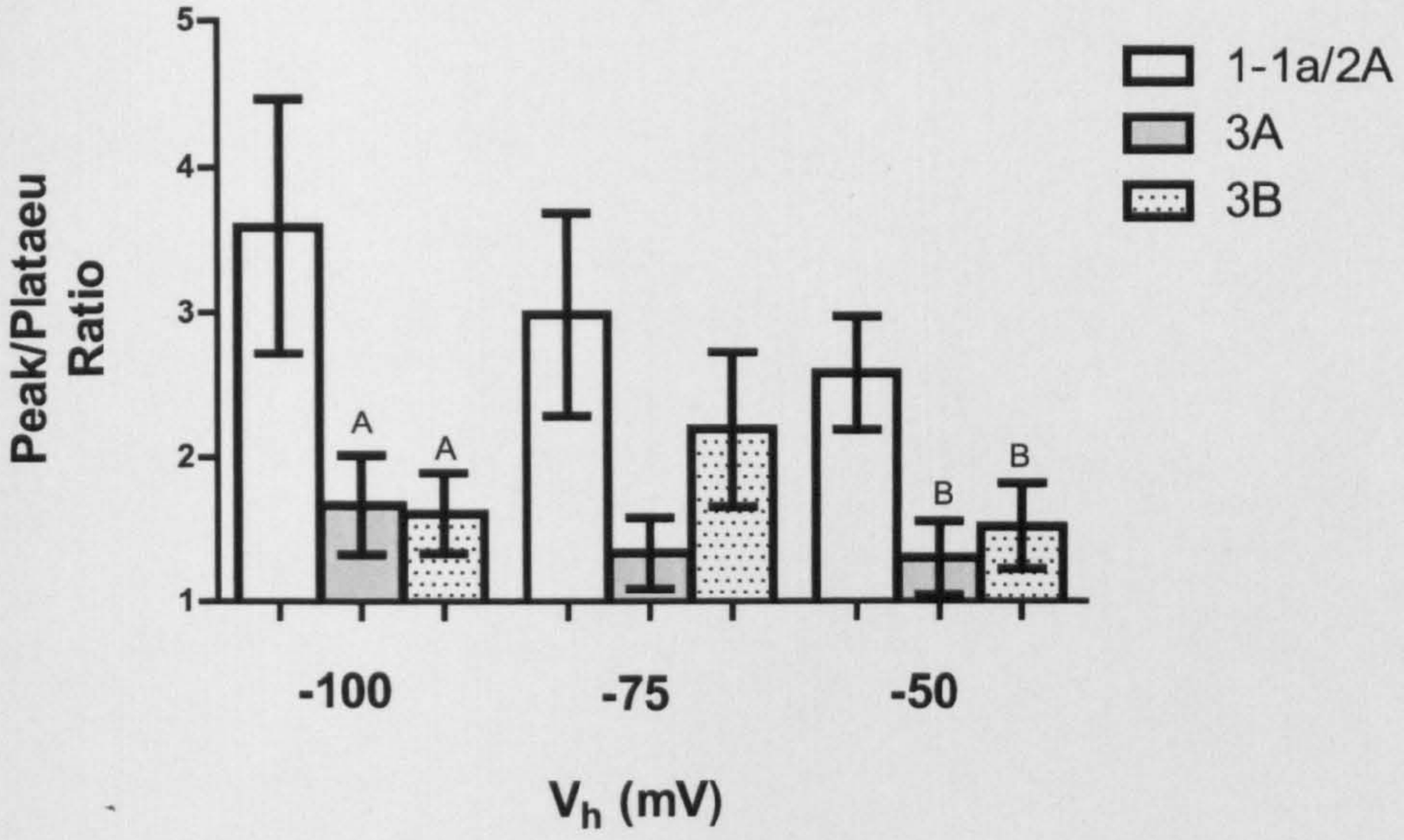

Figure 48: Effect of subunit on Peak/Plateau ratio. Bars show mean ratio (95% CI, n=40-85). Kruskal-Wallis test, subunit (P<0.001). Within a voltage, bars that do not share a letter are significantly different. PostHoc Dunn's Multiple Comparison Test (P<0.05).

3.4.4 Glycine Activation

It was found that 1 mM glycine, and 1 mM glycine with 1 mM Zn^{2+}, did not activate 3A containing receptors. When NMDA/glycine was applied the receptors showed inward current as expected (Figure 49).

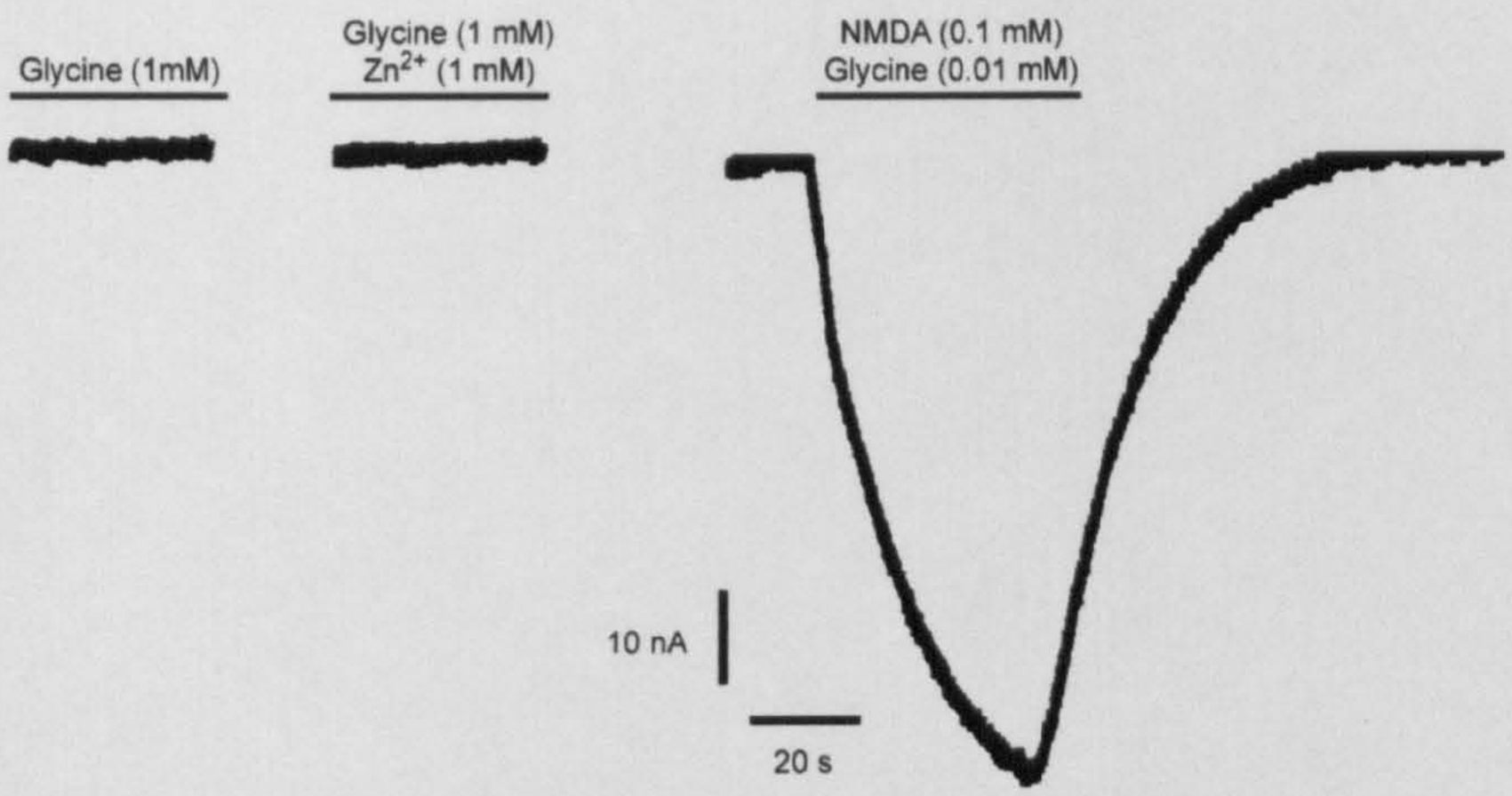

Figure 49: TEVC current recording of attempted glycine activation of currents mediated by 3A containing NMDA receptors at -50 mV. Recordings were made from the same oocyte.

3.4.5 NMDA Receptor Antagonism

Block by increasing concentrations of Mg^{2+} of NMDA/glycine responses for 1-1a/2A, 3A and 3B containing receptors were used to calculate the IC_{50} (Figure 50, Table 8). At all voltages, block by Mg^{2+} at 1-1a/2A had the lowest IC_{50} which was significantly lower than 3A and 3B. 3A had an intermediate IC_{50} for Mg^{2+} which was significantly lower than 3B. These data gave a subunit order of IC_{50} for Mg^{2+} at all voltages of as 1-1a/2A<3A<3B.

	IC_{50} (95% CI) µM		
Voltage (mV)	**1a/2A**	**3A**	**3B**
-100	**1.74** 1.48 to 20.44	**5.83** 4.99 to 6.81 ***P<0.001**	**15.74** 12.09 to 20.50 ***P<0.001** **†P<0.001**
-75	**4.23** 3.48 to 5.13	**22.35** 19.00 to 26.29 ***P<0.001**	**40.07** 30.14 to 53.28 ***P<0.001** **†P<0.001**
-50	**16.03** 12.77 to 20.12	**25.77** 1.92 to 3.46 ***P<0.001**	**71.59** 55.71 to 92.01 ***P<0.001** **†P<0.001**

Table 8: IC_{50} values for Mg^{2+} block of NMDA/glycine responses at 1-1a/2A, 3A and 3B containing NMDA receptors. * denotes statistical significance against 1-1a/2A and † denotes significance against 3A.

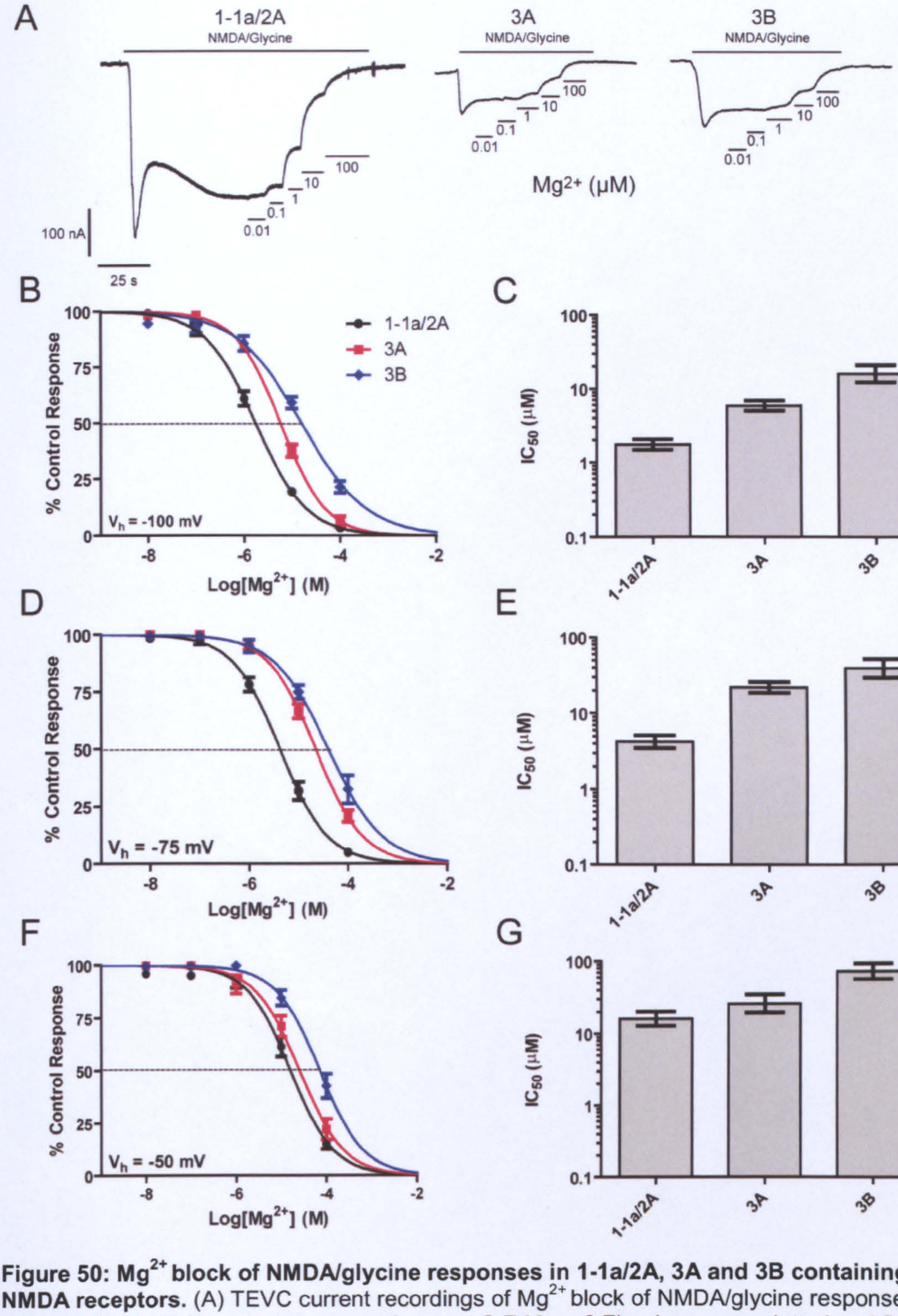

Figure 50: Mg^{2+} block of NMDA/glycine responses in 1-1a/2A, 3A and 3B containing NMDA receptors. (A) TEVC current recordings of Mg^{2+} block of NMDA/glycine responses at -100 mV. (B, D, F) % control response (mean ± S.E.M, n=6-7) values were plotted and fitted with the Hill equation to give estimates of IC_{50} (C, -100 mV; E, -75 mV; G, -50 mV). Bars show IC_{50} (95% CI) μM. Groups that do not share a letter are significantly different.

The IC_{50} for memantine was then calculated (Figure 51, Table 9). At -100 and -75 mV 1-1a/2A had the lowest IC_{50} (0.80 and 2.48 μM respectively) which was significantly lower than 3A and 3B. Memantine block of 3A had an intermediate IC_{50} which was significantly lower than 3B. The subunit order of IC_{50} for memantine at -100 and -75 mV was 1-1a/2A<3A<3B. At -50 mV 1-1a/2A had the lowest IC_{50}, which was significantly lower than 3A and 3B, but at this voltage 3A was not significantly different to that of 3B. The subunit order of IC_{50} at -50 mV was 1a/2A<3A≈3B.

	IC_{50} (95% CI) μM		
Voltage (mV)	**1a/2A**	**1a/2A/3A**	**1a/2A/3B**
-100	**0.80** 0.64 to 0.99	**2.55** 1.75 to 3.74 ***P<0.001**	**17.77** 8.49 to 37.20 ***P<0.001** **†P<0.001**
-75	**2.48** 2.04 to 3.02	**7.54** 6.27 to 9.07 ***P<0.001**	**17.54** 11.42 to 26.94 ***P<0.001** **†P<0.001**
-50	**3.94** 3.46 to 4.49	**15.89** 12.13 to 20.82 ***P<0.001**	**18.23** 12.51 to 26.56 ***P<0.001** †P<0.548

Table 9: IC_{50} values for memantine block of NMDA/glycine responses at 1-1a/2A, 3A and 3B containing NMDA receptors. * denotes statistical significance against 1-1a/2A and † denotes significance against 3A.

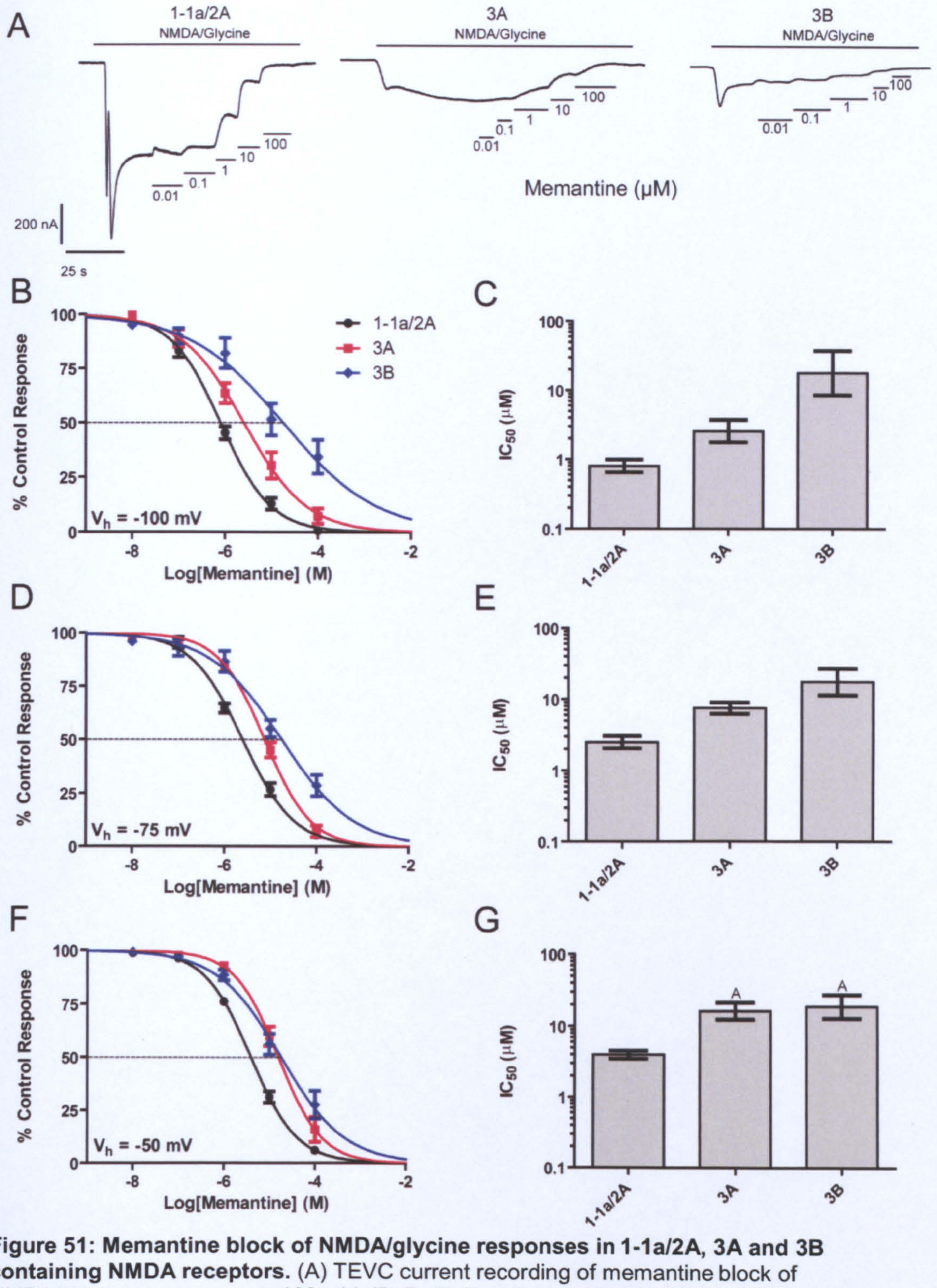

Figure 51: Memantine block of NMDA/glycine responses in 1-1a/2A, 3A and 3B containing NMDA receptors. (A) TEVC current recording of memantine block of NMDA/glycine responses at -100 mV. (B, D, F) % control response (mean ± S.E.M, n=6-9) values were plotted and fitted with the Hill equation to give estimates of IC_{50} (C, -100 mV; E, -75 mV; G, -50 mV. Bars show IC_{50} (95% CI) μM. Groups that do not share a letter are significantly different.

The IC_{50} for PhTX-343 was then established for all subunit combinations (Figure 52, Table 10). At -100 mV 1-1a/2A had the lowest IC_{50} which was significantly lower than 3A and 3B, but both the GluN3 containing receptors were not significantly different to each other. The subunit order of IC_{50} was 1a/2A<3A≈3B. At -75 mV no significant differences were found between all receptor subtype combinations tested. At -50 mV the IC_{50} at 3B significantly increased relative to both 1-1a/2A and 3A, while no significant difference between 1-1a/2A and 3A was found. The subunit order of IC_{50} was 1a/2A≈3A<3B at -50 mV.

	IC_{50} (95% CI) μM		
Voltage (mV)	**1a/2A**	**3A**	**3B**
-100	**0.30** 0.21 to 0.44	**1.40** 0.83 to 2.37 ***P<0.001**	**0.93** 0.63 to 1.36 ***P=0.001** †P=0.205
-75	**2.95** 1.57 to 5.54	**4.64** 3.10 to 6.94 *P=0.213	**5.74** 3.84 to 8.59 *P=0.065 †P=0.467
-50	**17.22** 9.19 to 32.27	**17.28** 8.72 to 34.25 *P=0.994	**62.80** 40.11 to 98.31 ***P=0.001** **†P=0.003**

Table 10: IC_{50} values for PhTX-343 block of NMDA/glycine responses at 1-1a/2A, 3A and 3B containing NMDA receptors. * denotes statistical significance against 1-1a/2A and † denotes significance against 3A.

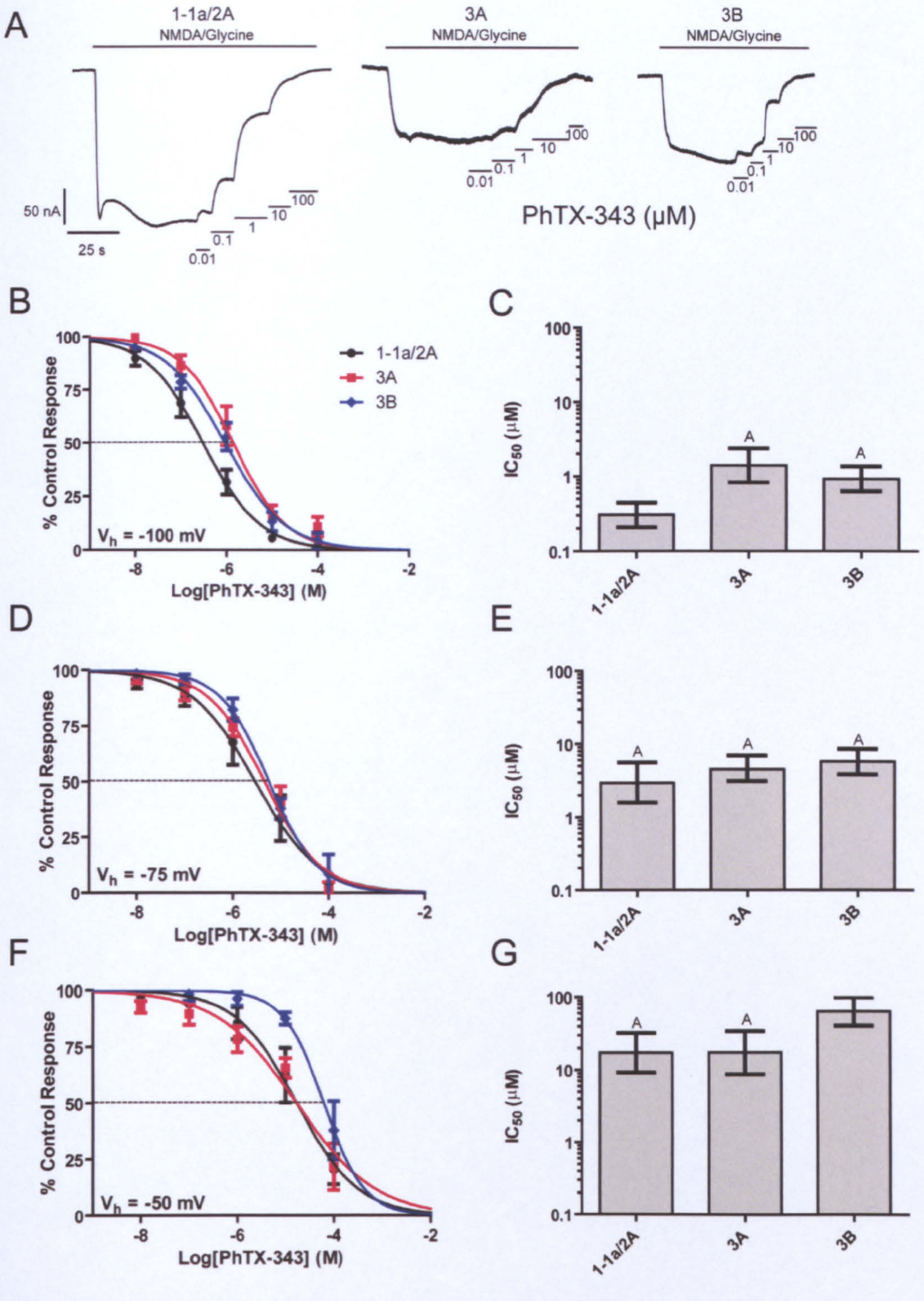

Figure 52: PhTX-343 block of NMDA/glycine responses in 1-1a/2A, 3A and 3B containing NMDA receptors. (A) TEVC current recording of PhTX-343 block of NMDA/glycine responses at -100 mV. (B, D, F) % control response (mean ± S.E.M, n=6-11) values were plotted and fitted with the Hill equation to give estimates of IC_{50} (C, -100 mV; E, -75 mV; G, -50 mV). Bars show IC_{50} (95% CI) μM. Groups that do not share a letter are significantly different.

The IC_{50} for methoctramine was calculated for at all subunit combinations (Figure 53, Table 11). At -100 mV, methoctramine had the lowest IC_{50} at 1-1a/2A which was significantly lower than at 3A and 3B, but the IC_{50} for methoctramine at both GluN3 containing receptors were not significantly different. This gave a subunit order of IC_{50} as 1a/2A<3A≈3B. At -75 mV 1-1a/2A and 3A were not significantly different to each other, but the IC_{50} for methoctramine at 3B increased so it was now significantly higher than 1-1a/2A and 3A. The subunit order of methoctramine IC_{50} was 1a/2A≈3A<3B at -75 mV. At -50 mV there were no significant differences between all the subunits combinations tested.

	IC_{50} (95% CI) μM		
Voltage (mV)	**1a/2A**	**3A**	**3B**
-100	**1.42** 0.98 to 2.05	**2.78** 2.33 to 3.32 ***P=0.003**	**3.07** 2.33 to 4.05 ***P=0.001** †P=0.574
-75	**1.94** 1.25 to 3.01	**2.63** 2.04 to 3.40 *P=0.252	**4.81** 3.43 to 6.74 ***P=0.002** **†P=0.006**
-50	**5.36** 3.83 to 7.50	**5.29** 3.68 to 7.61 *P=0.959	**4.69** 4.09 to 5.36 *P=0.537 †P=0.472

Table 11: IC_{50} values for methoctramine block of NMDA/glycine responses at 1-1a/2A, 3A and 3B containing NMDA receptors. * denotes statistical significance against 1-1a/2A and † denotes significance against 3A.

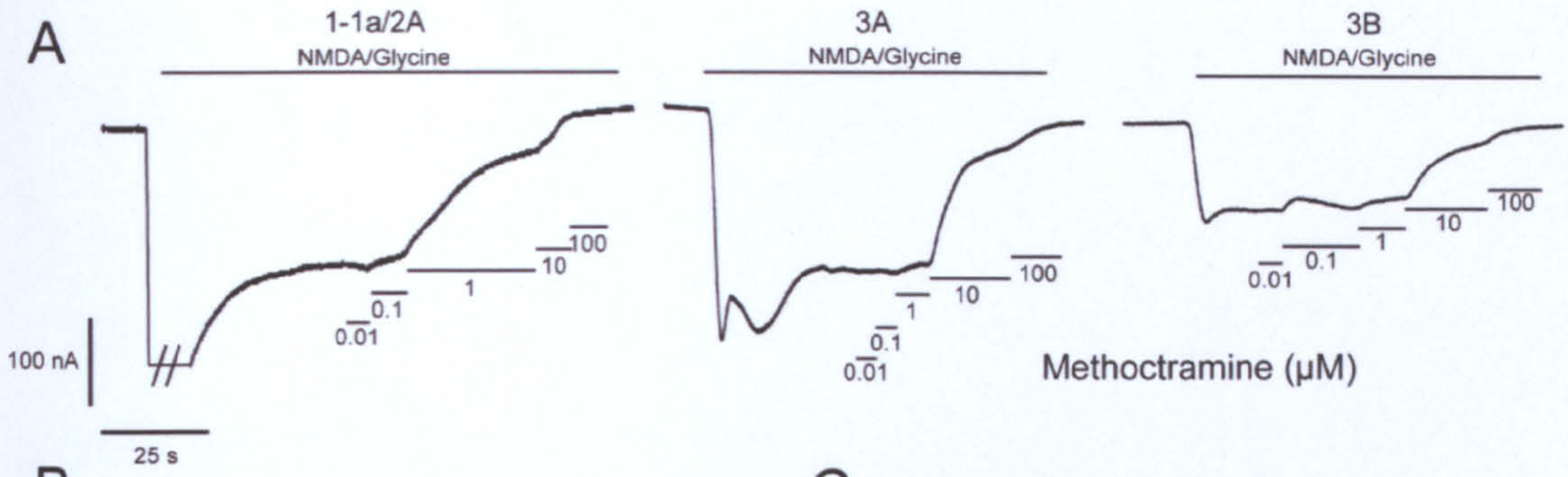

Figure 53: Methoctramine block of NMDA/glycine responses in 1-1a/2A, 3A and 3B containing NMDA receptors. (A) TEVC current recording of methoctramine block of NMDA/glycine responses at -100 mV. (B, D, F) % control response (mean ± S.E.M, n=5-8) values were plotted and fitted with the Hill equation to give estimates of IC_{50} (C, -100 mV; E, -75 mV; G, -50 mV). Bars show IC_{50} (95% CI) μM. Groups that do not share a letter are significantly different.

IC_{50} values for MK-801 inhibition were calculated (Figure 54, Table 12). At -100 mV 1-1a/2A had the lowest IC_{50} which was significantly lower than 3A and 3B, but 3A and 3B were not significantly different. This gave a subunit order of MK-801 IC_{50} as 1a/2A<3A≈3B. At -75 mV 1-1a/2A had an IC_{50} for MK-801 that was not significantly different to 3A, but the IC_{50} at 3B was increased so that it was significantly higher than both 1-1a/2A and 3A. At -75 the rank order of methoctramine IC_{50} was 1a/2A≈3A<3B. At -50 mV the same pattern was found as at 75 mV.

	IC_{50} (95% CI) μM		
Voltage (mV)	**1a/2A**	**3A**	**3B**
-100	**0.193** 0.12 to 0.31	**0.46** 0.40 to 0.54 ***P<0.001**	**0.68** 0.34 to 1.39 ***P=0.003** †P=0.212
-75	**0.21** 0.13 to 0.34	**0.31** 0.21 to 0.45 *P=0.204	**2.19** 0.97 to 4.96 ***P<0.001** **†P<0.001**
-50	**0.50** 0.29 to 0.85	**0.49** 0.37 to 0.64 *P=0.94	**3.56** 1.98 to 6.38 ***P<0.001** **†P<0.001**

Table 12: IC_{50} values for MK-801 block of NMDA/glycine responses at 1-1a/2A, 3A and 3B containing NMDA receptors. * denotes statistical significance against 1-1a/2A and † denotes significance against 3A.

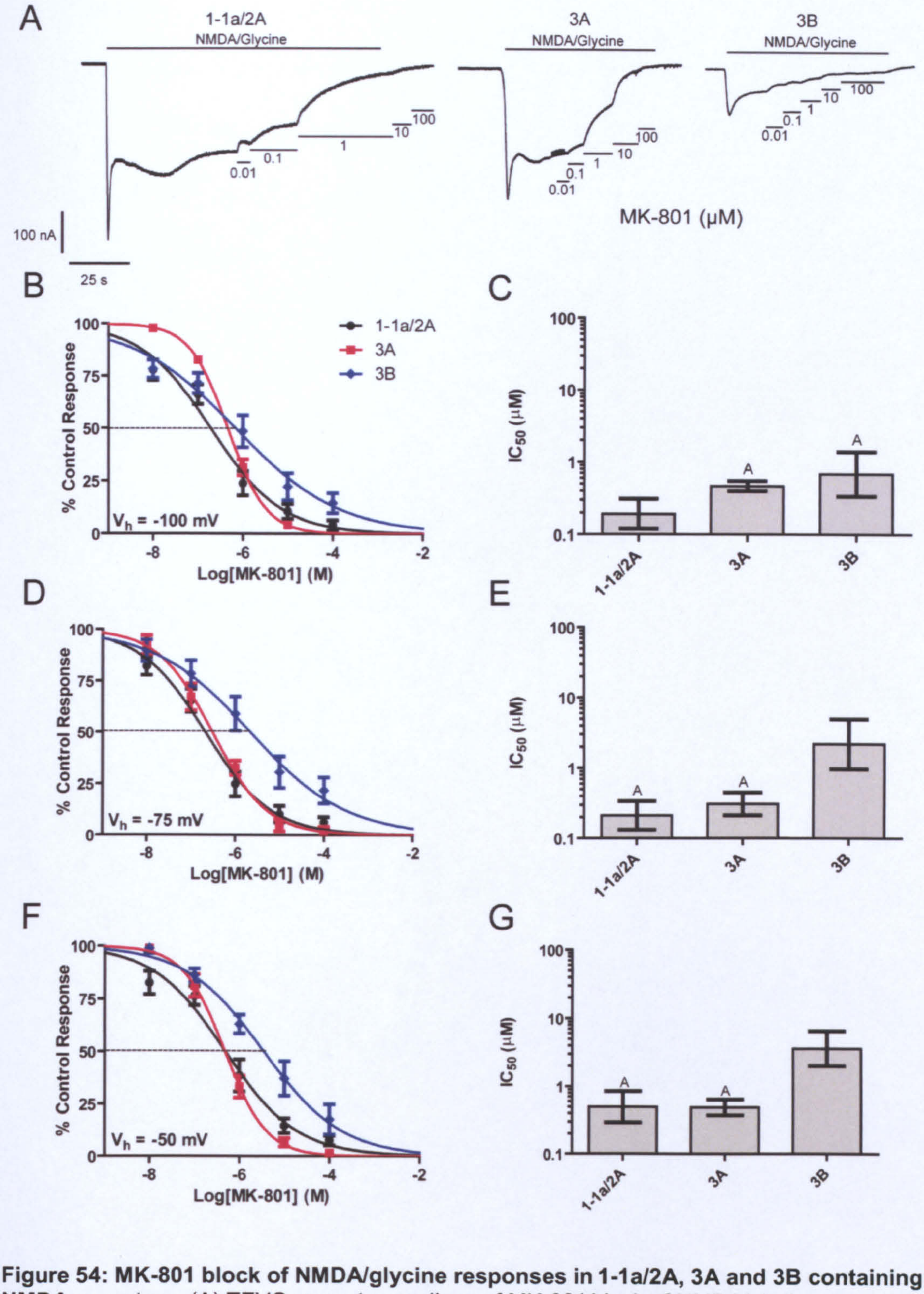

Figure 54: MK-801 block of NMDA/glycine responses in 1-1a/2A, 3A and 3B containing NMDA receptors. (A) TEVC current recordings of MK-801 block of NMDA/glycine responses at -100 mV. (B, D, F) % control response (mean ± S.E.M, n=5-7) values were plotted and fitted with the Hill equation to give estimates of IC_{50} (C, -100 mV; E, -75 mV; G, -50 mV). Bars show IC_{50} (95% CI) μM. Groups that do not share a letter are significantly different.

Concentration-inhibition data was used to produce IC_{50} values for PhTX-12 inhibition (Figure 55, Table 13). At -100 mV 3A had the lowest IC_{50} which was significantly lower than both 1-1a/2A and 3B. The IC_{50} for 1-1a/2A was not significantly different to 3B. This gave a subunit order of IC_{50} as 3A<1a/2A≈3B. At -75 mV the pattern remained; however, at – 50 mV the IC_{50} values for PhTX-12 were now not significantly different to each other for any subunit combination.

	IC_{50} (95% CI) µM		
Voltage (mV)	**1a/2A**	**3A**	**3B**
-100	**164.90** 127.30 to 213.50	**77.47** 45.99 to 130.50 ***P=0.014**	**157.00** 122.80 to 200.60 *P=0.779 **†P=0.023**
-75	**293.60** 209.00 to 412.40	**122.30** 75.57 to 200.50 ***P=0.031**	**402.30** 191.00 to 847.30 *P=0.390 **†P=0.033**
-50	**734.50** 348.20 to 155.00	**433.90** 144.90 to 129.90 *P=0.466	**476.00** 134.40 to 168.60 *P=0.912 †P=0.602

Table 13: IC_{50} values for PhTX-12 block of NMDA/glycine responses at 1-1a/2A, 3A and 3B containing NMDA receptors. * denotes statistical significance against 1-1a/2A and † denotes significance against 3A.

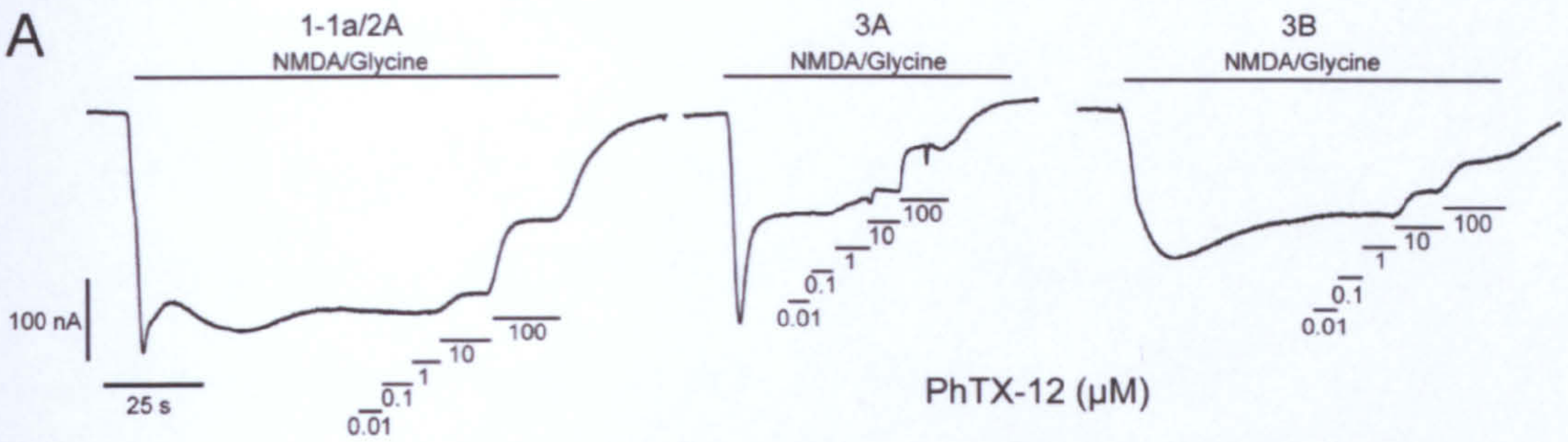

Figure 55: PhTX-12 block of NMDA/glycine responses in 1-1a/2A, 3A and 3B containing NMDA receptors. (A) TEVC current recordings of PhTX-12 block of NMDA/glycine responses at -100 mV. (B, D, F) % control response (mean ± S.E.M, n=6) values were plotted and fitted with the Hill equation to give estimates of IC_{50} (C, -100 mV; E, -75 mV; G, -50 mV). Bars show IC_{50} (95% CI) μM (note altered y-axis scale). Groups that do not share a letter are significantly different.

3.4.6 Voltage Dependence

Concentration-inhibition values were fitted with the Hill equation for Mg^{2+}, memantine, PhTX-343 methoctramine, MK-801 and PhTX-12 at the range of voltages tested for 1-1a/2A NMDA receptors (Figure 56). There was a significant ($P<0.001$), effect of voltage on the IC_{50} all the blockers.

Voltage was then determined for 3A receptors (Figure 57). There was a significant effect of voltage on IC_{50} for Mg^{2+} ($P<0.001$), memantine ($P<0.001$), PhTX-343 ($P<0.001$), methoctramine ($P=0.001$) and MK-801 ($P=0.046$). At 3A block by PhTX-12 was not voltage-dependent ($P=0.174$). Voltage-dependence was also tested at 3B containing receptors (Figure 58). There was a significant effect of voltage on IC_{50} for Mg^{2+} ($P<0.001$), PhTX-343 ($P<0.001$), methoctramine ($P=0.025$) and MK-801 ($P=0.002$). At 3B block by memantine ($P=0.987$) and PhTX-12 ($P=0.629$) were not voltage-dependent.

The δ value from the Woodhull equation was calculated for 1a/2A, 3A and 3B containing NMDA receptors (Figure 59, Table 14). Mg^{2+} showed a decrease in δ for 3A and 3B compared with 1-1a/2A. Memantine showed an increase in δ for 3A compared with 1-1a/2A, whereas 3B showed a large decrease. For PhTX-343 it was found that there was a decrease in δ for 3A, but an increase with 3B compared with 1-1a/2A. Methoctramine showed a decrease with 3A compared with 1-1a/2A, and there was a further decrease with 3B. MK-801 showed a large decrease with 3A, but an increase with 3B compared with 1-1a/2A. PhTX-12 showed no change between 3A and 1-1a/2A, but a decrease with 3B.

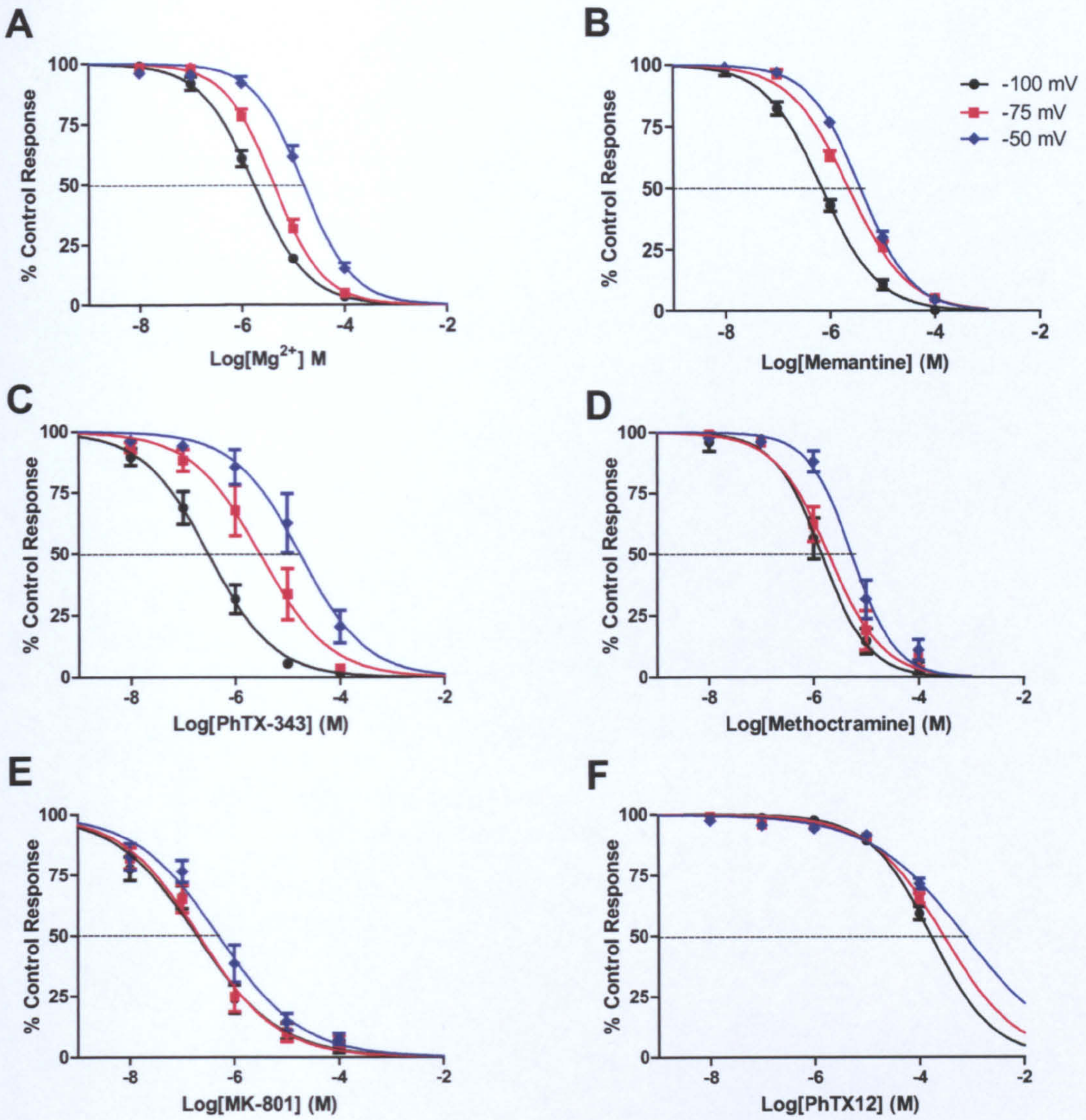

Figure 56: Concentration inhibition relationship showing block of NMDA-glycine-evoked responses mediated by 1-1a/2A NMDA receptors at -100, -75 and -50 mV. % control response (mean ± S.E.M) values were plotted and fitted with the Hill equation for (A) Mg^{2+}, (B) memantine, (C) PhTX-343, (D) methoctramine, (E) MK-801 and (F) PhTX-12.

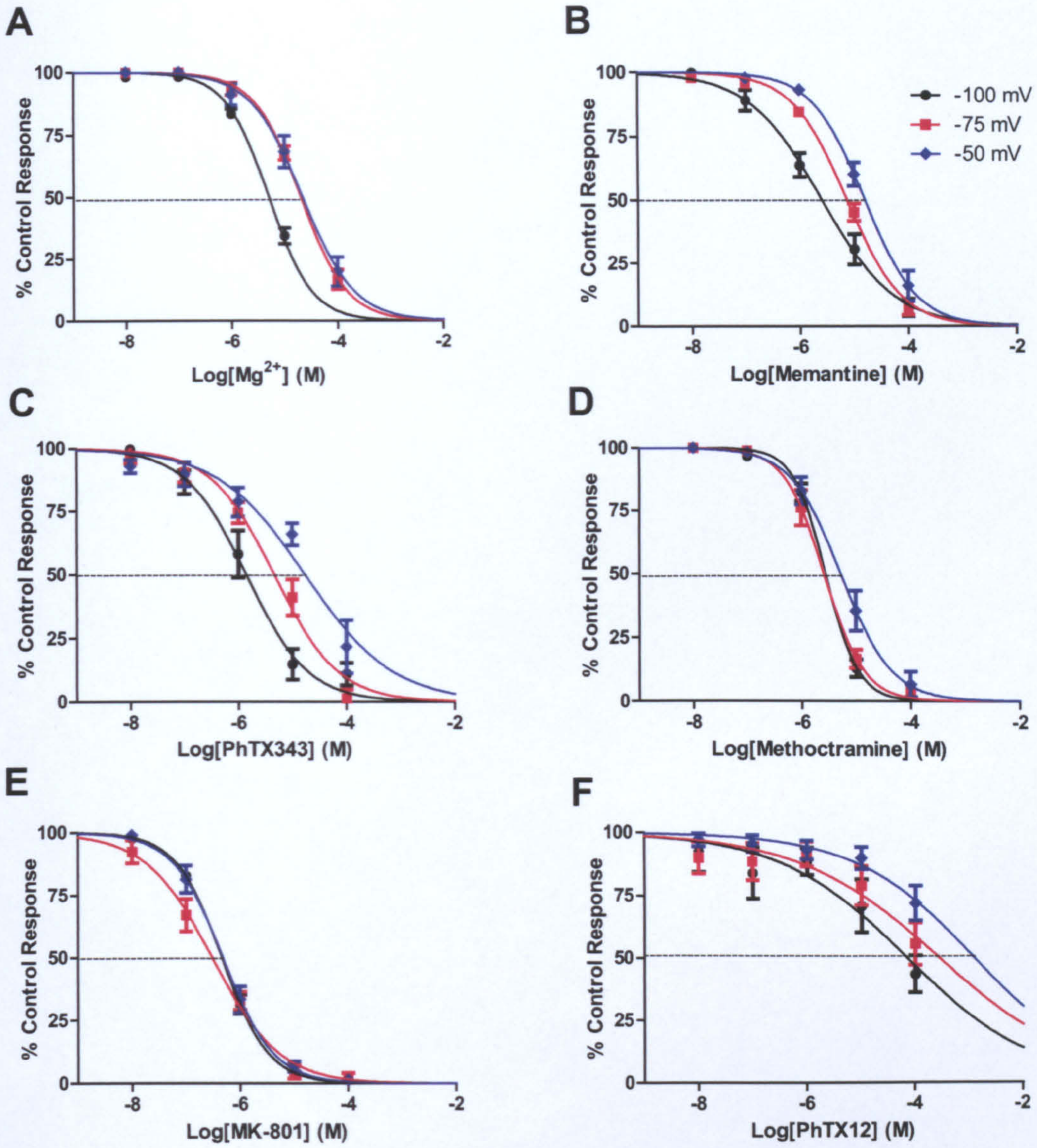

Figure 57: Concentration inhibition relationship showing voltage-dependence of block of NMDA/glycine-evoked responses mediated by 3A containing NMDA receptors at -100, -75 and -50 mV. % control response (mean ± S.E.M) values were plotted and fitted with the Hill equation for (A) Mg^{2+}, (B) memantine, (C) PhTX-343, (D) methoctramine, (E) MK-801 and (F) PhTX-12.

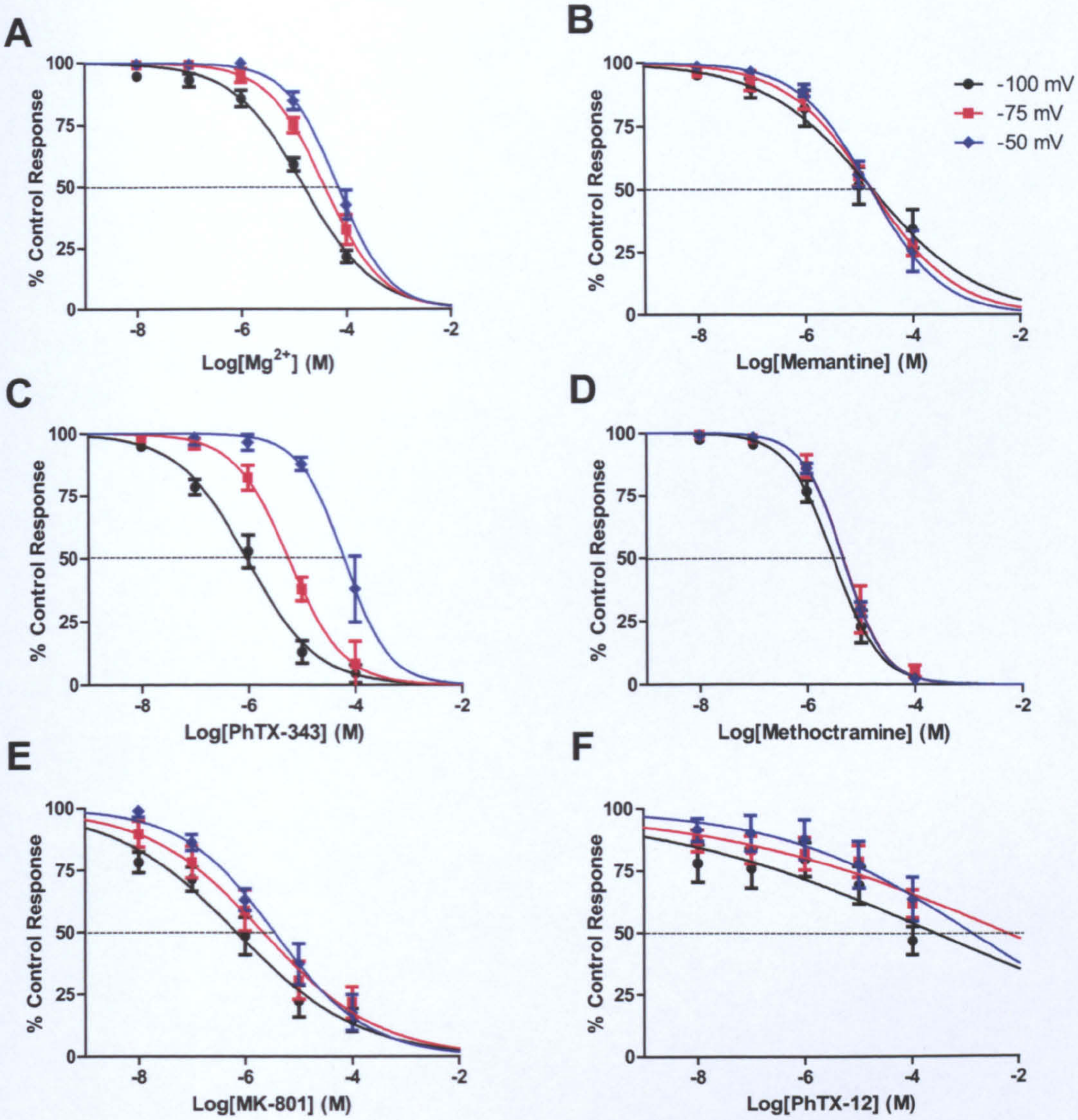

Figure 58: Concentration inhibition relationship showing voltage-dependence of block of NMDA/glycine-evoked responses mediated by 3B containing NMDA receptors at -100, -75 and -50 mV. % control response (mean ± S.E.M) values were plotted and fitted with the Hill equation for (A) Mg^{2+}, (B) memantine, (C) PhTX-343, (D) methoctramine, (E) MK-801 and (F) PhTX-12.

	δ (95% CI)		
Compound	**1a/2A**	**3A**	**3B**
Mg^{2+}	0.650 -0.065 to 1.365	0.250 -1.889 to 2.389	0.345 -0.282 to 0.972
Memantine	0.652 -1.691 to 2.995	0.839 -0.294 to 1.971	0.0133 -0.180 to 0.206
PhTX-343	0.610 0.335 to 0.885	0.454 0.262 to 0.646	0.812 0.521 to 1.103
Methoctramine	0.213 -0.436 to 0.861	0.104 -0.566 to 0.775	0.046 -0.414 to 0.506
MK-801	0.246 -2.165 to 3.400	0.034 -2.973 to 3.040	0.672 -1.686 to 3.029
PhTX-12	0.854 -0.460 to 2.167	0.855 0.530 to 1.181	0.434 -2.451 to 3.319

Table 14: Calculated δ values from the Woodhull equation for 1-1a/2A, 3A and 3B NMDA receptors.

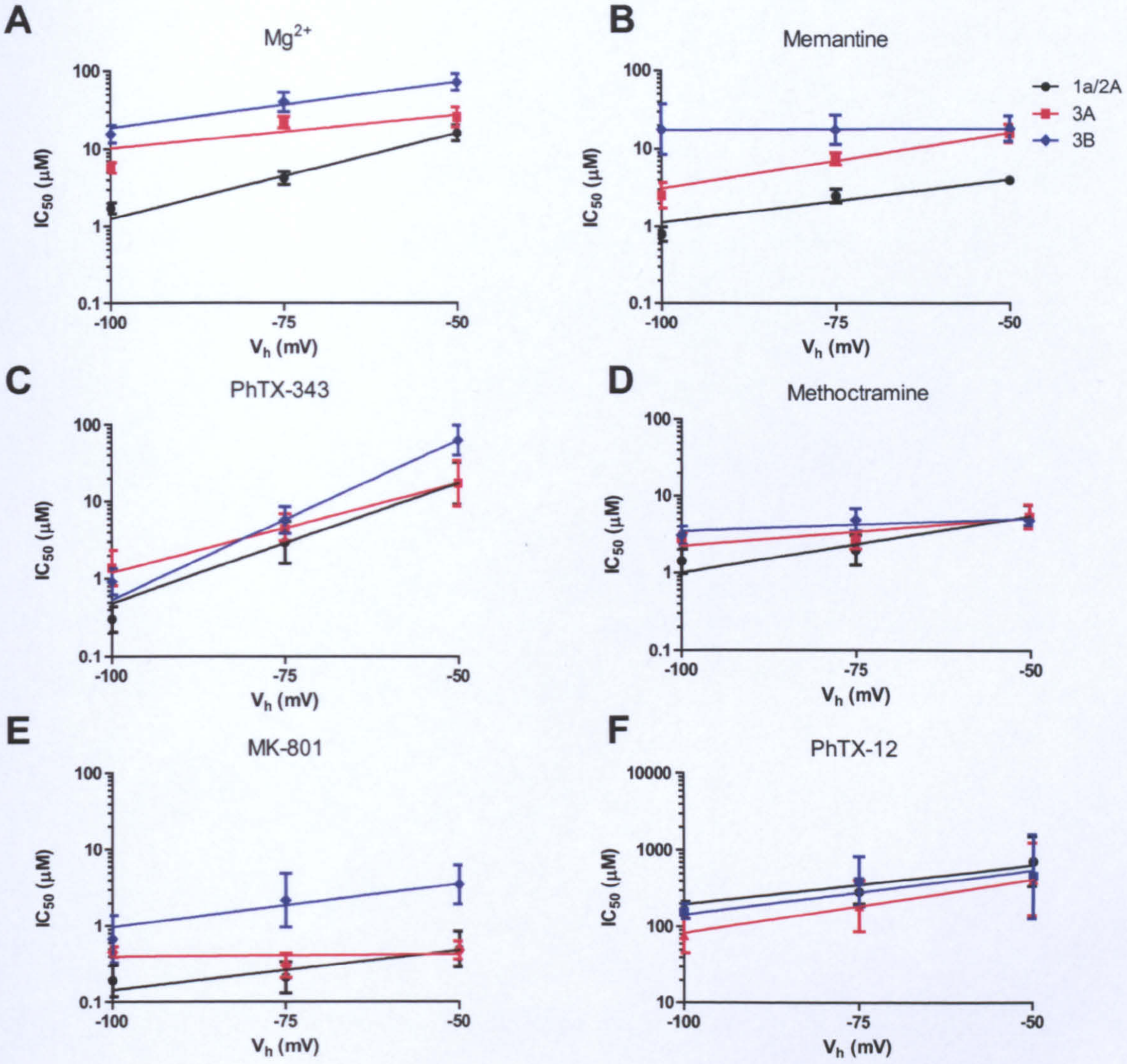

Figure 59: Voltage dependence of IC_{50} for memantine block of NMDA/glycine responses from 1-1a/2A, 3A and 3B containing receptors fitted with the Woodhull equation. IC_{50} (95% CI) μM for (A) Mg^{2+}, (B) memantine, (C) PhTX-343, (D) methoctramine, (E) MK-801 and (F) PhTX-12 (note altered y-axis).

3.4.7 Rank Order of IC_{50}

Concentration-inhibition curves for each blocker were used to calculate rank order of IC_{50} values (Figure 60). Statistical significance, and the direction of change, is represented by the < and ≈ separates compounds that are not significantly different to each other. At -100 mV for 1-1a/2A this gave a rank order of IC_{50} of MK-801 ≈ PhTX343 < memantine < methoctramine ≈ Mg < PhTX-12. At -75 mV the order was MK-801<methoctramine≈memantine≈ PhTX-343≈ Mg^{2+}<PhTX-12. At -50 mV the rank order IC_{50} was MK-801<memantine ≈methoctramine≈ PhTX-343≈ Mg^{2+}≈PhTX-12.

Rank of IC_{50} was then established for the blockers at 3A containing receptors (Figure 61). At -100 mV rank was MK-801 < PhTX-343 ≈ methoctramine ≈ memantine < Mg^{2+}< PhTX-12. At -75 mV it was MK-801 < methoctramine < PhTX-343 < memantine < Mg^{2+}< PhTX-12. Finally, at -50 mV was MK-801 < methoctramine < memantine ≈ PhTX-343 ≈ Mg^{2+} < PhTX-12. Rank was again established for 3B containing receptors (Figure 62). The order was MK-801 ≈ PhTX-343 < methoctramine < Mg^{2+}≈ memantine < PhTX-12 at -100 mV. At -75 mV it was MK-801 < PhTX-343 ≈ methoctramine < memantine < Mg^{2+} < PhTX-12. Lastly, at -50 mV the rank order was MK-801 < methoctramine < memantine < PhTX-343 ≈ Mg^{2+}< PhTX-12. A full list of statistical comparisons is given in the appendix.

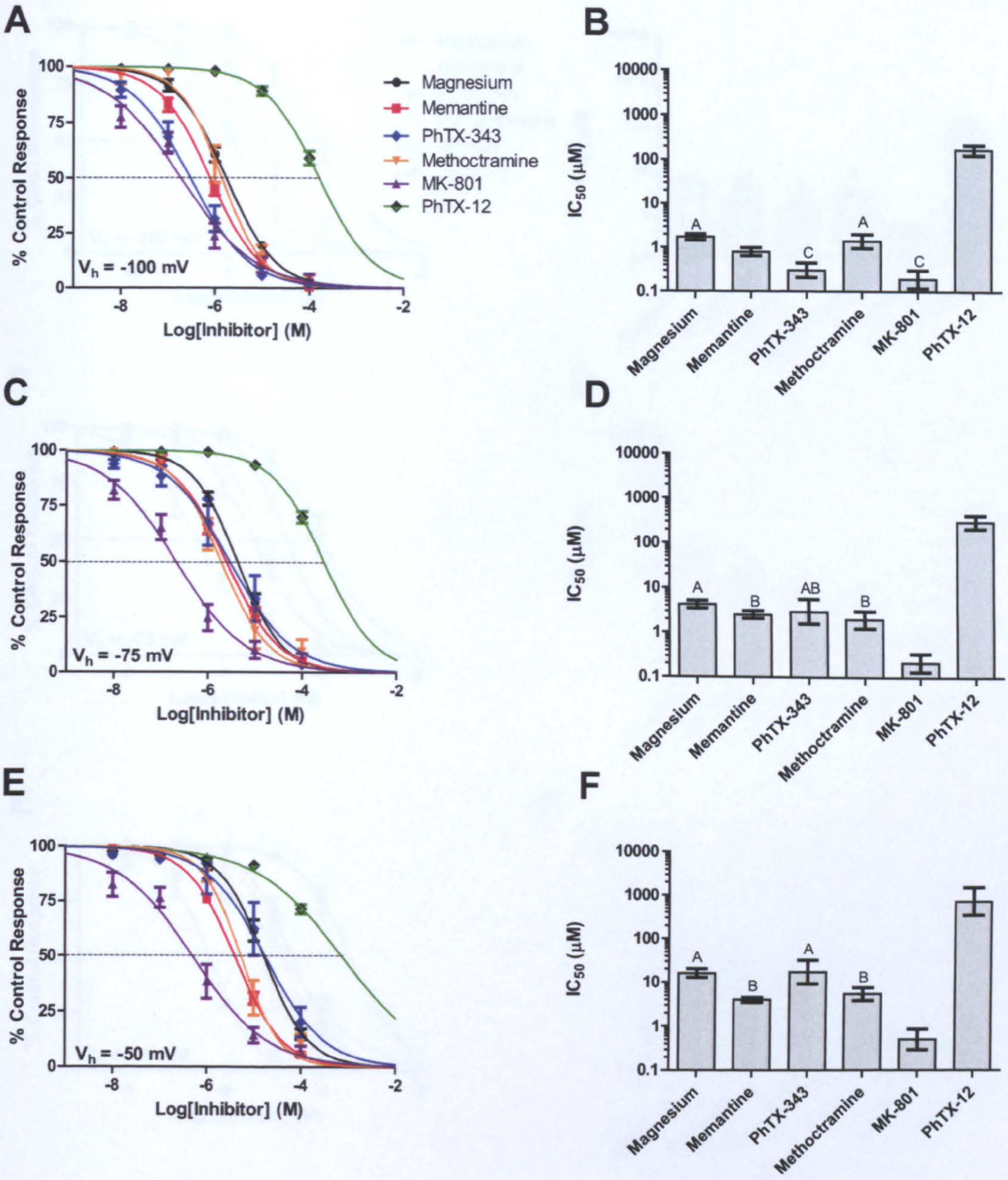

Figure 60: Concentration-inhibition relationships for rank order of block of NMDA/Glycine-evoked responses mediated by 1-1a/2A NMDA receptors at -100, -75 and -50 mV. (A, C, E) % control response (mean ± S.E.M) values were plotted and fitted with the Hill equation to give estimates of IC_{50} (B, -100 mV; D, -75 mV; F, -50 mV). Bars show IC_{50} (95% CI) μM Groups that do not share a letter are significantly different.

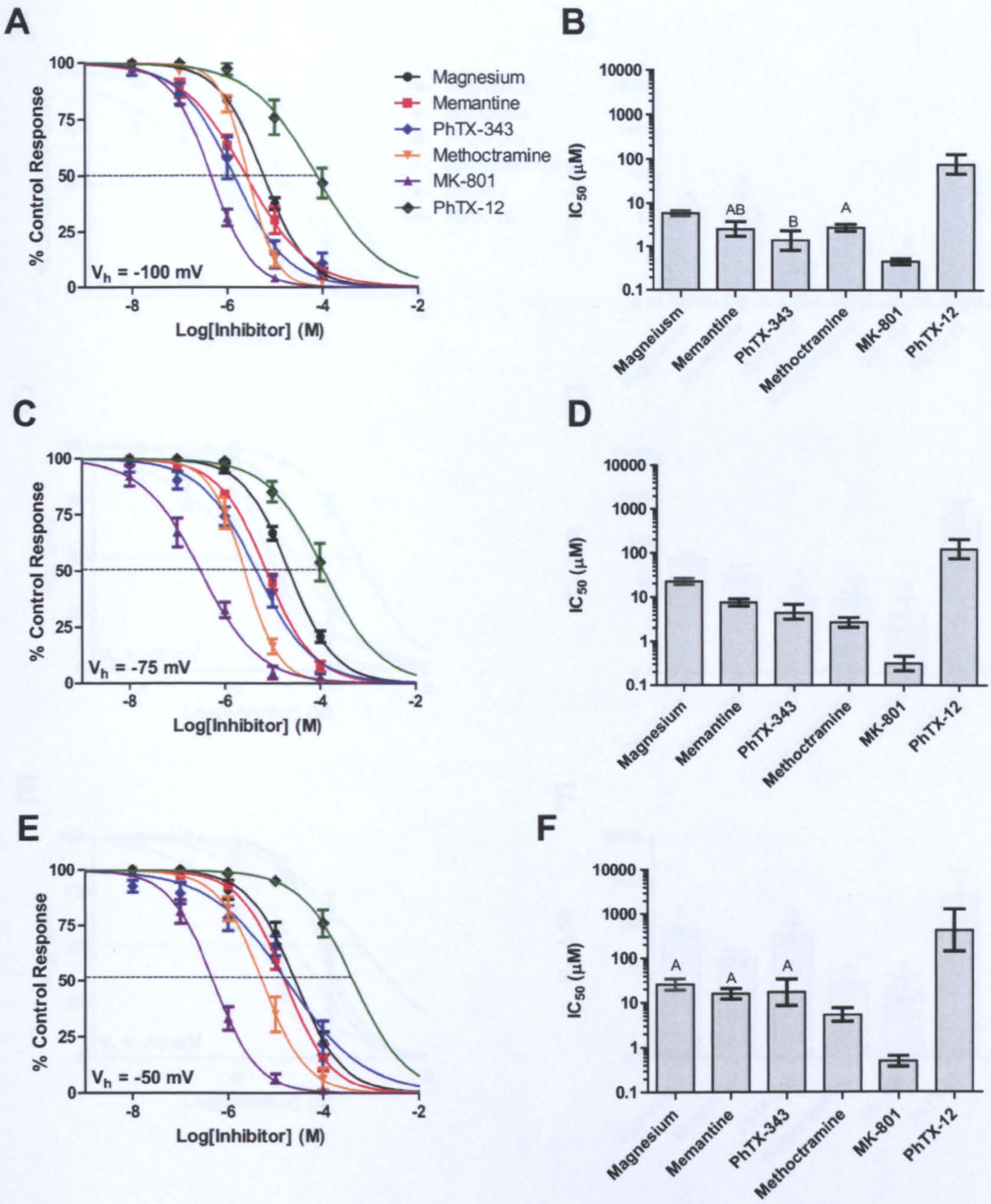

Figure 61: Concentration-inhibition relationships for rank order of block of NMDA/Glycine-evoked responses mediated by 3A NMDA receptors at -100, -75 and -50 mV. (A, B, C) % control response (mean ± S.E.M) values were plotted and fitted with the Hill equation to give estimates of IC_{50} (B, -100 mV; D, -75 mV; F, -50 mV). Bars show IC_{50} (95% CI) μM Groups that do not share a letter are significantly different

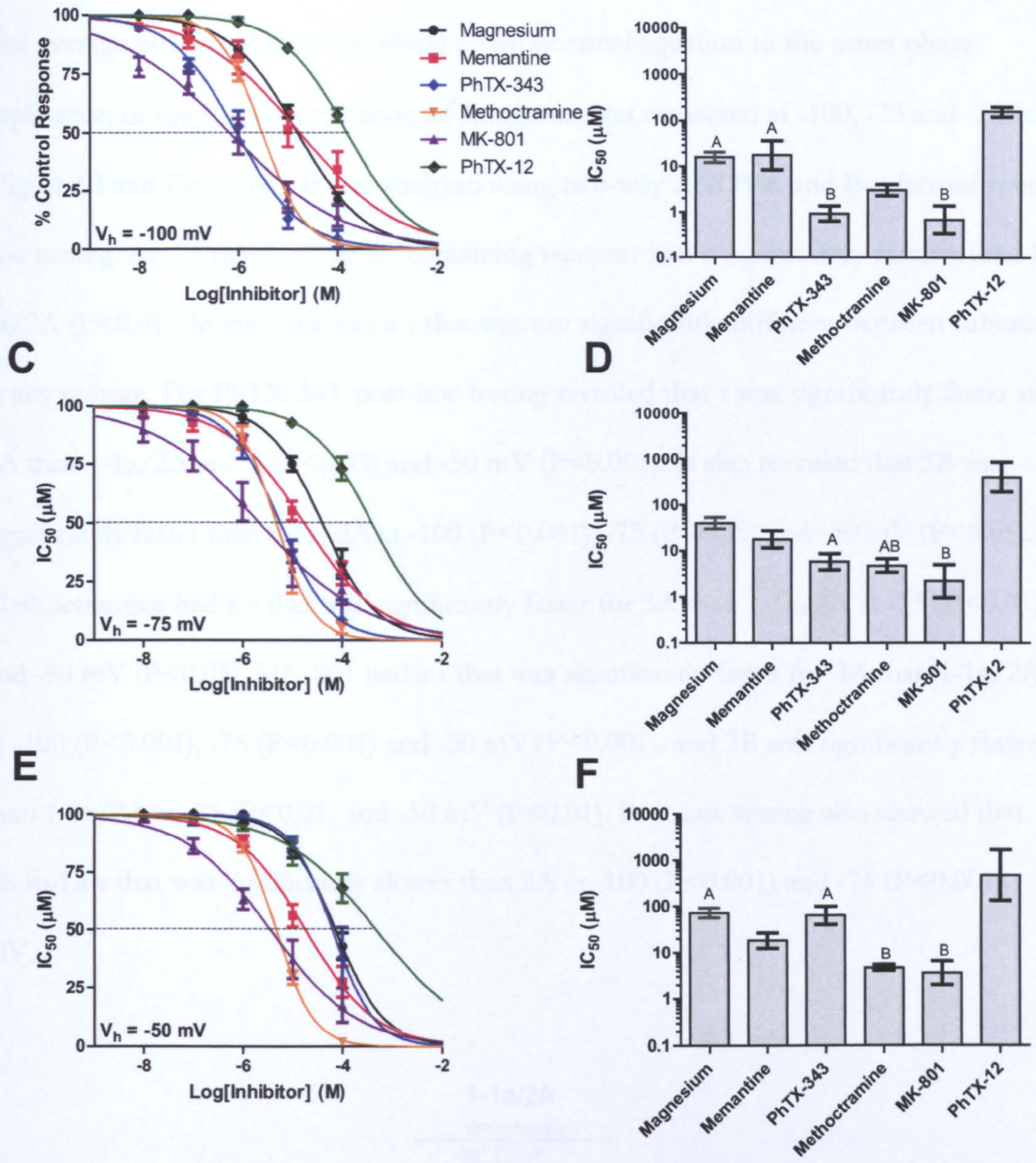

Figure 62: Concentration-inhibition relationships for rank order of block of NMDA/Glycine-evoked responses mediated by 3B NMDA receptors at -100, -75 and -50 mV. (A, C, E) % control response (mean ± S.E.M) values were plotted and fitted with the Hill equation to give estimates of IC_{50} (C, -100 mV; E, -75 mV; G, -50 mV). Bars show IC_{50} (95% CI) μM Groups that do not share a letter are significantly different

3.4.8 On Rate of Block

The average time constant τ describing an exponential equation to the onset phase application of the IC_{50} concentration of antagonist was measured at -100, -75 and -50 mV (Figure 63 and Figure 64). It was analysed using two-way ANOVA and Bonferroni post-hoc testing. At -75 mV Mg^{2+} at 3A containing receptor had a significantly faster τ than 1-1a/2A ($P<0.01$). Memantine had a τ that was not significantly different between subunits at any voltage. For PhTX-343, post-hoc testing revealed that τ was significantly faster at 3A than 1-1a/2A at -75 ($P<0.05$) and -50 mV ($P<0.001$). It also revealed that 3B was significantly faster than 1-1a/2A at -100 ($P<0.001$), -75 ($P<0.05$) and -50 mV ($P<0.05$). Methoctramine had a τ that was significantly faster for 3A than 1-1a/2A at -75 ($P<0.01$) and -50 mV ($P<0.05$). MK-801 had a τ that was significantly faster for 3A than 1-1a/2A at -100 ($P<0.001$), -75 ($P<0.001$) and -50 mV ($P<0.001$), and 3B was significantly faster than 1-1a/2A at -75 ($P<0.01$) and -50 mV ($P<0.01$). Post-hoc testing also showed that 3B had a τ that was significantly slower than 3A at -100 ($P<0.001$) and -75 ($P<0.001$) mV.

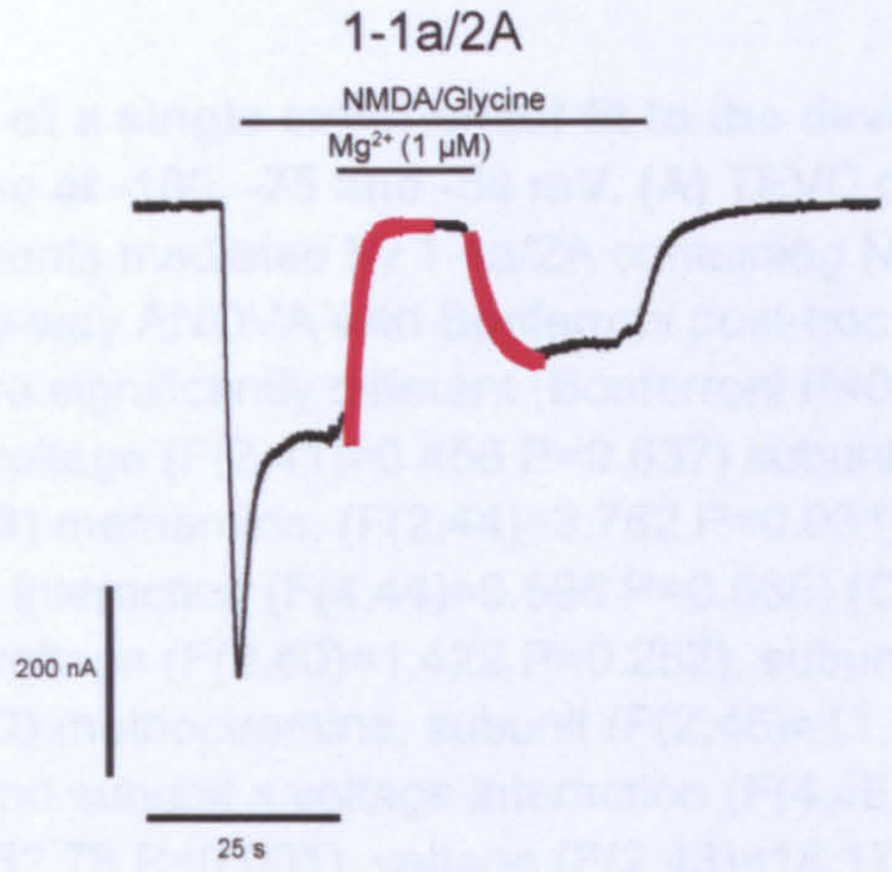

Figure 63: TEVC current recording of Mg^{2+} block of NMDA/glycine currents mediated by 1-1a/2A NMDA receptors at -100 mV. The onset and decay of block are shown by the exponential fit highlighted in red.

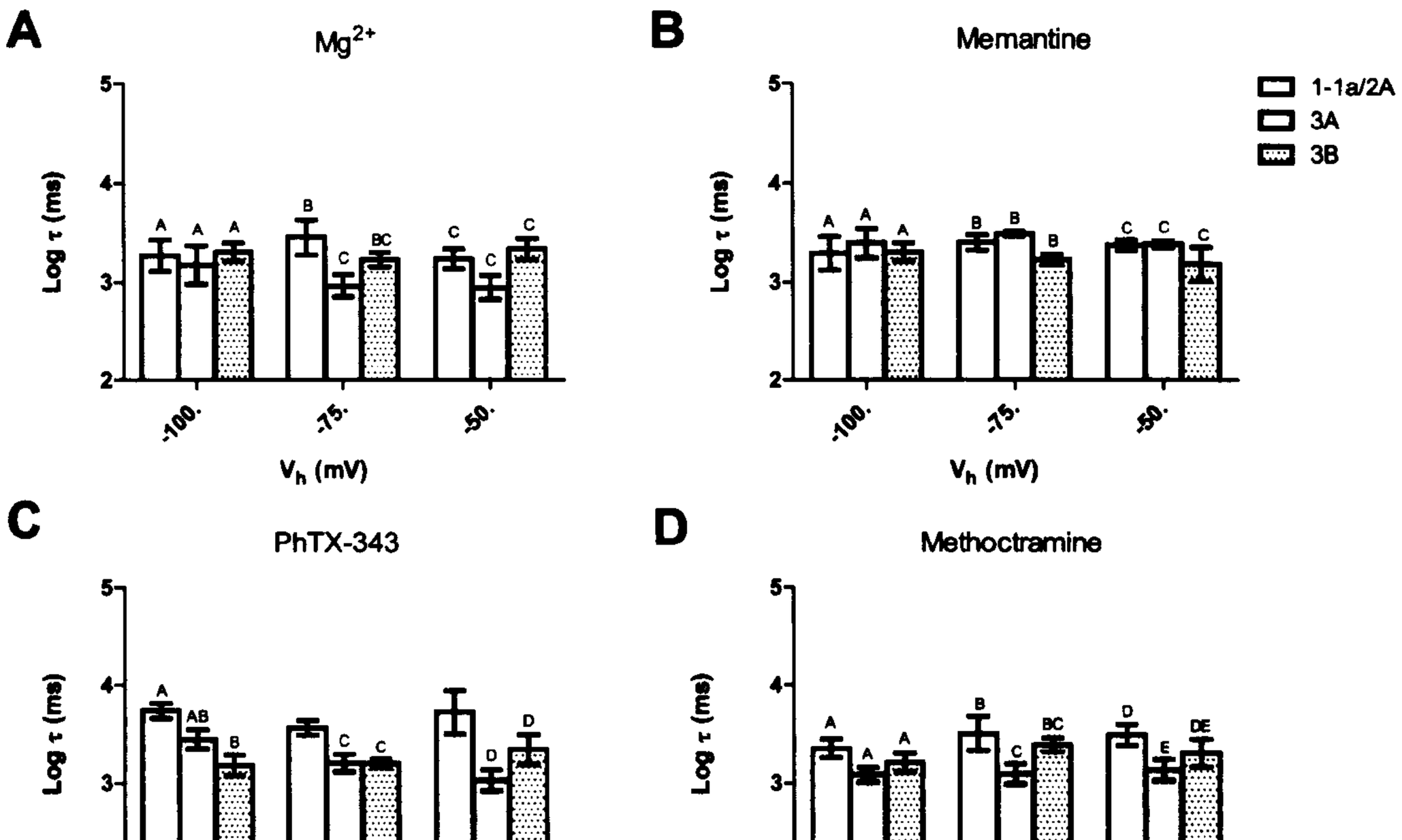

Figure 64: Time constant of a single exponential fit to the development phase of block of NMDA/glycine response at -100, -75 and -50 mV. (A) TEVC current recording of Mg^{2+} block of NMDA/glycine currents mediated by 1-1a/2A containing NMDA receptors at -100 mV. Log τ (95% CI, n=5-7). Two-way ANOVA with Bonferroni post-hoc test. Within a voltage, bars that do not share a letter are significantly different (Bonferroni $P<0.05$). **(A)** Mg^{2+}, subunit ($F(2,41)=7.935$ $P=0.002$), voltage ($F(2,41)=0.456$ $P=0.637$) subunit x voltage interaction ($F(4,41)=1.338$ $P=0.272$) **(B)** memantine, ($F(2,44)=3.762$ $P=0.031$), voltage ($F(2,44)=0.399$ $P=0.674$) subunit voltage x interaction ($F(4,44)=0.596$ $P=0.668$) **(C)** PhTX-343, subunit ($F(2,40)=20.74$ $P<0.001$), voltage ($F(2,40)=1.429$ $P=0.252$), subunit x voltage interaction ($F(4,40)=2.853$ $P=0.036$) **(D)** methoctramine, subunit ($F(2,46)=11.82$ $P<0.001$), voltage ($F(2,46)=1.265$ $P=0.865$) and subunit x voltage interaction ($F(4,46)=0.3177$ $P=0.292$). and **(E)** MK-801, subunit ($F(2,43)=52.78$ $P<0.001$), voltage ($F(2,43)=18.17$ $P<0.001$) and subunit x voltage interaction ($F(4,43)=6.890$ $P<0.001$).

3.4.9 Off Rate of Block

The average time constant τ describing an exponential equation fitted to the recovery phase of block was measured and analysed by two-way ANOVA (Figure 65). For Mg^{2+} block, Bonferroni multiple comparison tests revealed that at -100 mV, 1-1a/2A had a τ that was significantly slower than that of 3A ($P<0.001$) and 3B ($P<0.05$), and that at -50 mV the τ for 3B was significantly slower than 3A ($P<0.05$). Post-hoc testing for memantine revealed that τ was significantly slower for 3A than 1-1a/2A at -100 ($P<0.05$), -75 ($P<0.001$) and -50 ($P<0.001$) mV. It also found that for 3A τ was significantly slower than that of 3B at -75 ($P<0.05$) and -50 ($P<0.01$) mV.

Block by PhTX-343 showed that 3A had a τ that was significantly faster than 1-1a/2A at -100 ($P<0.05$), -75 ($P<0.001$) and -50 mV ($P<0.001$). 3B also had a τ that was significantly faster than 1-1a/2A at -100 ($P<0.01$), -75 ($P<0.001$) and -50 mV ($P<0.01$). It was also found that at -50 mV τ for 3A was significantly faster than 3B ($P<0.01$).

Methoctramine showed no significant differences between subunits at any voltage. MK-801 post-hoc testing revealed that τ for 3A was significantly faster than 1-1a/2A at -100 ($P<0.001$), -75 ($P<0.001$) and -50 ($P<0.001$) mV and that 3A was significantly faster than 3B at -100 ($P<0.001$) and -75 ($P<0.001$) mV.

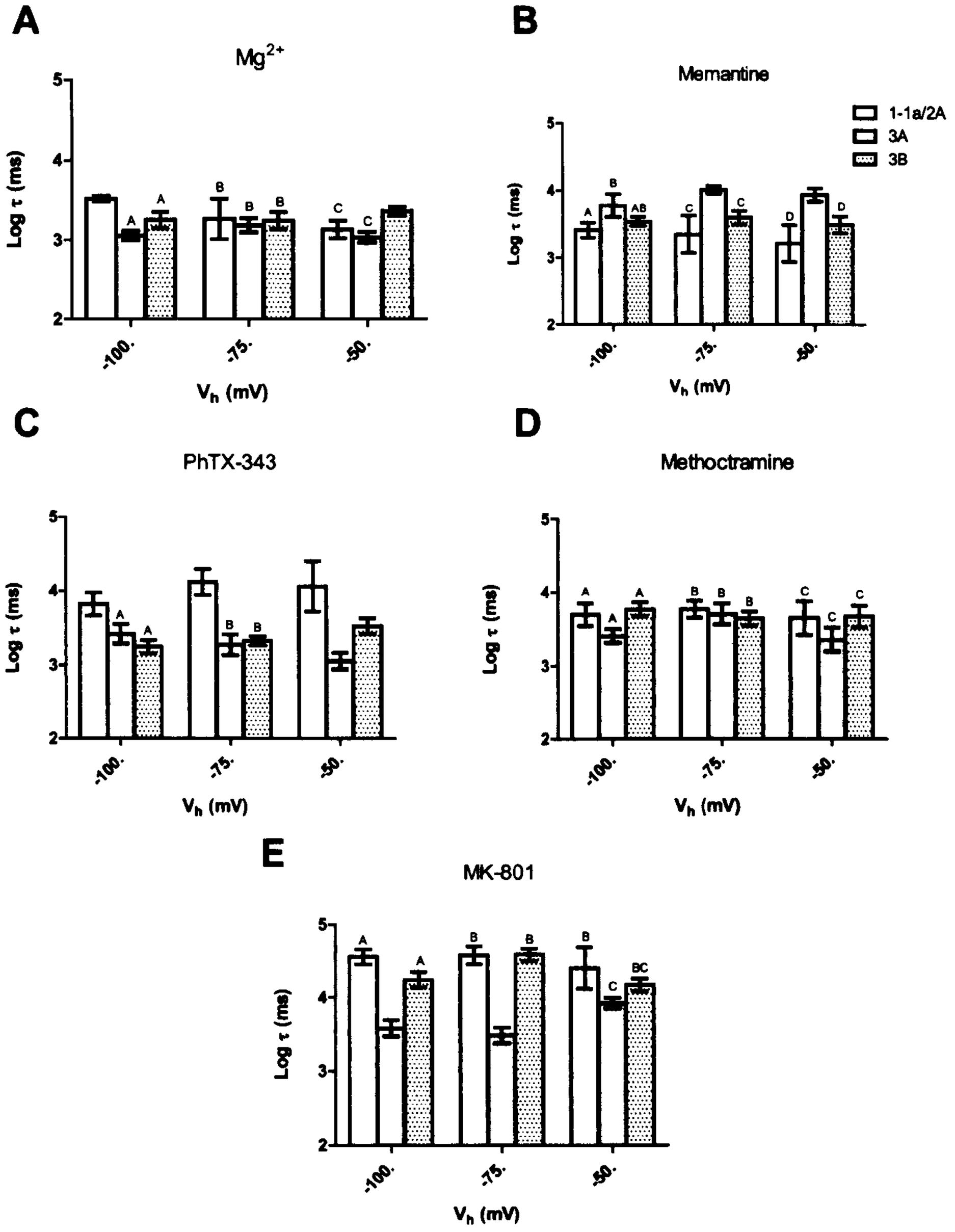

Figure 65: Time constant of a single exponential fit to the recovery phase of block of NMDA/glycine response at -100, -75 and -50 mV. Two-way ANOVA with Bonferroni post-hoc test. Within a voltage, bars that do not share a letter are significantly different (Bonferroni $P<0.05$). Shown are Log τ (95% CI) (n=6-7) for **(A)** Mg^{2+}, subunit ($F(2,43)=7.118$ $P=0.002$), voltage ($F(2,43)=1.331$ $P=0.275$) and subunit x voltage interaction ($F(4,43)=3.952$ $P=0.008$) **(B)** memantine, subunit ($F(2,44)=25.64$ $P<0.001$), voltage ($F(2,44)=0.826$ $P=0.444$) and subunit x voltage interaction ($F(4,44)=0.938$ $P=0.451$) **(C)** PhTX-343, subunit ($F(2,41)=44.83$ $P<0.001$), voltage ($F(2,41)=0.4453$ $P=0.645$) and subunit x voltage interaction ($F(4,41)=3.769$ $P=0.011$) **(D)** methoctramine, subunit $F(2,44)=3.544$ $P=0.037$), voltage ($F(2,44)=1.261$ $P=0.299$) and subunit x voltage interaction ($F(4,44)=1.114$ $P=0.362$) **(E)** MK-801, subunit ($F(2,38)=74.37$ $P<0.001$), voltage ($F(2,38)=0.6476$ $P=0.529$) and subunit x voltage interaction ($F(4,38)=6.376$ $P=0.011$).

3.5 Mutations

3.5.1 Steady State Current

In order to determine if the presence of the GluN3 subunit had any effect on inward current, two-way ANOVA was carried out. Post-hoc analysis using the Bonferroni test for multiple comparisons revealed that there was significantly less inward current for 3A compared with G703N ($P<0.001$), R704N ($P<0.001$), and R704D ($P<0.001$) at all voltages. It was also found that R704N had significantly less current than R703N ($P<0.001$) at all voltages.

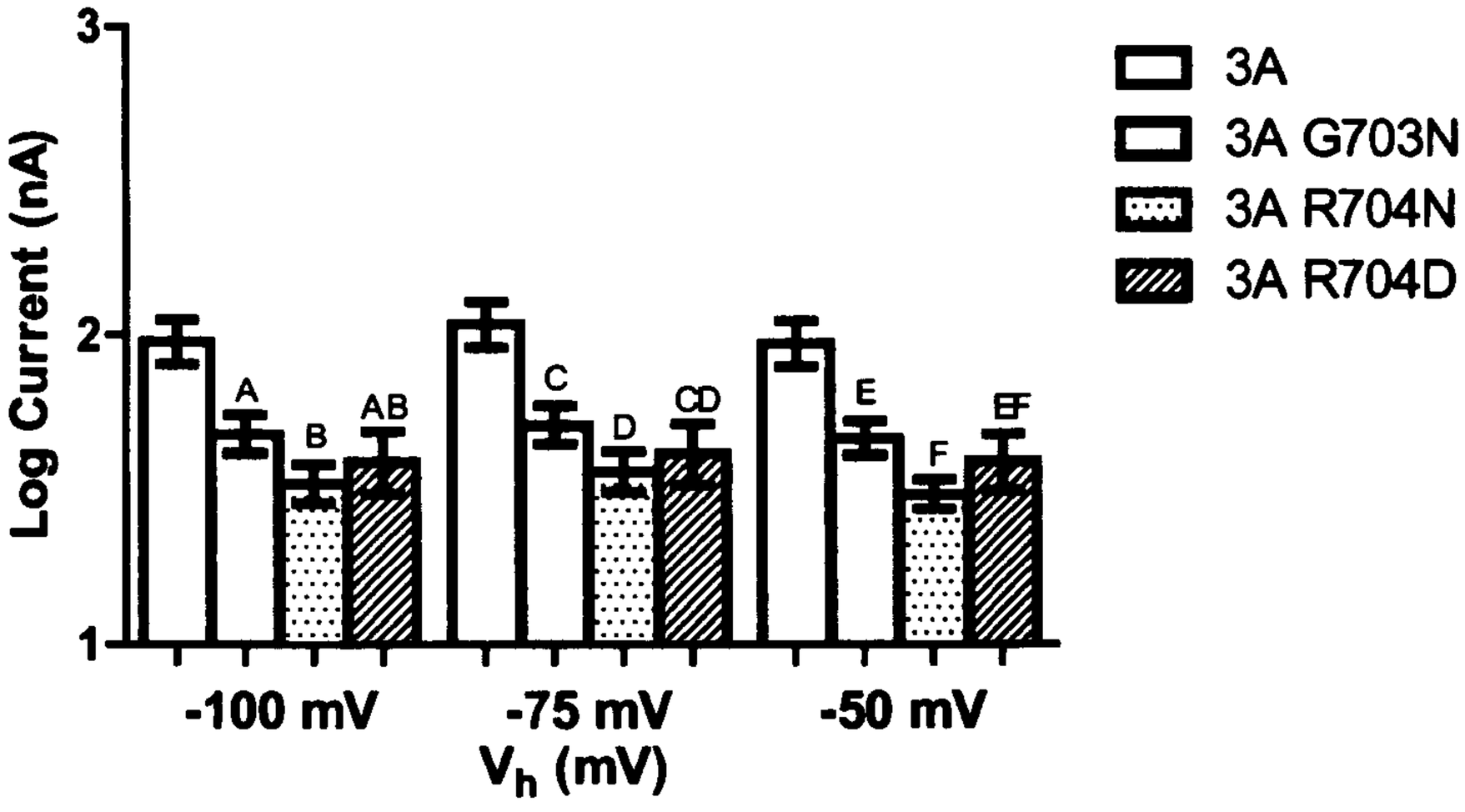

Figure 66: Effect of mutation and voltage on steady-state current recorded from Xenopus oocytes. Bars represent mean (95% CI, n=39-64). Two-way ANOVA subunit ($P<0.001$), voltage ($P=0.124$) and subunit x voltage interaction ($P=0.995$). Bars that do not share a letter within a voltage are significantly different.

3.5.2 NMDA Receptor Antagonism

The IC_{50} for Mg^{2+} at $3A^{G703N}$, $3A^{R704N}$ and $3A^{R704D}$ was calculated and compared to 1-1a/2A and 3A wild-type (Figure 67, Table 15). At -100 and -75 mV $3A^{G703N}$ resulted in an intermediate IC_{50} for Mg^{2+} that was significantly lower than that for 3A wild-type, but still significantly higher than that of 1-1a/2A. At -50 mV the pattern changed and the IC_{50} for $3A^{G703N}$ increased relative to the other subunits and was now significantly higher than both wild-type 3A and 1-1a/2A. At -100 mV the $3A^{R704N}$ mutation also produced an intermediate IC_{50} for Mg^{2+} that was significantly lower than that for wild-type and significantly higher than that of 1-1a/2A. At -75 mV the IC_{50} was again significantly lower ($P=0.0072$) than 3A wild-type, but was now reduced to a level that was not significantly different to 1-1a/2A. At -50 mV $3A^{G704N}$ had an IC_{50} for Mg^{2+} that was not significantly different to wild-type 3A or 1-1a/2A. With the $3A^{R704D}$ mutation at -100 mV there was no effect on the IC_{50} for Mg^{2+} as it was not significantly different than that for wild-type 3A. At -75 mV the IC_{50} for Mg^{2+} was now intermediate and was significantly lower than 3A wild-type and significantly higher than 1-1a/2A. At -50 mV Mg^{2+} was found to have an IC_{50} that was increased relative to 3A and was now significantly higher than both wild-type 3A and 1-1a/2A.

The IC_{50} for Mg^{2+} at the mutated 3A subunits was also compared at each voltage. $3A^{G703N}$ and $3A^{R704N}$ had IC_{50} values for Mg^{2+} that were not significantly different to each other ($P=0.5786$). $3A^{R704D}$ had the highest IC_{50} which was significantly higher than both $3A^{G703N}$ ($P<0.001$) and $3A^{R704N}$ ($P<0.003$). At -75 mV again $3A^{G703N}$ and $3A^{R704N}$ had IC_{50} values for Mg^{2+} that were not significantly different to each other ($P<0.995$). Again, $3A^{R704D}$ had the highest IC_{50} that was significantly higher than $3A^{G703N}$ ($P<0.001$), but was not

significantly different to $3A^{R704N}$ (P=0.083). At -50 mV there were no significant differences between the mutated subunits.

	IC_{50} (95% CI) μM		
Voltage (mV)	**$3A^{G703N}$**	**$3A^{R704N}$**	**$3A^{R704D}$**
-100	**3.17** 2.53 to 3.98 ***P<0.001** **†P<0.001**	**2.77** 1.71 to 4.48 ***P=0.050** **†P=0.002**	**5.92** 4.89 to 7.18 ***P<0.001** †P=0.891
-75	**7.58** 5.56 to 10.33 ***P=0.003** **†P<0.001**	**7.56** 3.35 to 17.00 *P=0.138 **†P=0.007**	**14.53** 12.56 to 16.81 ***P<0.001** **†P<0.001**
-50	**48.83** 38.02 to 62.70 ***P<0.001** **†P<0.001**	**27.01** 13.47 to 54.15 *P=0.138 †P=0.898	**46.38** 37.24 to 57.77 ***P<0.001** **†P=0.016**

Table 15: IC_{50} values for Mg^{2+} at $3A^{G703N}$, $3A^{G703N}$ and $3A^{R704D}$ containing receptors. * denotes statistical significance against 1-1a/2A and † denotes significance against 3A.

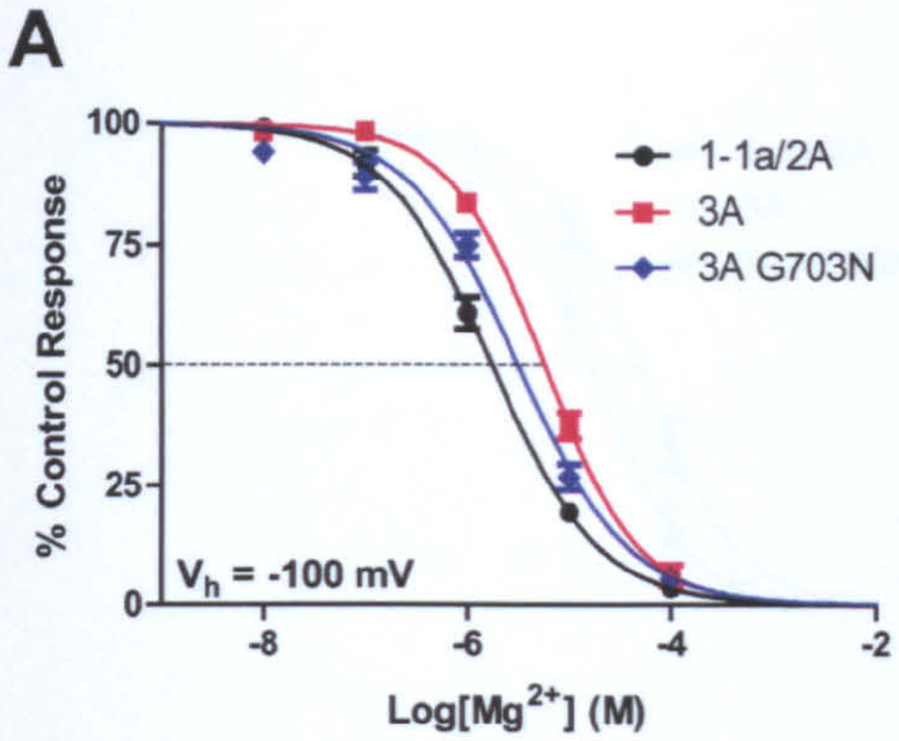
A
100
75
50
25
0
% Control Response
V_h = -100 mV
-8
-6
-4
-2
Log[Mg^{2+}] (M)
1-1a/2A
3A
3A G703N

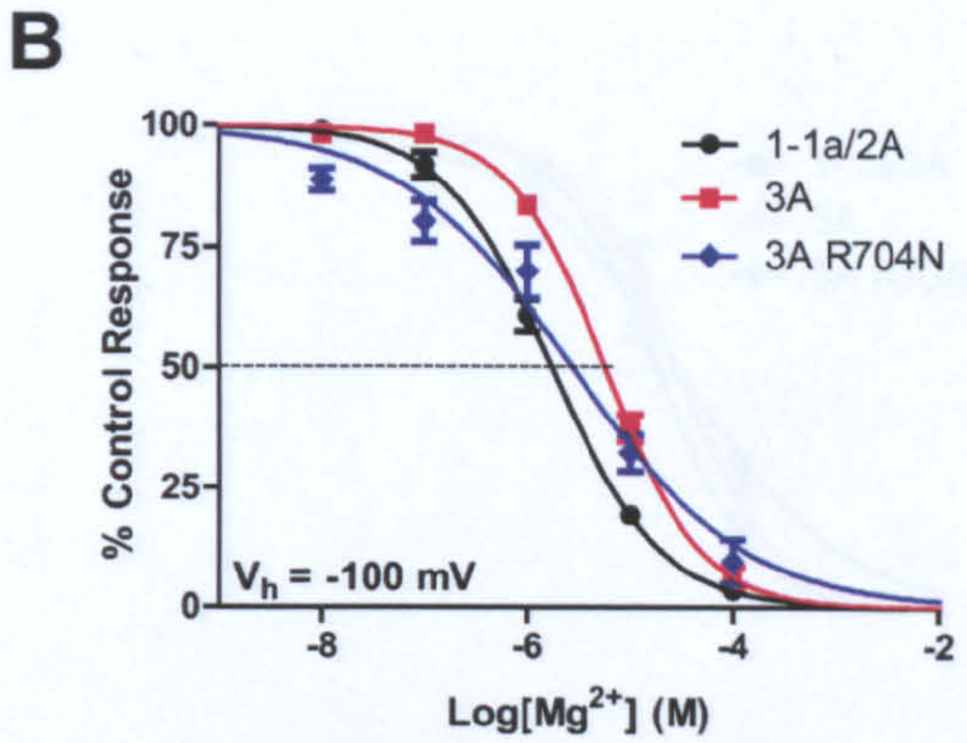
B
100
75
50
25
0
% Control Response
V_h = -100 mV
-8
-6
-4
-2
Log[Mg^{2+}] (M)
1-1a/2A
3A
3A R704N

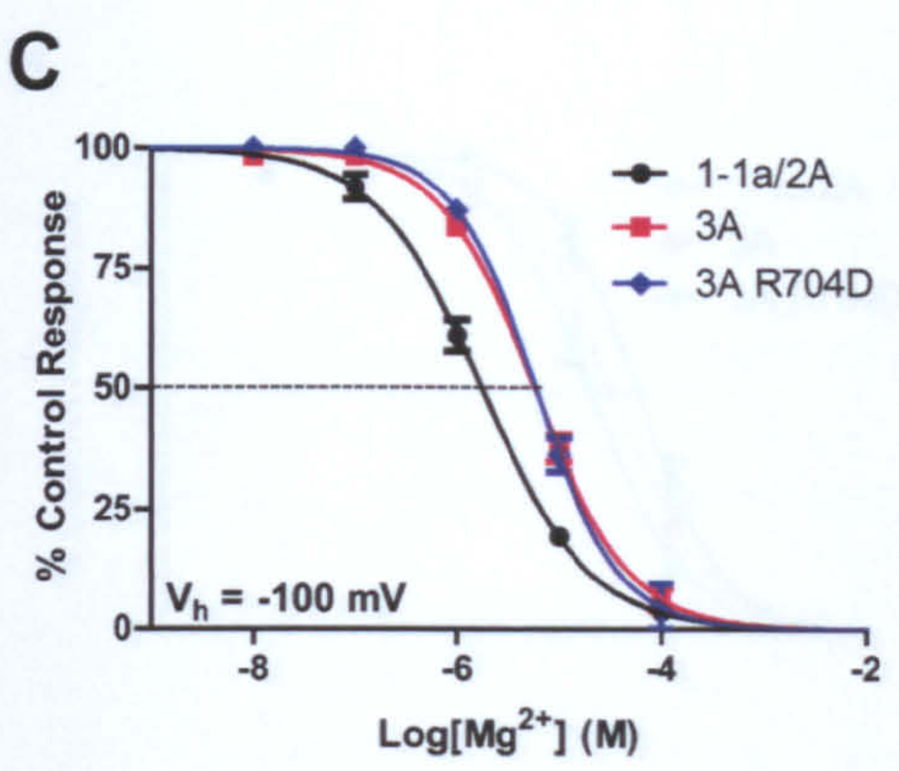
C
100
75
50
25
0
% Control Response
V_h = -100 mV
-8
-6
-4
-2
Log[Mg^{2+}] (M)
1-1a/2A
3A
3A R704D

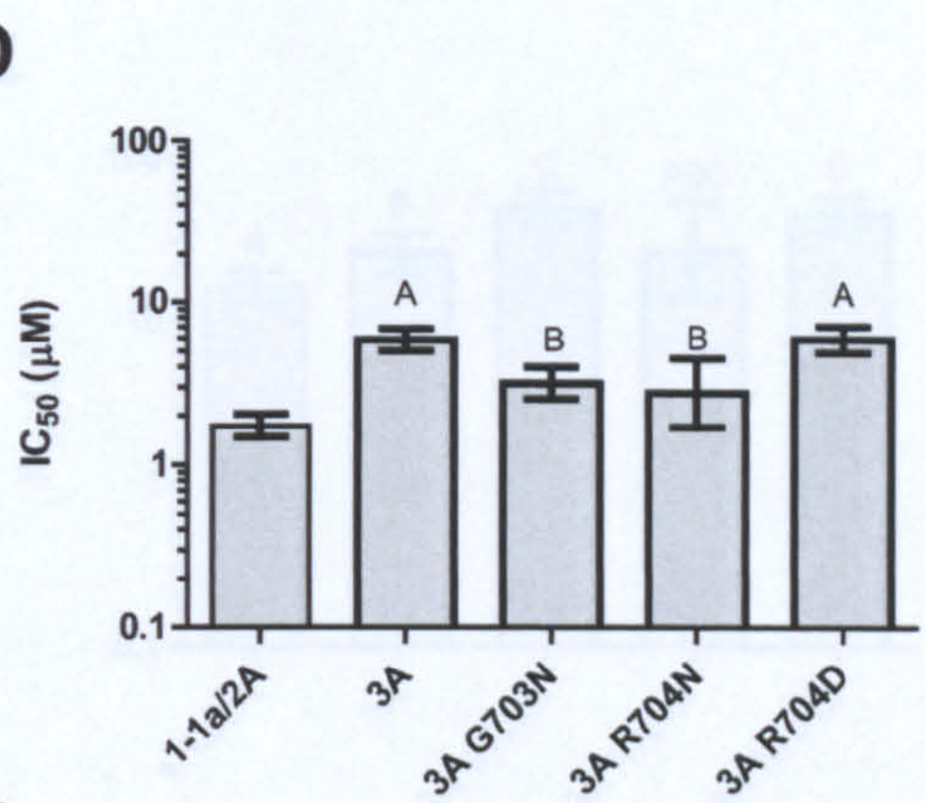
D
100
10
1
0.1
IC_{50} (μM)
A
B
B
A
1-1a/2A
3A
3A G703N
3A R704N
3A R704D

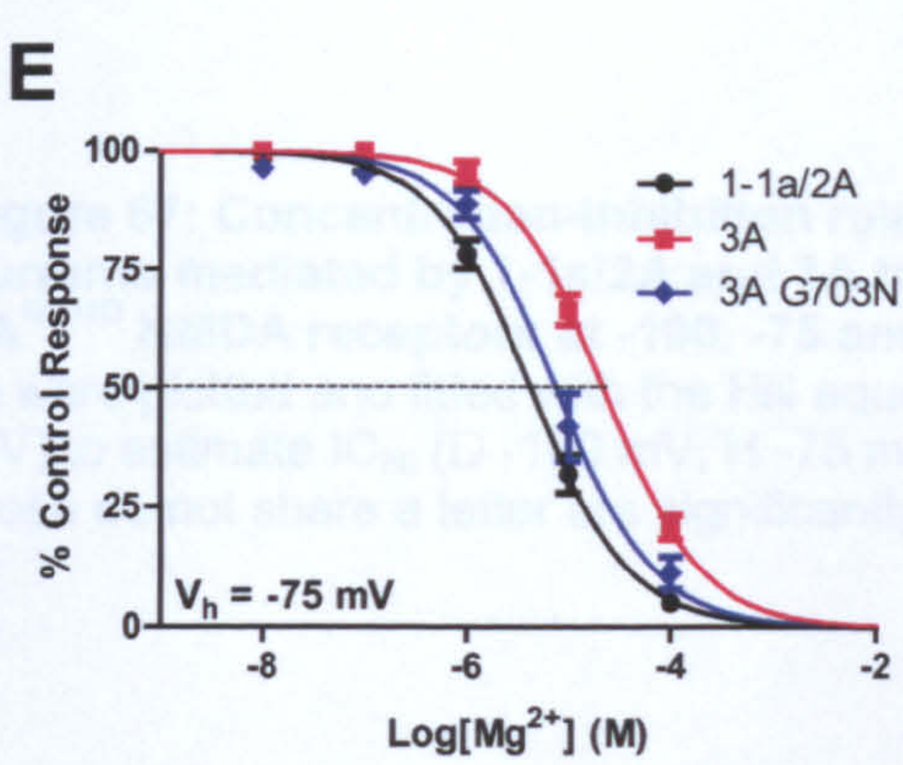
E
100
75
50
25
0
% Control Response
V_h = -75 mV
-8
-6
-4
-2
Log[Mg^{2+}] (M)
1-1a/2A
3A
3A G703N

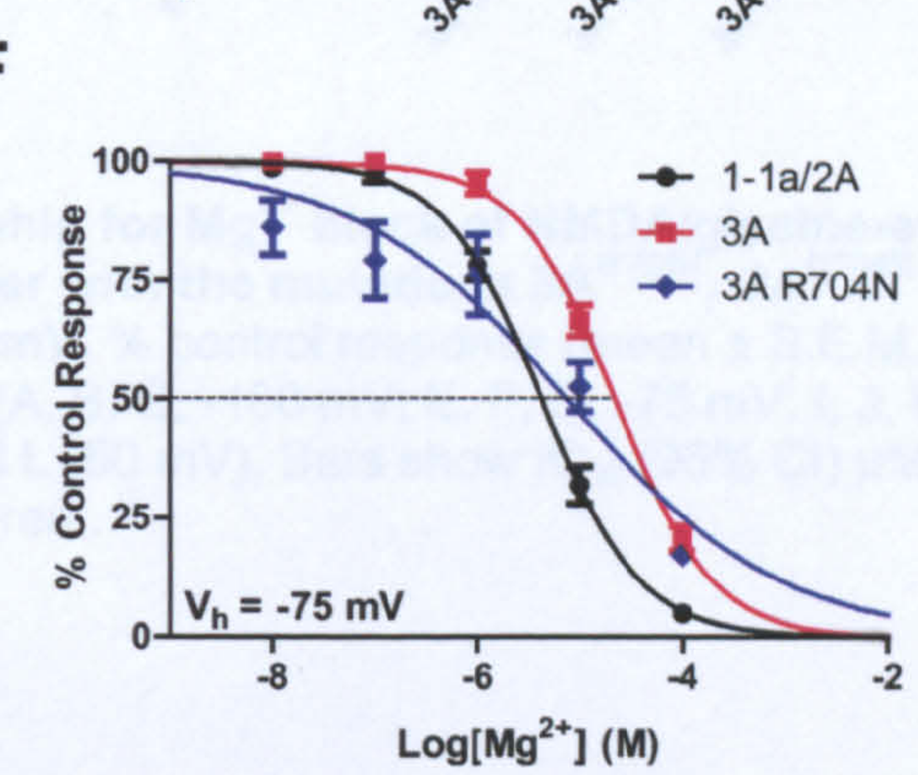
F
100
75
50
25
0
% Control Response
V_h = -75 mV
-8
-6
-4
-2
Log[Mg^{2+}] (M)
1-1a/2A
3A
3A R704N

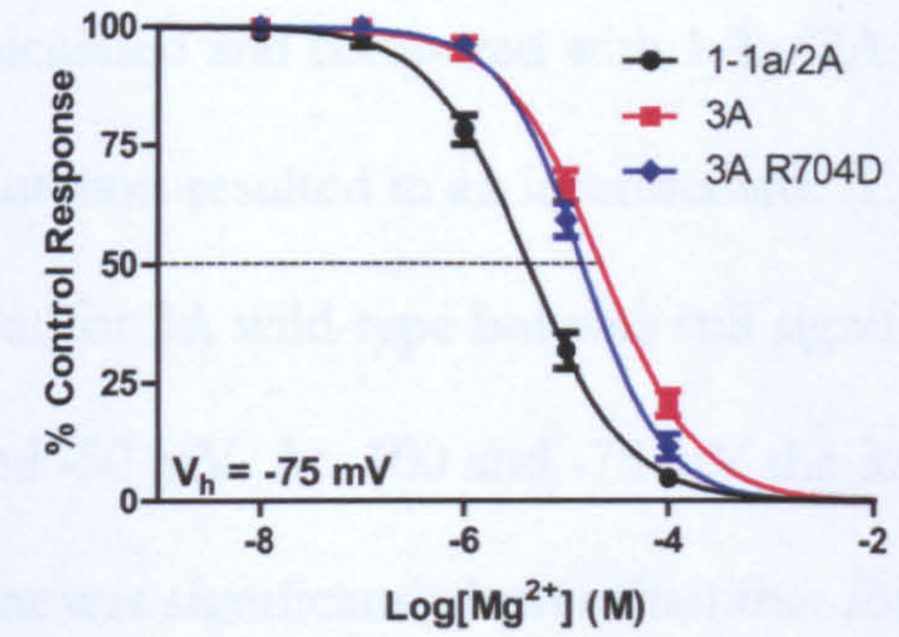
G
100
75
50
25
0
% Control Response
V_h = -75 mV
-8
-6
-4
-2
Log[Mg^{2+}] (M)
1-1a/2A
3A
3A R704D

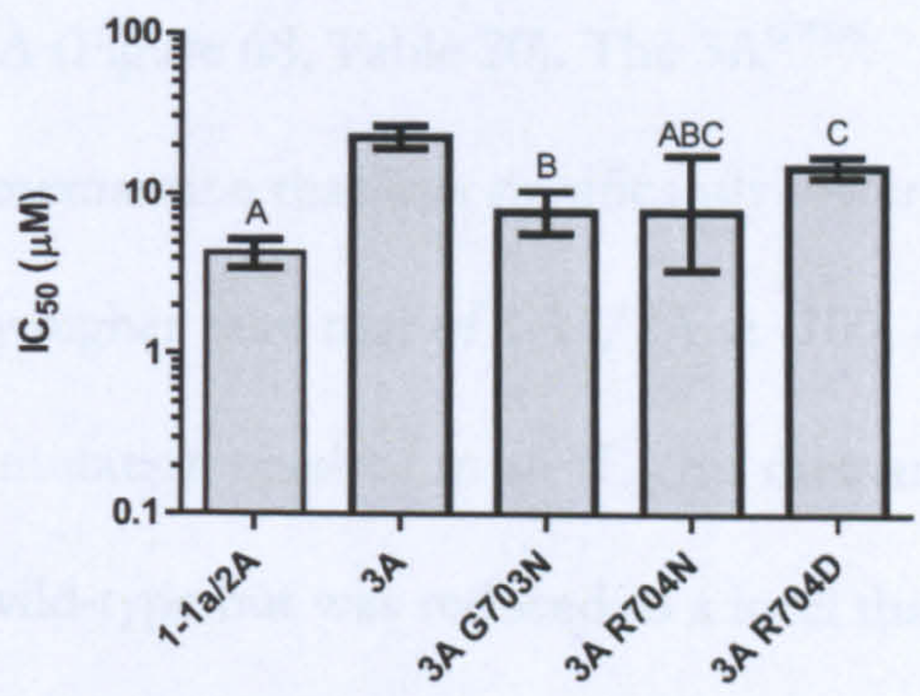
H
100
10
1
0.1
IC_{50} (μM)
A
B
ABC
C
1-1a/2A
3A
3A G703N
3A R704N
3A R704D

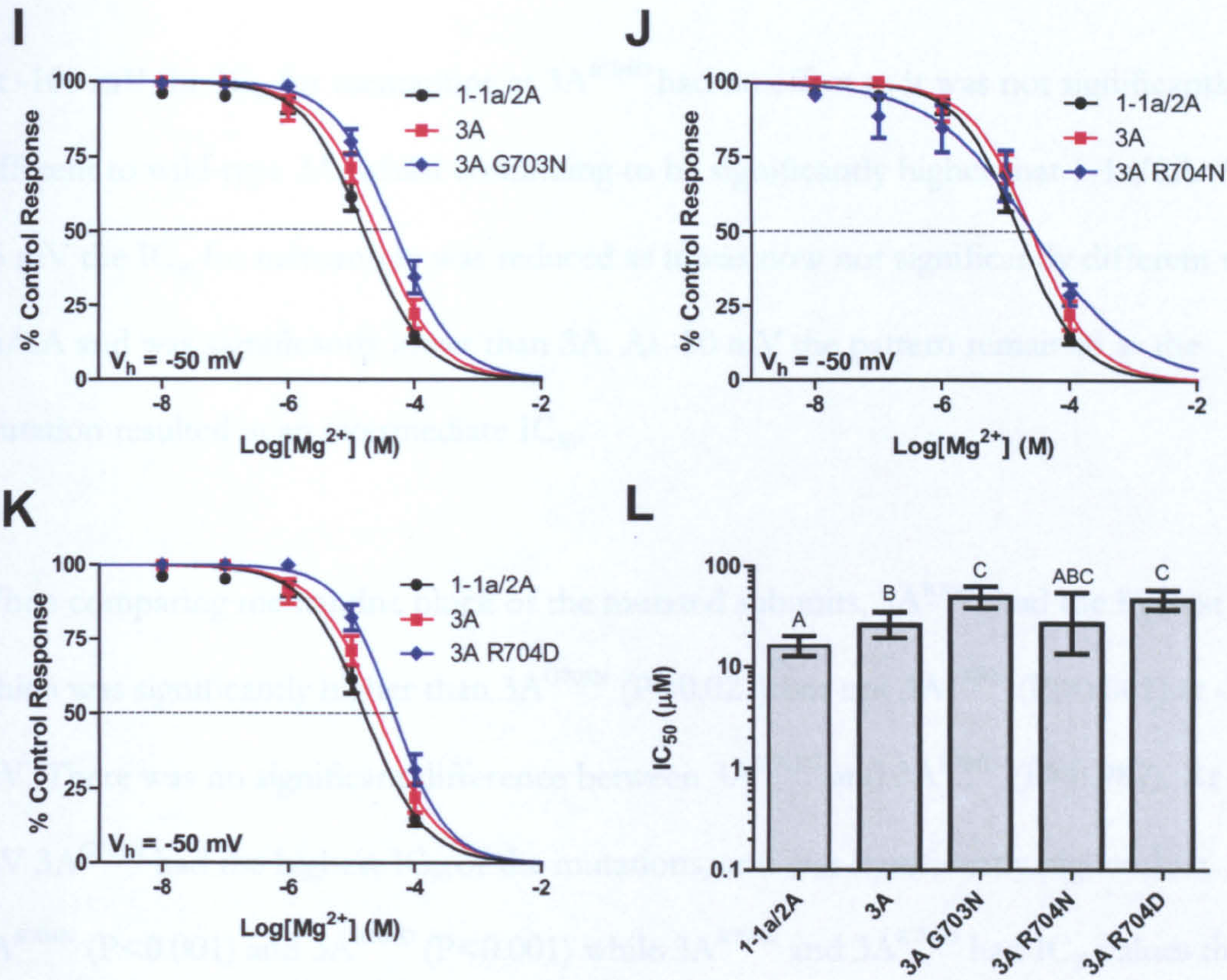

Figure 67: Concentration-inhibition relationship for Mg^{2+} block of NMDA/glycine-evoked currents mediated by 1-1a/2A and 3A together with the mutations $3A^{G703N}$, $3A^{R704N}$ and $3A^{R704D}$ NMDA receptors at -100, -75 and -50 mV. % control response (mean ± S.E.M, n=5-8) were plotted and fitted with the Hill equation (A, B, C, -100 mV; E, F, G, -75 mV; I, J, K -50 mV) to estimate IC_{50} (D -100 mV, H -75 mV and L -50 mV). Bars show IC_{50} (95% CI) μM and those do not share a letter are significantly different.

The IC_{50} for memantine block of $3A^{G703N}$, $3A^{R704N}$ and $3A^{R704D}$ NMDA receptors were calculated and compared with 1-1a/2A and 3A (Figure 68, Table 20). The $3A^{G703N}$ mutation resulted in an intermediate IC_{50} for memantine that was significantly lower than that for 3A wild-type but was still significantly higher than that of 1-1a/2A at -100, -75 and -50 mV. At -100 and -75 mV the $3A^{R704N}$ mutation resulted in an IC_{50} for memantine that was significantly lower than that for 3A wild-type but was reduced to a level that was not significantly different to that of 1-1a/2A. At -50 mV the IC_{50} for $3A^{R704N}$ was now intermediate, as it was found to be significantly lower than wild-type and significantly higher than 1-1a/2A.

At -100 mV the IC_{50} for memantine at $3A^{R704D}$ had no effect as it was not significantly different to wild-type 3A, whilst continuing to be significantly higher that 1-1a/2A. At -75 mV the IC_{50} for memantine was reduced as it was now not significantly different to 1-1a/2A and was significantly lower than 3A. At -50 mV the pattern remained as the mutation resulted in an intermediate IC_{50}.

When comparing memantine block of the mutated subunits, $3A^{R704D}$ had the highest IC_{50} which was significantly higher than $3A^{G703N}$ ($P=0.021$) but not $3A^{R704N}$ ($P=0.061$) at -100 mV. There was no significant difference between $3A^{G703N}$ and $3A^{R704N}$ ($P=0.982$). At -75 mV $3A^{G703N}$ had the highest IC_{50} of the mutations, and was significantly higher than $3A^{R704N}$ ($P<0.001$) and $3A^{R704D}$ ($P<0.001$) while $3A^{R704N}$ and $3A^{R704D}$ had IC_{50} values that were not significantly different to each other ($P=0.951$). At -50 mV $3A^{R704D}$ had the lowest IC_{50} which was significantly lower than $3A^{G703N}$ ($P<0.001$) and $3A^{R704N}$ ($P<0.001$). There was no significant difference between $3A^{G703N}$ and $3A^{R704N}$ at -50 mV ($P=0.124$).

	IC_{50} (95% CI) μM		
Voltage (mV)	**$3A^{G703N}$**	**$3A^{R704N}$**	**$3A^{R704D}$**
-100	**1.18** 0.90 to 1.55 ***P<0.023** **†P=0.001**	**1.190** 0.77 to 1.83 *P=0.081 **†P=0.009**	**2.11** 1.40 to 3.20 ***P<0.001** †P=0.499
-75	**5.39** 4.72 to 6.14 ***P<0.001** **†P=0.006**	**2.68** 1.90 to 3.77 *P=0.689 **†P<0.001**	**2.644** 2.019 to 3.460 *P=0.708 **†P<0.001**
-50	**5.53** 4.81 to 6.36 ***P<0.001** **†P<0.001**	**7.01** 5.23 to 9.39 ***P<0.001** **†P<0.001**	**3.25** 2.51 to 4.20 *P=0.154 **†P<0.001**

Table 16: IC_{50} values for memantine at $3A^{G703N}$, $3A^{G703N}$ and $3A^{R704D}$ containing receptors.
* denotes statistical significance against 1-1a/2A and † denotes significance against 3A.

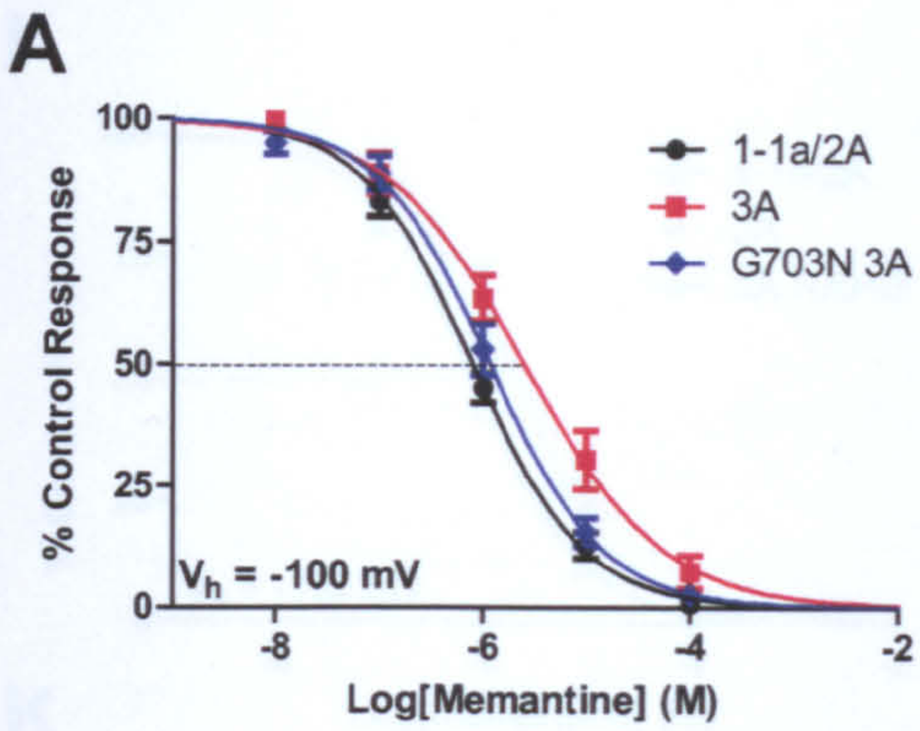
A
100
75
50
25
0
% Control Response
V_h = -100 mV
-8
-6
-4
-2
Log[Memantine] (M)
1-1a/2A
3A
G703N 3A

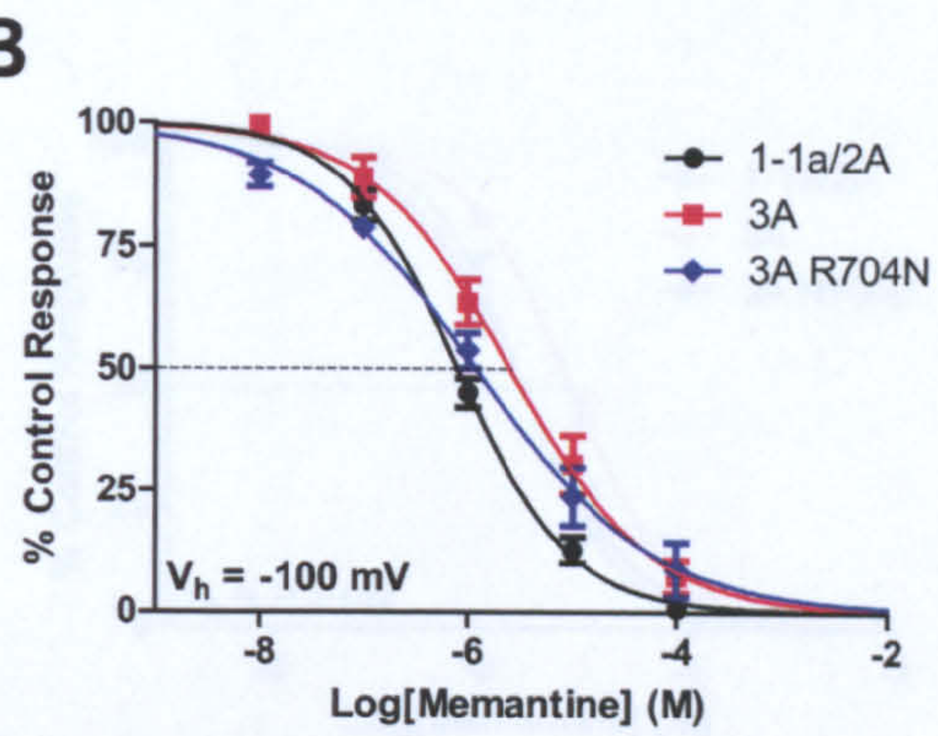
B
100
75
50
25
0
% Control Response
V_h = -100 mV
-8
-6
-4
-2
Log[Memantine] (M)
1-1a/2A
3A
3A R704N

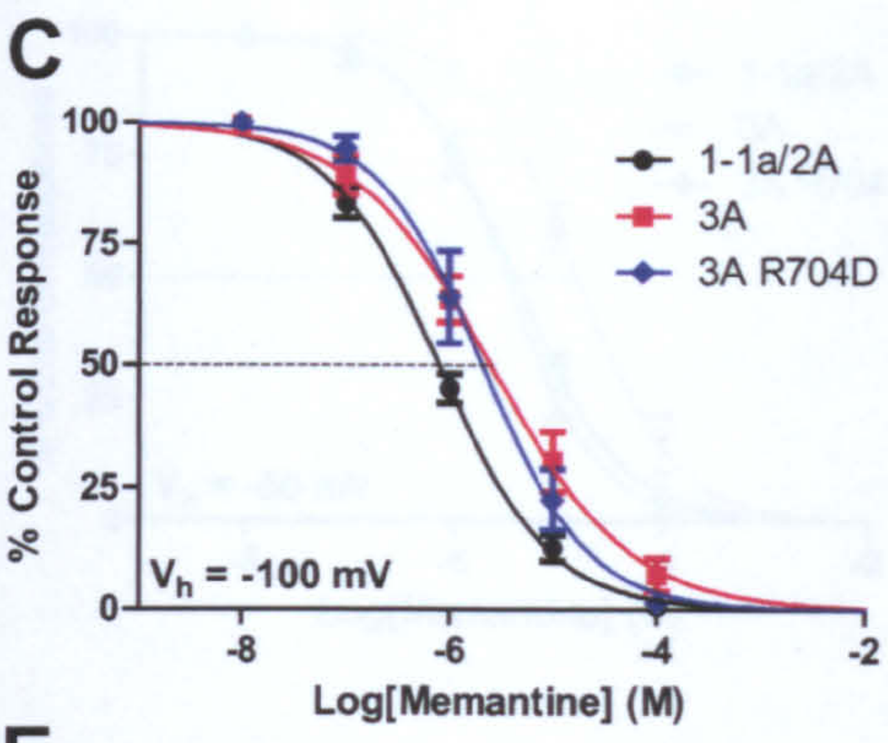
C
100
75
50
25
0
% Control Response
V_h = -100 mV
-8
-6
-4
-2
Log[Memantine] (M)
1-1a/2A
3A
3A R704D

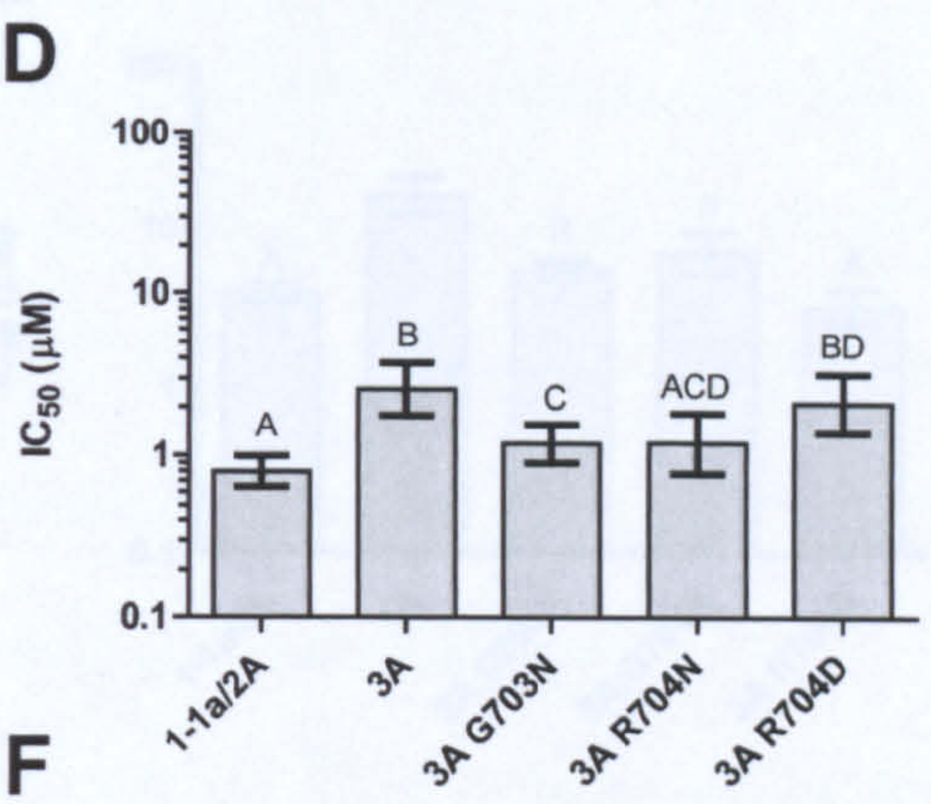
D
100
10
1
0.1
IC_{50} (μM)
A
B
C
ACD
BD
1-1a/2A
3A
3A G703N
3A R704N
3A R704D

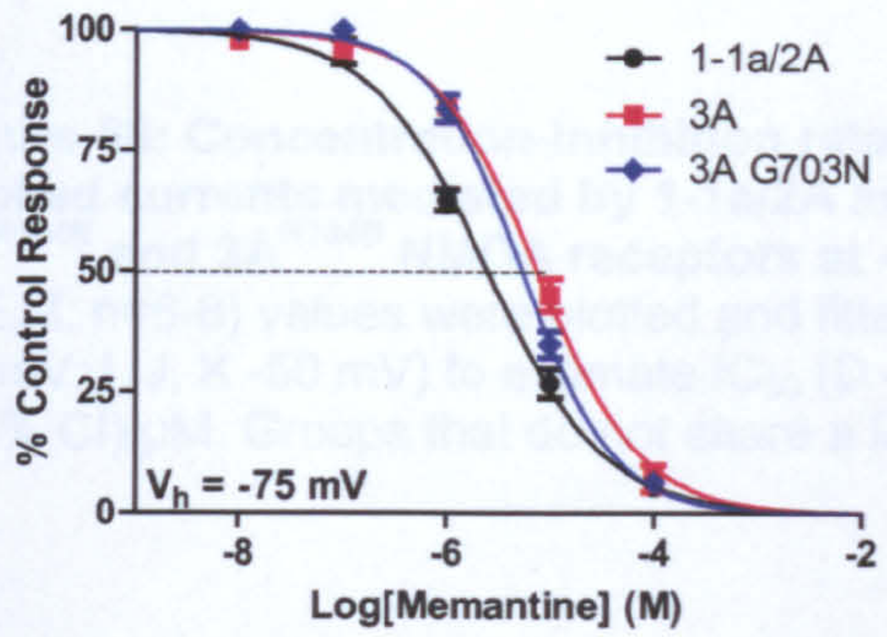
E
100
75
50
25
0
% Control Response
V_h = -75 mV
-8
-6
-4
-2
Log[Memantine] (M)
1-1a/2A
3A
3A G703N

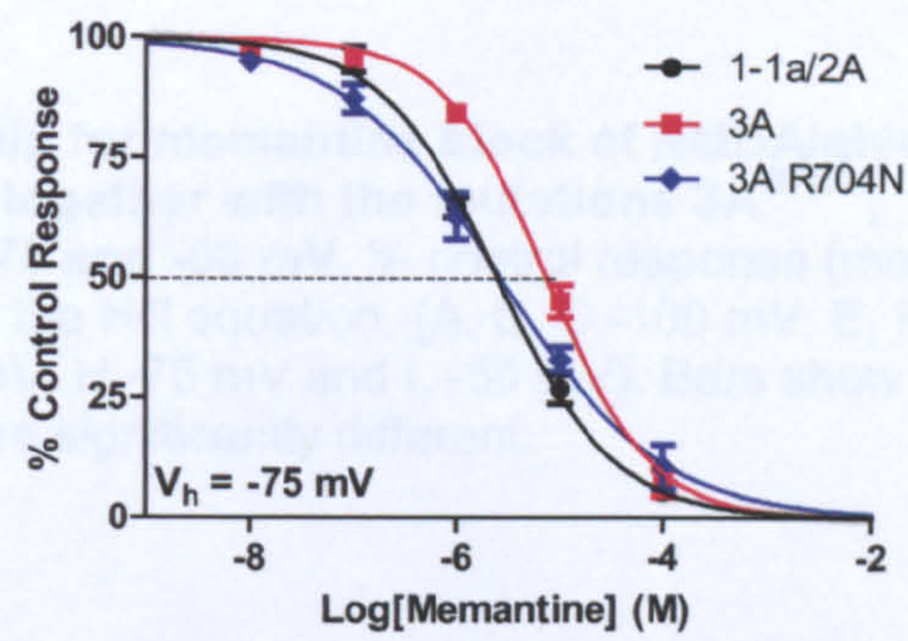
F
100
75
50
25
0
% Control Response
V_h = -75 mV
-8
-6
-4
-2
Log[Memantine] (M)
1-1a/2A
3A
3A R704N

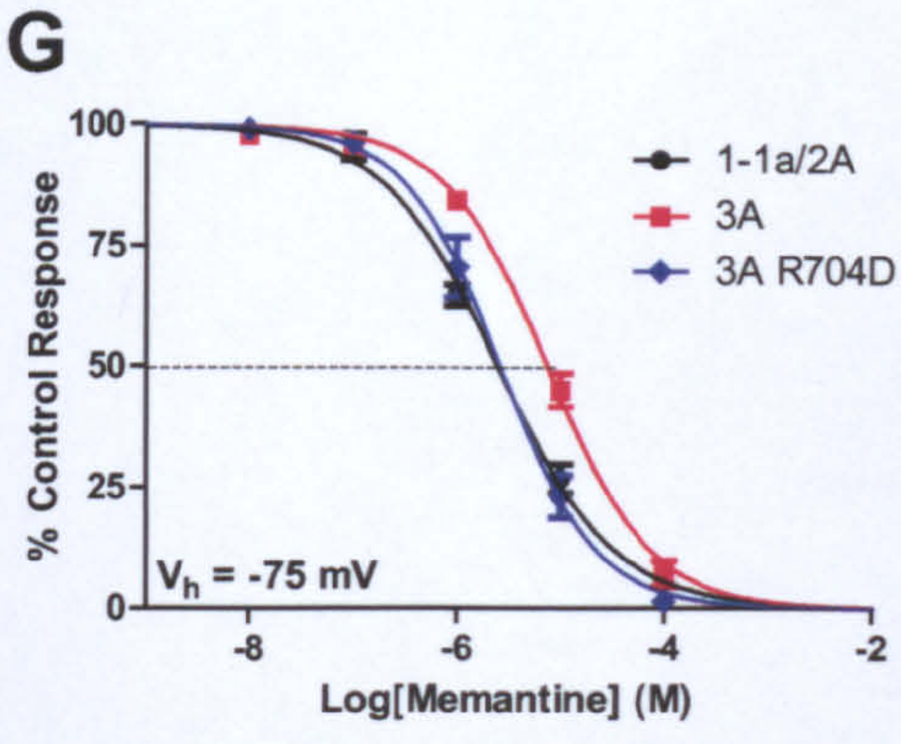
G
100
75
50
25
0
% Control Response
V_h = -75 mV
-8
-6
-4
-2
Log[Memantine] (M)
1-1a/2A
3A
3A R704D

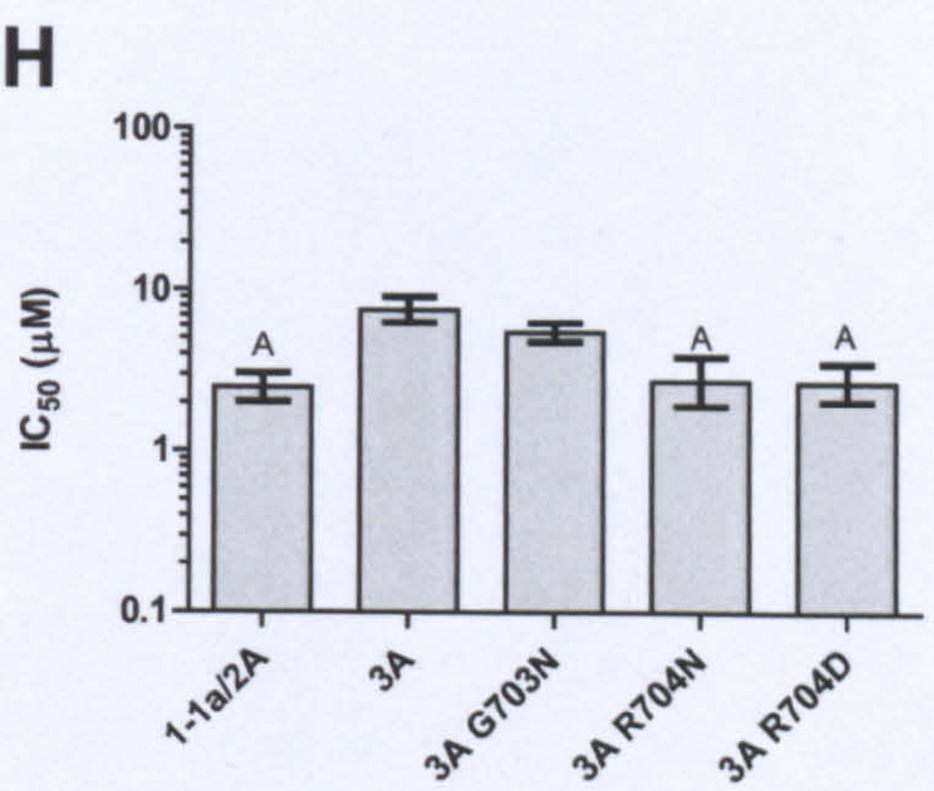
H
100
10
1
0.1
IC_{50} (μM)
A
A
A
1-1a/2A
3A
3A G703N
3A R704N
3A R704D

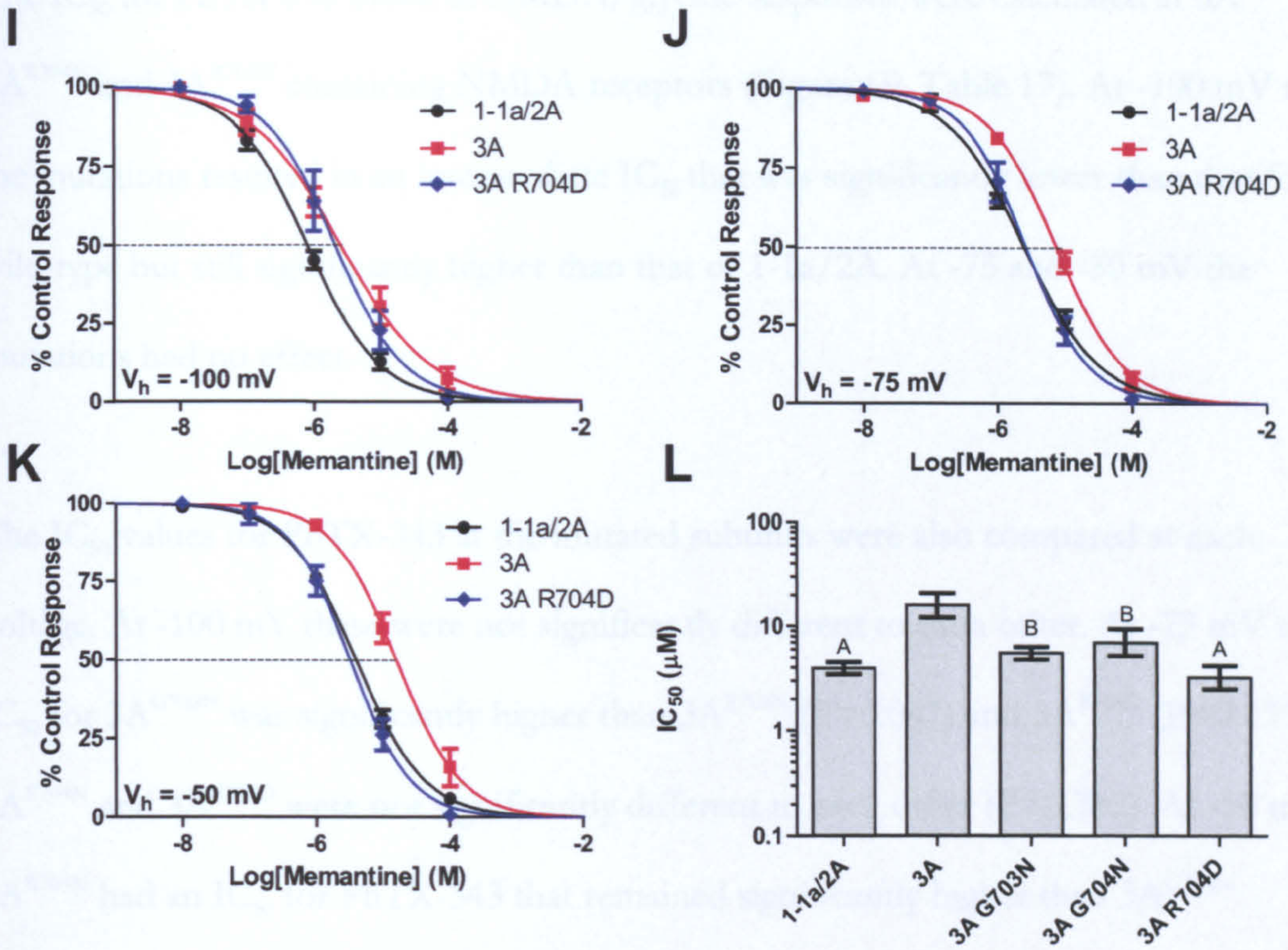

Figure 68: Concentration-inhibition relationship for memantine block of NMDA/glycine-evoked currents mediated by 1-1a/2A and 3A together with the mutations $3A^{G703N}$, $3A^{R704N}$ and $3A^{R704D}$ NMDA receptors at -100, -75 and -50 mV. % control response (mean ± S.E.M, n=6-8) values were plotted and fitted with the Hill equation. (A, B, C -100 mV; E, F, G -75 mV; I, J, K -50 mV) to estimate IC_{50} (D -100 mV, H -75 mV and L -50 mV). Bars show IC_{50} (95% CI) μM. Groups that do not share a letter are significantly different.

The IC_{50} for PhTX-343 block of NMDA/glycine responses were calculated at $3A^{G703N}$, $3A^{R704N}$ and $3A^{R704D}$ containing NMDA receptors (Figure 69, Table 17). At -100 mV all the mutations resulted in an intermediate IC_{50} that was significantly lower than that for wild-type but still significantly higher than that of 1-1a/2A. At -75 and -50 mV the mutations had no effect.

The IC_{50} values for PhTX-343 at the mutated subunits were also compared at each voltage. At -100 mV these were not significantly different to each other. At -75 mV the IC_{50} for $3A^{G703N}$ was significantly higher than $3A^{R704N}$ (P=0.047) and $3A^{R704D}$ (P=0.031). $3A^{R704N}$ and $3A^{R704D}$ were not significantly different to each other (P=0.782). At -50 mV $3A^{R704N}$ had an IC_{50} for PhTX-343 that remained significantly higher than $3A^{G703N}$ (P=0.006) and $3A^{R704D}$ (P<0.001), while $3A^{G703N}$ and $3A^{R704D}$ again were not significantly different to each other (P=0.059).

	IC_{50} (95% CI) µM		
Voltage (mV)	**$3A^{G703N}$**	**$3A^{R704N}$**	**$3A^{R704D}$**
-100	**0.49** 0.62 to 0.39 ***P=0.032** **†P=0.002**	**0.51** 0.36 to 0.71 ***P=0.046** **†P=0.003**	**0.51** 0.41 to 0.64 ***P=0.017** **†P<0.001**
-75	**5.40** 3.61 to 8.08 *P=0.0988 †P=0.6206	**3.12** 2.15 to 4.52 *P=0.876 †P=0.204	**3.30** 2.65 to 4.11 *P=0.718 †P=0.213
-50	**22.04** 18.73 to 25.94 *P=0.400 †P=0.468	**29.67** 25.91 to 33.97 *P=0.065 †P=0.111	17.41 14.46 to 20.97 *P=0.970 †P=0.982

Table 17: IC_{50} values for PhTX-343 at $3A^{G703N}$, $3A^{G703N}$ and $3A^{R704D}$ containing receptors. * denotes statistical significance against 1-1a/2A and † denotes significance against 3A.

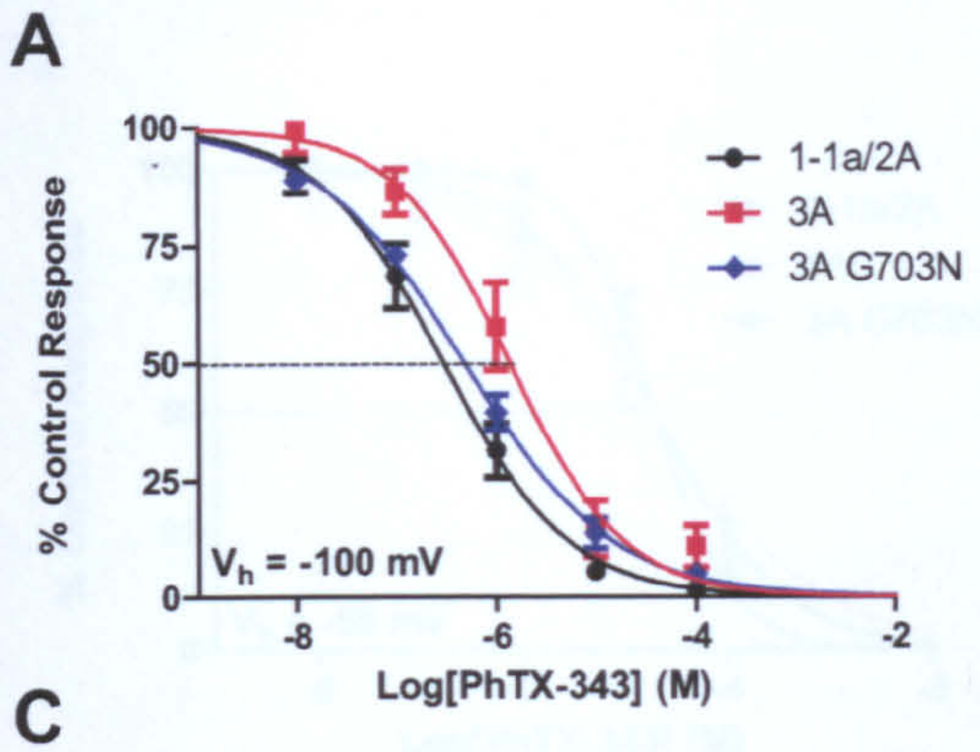
A
100
75
50
25
0
% Control Response
1-1a/2A
3A
3A G703N
V_h = -100 mV
-8
-6
-4
-2
Log[PhTX-343] (M)

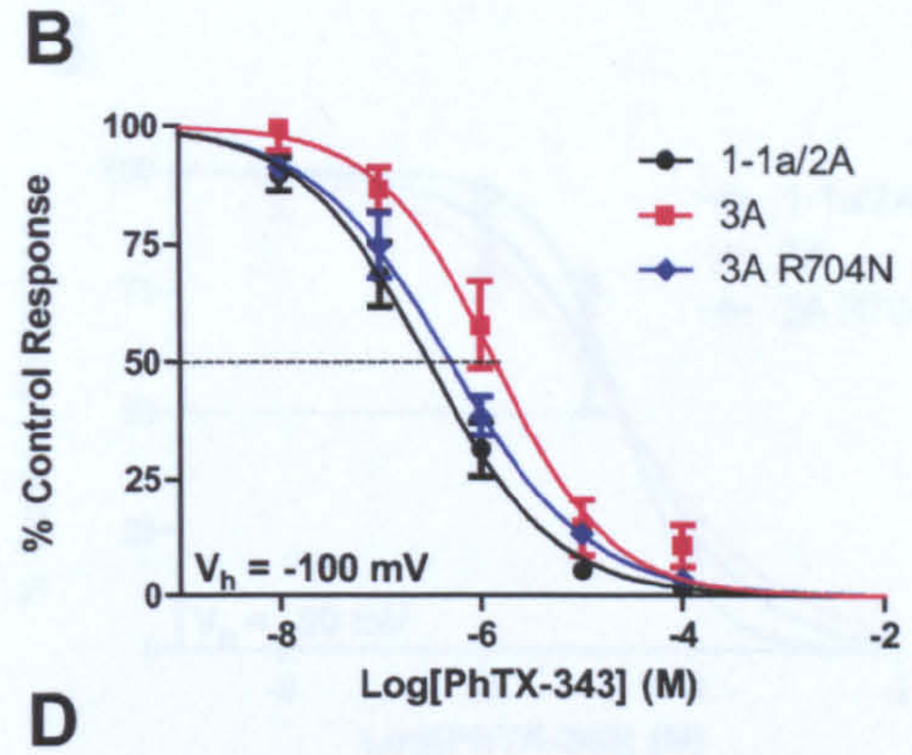
B
100
75
50
25
0
% Control Response
1-1a/2A
3A
3A R704N
V_h = -100 mV
-8
-6
-4
-2
Log[PhTX-343] (M)

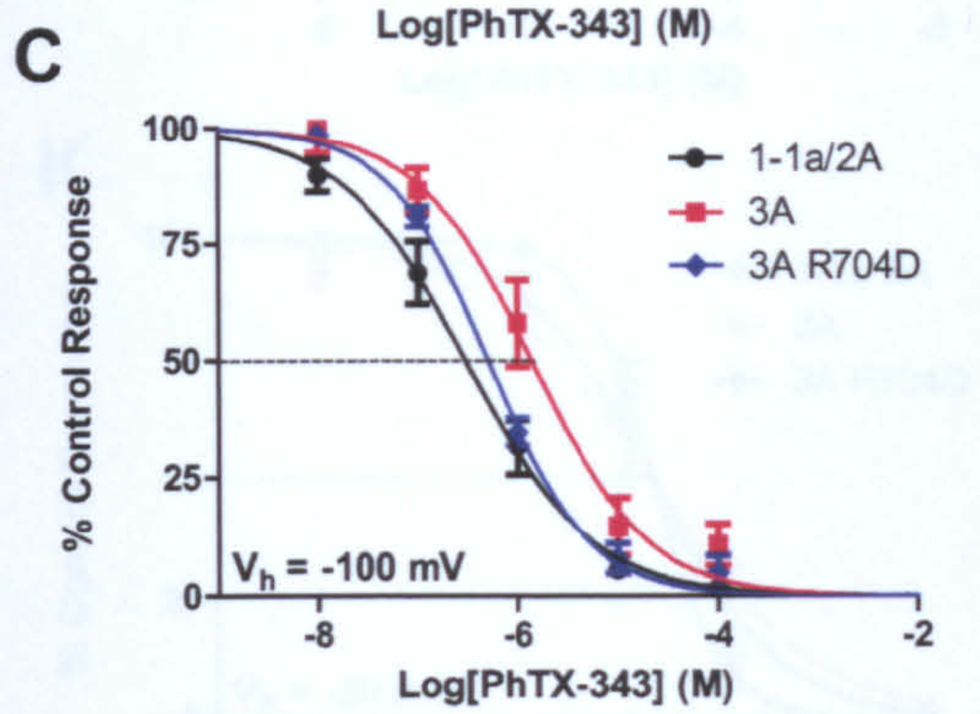
C
100
75
50
25
0
% Control Response
1-1a/2A
3A
3A R704D
V_h = -100 mV
-8
-6
-4
-2
Log[PhTX-343] (M)

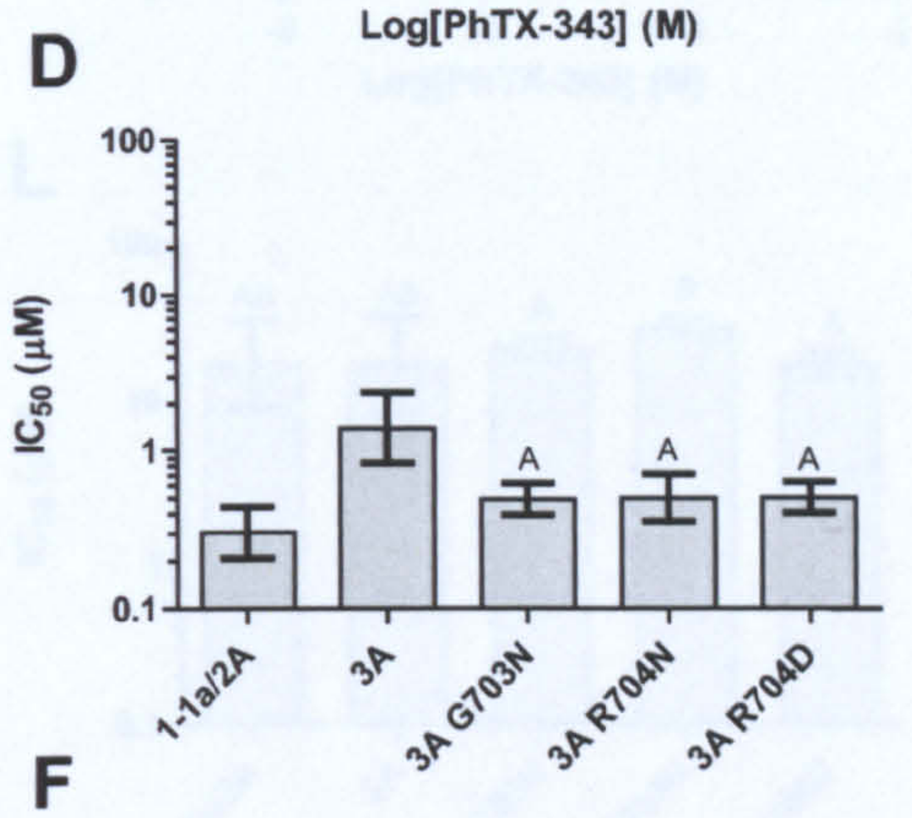
D
100
10
1
0.1
IC_{50} (μM)
A
A
A
1-1a/2A
3A
3A G703N
3A R704N
3A R704D

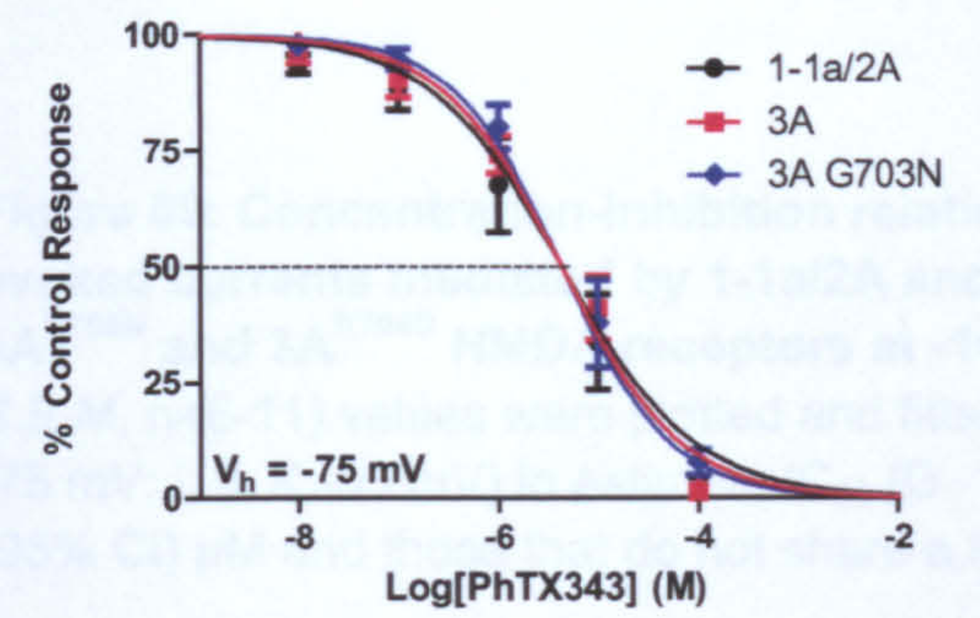
E
100
75
50
25
0
% Control Response
1-1a/2A
3A
3A G703N
V_h = -75 mV
-8
-6
-4
-2
Log[PhTX343] (M)

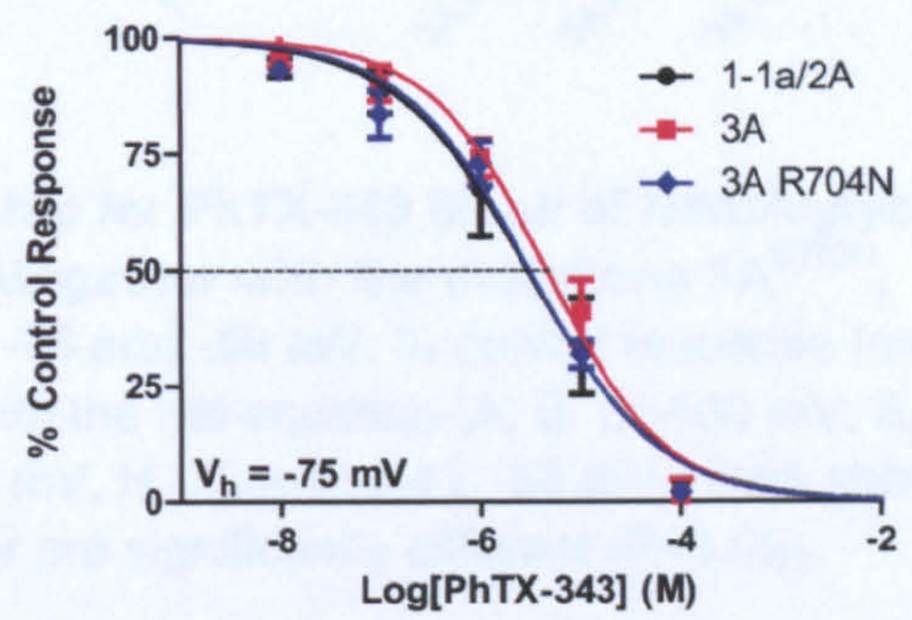
F
100
75
50
25
0
% Control Response
1-1a/2A
3A
3A R704N
V_h = -75 mV
-8
-6
-4
-2
Log[PhTX-343] (M)

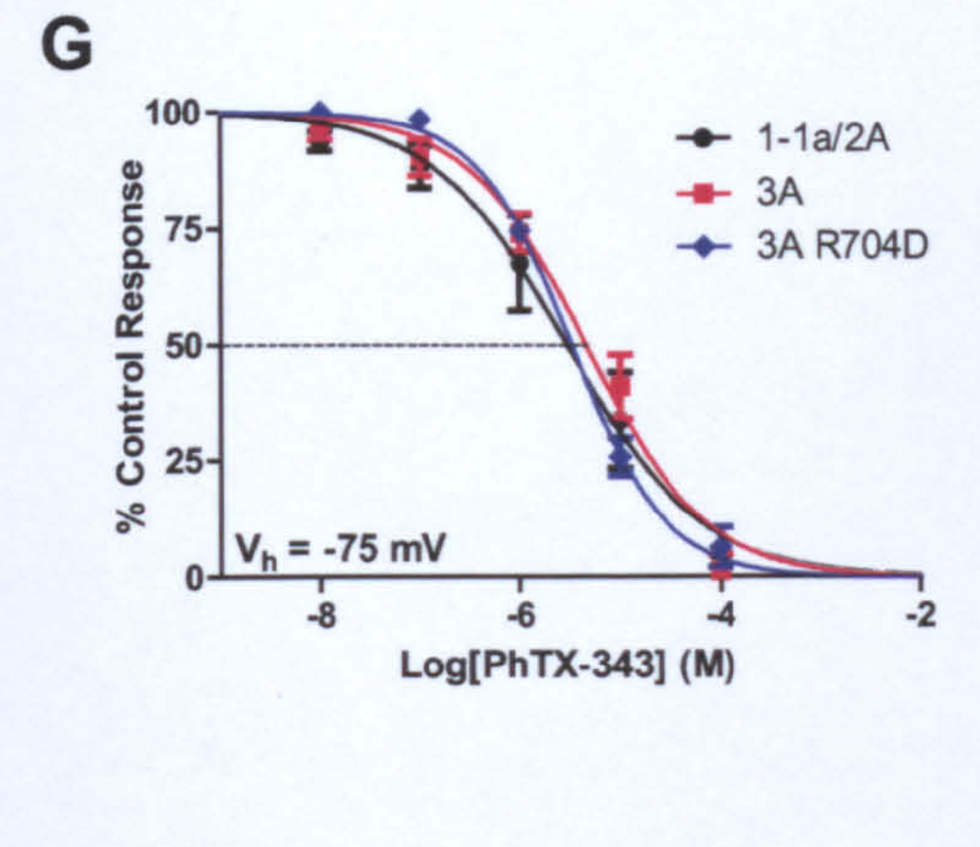
G
100
75
50
25
0
% Control Response
1-1a/2A
3A
3A R704D
V_h = -75 mV
-8
-6
-4
-2
Log[PhTX-343] (M)

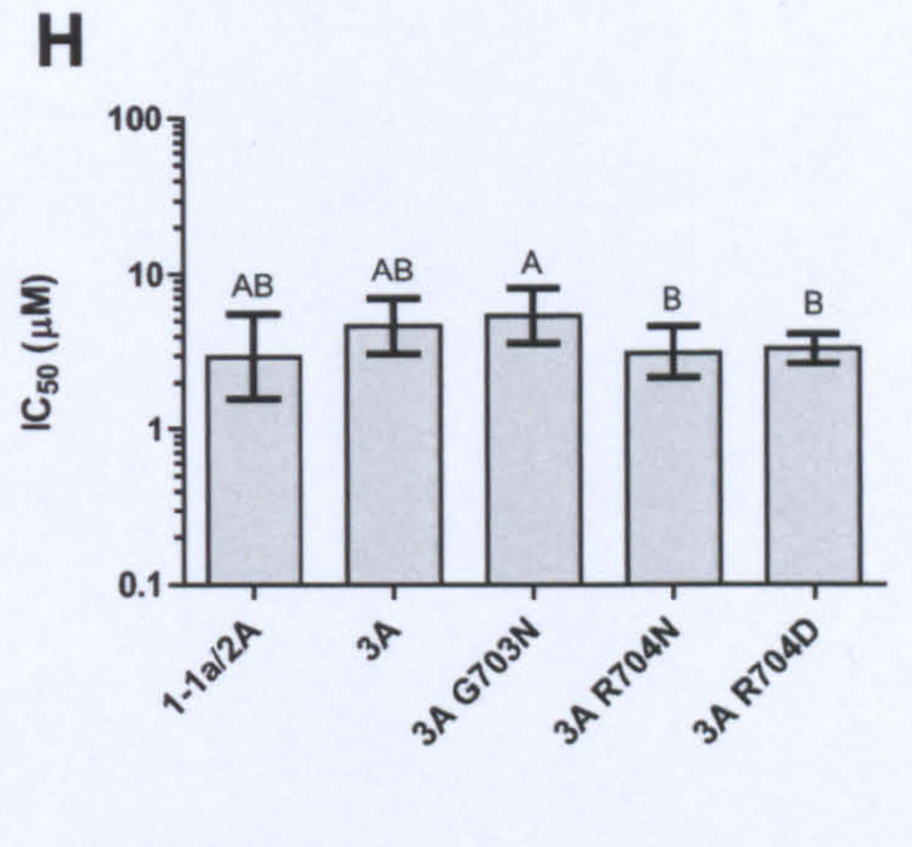
H
100
10
1
0.1
IC_{50} (μM)
AB
AB
A
B
B
1-1a/2A
3A
3A G703N
3A R704N
3A R704D

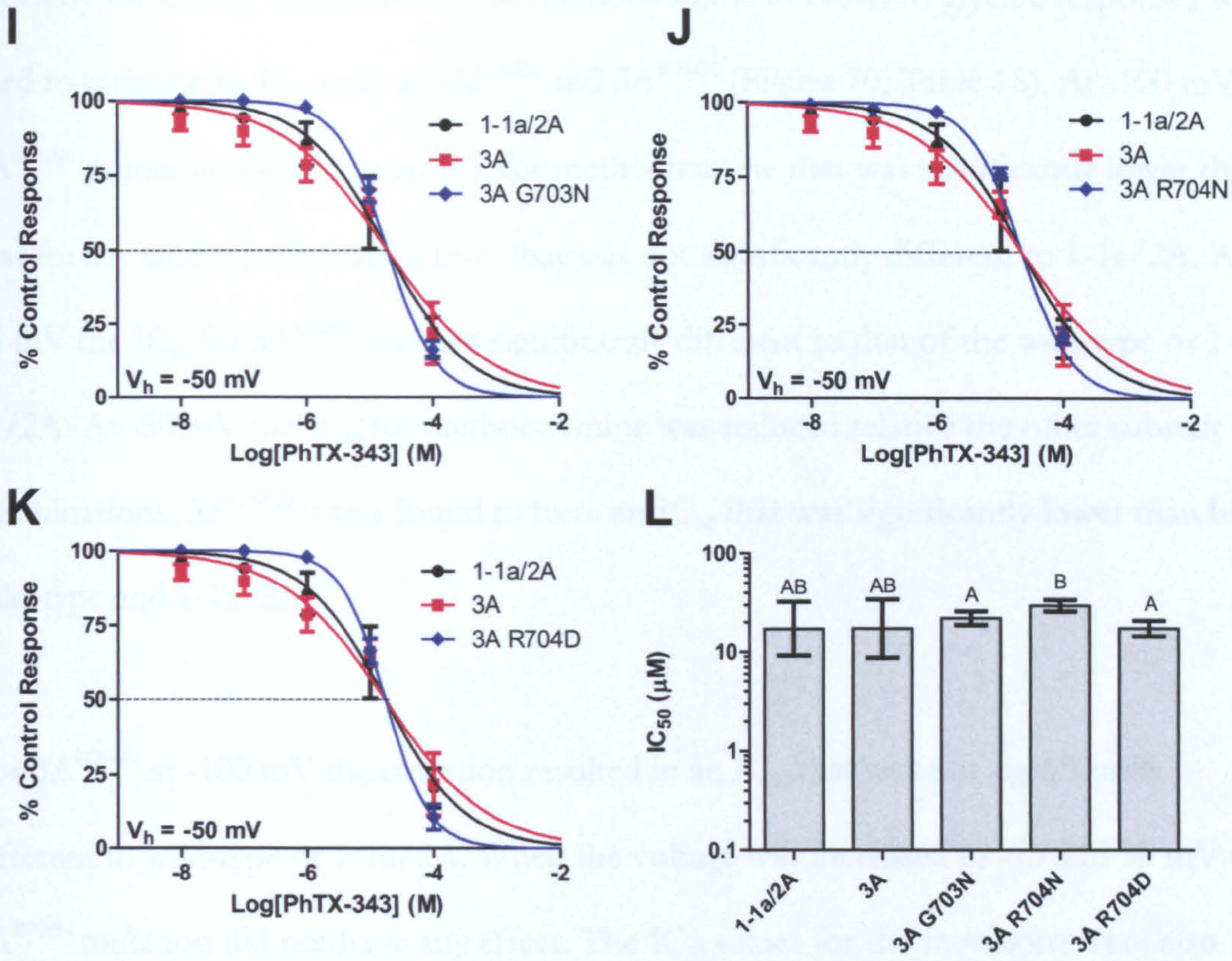

Figure 69: Concentration-inhibition relationship for PhTX-343 block of NMDA/glycine-evoked currents mediated by 1-1a/2A and 3Atogether with the mutations $3A^{G703N}$, $3A^{R704N}$ and $3A^{R704D}$ NMDA receptors at -100, -75 and -50 mV. % control response (mean ± S.E.M, n=6-11) values were plotted and fitted with the Hill equation (A, B, C -100 mV; E, F, G -75 mV; I, J, K -50 mV) to estimate IC_{50} (D -100 mV, H -75 mV and L -50 mV). Bars show IC_{50} (95% CI) μM and those that do not share a letter are significantly different (P<0.05)

Block by increasing concentrations of methoctramine to NMDA/glycine responses were used to estimate its IC_{50} only at $3A^{G703N}$ and $3A^{R704N}$ (Figure 70, Table 18). At -100 mV the $3A^{G703N}$ mutation resulted in an IC_{50} for methoctramine that was significantly lower than that for 3A wild-type, toward a level that was not significantly different to 1-1a/2A. At -75 mV the IC_{50} for $3A^{G703N}$ was not significantly different to that of the wild-type or 1-1a/2A. At -50 mV the IC_{50} for methoctramine was reduced relative the other subunit combinations, $3A^{G703N}$ it was found to have an IC_{50} that was significantly lower than both wild-type and 1-1a/2A.

For $3A^{G704N}$ at -100 mV the mutation resulted in an IC_{50} that was not significantly different to wild-type or 1-1a/2A. When the voltage was increased to -75 and 50 mV the $3A^{R704N}$ mutation did not have any effect. The IC_{50} values for the mutations were also compared with each other at each voltage tested. At -100 and -75 mV they were not significantly different to each other. At -50 mV $3A^{G703N}$ had an IC_{50} that was significantly lower than $3A^{R704N}$ (P=0.002).

	IC_{50} (95% CI) µM	
Voltage (mV)	**$3A^{G703N}$**	**$3A^{R704N}$**
-100	**1.85** 1.29 to 2.64 *P=0.297 **†P=0.039**	**1.83** 1.18 to 2.84 *P=0.379 †P=0.056
-75	**2.50** 2.08 to 3.01 *P=0.316 †P=0.735	**3.28** 1.96 to 5.49 *P=0.139 †P=0.416
-50	**2.80** 2.02 to 3.89 ***P=0.009** **†P=0.015**	**6.08** 4.24 to 8.71 *P=0.608 †P=0.591

Table 18: IC_{50} values for methoctramine at $3A^{G703N}$, $3A^{G703N}$ containing receptors. * denotes statistical significance against 1-1a/2A and † denotes significance against 3A.

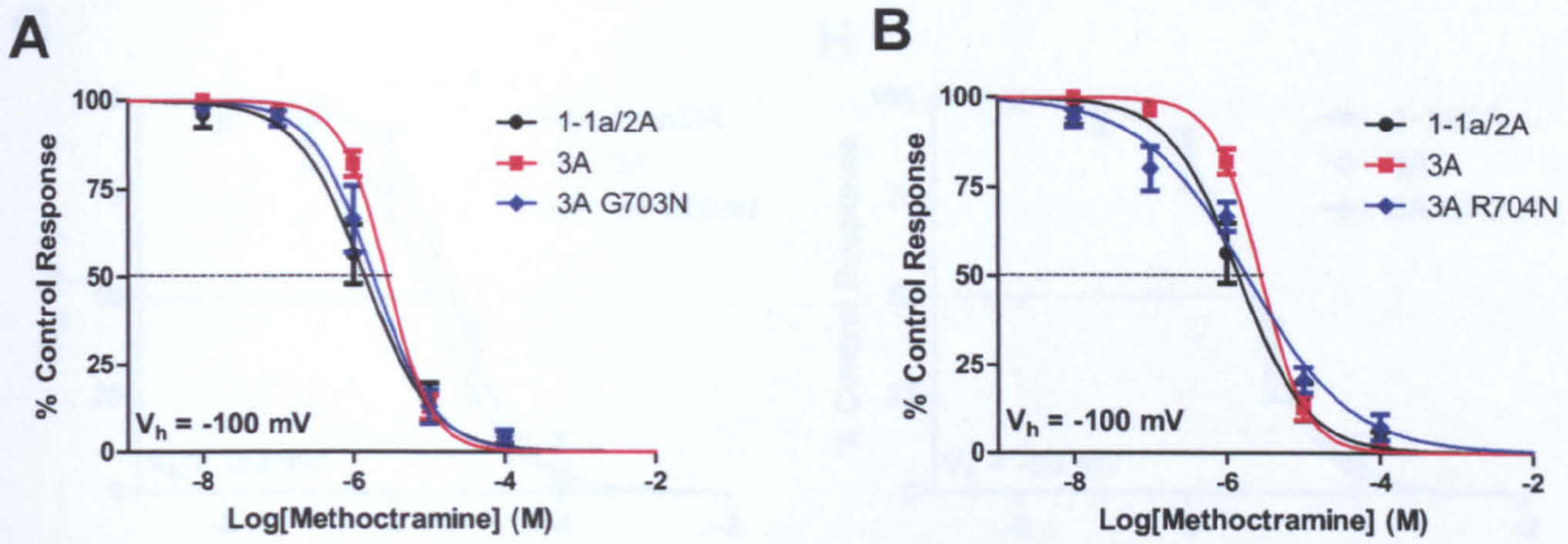
A
100
75
50
25
0
% Control Response
V_h = -100 mV
-8
-6
-4
-2
Log[Methoctramine] (M)
1-1a/2A
3A
3A G703N
B
100
75
50
25
0
% Control Response
V_h = -100 mV
-8
-6
-4
-2
Log[Methoctramine] (M)
1-1a/2A
3A
3A R704N

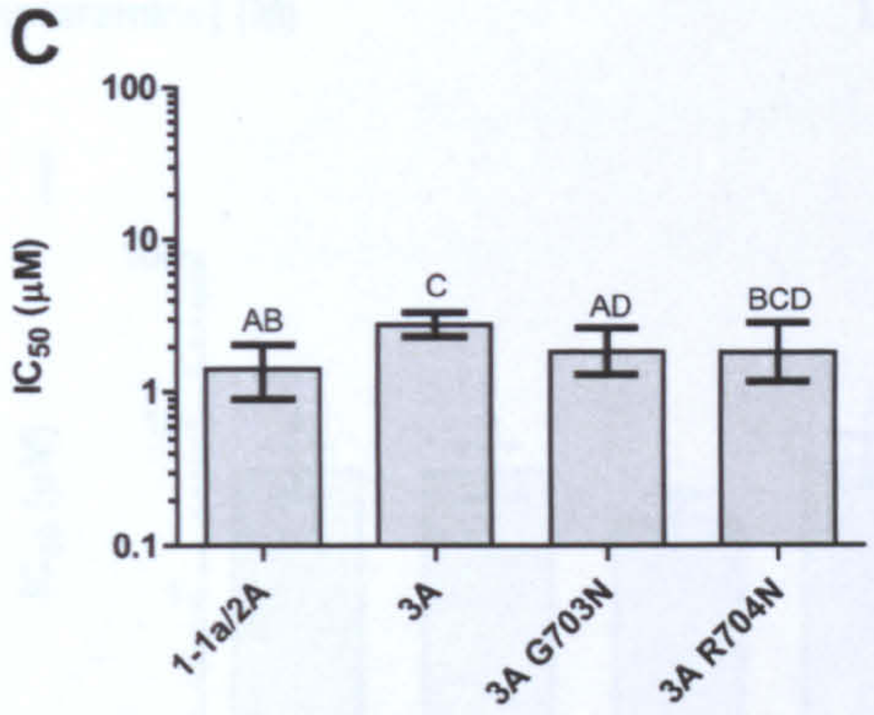
C
100
10
1
0.1
IC_{50} (μM)
AB
C
AD
BCD
1-1a/2A
3A
3A G703N
3A R704N

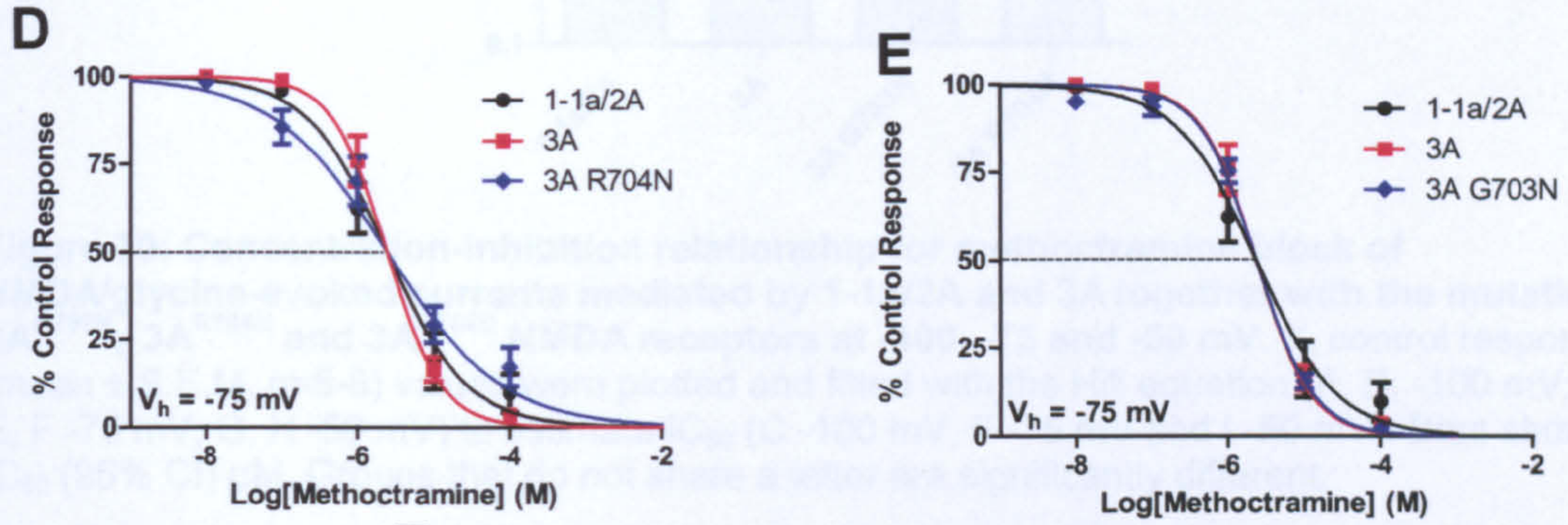
D
100
75
50
25
0
% Control Response
V_h = -75 mV
-8
-6
-4
-2
Log[Methoctramine] (M)
1-1a/2A
3A
3A R704N
E
100
75
50
25
0
% Control Response
V_h = -75 mV
-8
-6
-4
-2
Log[Methoctramine] (M)
1-1a/2A
3A
3A G703N

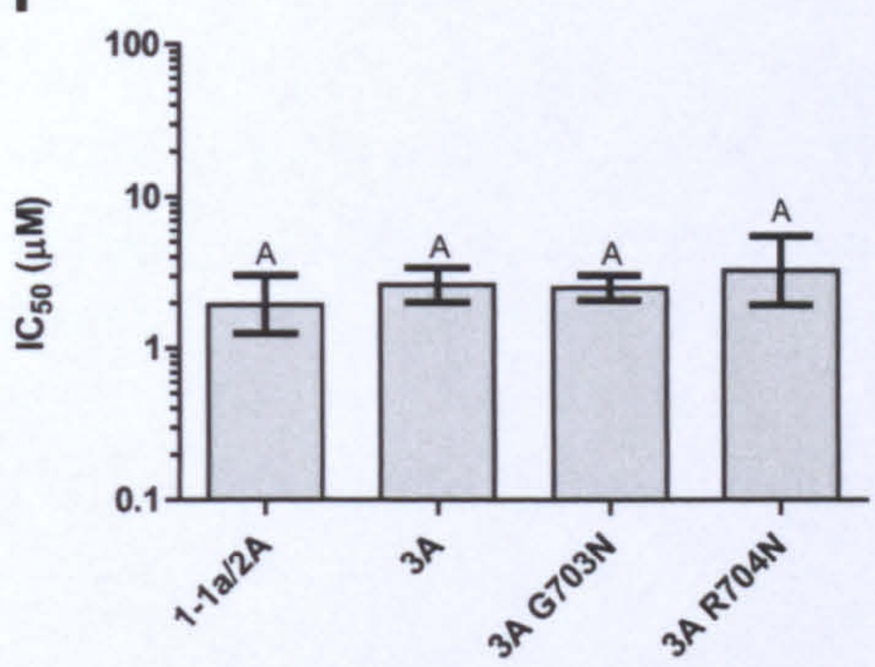
F
100
10
1
0.1
IC_{50} (μM)
A
A
A
A
1-1a/2A
3A
3A G703N
3A R704N

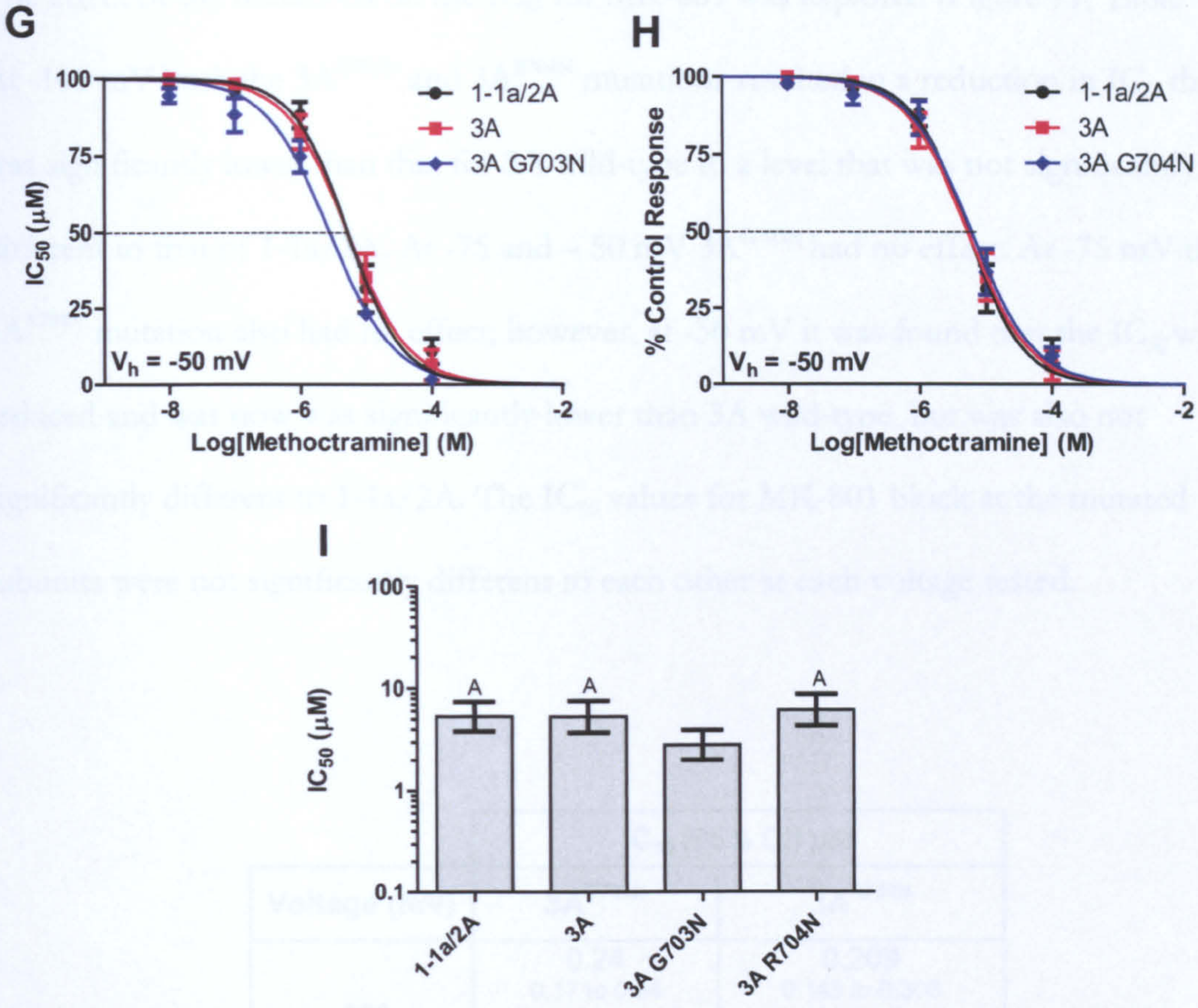

Figure 70: Concentration-inhibition relationship for methoctramine block of NMDA/glycine-evoked currents mediated by 1-1a/2A and 3A together with the mutations $3A^{G703N}$, $3A^{R704N}$ and $3A^{R704D}$ NMDA receptors at -100, -75 and -50 mV. % control response (mean ± S.E.M, n=5-8) values were plotted and fitted with the Hill equation (A, B, -100 mV; D, E, F -75 mV; G, H -50 mV) to estimate IC_{50} (C -100 mV, F -75 mV and I -50 mV). Bars show IC_{50} (95% CI) μM. Groups that do not share a letter are significantly different.

The effect of the mutations on the IC_{50} for MK-801 was explored (Figure 71, Table 19). At -100 mV both the $3A^{G703N}$ and $3A^{R704N}$ mutations resulted in a reduction in IC_{50} that was significantly lower than that for 3A wild-type to a level that was not significantly different to that of 1-1a/2A. At -75 and – 50 mV $3A^{G703N}$ had no effect. At -75 mV the $3A^{R704N}$ mutation also had no effect; however, at -50 mV it was found that the IC_{50} was reduced and was now was significantly lower than 3A wild-type, but was also not significantly different to 1-1a/2A. The IC_{50} values for MK-801 block at the mutated subunits were not significantly different to each other at each voltage tested.

	IC_{50} (95% CI) µM	
Voltage (mV)	**$3A^{G703N}$**	**$3A^{R704N}$**
-100	0.24 0.17 to 0.34 *P=0.453 †P<0.001	0.209 0.143 to 0.306 *P=0.788 †P<0.001
-75	0.39 0.26 to 0.66 *P=0.084 †P=0.467	0.21 0.13 to 0.33 *P=0.204 †P=0.187
-50	0.39 0.26 to 0.66 *P=0.29 †P=0.18	0.21 0.14 to 0.33 *P=0.051 †P=0.008

Table 19: IC_{50} values for MK-801 at $3A^{G703N}$, $3A^{G703N}$ containing receptors. * denotes statistical significance against 1-1a/2A and † denotes significance against 3A.

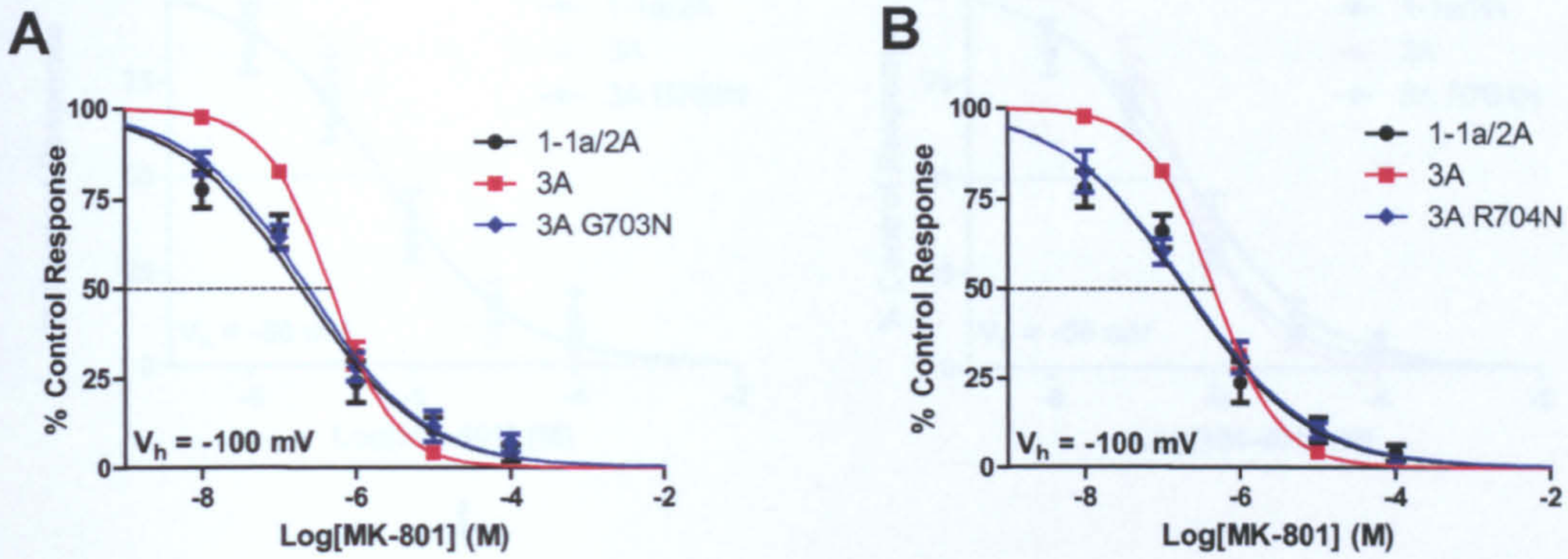
A
100
75
50
25
0
% Control Response
V_h = -100 mV
-8
-6
-4
-2
Log[MK-801] (M)
1-1a/2A
3A
3A G703N
B
100
75
50
25
0
% Control Response
V_h = -100 mV
-8
-6
-4
-2
Log[MK-801] (M)
1-1a/2A
3A
3A R704N

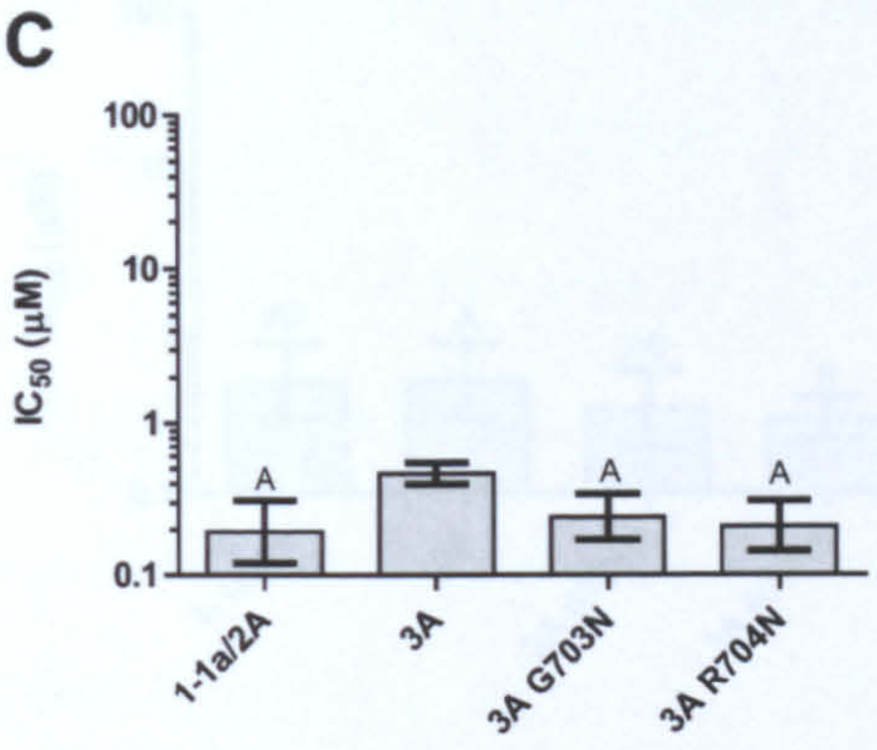
C
100
10
1
0.1
IC_{50} (μM)
A
A
A
1-1a/2A
3A
3A G703N
3A R704N

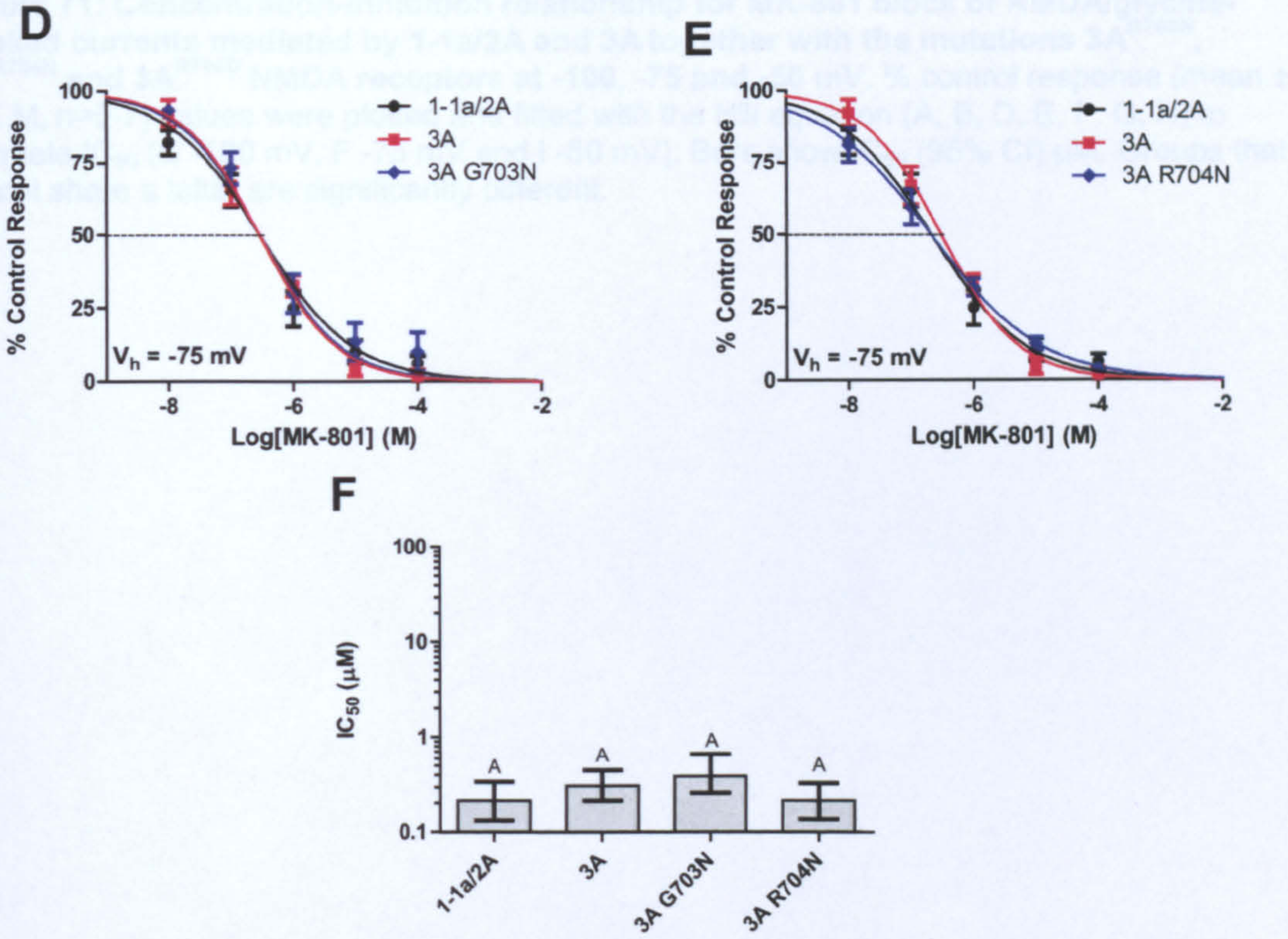
D
100
75
50
25
0
% Control Response
V_h = -75 mV
-8
-6
-4
-2
Log[MK-801] (M)
1-1a/2A
3A
3A G703N
E
100
75
50
25
0
% Control Response
V_h = -75 mV
-8
-6
-4
-2
Log[MK-801] (M)
1-1a/2A
3A
3A R704N
F
100
10
1
0.1
IC_{50} (μM)
A
A
A
A
1-1a/2A
3A
3A G703N
3A R704N

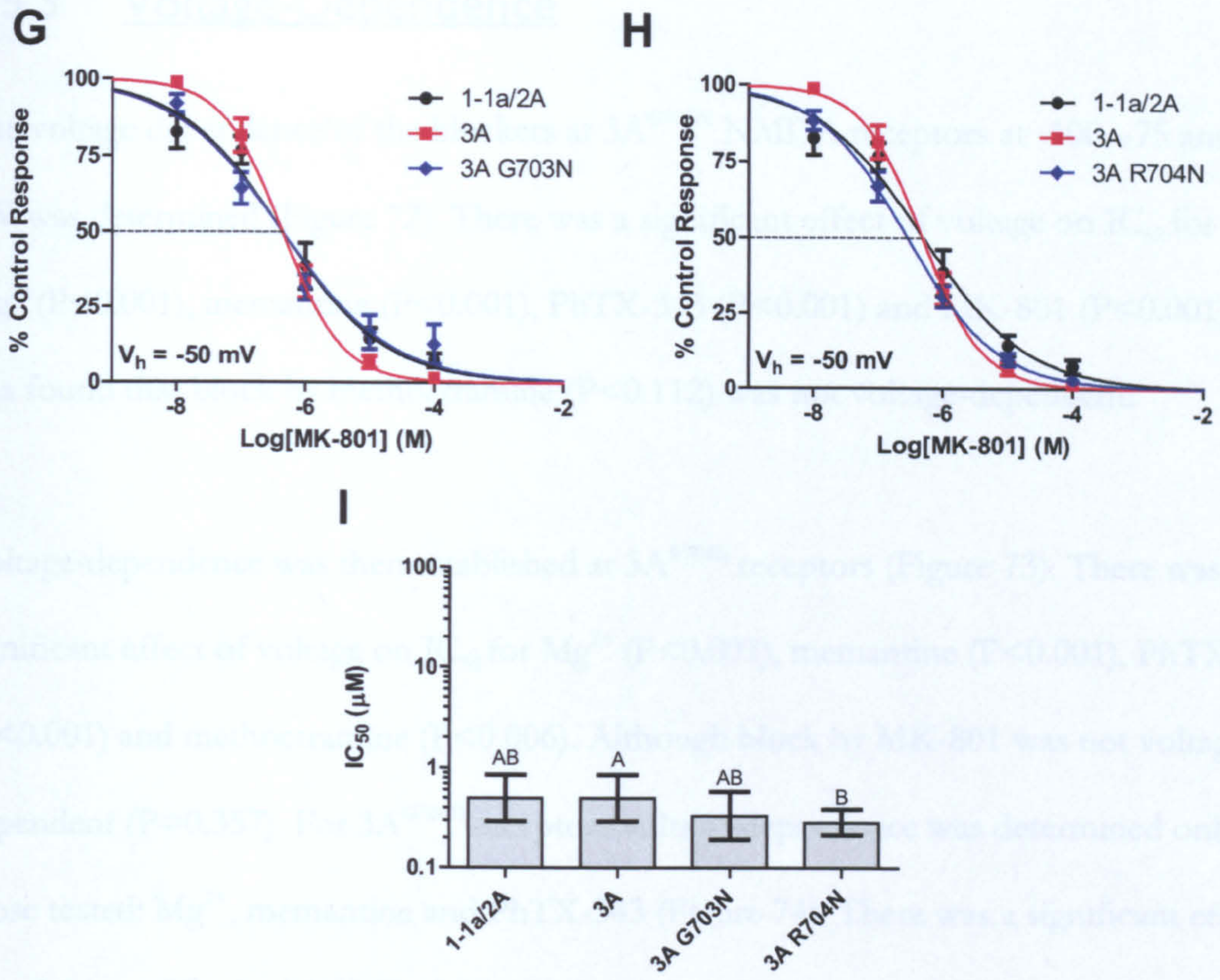

Figure 71: Concentration-inhibition relationship for MK-801 block of NMDA/glycine-evoked currents mediated by 1-1a/2A and 3A together with the mutations $3A^{G703N}$, $3A^{R704N}$ and $3A^{R704D}$ NMDA receptors at -100, -75 and -50 mV. % control response (mean ± S.E.M, n=5-7) values were plotted and fitted with the Hill equation (A, B, D, E, F, G, H) to estimate IC_{50} (C -100 mV, F -75 mV and I -50 mV). Bars show IC_{50} (95% CI) μM. Groups that do not share a letter are significantly different.

3.5.3 Voltage-Dependence

The voltage dependence of the blockers at $3A^{G703N}$ NMDA receptors at -100, -75 and -50 mV was determined (Figure 72). There was a significant effect of voltage on IC_{50} for Mg^{2+} ($P<0.001$), memantine ($P<0.001$), PhTX-343 ($P<0.001$) and MK-801 ($P<0.001$). It was found that block by methoctramine ($P<0.112$) was not voltage-dependent.

Voltage-dependence was then established at $3A^{R704N}$ receptors (Figure 73). There was a significant effect of voltage on IC_{50} for Mg^{2+} ($P<0.001$), memantine ($P<0.001$), PhTX-343 ($P<0.001$) and methoctramine ($P<0.006$). Although block by MK-801 was not voltage-dependent ($P=0.357$). For $3A^{G704D}$ receptors voltage-dependence was determined only for those tested: Mg^{2+}, memantine and PhTX-343 (Figure 74). There was a significant effect of voltage on IC_{50} for Mg^{2+} ($P<0.001$) and PhTX-343 ($P<0.001$). With this mutation the IC_{50} for memantine was not voltage-dependent ($P=0.184$).

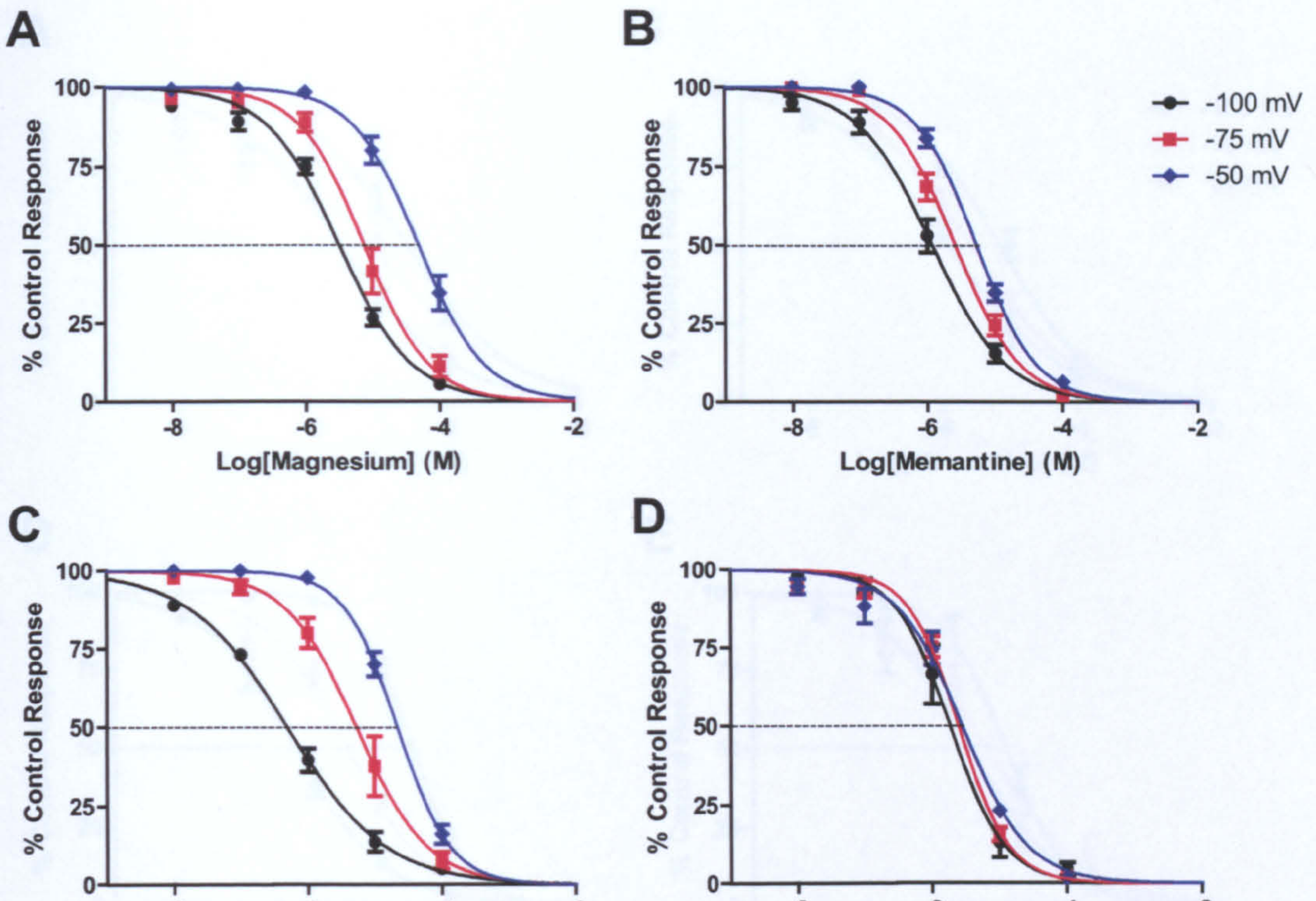

Figure 72: Concentration inhibition relationship showing voltage-dependence of block of NMDA-glycine-evoked responses mediated by $3A^{G703N}$ NMDA receptors at -100, -75 and -50 mV. % control response (mean ± S.E.M) values were plotted and fitted with the Hill equation for (A) Mg^{2+}, (B) memantine, (C) PhTX-343, (D) methoctramine and (E) MK-801.

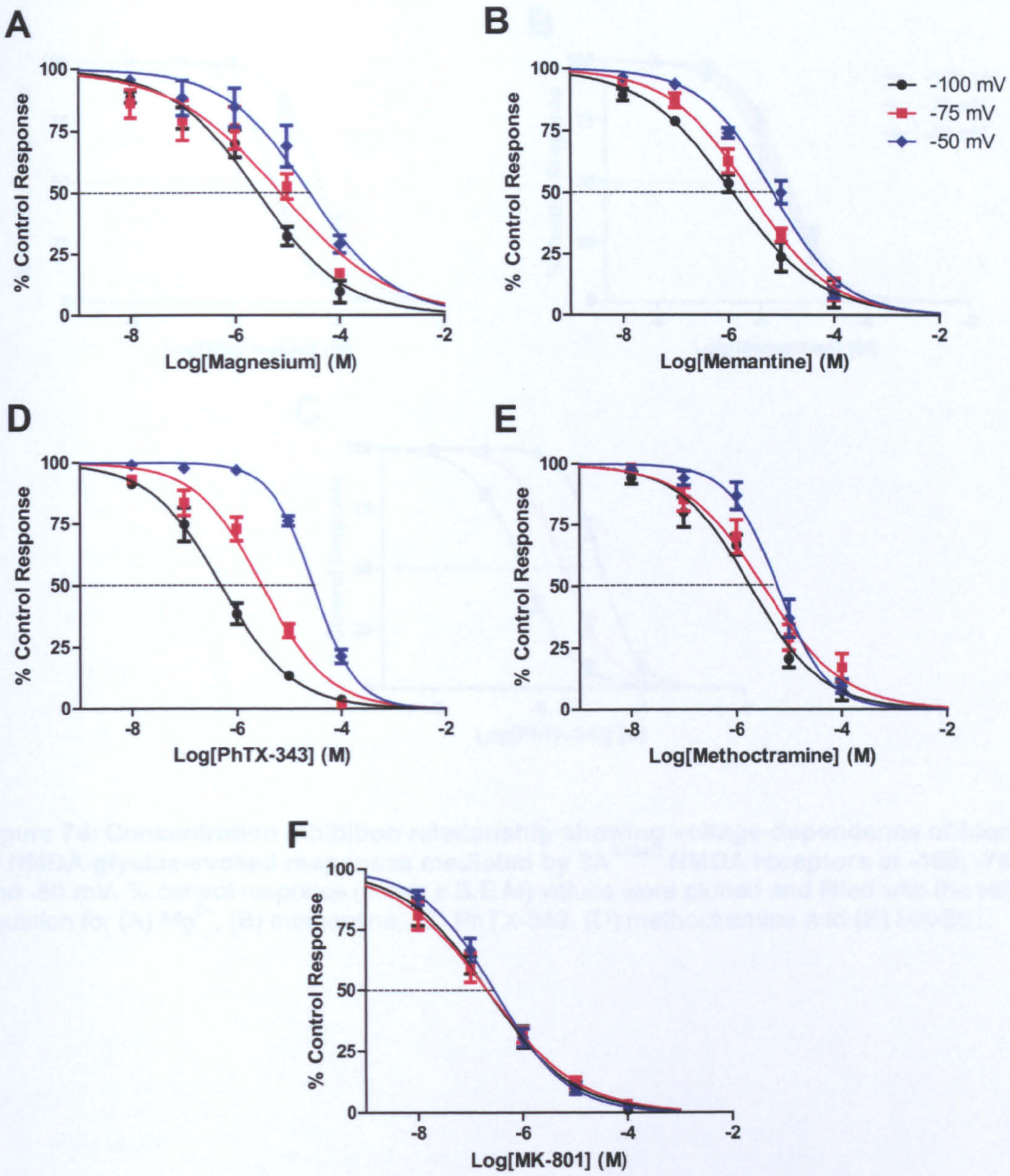

Figure 73: Concentration inhibition relationship showing voltage-dependence of block of NMDA-glycine-evoked responses mediated by $3A^{R704N}$ NMDA receptors at -100, -75 and -50 mV. % control response (mean ± S.E.M) values were plotted and fitted with the Hill equation for (A) Mg^{2+}, (B) memantine, (C) PhTX-343, (D) methoctramine and (E) MK-801.

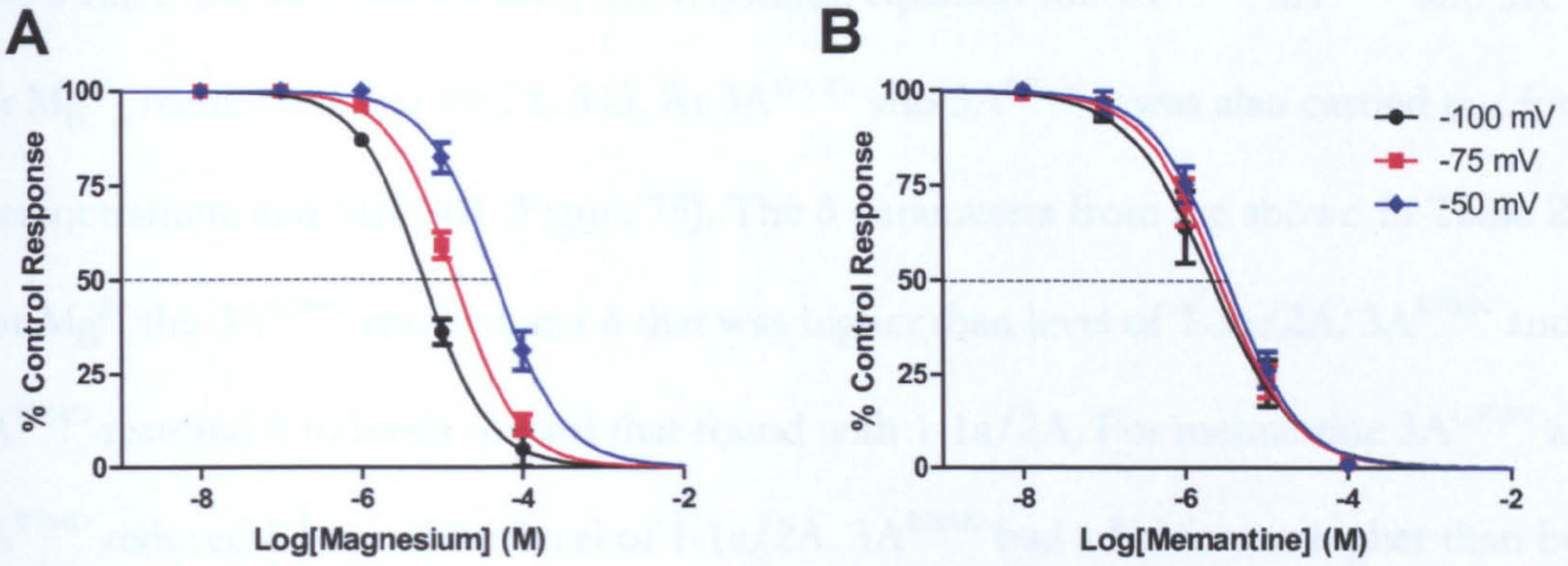

Figure 74: Concentration inhibition relationship showing voltage-dependence of block of NMDA-glycine-evoked responses mediated by $3A^{R704D}$ NMDA receptors at -100, -75 and -50 mV. % control response (mean ± S.E.M) values were plotted and fitted with the Hill equation for (A) Mg^{2+}, (B) memantine, (C) PhTX-343, (D) methoctramine and (E) MK-801.

The δ value was determined from the Woodhull equation for $3A^{G703N}$, $3A^{R704N}$ and $3A^{R704D}$ for Mg^{2+}, memantine and PhTX-343. At $3A^{G703N}$ and $3A^{R704N}$ it was also carried out for methoctramine and MK-801 (Figure 75). The δ parameters from are shown in Table 20. For Mg^{2+} the $3A^{G703N}$ resulted in a δ that was higher than level of 1-1a/2A. $3A^{R704N}$ and $3A^{R704D}$ restored δ to levels toward that found with 1-1a/2A. For memantine $3A^{G703N}$ and $3A^{R704D}$ reduced δ beyond the level of 1-1a/2A. $3A^{R704N}$ had a δ that was higher than both 3A and 1-1a/2A. The δ for PhTX-343 at $3A^{R704N}$ and $3A^{R704D}$ restored it to levels toward that found with 1-1a/2A, but for $3A^{R704N}$ it was highly reduced. For methoctramine there was no change for $3A^{R704N}$, but a reduction was found with $3A^{G703N}$. For MK-801 $3A^{G703N}$ and $3A^{R704N}$ had an intermediate δ between that of 1-1a/2A and 3A.

	δ (95% CI)				
Compound	**1-1a/2A**	**3A**	**G703N**	**R704N**	**R704D**
Mg^{2+}	0.650 -0.065 to 1.365	0.250 -1.889 to 2.389	0.914 -0.536 to 2.364	0.632 0.213 to 1.051	0.571 0.136 to 1.006
Memantine	0.652 -1.691 to 2.995	0.839 -0.294 to 1.971	0.467 -4.795 to 5.729	0.952 0.433 to 1.470	0.218 0.144 to 0.293
PhTX-343	0.610 0.335 to 0.885	0.454 0.262 to 0.646	0.183 -2.149 to 2.515	0.765 0.528 to 1.002	0.571 0.433 to 0.709
Methoctramine	0.213 -0.436 to 0.861	0.104 -0.566 to 0.775	0.0501 -0.129 to 0.223	0.155 0.122 to 0.189	-
MK-801	0.246 -2.165 to 3.400	0.034 -2.973 to 3.040	0.132 -2.313 to 2.577	0.176 -0.909 to 1.261	-

Table 20: δ values from the Woodhull equation for $3A^{G703N}$, $3A^{R704N}$ and $3A^{R704D}$ NMDA receptors.

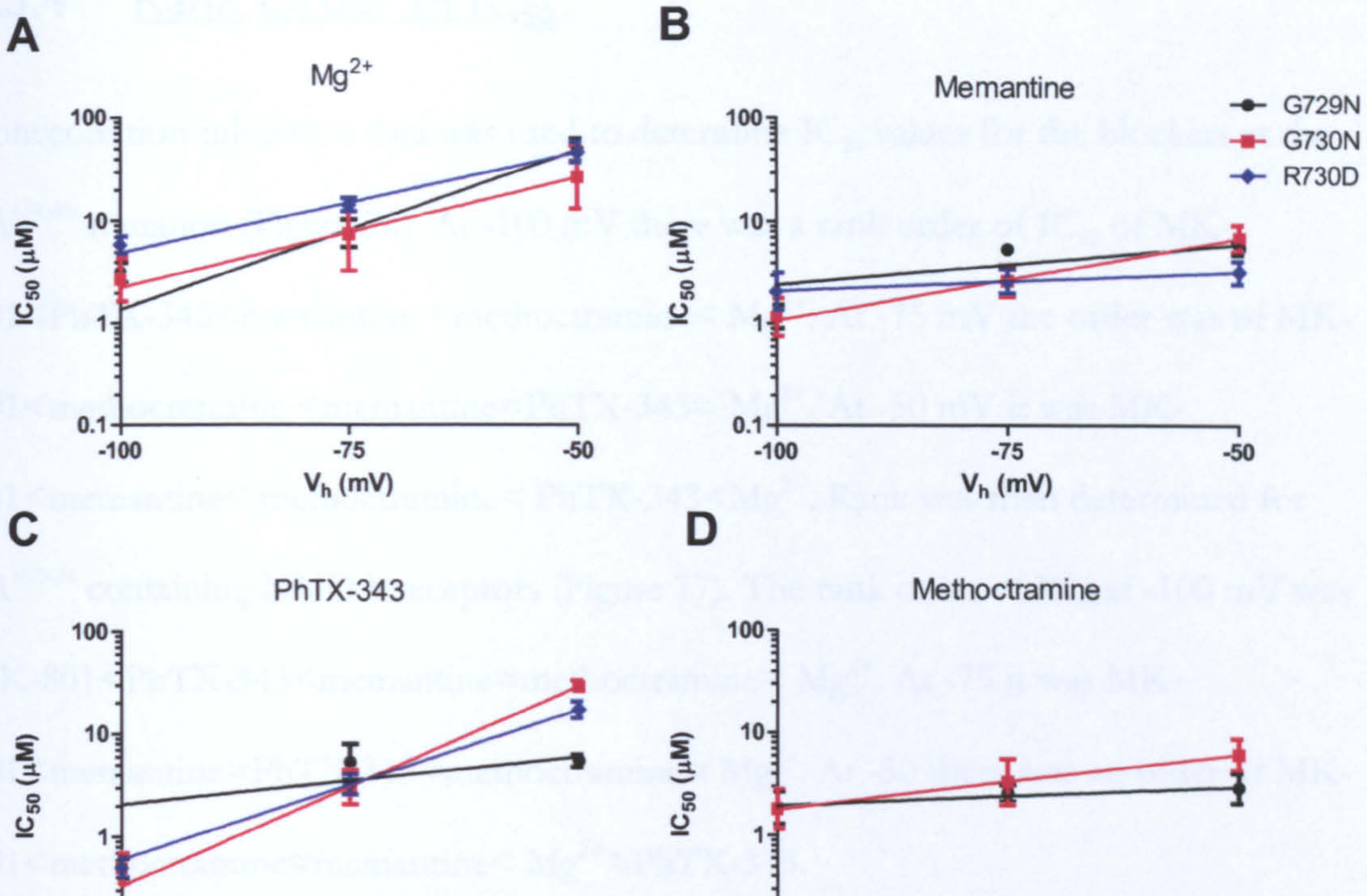

Figure 75: Voltage dependence of IC_{50} for memantine block of 1-1a/2A, 3A and 3B NMDAR-mediated responses fitted with the Woodhull equation. IC_{50} (95% CI) μM for (A) Mg^{2+}, (B) memantine, (C) PhTX-343, (D) methoctramine and (E) MK-801.

3.5.4 Rank Order of IC_{50}

Concentration-inhibition data was used to determine IC_{50} values for the blockers at the $3A^{G703N}$ mutation (Figure 76). At -100 mV there was a rank order of IC_{50} of MK-801<PhTX-343<memantine <methoctramine< Mg^{2+}. At -75 mV the order was of MK-801<methoctramine <memantine≈PhTX-343≈ Mg^{2+}. At -50 mV it was MK-801<memantine< methoctramine< PhTX-343<Mg^{2+}. Rank was then determined for $3A^{R704N}$ containing NMDA receptors (Figure 77). The rank order of IC_{50} at -100 mV was MK-801<PhTX-343<memantine≈methoctramine≈ Mg^{2+}. At -75 it was MK-801<memantine≈PhTX-343≈methoctramine≈ Mg^{2+}. At -50 there was an order of MK-801<methoctramine≈memantine< Mg^{2+}≈PhTX-343.

Inhibition by increasing concentrations of blocker were used estimate IC_{50} at $3A^{R704D}$ receptors (Figure 78). At -100 mV there was a rank order of IC_{50} as PhTX-343 <memantine< Mg^{2+}. At -75 mV the rank was memantine≈PhTX-343<Mg^{2+}. At -50 mV there was a rank order of IC_{50} of memantine<PhTX-343<Mg^{2+}. A full list of statistical comparisons is given in the appendix.

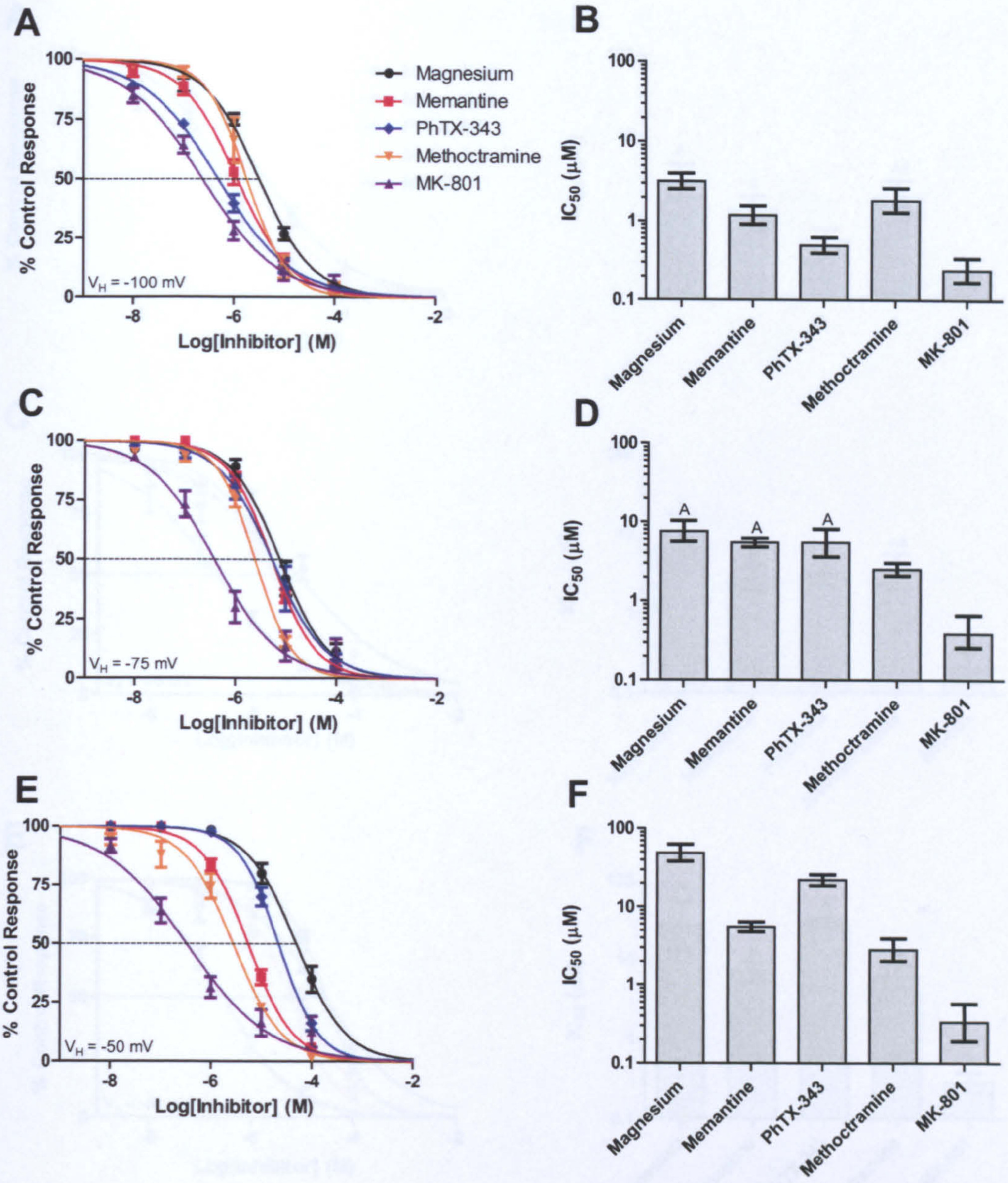

Figure 76: Concentration-inhibition relationships for rank order of block of NMDA/Glycine-evoked responses mediated by $3A^{G703N}$ NMDA receptors at -100, -75 and -50 mV. (A, C, E) % control response (mean ± S.E.M) values were plotted and fitted with the Hill equation to give estimates of IC_{50} (B, -100 mV; D, -75 mV; F, -50 mV). Bars show IC_{50} (95% CI) μM Groups that do not share a letter are significantly different.

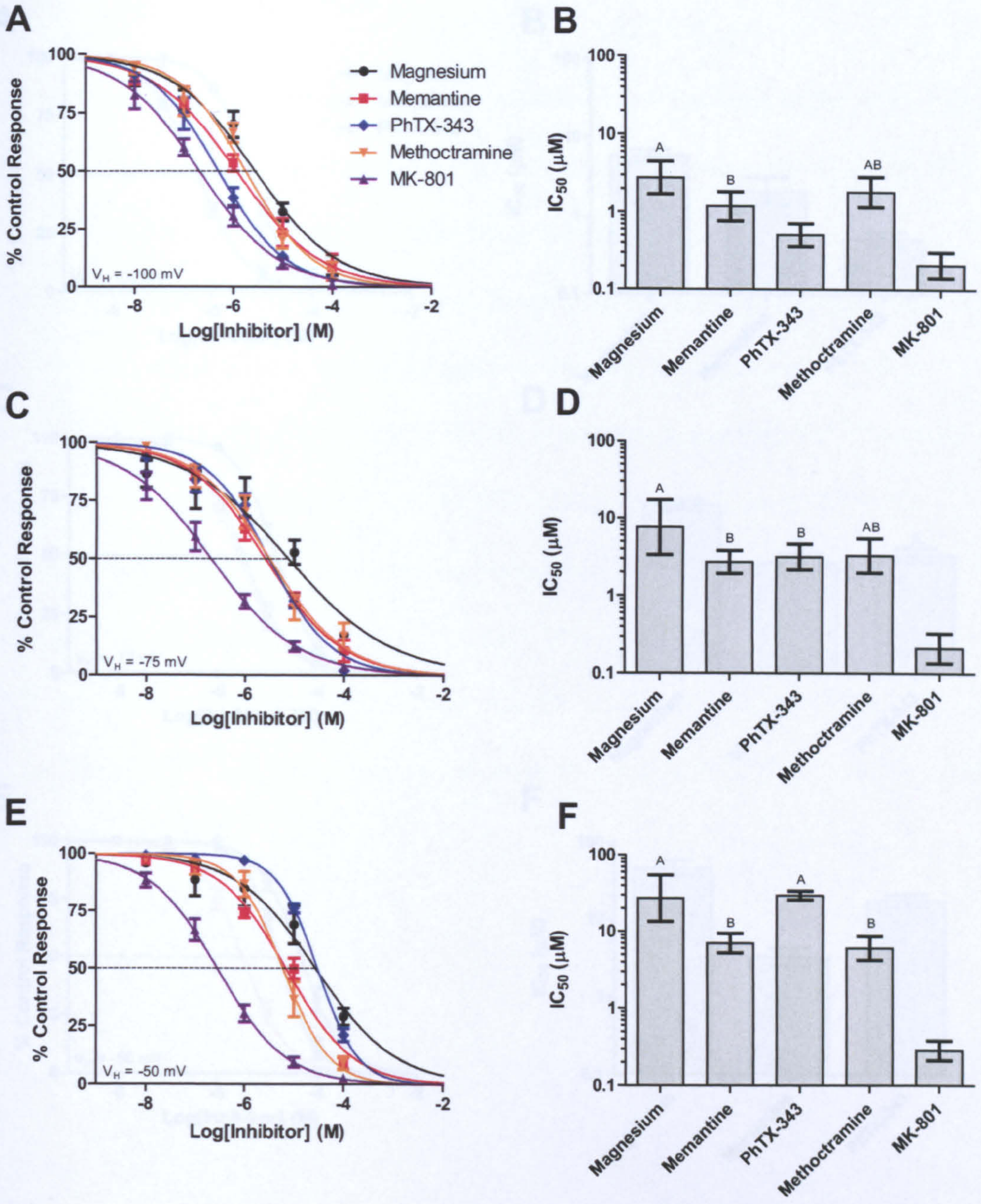

Figure 77: Concentration-inhibition relationships for rank order of block of NMDA/Glycine-evoked responses mediated by $3A^{R704N}$ NMDA receptors at -100, -75 and -50 mV. (A, C, E) % control response (mean ± S.E.M) values were plotted and fitted with the Hill equation to give estimates of IC_{50} (B, -100 mV; D, -75 mV; F, -50 mV). Bars show IC_{50} (95% CI) μM. Groups that do not share a letter are significantly different.

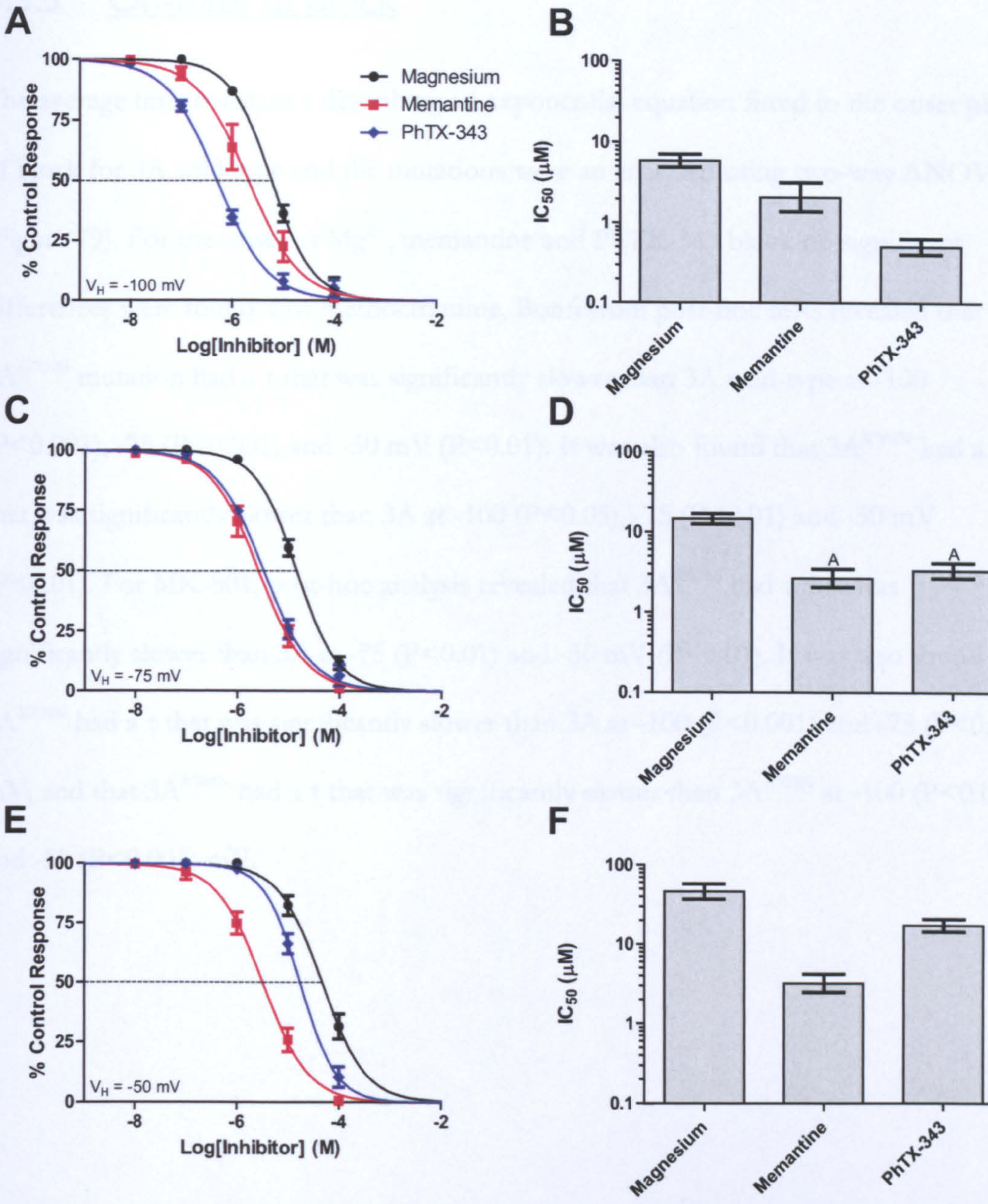

Figure 78: Concentration-inhibition relationships for rank order of block of NMDA/Glycine-evoked responses mediated by $3A^{R704D}$ NMDA receptors at -100, -75 and -50 mV. (A, C, E) % control response (mean ± S.E.M) values were plotted and fitted with the Hill equation to give estimates of IC_{50} (B, -100 mV; D, -75 mV; F, -50 mV). Bars show IC_{50} (95% CI) μM. Groups that do not share a letter are significantly different.

3.5.5 On-Rate of Block

The average time constant τ describing an exponential equation fitted to the onset phase of block for 3A wild-type and the mutations were an analysed using two-way ANOVA (Figure 79). For the onset of Mg^{2+}, memantine and PhTX-343 block no significant differences were found. For methoctramine, Bonferroni post-hoc tests revealed that the $3A^{G703N}$ mutation had a τ that was significantly slower than 3A wild-type at -100 ($P<0.001$), -75 ($P<0.001$) and -50 mV ($P<0.01$). It was also found that $3A^{R704N}$ had a τ that was significantly slower than 3A at -100 ($P<0.05$), -75 ($P<0.01$) and -50 mV ($P<0.01$). For MK-801, post-hoc analysis revealed that $3A^{R703N}$ had τ that was significantly slower than 3A at -75 ($P<0.01$) and -50 mV ($P<0.01$). It was also found that $3A^{R704N}$ had a τ that was significantly slower than 3A at -100 ($P<0.001$) and -75 ($P<0.001$) mV, and that $3A^{R704N}$ had a τ that was significantly slower than $3A^{R703N}$ at -100 ($P<0.01$) and -50 ($P<0.001$) mV.

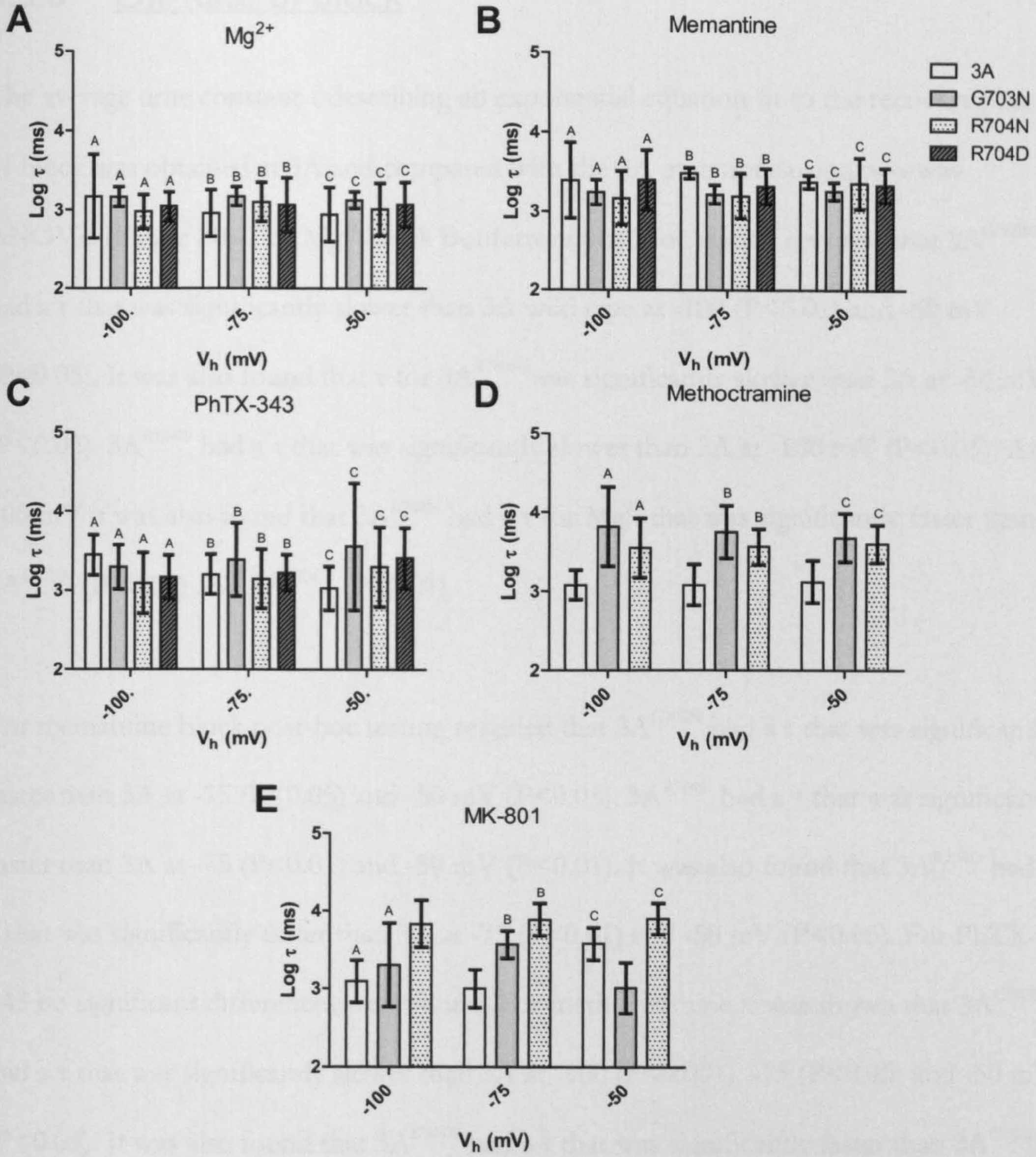

Figure 79: Time constant of a single exponential fit to the development phase of block of NMDA/glycine responses from $3A^{G703N}$, $3A^{R704N}$ and $3A^{R704D}$ NMDA receptors at -100, -75 and -50 mV. Bars show Log τ (95% CI, n=5-6) Two-way ANOVA with Bonferroni post-hoc test (P<0.05). Within a voltage, groups that do not share a letter are significantly different. **(A)** Mg^{2+}, subunit (F(3,51)=0.956 P=0.421), voltage (F(2,51)=0.286 P=0.752) subunit x voltage interaction (F(6,51)=0.522 P=0.789) **(B)** memantine, subunit (F(3,60)=2.210 P=0.096), voltage (F(2,60)=0.1428 P=0.867) and no subunit x voltage interaction (F(6,60)=0.5255 P=0.787). **(C)** PhTX-343, subunit (F(3,50)=1.235 P=0.307), voltage (F(2,50)=0.4097 P=0.666) and subunit x voltage interaction (F(6,50)=1.620 P=0.161) **(E)** methoctramine, subunit (F(2,41)=27.91 P<0.001), voltage (F(2,41)=0.02649 P=0.974) and subunit x voltage interaction (F(4,41)=0.228 P=0.921) and **(F)** MK-801, subunit (F(2,45)=35.00 P<0.001), voltage (F(2,45)=0.5779 P=0.565) and subunit x voltage interaction (F(4,45)=7.006 P<0.001).

3.5.6 Off-Rate of block

The average time constant τ describing an exponential equation fit to the recovery phase of block was obtained at 3A and compared with the 3A mutations using two-way ANOVA (Figure 80). For Mg^{2+} block Bonferroni post-hoc testing revealed that $3A^{G703N}$ had a τ that was significantly slower than 3A wild type at -100 ($P<0.01$) and -50 mV ($P<0.05$). It was also found that τ for $3A^{R704N}$ was significantly slower than 3A at -50 mV ($P<0.05$). $3A^{R704D}$ had a τ that was significantly slower than 3A at -100 mV ($P<0.05$). At -100 mV it was also found that $3A^{R704N}$ had a τ for Mg^{2+} that was significantly faster than $3A^{G703N}$ ($P<0.05$) and $3A^{R704D}$ ($P<0.01$).

For memantine block post-hoc testing revealed that $3A^{G703N}$ had a τ that was significantly faster than 3A at -75 ($P<0.05$) and -50 mV ($P<0.05$). $3A^{R704N}$ had a τ that was significantly faster than 3A at -75 ($P<0.01$) and -50 mV ($P<0.01$). It was also found that $3A^{R704D}$ had a τ that was significantly faster than 3A at -75 ($P<0.01$) and -50 mV ($P<0.05$). For PhTX-343 no significant differences were found. For methoctramine it was shown that $3A^{G703N}$ had a τ that was significantly slower than 3A at -100 ($P<0.001$), -75 ($P<0.05$) and -50 mV ($P<0.05$). It was also found that $3A^{R704N}$ had a τ that was significantly faster than $3A^{G703N}$ at -100 mV ($P<0.01$). For MK-801 post-hoc analysis revealed that $3A^{R704N}$ had a τ that was significantly slower than 3A at -100 ($P<0.001$) -75 ($P<0.001$) and -50 mV ($P<0.05$). It was also found that $3A^{G703N}$ had a τ that was significantly faster than $3A^{R704N}$ at -100 mV ($P<0.01$).

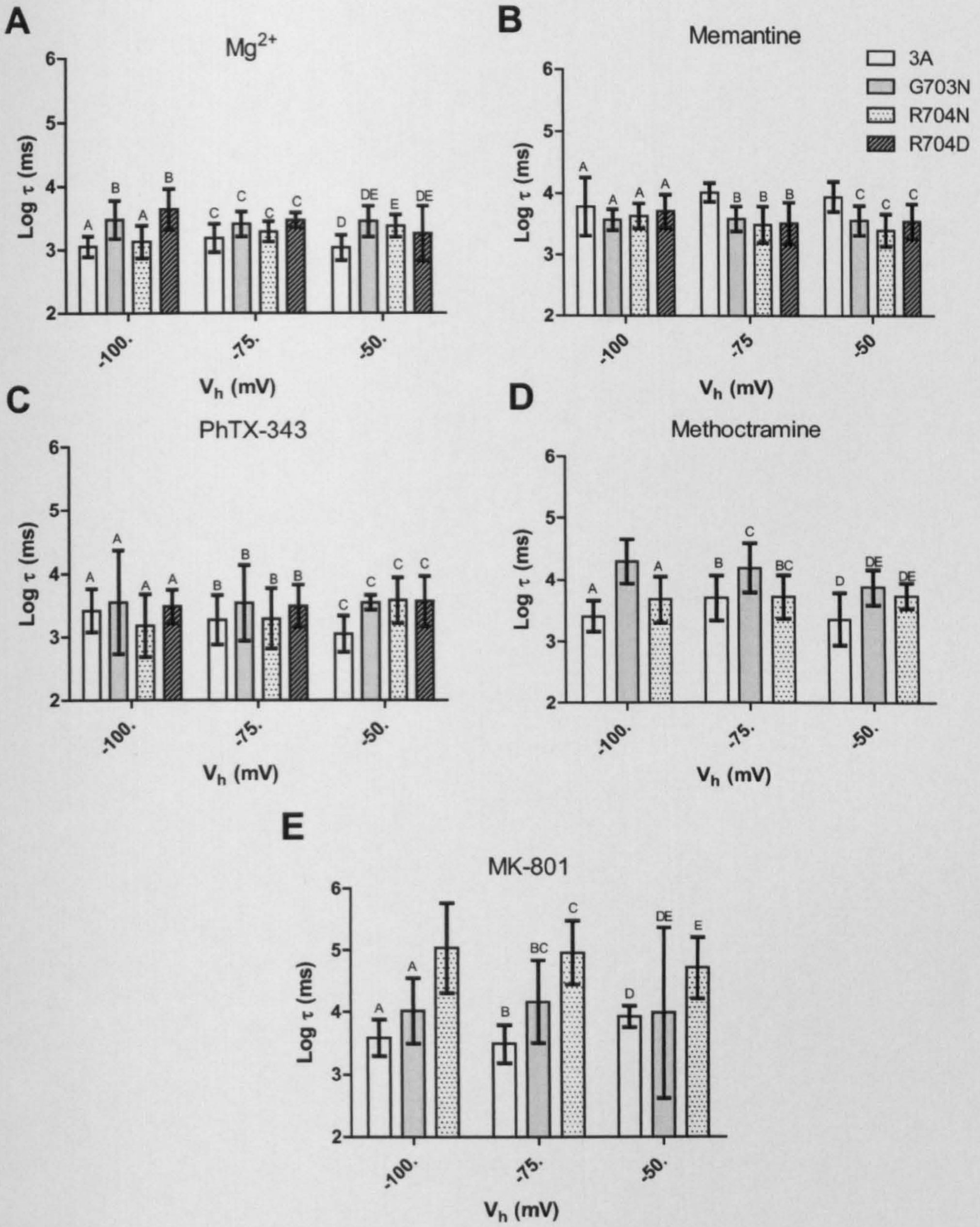

Figure 80: Time constant of a single exponential fit to the recovery phase of block of NMDA/glycine responses from $3A^{G703N}$, $3A^{R704N}$ and $3A^{R704D}$ NMDA receptors at -100, -75 and -50 mV. Log τ (95% CI, n=5-6). Two-way ANOVA with Bonferroni post-hoc test. Within a voltage bars that do not share a letter are significantly different **(A)** Mg^{2+}, subunit ($F(3,52)=9.925$ $P<0.001$), voltage ($F(2,52)=0.4118$ $P=0.665$) and subunit x voltage interaction ($F(6,52)=2.114$ $P=0.064$). **(B)** memantine, subunit ($F(3,61)=7.791$ $P<0.001$), voltage ($F(2,61)=0.336$ $P=0.716$) and no subunit x voltage interaction ($F(6,61)=0.950$ $P=0.470$) **(C)** PhTX-343, subunit ($F(3,49)=2.423$ $P=0.077$), voltage ($F(2,49)=0.057$) and voltage x subunit interaction ($F(6,49)=1.331$ $P=0.262$) **(D)** methoctramine, subunit ($F(2,40)=18.53$ $P<0.001$), voltage ($F(2,40)=2.344$ $P=0.109$) and subunit x voltage interaction ($F(4,40)=1.474$ $P=0.228$) **(E)** MK-801, subunit ($F(2,39)=31.91$ $P<0.001$), voltage ($F(2,39)=0.002$ $P=0.998$) and no voltage x subunit interaction ($F(4,39)=1.146$ $P=0.349$).

3.6 MTDL Drug Design for Alzheimer's Disease

The compounds were successfully produced by the collaborators at the University of Bologna and are shown again in (Figure 81).

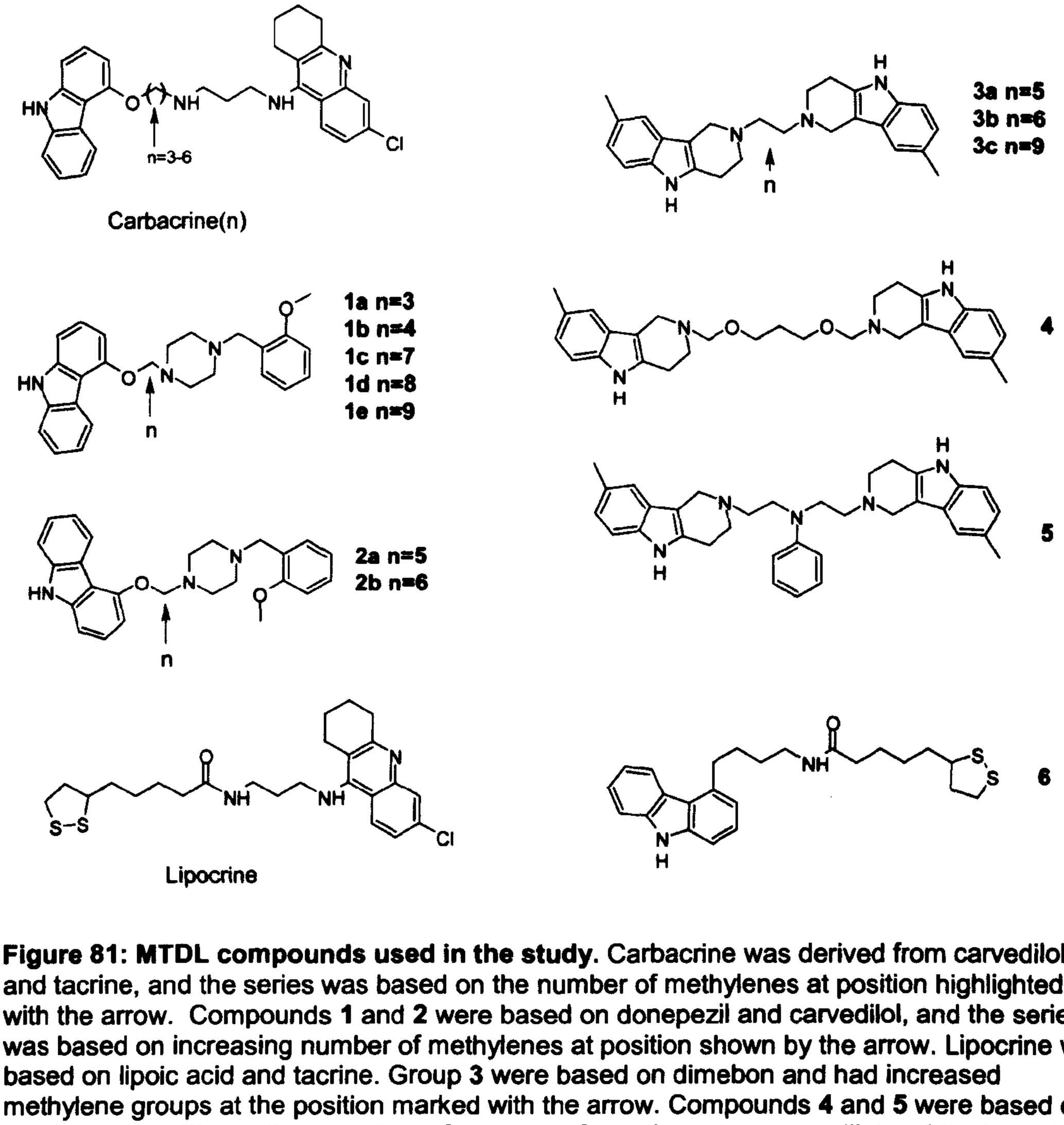

Figure 81: MTDL compounds used in the study. Carbacrine was derived from carvedilol and tacrine, and the series was based on the number of methylenes at position highlighted with the arrow. Compounds **1** and **2** were based on donepezil and carvedilol, and the series was based on increasing number of methylenes at position shown by the arrow. Lipocrine was based on lipoic acid and tacrine. Group **3** were based on dimebon and had increased methylene groups at the position marked with the arrow. Compounds **4** and **5** were based on dimebon with differing linker regions. Compound **6** was based on carvedilol and lipoic acid.

3.6.1 Memantine

Concentration-inhibition data for memantine was plotted and fitted with the Hill equation in order to estimate IC_{50} (Figure 82). The range of voltages required for this chapter was different to that in chapter 3, where -80mV was used as the intermediate voltage (Figure 82).

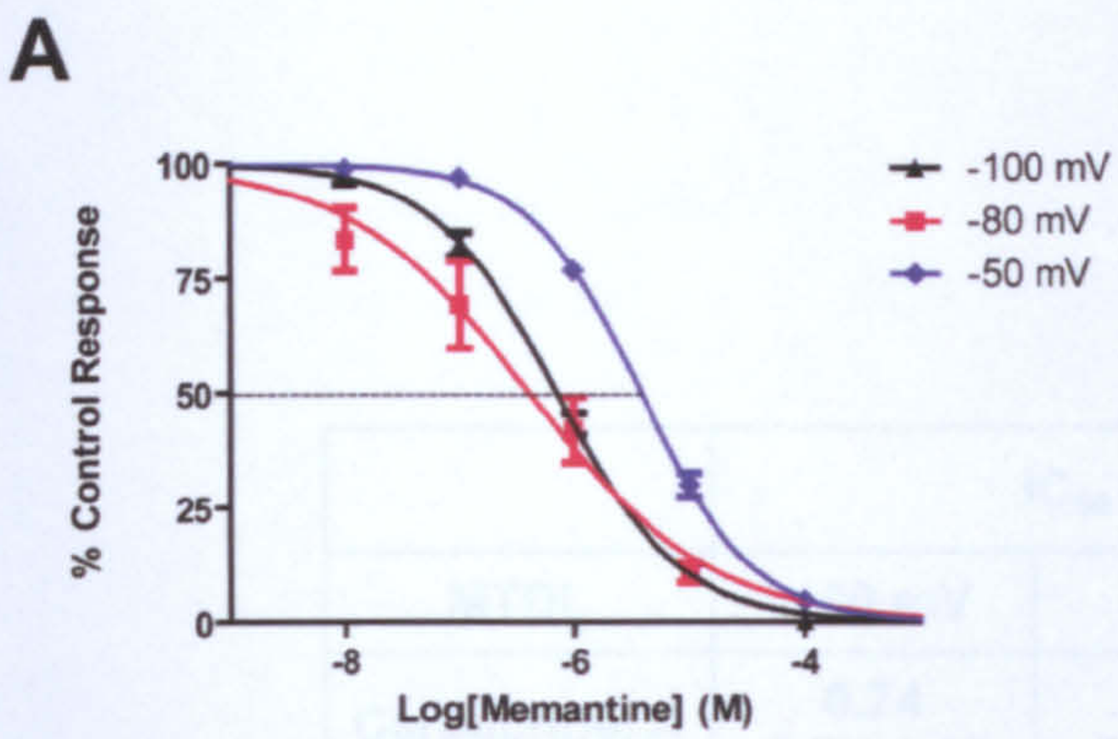

Memantine	
Voltage (mV)	**IC_{50} (95% CI) µM**
-100	0.71 0.64 to 0.99
-80	0.41 0.22 to 0.84
-50	3.94 3.46 to 4.49

Figure 82: Memantine block of NMDA/glycine-evoked currents mediated by 1-1a/2A receptors at -100, -80 and -50 mV. (A) Concentration-inhibition relationships for memantine block. % control response (mean ± S.E.M., n=6) values were plotted and fitted with the Hill equation (A) to give estimates of IC_{50} (B).

3.6.2 Carbacrine Series

Concentration-inhibition curves were produced for the carbacrine compounds at GluN1-1a/2A receptors to establish a rank of potency amongst each other and with memantine (Figure 83). These were then used to calculate IC_{50} values for the blockers tested (Figure 83). The rank order of IC_{50} at -100 mV was carbacrine(3)≈memantine>carbacrine (6)≈carbacrine(5) ≈carbacrine(4) comparison. At -80 mV it was memantine≈ carbacrine(3)<carbacrine(6)≈carbacrine(4)≈carbacrine(5). At -50 mV, the rank order of

IC_{50} was carbacrine(3)≈memantine<carbacrine(6)≈ carbacrine(4)≈carbacrine(5). See appendix for a full statistical comparison.

Block by increasing concentrations of the carbacrine compounds of NMDA/glycine responses at -100, -80 and -50 mV were plotted and fitted with the Hill equation to determine voltage-dependence (Figure 84). There was a significant effect of voltage on IC_{50} for carbacrine(3) (P<0.001) and carbacrine(5) (P=0.034). Block was not voltage dependent for carbacrine(4) (P=0.686) and carbacrine(6) (P=0.613).

	IC_{50} (95% CI) μM		
MTDL	**-100 mV**	**-80 mV**	**-50 mV**
Carbacrine(3)	**0.74** 0.43 to 1.28	**1.14** 0.74 to 1.76	**3.35** 2.15 to 5.24
Carbacrine(4)	**30.25** 18.93 to 48.31	**23.07** 13.04 to 40.83	**32.23** 15.55 to 66.80
Carbacrine(5)	**18.24** 8.095 to 41.11	**53.41** 25.78 to 110.70	**107.00** 20.18 to 567.70
Carbacrine(6)	**12.99** 6.19 to 27.26	**14.22** 6.84 to 29.56	**20.08** 10.87 to 37.11

Table 21: IC_{50} values for carbacrine compounds

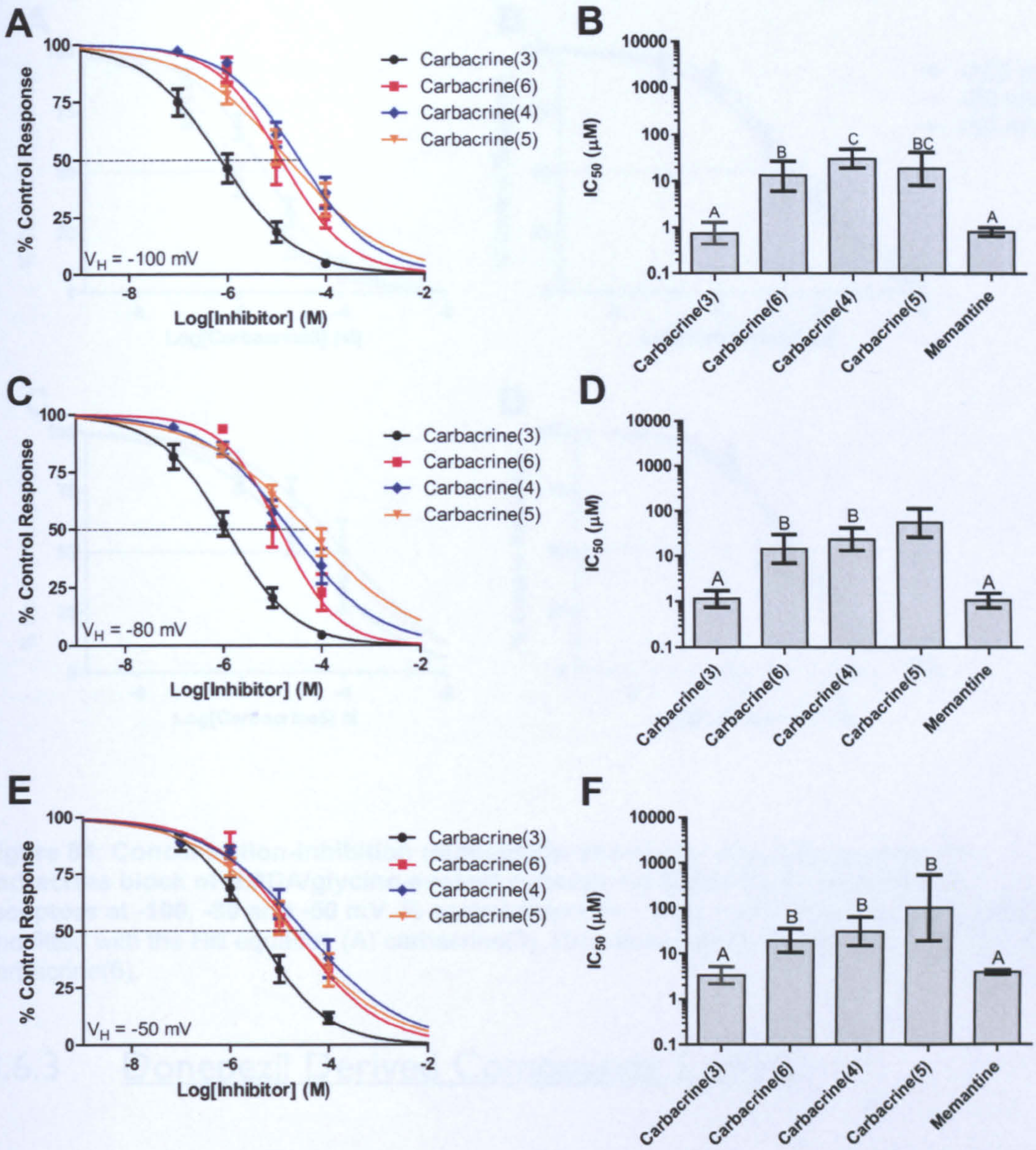

Figure 83: Concentration-inhibition relationships for rank order of carbacrine block of NMDA/glycine-evoked currents mediated by 1-1a/2A NMDA receptors at -100, -80 and -50 mV. % control response (mean ± S.E.M., n=5-12) values were plotted and fitted with the Hill equation (A, C, E) to give estimates of IC_{50} (B, D, F). Bars show IC_{50} (95% CI) and those that do not share a letter are significantly different.

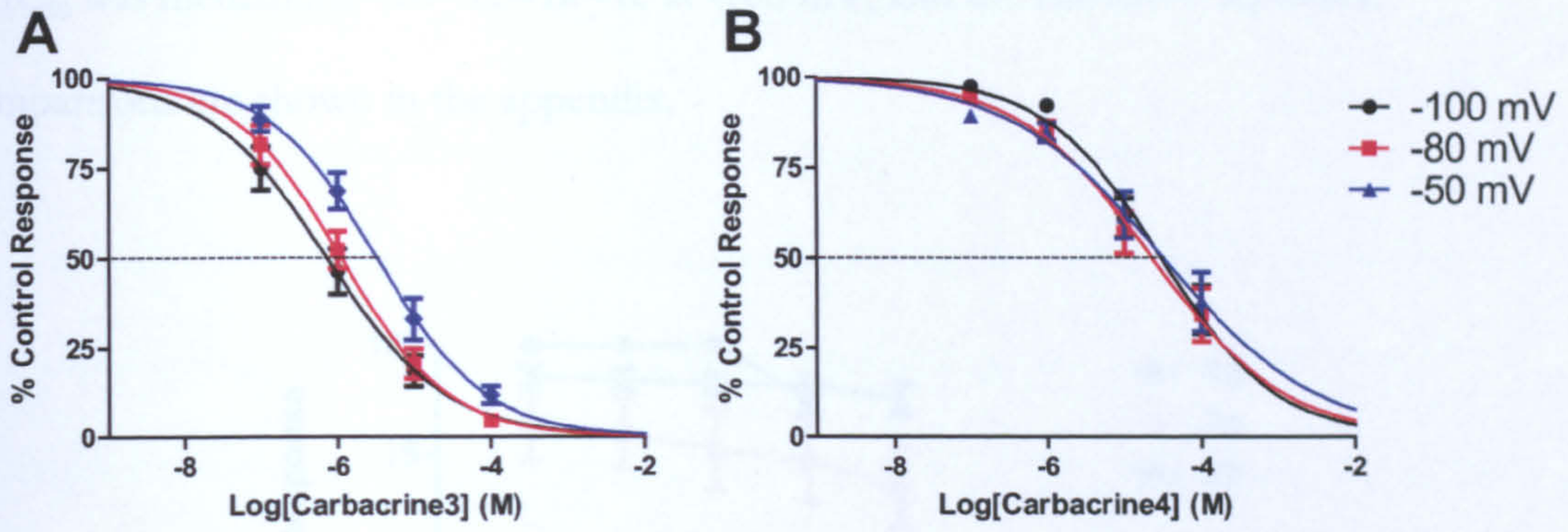

Figure 84: Concentration-inhibition relationship showing voltage dependence of carbacrine block of NMDA/glycine-evoked currents mediated by 1-1a/2A NMDA receptors at -100, -80 and -50 mV. % control response (mean ± S.E.M) values were plotted and fitted with the Hill equation (A) carbacrine(3), (B) carbacrine(4), (C) carbacrine(5) and (D) carbacrine(6).

3.6.3 Donepezil Derived Compounds 1 and 2

2b, **2a** and **1d** were found to weak blockers of NMDA receptor responses (Figure 85). **2b** was shown to only inhibit the control response to a level of 87.5% ± 3.5 (mean ± S.E.M) with 100 μM. **2a** also showed little activity, with only 66.8% ± 9.4 control response remaining with 100 μM. **1d** was not soluble at 100 μM, but inhibited control responses to 87.30 ± 3.26 % at 10 μM.

The remaining compounds had increased potency at the NMDA receptor.

Concentration-inhibition curves were produced at -100 mV (Figure 86). The rank order

of IC_{50} was memantine<**1b**<**1e**≈**1a**≈**1c** at -100 mV, and the full list of statistical comparisons are shown in the appendix.

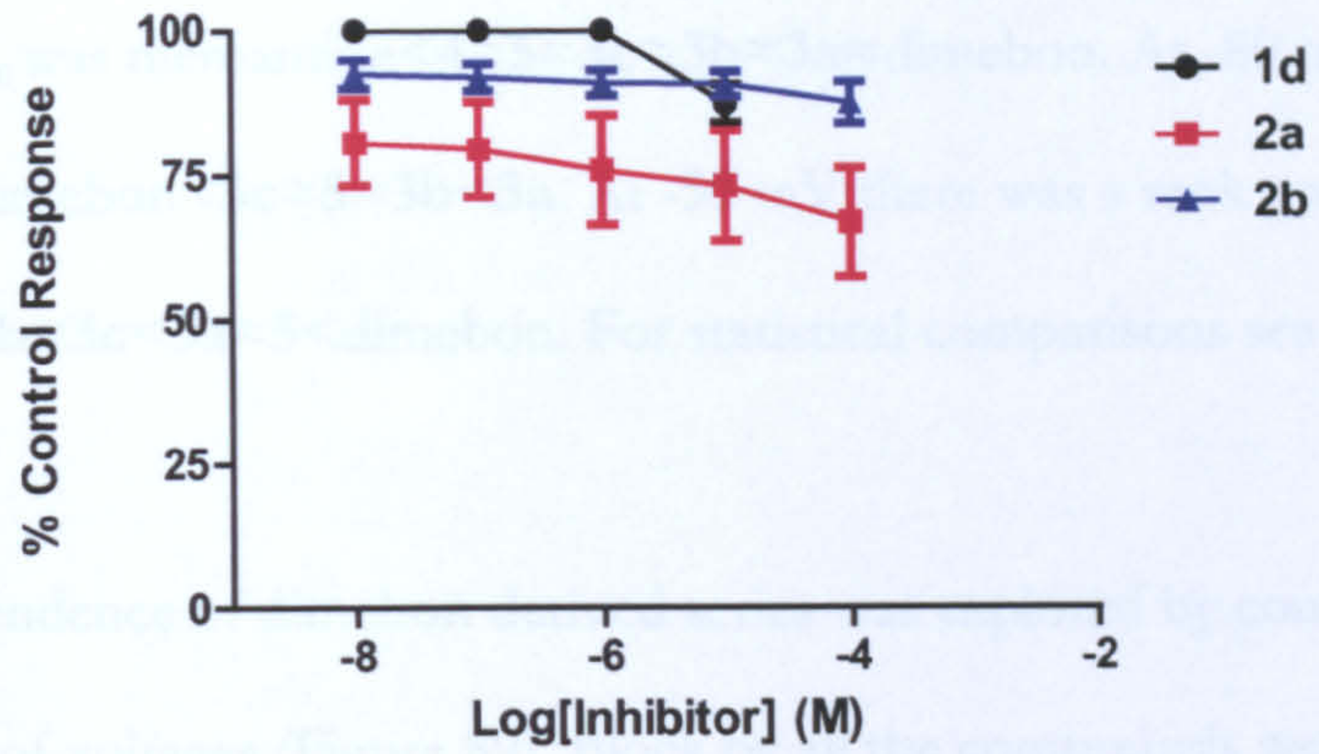

Figure 85: Concentration-inhibition relationship for 1 and 2 block of NMDA/glycine-evoked currents mediated by 1-1a/2A receptors. % control response (mean ± S.E.M, n=6-7). Curves were constructed for **1d, 2a** and **2d**.Shown are connecting lines for clarity.

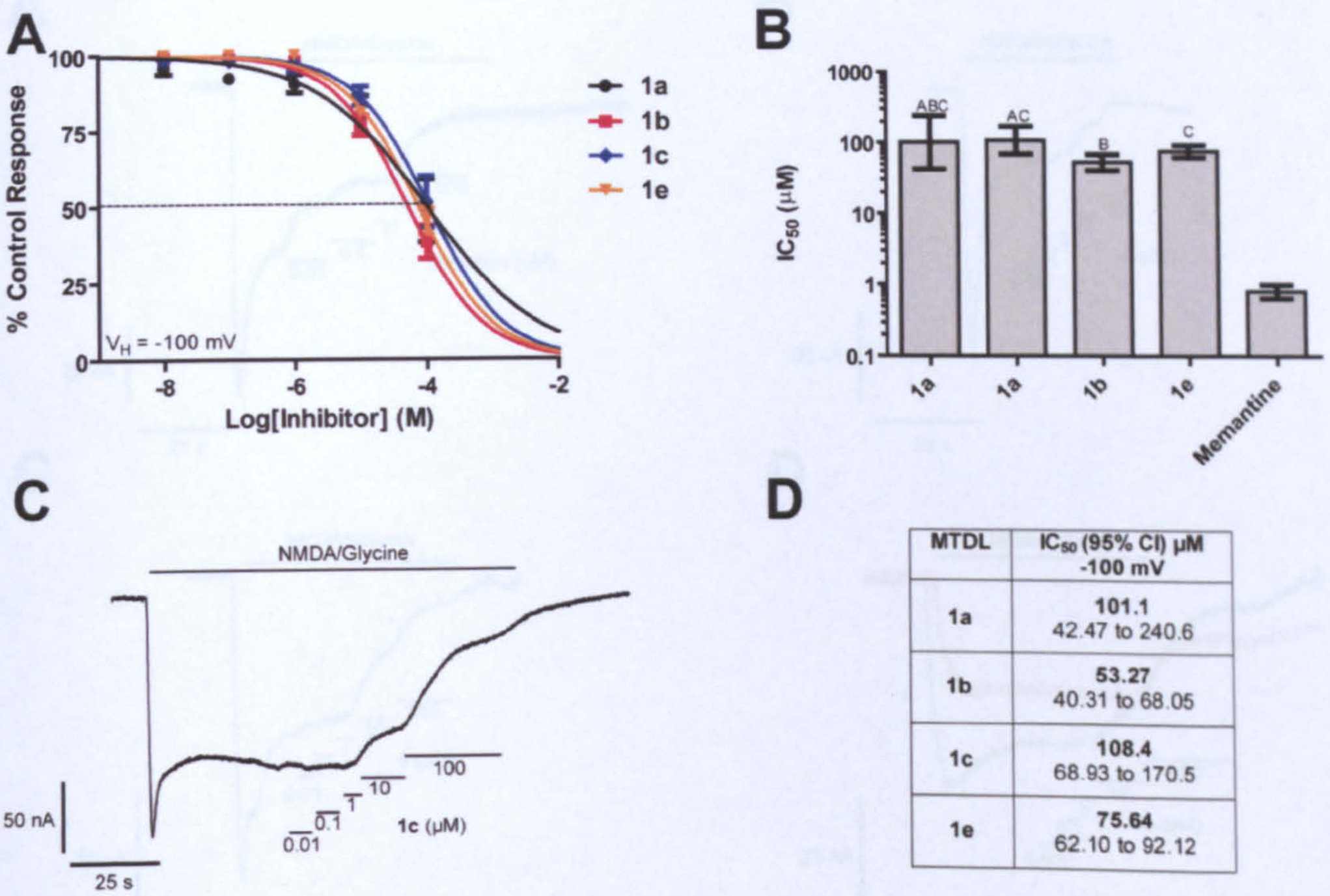

MTDL	IC_{50} (95% CI) μM -100 mV
1a	**101.1** 42.47 to 240.6
1b	**53.27** 40.31 to 68.05
1c	**108.4** 68.93 to 170.5
1e	**75.64** 62.10 to 92.12

Figure 86: Compound 1 and 2 block of NMDA/glycine-evoked currents mediated by 1-1a/2A receptors at -100 mV. (A) Concentration-inhibition relationships for **1** and **2** block. % control response (mean ± S.E.M., n=6) values were plotted and fitted with the Hill equation (A) to give estimates of IC_{50} (B,D). Bars show IC_{50} (95% CI) and those that do not share a letter are significantly different. (C) TEVC current recording of 1c block of NMDA/glycine evoked currents mediated by 1-1a/2A NMDA receptors at -100 mV.

3.6.4 Dimebon Derived Compounds

Block by increasing concentrations of **3**, **4**, **5** and dimebon of NMDA/glycine responses were plotted and fitted with the Hill equation to estimate IC_{50} (Figure 88, Table 22). The rank order of IC_{50} was memantine<**4**≈**5**≈**3c**≈**3b**≈**3a**≈dimebon. At -80 mV this was memantine<**4**<dimebon≈**3c**≈**5**≈**3b**<**3a**. At -50 mV there was a rank order of IC_{50} of memantine<**4**<**3b**≈**3c**<**3a**≈**5**<dimebon. For statistical comparisons see appendix.

The voltage-dependence of dimebon derived series was explored by comparing IC_{50} values at a range of voltages (Figure 89). Block by all the compounds were found to be voltage-dependent, showing a significant effect of voltage on IC_{50} for dimebon ($P<0.001$), **3a** ($P<0.001$), **3b** ($P<0.001$), **3c** ($P<0.001$), **4** ($P<0.001$) and **5** ($P<0.001$).

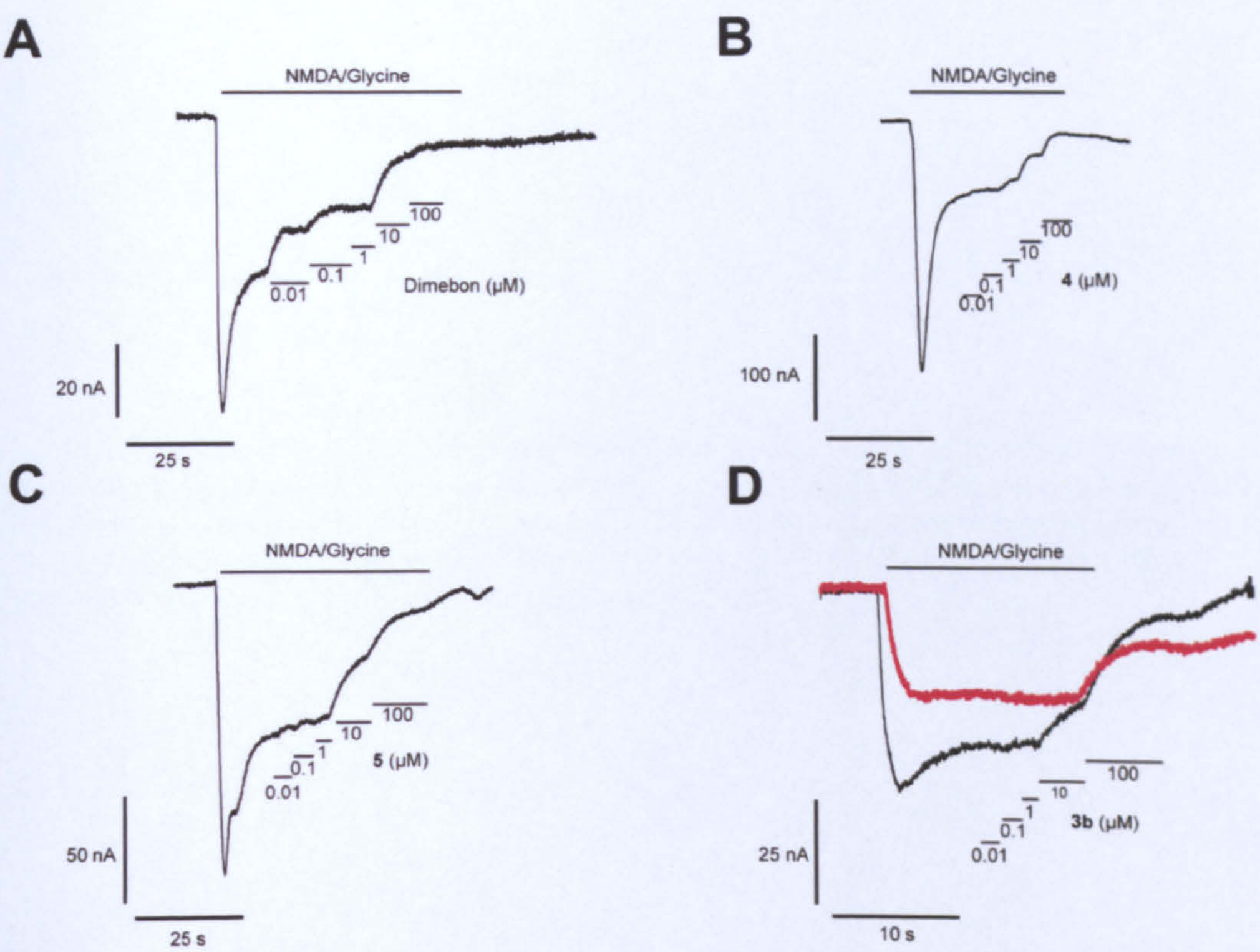

Figure 87: TEVC current recording of dimebon and 3 and 4 block of NMDA/glycine evoked currents mediated by 1-1a/2A NMDA receptors. (A) Dimebon, (B) **4**, (C) **5** at -100 mV. (D) **3b** at -100 (black) and -50 mV (red).

	IC_{50} (95% CI) μM		
MTDL	**-100 mV**	**-80 mV**	**-50 mV**
Dimebon	**13.85** 7.66 to 25.05	**11.98** 5.82 to 24.65	**149.10** 84.05 to 265.6
3a	**12.58** 9.00 to 17.60	**29.14** 21.14 to 40.18	**51.11** 37.96 to 68.82
3b	**10.95** 8.22 to 14.57	**17.94** 14.19 to 22.68	**27.53** 20.76 to 36.52
3c	**9.66** 7.77 to 12.01	**14.76** 11.22 to 19.41	**35.20** 28.99 to 42.74
4	**9.66** 7.77 to 12.01	**14.76** 11.22 to 19.41	**35.20** 28.99 to 42.74
5	**8.72** 4.72 to 16.13	**15.22** 9.05 to 25.60	**57.33** 34.20 to 96.11

Table 22: IC_{50} values for Dimebon, 3, 4 and 5. Shown is IC_{50} (95% CI) calculated from the Hill equation.

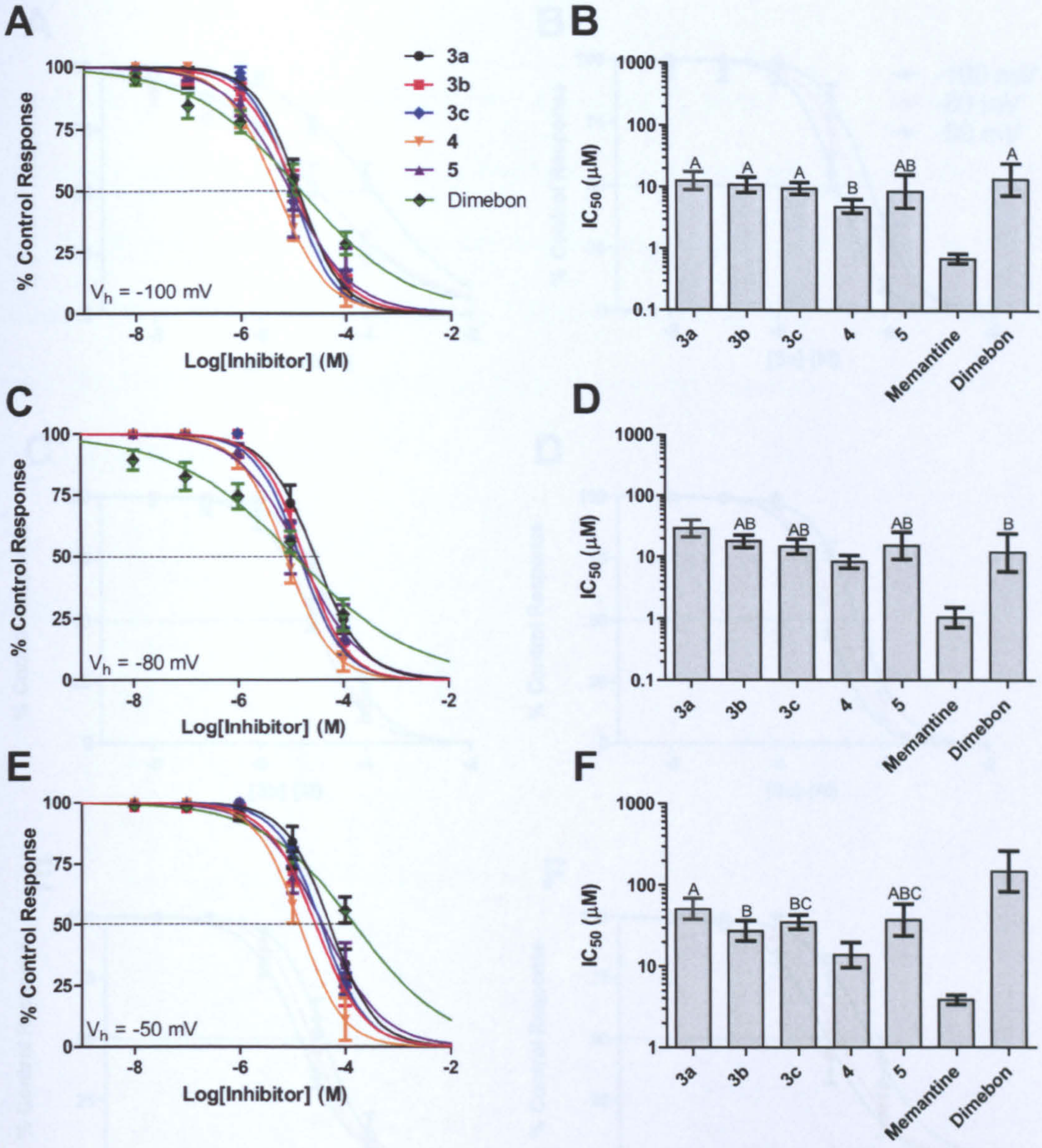

Figure 88: Concentration-inhibition relationships for rank order of 3, 4 and dimebon block of NMDA/glycine-evoked currents mediated by 1-1a/2A NMDA receptors at -100, -80 and -50 mV. % control response (mean ± S.E.M., n=5-6) values were plotted and fitted with the Hill equation (A, C, E) to give estimates of IC_{50} (B, D, F). Bars show IC_{50} (95% CI) and those that do not share a letter are significantly different.

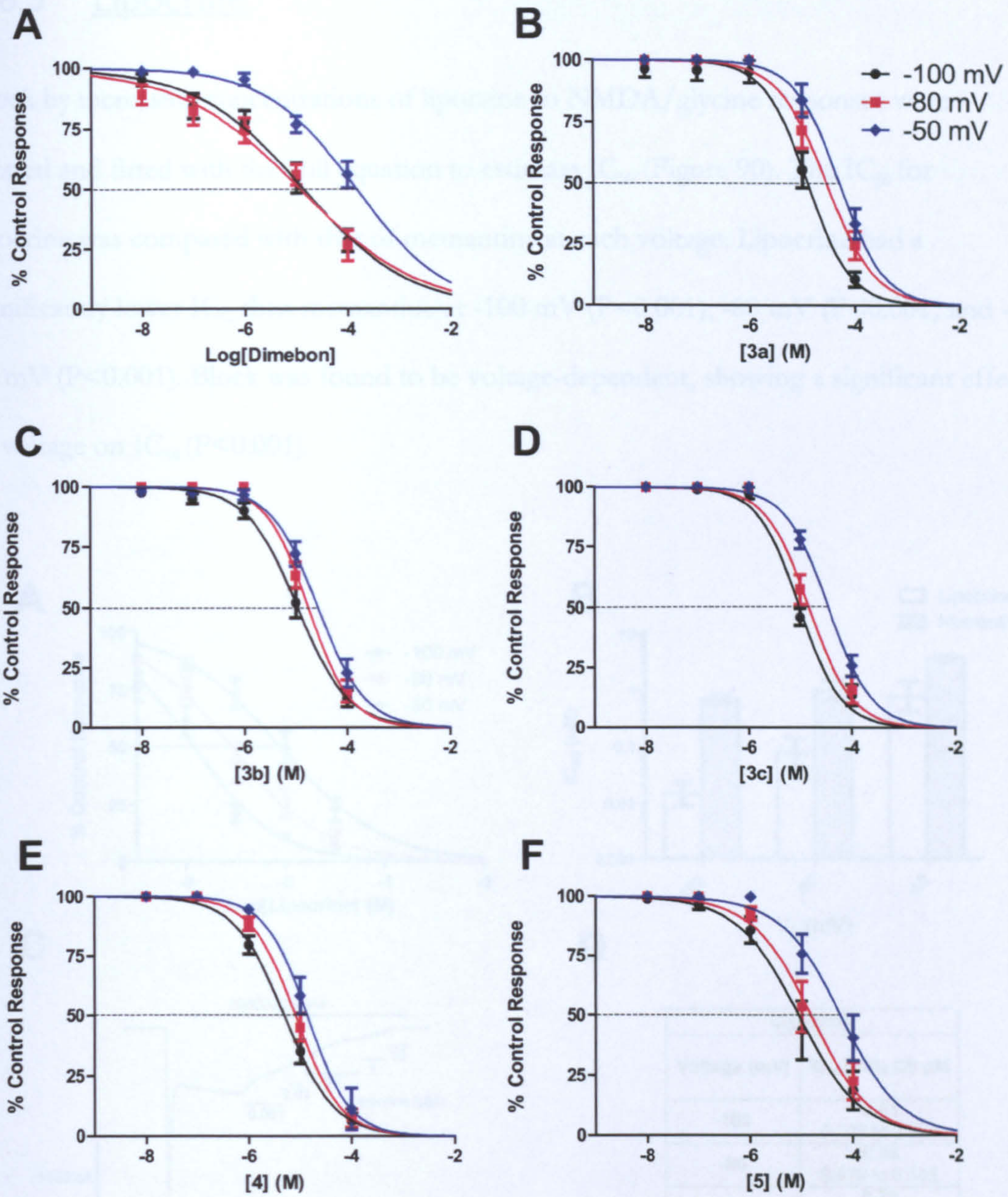

Figure 89: Concentration-inhibition relationship showing voltage-dependence of dimebon and RG block of NMDA/glycine-evoked currents mediated by 1-1a/2A NMDA receptors at -100, -80 and -50 mV. % control response (mean ± S.E.M) values were plotted and fitted with the Hill equation for (A) dimebon, (B) **3a**, (C) **3b**, (D) **3c**, (E) **4** and (F) **5**.

3.6.5 Lipocrine

Block by increasing concentrations of lipocrine to NMDA/glycine responses were plotted and fitted with the Hill equation to estimate IC_{50} (Figure 90). The IC_{50} for lipocrine was compared with that of memantine at each voltage. Lipocrine had a significantly lower IC_{50} than memantine at -100 mV ($P<0.001$), -80 mV ($P<0.001$) and -50 mV ($P<0.001$). Block was found to be voltage-dependent, showing a significant effect of voltage on IC_{50} ($P<0.001$).

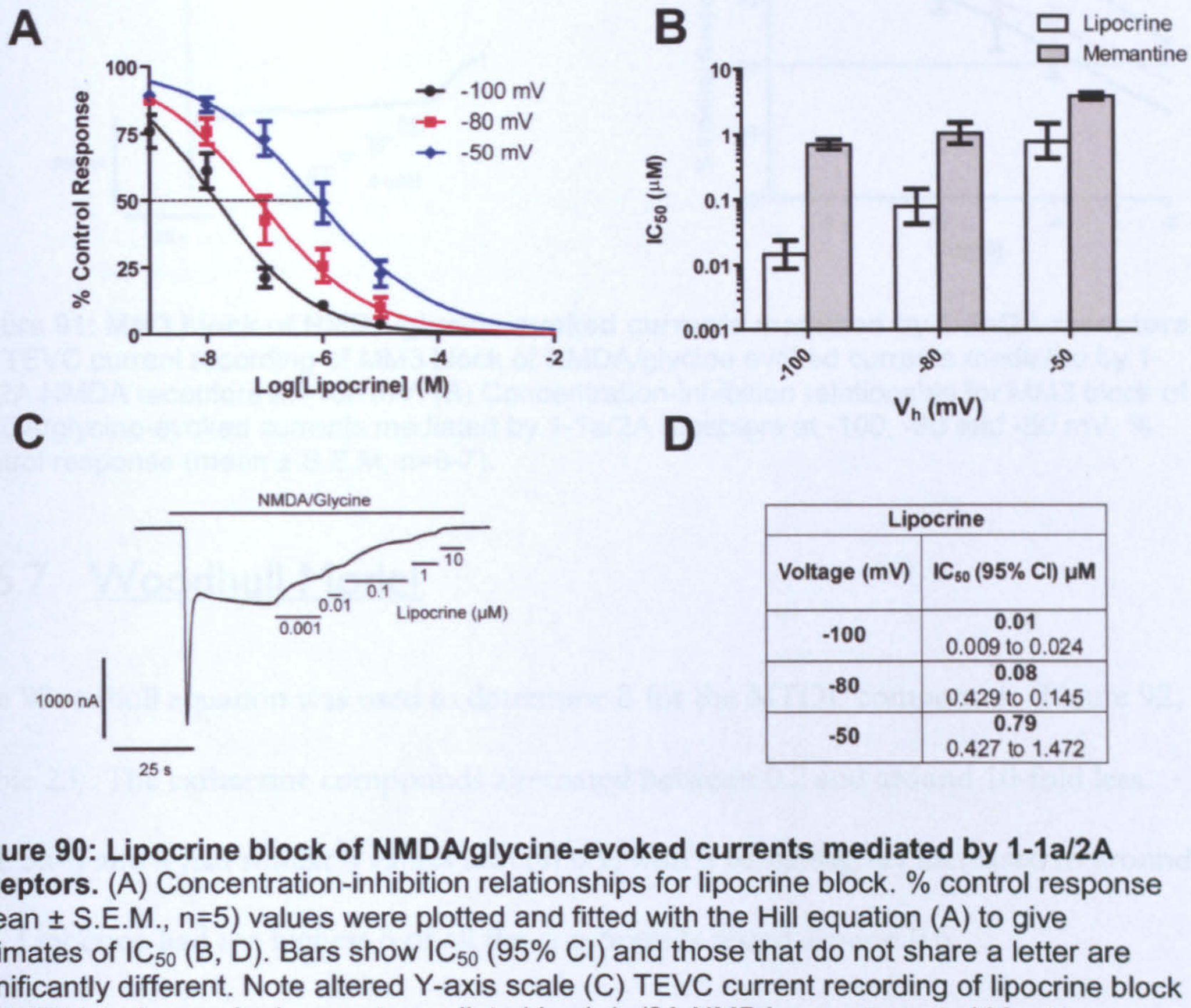

Lipocrine	
Voltage (mV)	**IC_{50} (95% CI) μM**
-100	**0.01** 0.009 to 0.024
-80	**0.08** 0.429 to 0.145
-50	**0.79** 0.427 to 1.472

Figure 90: Lipocrine block of NMDA/glycine-evoked currents mediated by 1-1a/2A receptors. (A) Concentration-inhibition relationships for lipocrine block. % control response (mean ± S.E.M., n=5) values were plotted and fitted with the Hill equation (A) to give estimates of IC_{50} (B, D). Bars show IC_{50} (95% CI) and those that do not share a letter are significantly different. Note altered Y-axis scale (C) TEVC current recording of lipocrine block of NMDA/glycine evoked currents mediated by 1-1a/2A NMDA receptors at -100 mV.

3.6.6 Carvedilol and Lipoic Acid derived Compound 6

Compound **6** was found to be a weak inhibitor of NMDA/glycine current, with 100 μM inhibiting the control response to 56.44 ± 11.12 (mean ± S.E.M) % control response at -100 mV (Figure 91). Showing some voltage-dependence, inhibition at -80 mV was to 63.52 ± 9.19 % and at -50 mV was reduced to 84.69 ± 6.52 % of the control response with 100 μM.

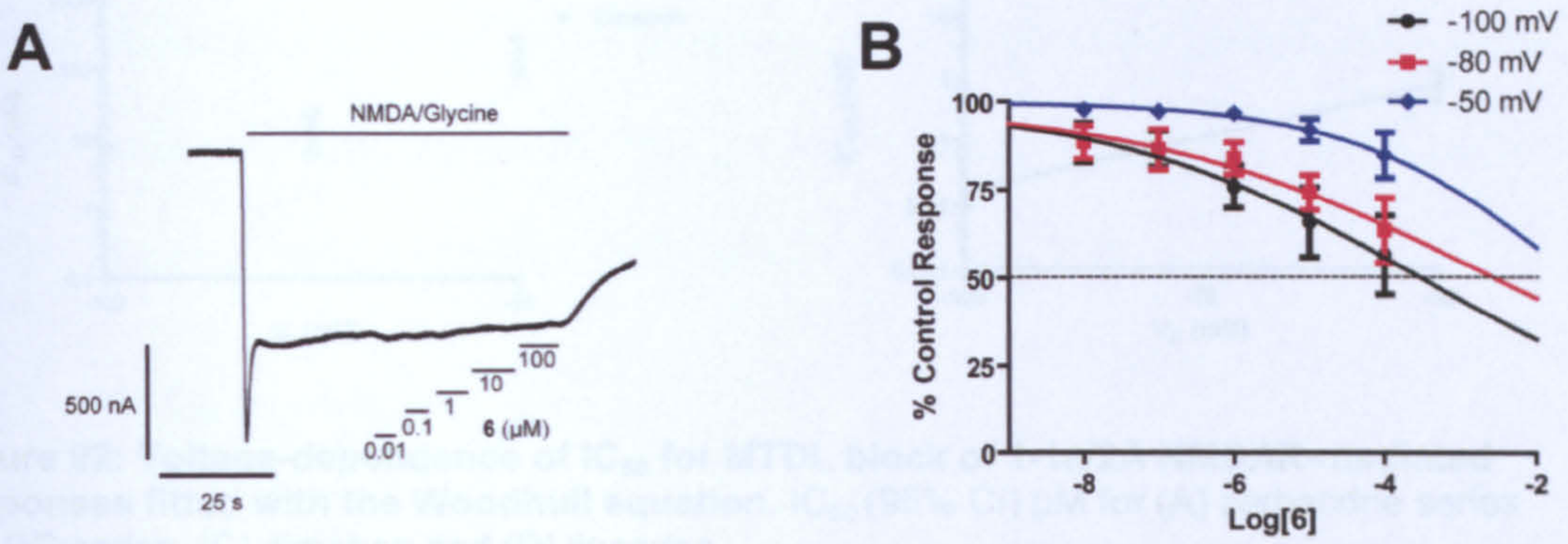

Figure 91: MM3 block of NMDA/glycine-evoked currents mediated by 1-1a/2A receptors. (A) TEVC current recording of MM3 block of NMDA/glycine evoked currents mediated by 1-1a/2A NMDA receptors at -100 mV. (B) Concentration-inhibition relationship for MM3 block of NMDA/glycine-evoked currents mediated by 1-1a/2A receptors at -100, -80 and -50 mV. % control response (mean ± S.E.M, n=6-7).

3.6.7 Woodhull Model

The Woodhull equation was used to determine δ for the MTDL compounds (Figure 92, Table 23). The carbacrine compounds alternated between 0.2 and around 10-fold less. The **3a-d** and **4** had similar δ values around 0.1, with 5 being slightly increased to around 0.2. Lipocrine had the highest δ of all the compounds tested around 0.6.

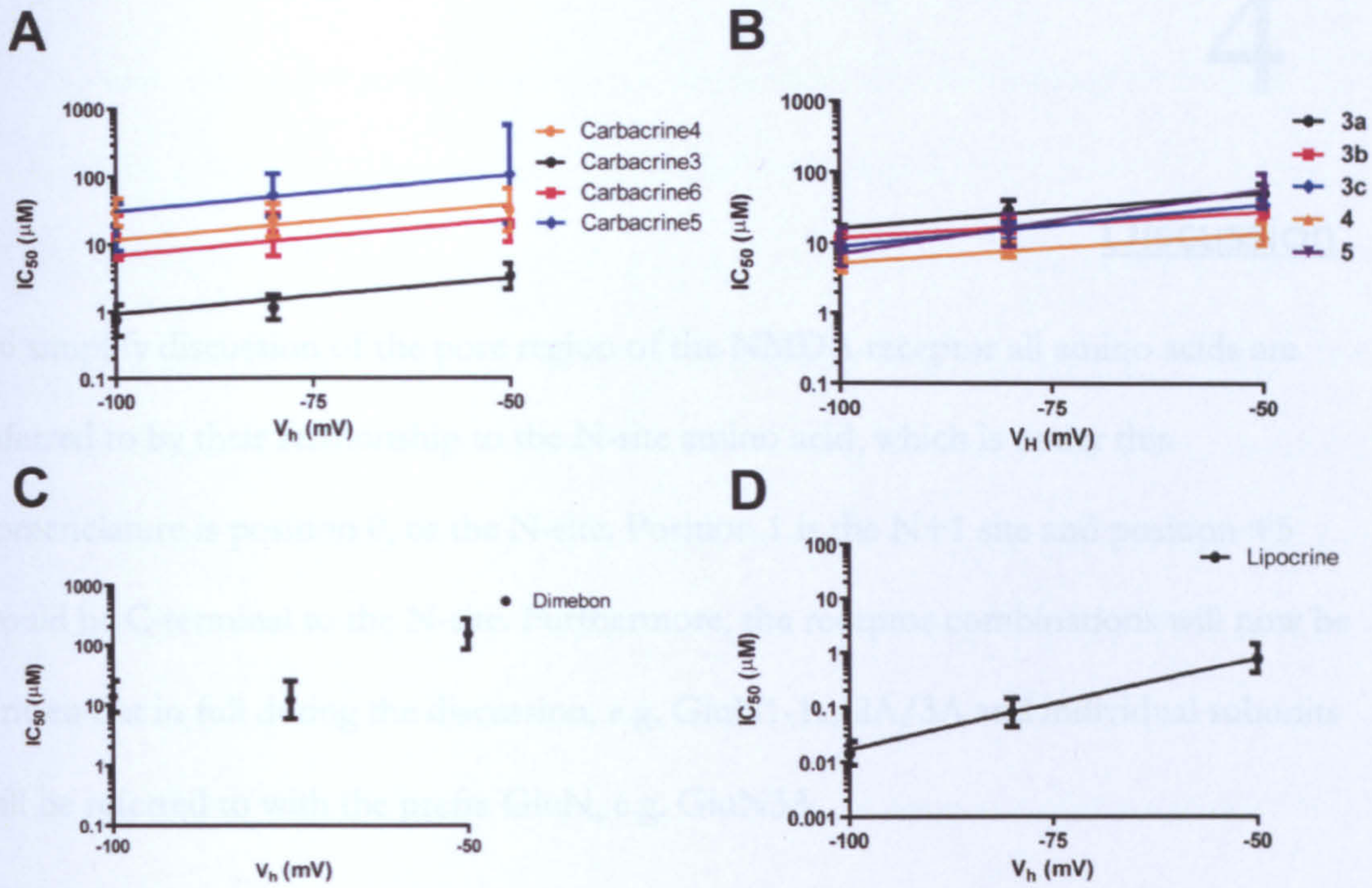

Figure 92: Voltage-dependence of IC_{50} for MTDL block of 1-1a/2A NMDAR-mediated responses fitted with the Woodhull equation. IC_{50} (95% CI) μM for (A) carbacrine series (B) RG series, (C) dimebon and (D) lipocrine.

	MTDL				
	Carbacrine(3)	**Carbacrine(4)**	**Carbacrine(5)**	**Carbacrine(6)**	**Lipocrine**
δ (95% CI)	**0.283** -0.054 to 0.621	**0.020** -0.661 to 0.701	**0.243** -0.439 to 0.925	**0.080** -0.108 to 0.268	**0.660** 0.554 to 0.765
	MTDL				
	3a	**3b**	**3c**	**4**	**5**
δ (95% CI)	**0.150** -0.267 to 0.568	**0.108** -0.093 to 0.309	**0.175** 0.034 to 0.315	**0.124** -0.034 to 0.282	**0.267** -0.012 to 0.545

Table 23: δ values for the MTDL compounds. δ (95% CI).

4

Discussion

To simplify discussion of the pore region of the NMDA receptor all amino acids are referred to by their relationship to the N-site amino acid, which is under this nomenclature is position 0, or the N-site. Position 1 is the N+1 site and position +5 would be C-terminal to the N-site. Furthermore, the receptor combinations will now be written out in full during the discussion, e.g. GluN1-1a/2A/3A and individual subunits will be referred to with the prefix GluN, e.g. GluN3A.

4.1 Molecular Biology

There was a single consensus difference in the GluN3B subunit when it was sequenced with T7. However, A BLAST search revealed no SNP at this position and so may have been a reading error. There was also a single consensus difference for GluN3A^{R704D} mutation that was not in the same region as the mutation. But as this did not appear on any other GluN3A sequence, this is likely a further reading error.

4.2 Agonist

For both agonists, the concentrations used in the study were at maximal efficacy. Therefore, these were considered saturating for glycine and NMDA at all combinations of receptor, which is required when investigating the activity of open channel blockers (Li, 1999). There was a decrease in efficacy with concentrations above these levels which has been previously reported for glycine, but not NMDA in Xenopus oocytes (Mirshahi and Woodward, 1995, de Carvalho et al., 1996).

It was shown that the EC_{50} values for NMDA were not significantly different for all the subunit combinations tested suggesting that the number of GluN2 subunits did not change. The glycine EC_{50} was found to be significantly reduced for GluN1-1a/2A/3A and GluN1-1a/2A/3B compared with GluN1-1a/2A which was consistent with the subunit being present in the receptor assembly, as glycine has been shown to bind to the GluN3A subunit with a 650-fold lower K_d than GluN1 (Yao and Mayer, 2006). However, a previous study found that that the EC_{50} for glutamate and glycine was not significantly different between wild-type and transgenic mice overexpressing GluN3A (Tong et al., 2007). GluN2A/3A has been shown to form dimers, but only a heteromeric complex containing GluN1 were able to exit from the ER (Perez-Otano et al., 2001). If there was a GluN2A/3A dimer in the heteromeric receptor complex then there would possibly have to be an additional GluN1-1a/2A or GluN1-1a/3 dimer, and the former outcome may be more likely as the EC_{50} for NMDA was shown in the current study to be unchanged. Such an interpretation is required because GluN3 lacking NMDA receptors have two GluN2 subunits (Sobolevsky et al., 2009).

4.3 NMDA Receptor Antagonism

4.3.1 Mg^{2+}

At all voltages tested Mg^{2+} showed an increase in IC_{50} for between GluN1-1a/2A/3A (~5-fold) and GluN1-1a/2A/3B (~10-fold) compared with the IC_{50} for GluN1-1a/2A, and GluN1-1a/2A/3B was significantly higher than GluN1-1a/2A/3A. The N-site of GluN1 and GluN2 and the N+1 site of GluN2 have been shown to form the Mg^{2+} binding sites of the NMDA receptor (Wollmuth et al., 1998a, Wollmuth et al., 1998b). The GluN3 subunits have a G then the positively charged R at these positions and it may be that the loss of the polar partial negative charge of N, as well as the addition of the

positive R, reduced Mg^{2+} affinity. The amino group of MK-801 may also interact with the N-site, as well as the amino group of memantine accounting the increased IC_{50} values found (Tikhonov et al., 2002, Chen and Lipton, 2005).

The binding site for Mg^{2+} for GluN3 containing receptors may have been lost. The orientation of the threonines in the M3 SYTANLAAF motif in GluN1/3A receptors has been shown to form a narrow constriction restricting entry to the pore (Wada et al., 2006). Entry to the N-site may be impaired and due to the constriction it may form a new binding site for open channel blockers that has a lower affinity (Figure 93). Woodhull analysis supported such a conclusion for Mg^{2+} as it suggested that depth of block occurred at 0.6 similar to previous reports of the N-site, which was decreased with the presence of GluN3A and GluN3B (Zhu and Auerbach, 2001). Current flow, and the relative speeds of the ions through the channel, have been shown to affect Mg^{2+} affinity (Yang et al., 2009). It may therefore be that the threonine ring reduced ion flux through the channel leading to reduced affinity for Mg^{2+} at the N-site of the GluN1-1a and GluN2A subunits, rather than through modified interactions with specific binding sites.

A further constricted region has been found at the tip of M3 at P +45 of GluN1, but with the GluN3A and GluN3B subunits the cyclic side chains are lost, possibly expanding the pore (Sobolevsky et al., 2009). Furthermore, the bulky W residue at -8 has been shown to influence Mg^{2+} block, but mutations here only resulted in a loss of activity if there was a loss of the aromatic ring, indicating there may be a cation-Π interaction (Williams et al., 1998). The Aromatic ring structure may contribute to the high energy barrier and further constrain the pore.

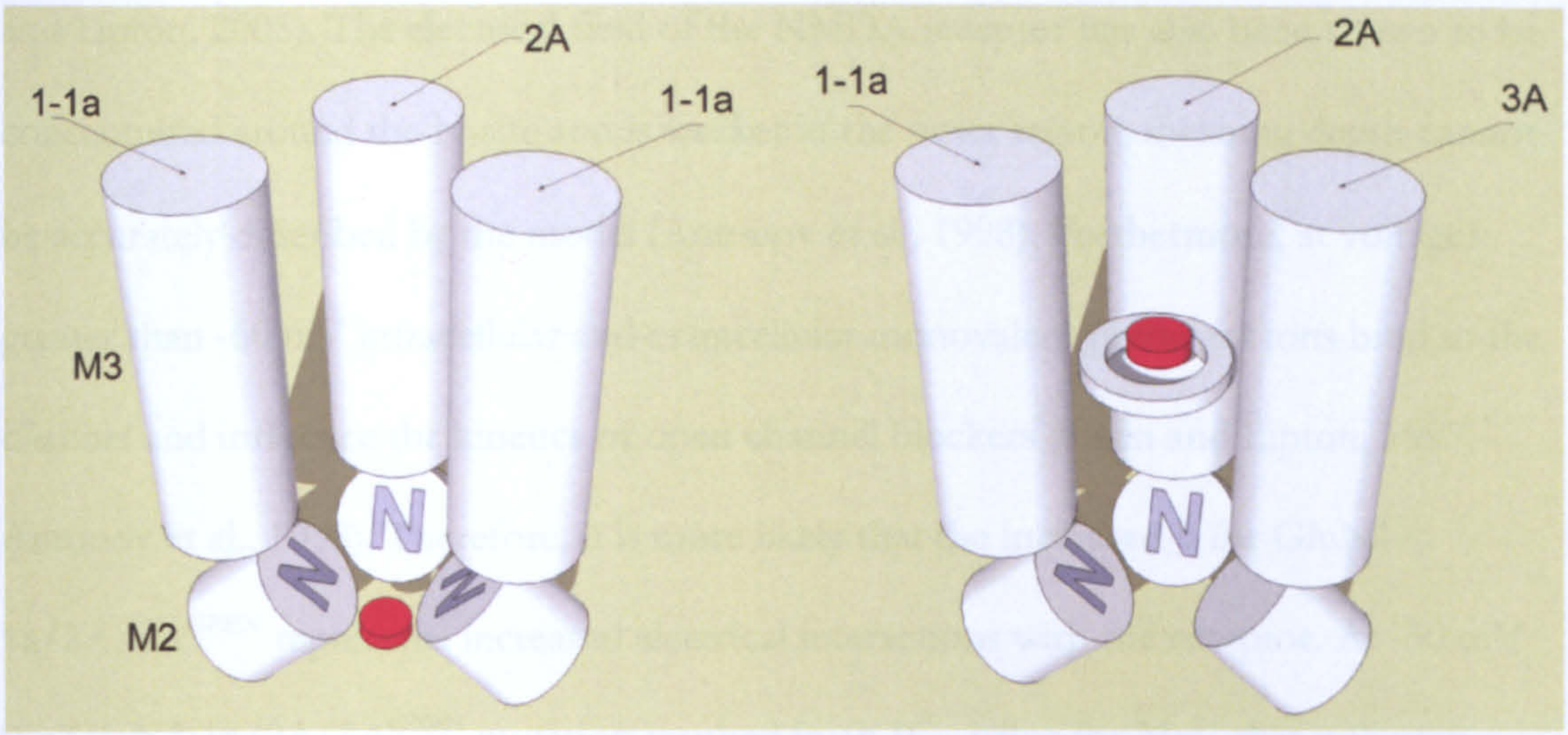

Figure 93: Model of open channel block of NMDA receptors. One subunit has been omitted for clarity. Shown on the left is 1-1a/2A and on the right a GluN3 containing receptor. Position of block shown by the red disc.

The N mutations at position 703 and 704 of GluN3A partially restored IC_{50} for Mg^{2+} toward levels seen with 1-1a/2A at -100 and -75 mV. By restoring the deep binding site, while retaining the threonine ring, it may have led to a situation where block was mediated by the mixed properties of both sites (Chen and Lipton, 2005). Or it may have been that restoring binding at the N-site, without restoring flux (as the ring is unaffected), led to a situation where only a proportion of block could be restored (Yang et al., 2009). Full restoration of block could require double N mutation at N and N+1 as it has been shown that the GluN2 subunit requires both asparagines to provide its binding site (Wollmuth et al., 1998a).The GluN1-1a/2A/GluN3A^{R704N} mutation seemed to show that there was a return to the N-site, as δ was restored to 0.6; however, GluN1-1a/2A/ GluN3A^{G703N} resulted in a δ value that was greater than 1-1a/2A so this interpretation may be unlikely.

The Woodhull model was originally developed to measure depth of block by H^+ through the Na^+ channel, but it has been more recently thought to represent voltage-dependence or electrical interactions, rather than an actual position in space (Woodhull, 1973, Chen

and Lipton, 2005). The electrical field of the NMDA receptor has also been shown to be concentrated around the N-site and is weaker in the outer region, meaning depth cannot be accurately described by the model (Antonov et al., 1998). Furthermore, at voltages greater than -60 mV intracellular and extracellular monovalent permeant ions bind to the channel and influence the kinetics of open channel blockers (Chen and Lipton, 1997, Antonov et al., 1998). Therefore, it is more likely that the increased δ for GluN1-1a/2A/3A^{G703N} represents increased electrical interactions with the receptor. At -50 mV the GluN1-1a/2A/3A^{G703N} mutation resulted in an IC_{50} value for Mg^{2+} that was now significantly higher than GluN1-1a/2A/3A wild-type. As the Woodhull analysis found the GluN1-1a/2A/3A^{G703N} mutation had the most electrical interactions, then it would mean that block was more influenced by the increase in voltage, leading to the higher IC_{50} compared to the other mutants and that was what was found.

The GluN1-1a/2A/3A^{R704D} mutation had no effect on Mg^{2+} block at -100 mV which may mean that changing the charge to negative at this position had no effect. However, as the voltage was increased to-75 mV the IC_{50} for Mg^{2+} was intermediate, and at -50 mV it was increased relative to GluN1-1a/2A/3A similar to GluN1-1a/2A/3A^{G703N}. Therefore, at increased voltages these mutations may have had equivalent effects on Mg^{2+} block, possibly mainly due to removal of the positive charge, rather than the addition of the negative charge.

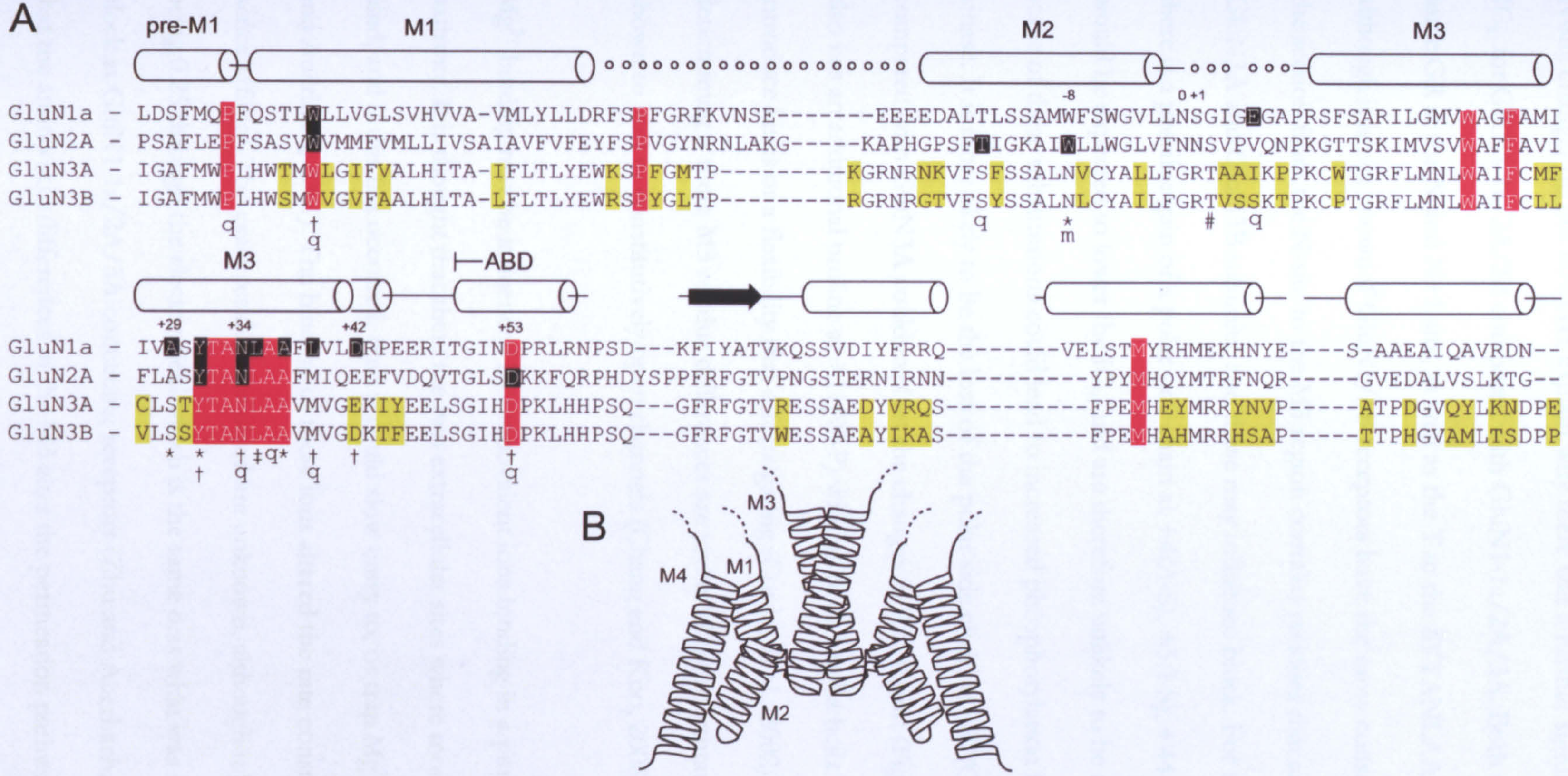

Figure 94: NMDA receptor sequences. (A) Sequence alignment. Residues are numbered in relation to the N site which is 0. Residues highlighted in red are those which are conserved across all subunits. Those which are highlighted in yellow are consensus differences between 3A and 3B. Those which are highlighted in black have been shown to be involved in block by memantine (*), MK-801 (†), AQ343 (q) and Mg2+ (m) at NMDA receptors in addition to the N-site (Williams et al., 1998, Kashiwagi et al., 2002, Kashiwagi et al., 2007, Sobolevsky et al., 2009). Also shown is a residue that was predicted to be involved in PhTX block of AMPA receptors (#) (Andersen et al., 2006). (B) Quaternary structure of the AMPA crystal in the closed configuration (Sobolevsky et al., 2009).

N-site changes do not however explain why there was a further significant increase in IC_{50} for GluN1-1a/2A/3B compared with GluN1-1a/2A/3A. Both subunits have the same GR at the N and N+1 site, as well as the T in the SYTANLAAF motif (Figure 94), although it is not known if GluN1/3B receptors have the same constriction. However, the section from the N-site to the M3 region contains residues that are different for the GluN3A and GluN3B subunits, and these may influence block. For the GluN3B subunit there is a possible gain of a polar side chain at +4(A-S), +5(I-S), +44(I-T) but these would be expected to lower the IC_{50} and are therefore unlikely to be involved, although some of these substitutions could lead to increased phosphorylation by serine/threonine kinase. It is more likely to be the loss of the polar side chain at +27(C-V) for GluN3B compared with GluN3A could explain the changes in IC_{50} found (Figure 94). GluN3B also has an additional proline at +11(W-P) within the M3 alpha helix which may introduce kinks or a flexibility that affects gating (Cordes et al., 2002). The difficulty in determining if these M3 residue differences are involved is that mutations have been shown to lead to constitutively open channels (Chang and Kuo, 2008).

Mg^{2+} binding may be influenced by monovalent ions binding in a putative permeation pathway. It is thought that there are two extracellular sites where monovalent ions can bind, and if this has occurred, then it could slow entry to, or trap Mg^{2+} at the N-site (Zhu and Auerbach, 2001). The binding of these ions altered the rate constants for Mg^{2+} and hence affinity. The exact residues involved are unknown, although it has been reported as being 0.25 through the electric field which is the same δ as what was found for Mg^{2+} block at GluN1-1a/2A/3A containing receptors (Zhu and Auerbach, 2001). It may be that the amino acid differences in the M3 alter the permeation pathway leading to increases in IC_{50} for GluN1-1a/2A/3A and GluN1-1a/2A/3B.

A constricted pore region is not supported by rates that were measured for block. The on-rate of Mg^{2+} was shown to be significantly faster at GluN1-1a/2A/3A than GluN1-1a/2A at -75 mV, but in general the GluN3 subunits and the GluN3A mutations had no effect. Changes in the Mg^{2+} off-rate were also not uniform across the voltages. GluN1-1a/2A was significantly slower at -100 mV while GluN1-1a/2A/3B had a significantly slower off-rate at -50 mV, compared to the remaining subunit combinations. The on-rates and off-rates for the blockers do not form a clear pattern across voltage, across subunits and across the blockers tested. The IC_{50} concentration was used to determine the rates. So the different concentrations may have been altering the rates, rather than the subunits or changes in voltage, although off-rate is not concentration-dependent. The variance of τ was also large between oocytes and would mean that the ANOVA could not detect the differences. Power analysis should have been carried out to determine the number of repeats required to show the differences sufficiently. Furthermore, the variability could also be due to differences in perfusion when the solutions were changed although it was kept at a minimum.

These data have shown that the effect of the GluN3 subunits on Mg^{2+} sensitivity was smaller than expected from the N-site changes alone, and that the GluN3B impaired block more than GluN3A. What was found is less substantial than claims in review papers that the receptor becomes completely resistant with GluN3 present (Petrenko et al., 2003, Paoletti and Neyton, 2006). In fact, evidence was weak, and seemed to be based only on the bioinformatic analysis of the N-site site rather than from experimental data. One study did however show that the IC_{50} for Mg^{2+} in hippocampal neurones from transgenic mice overexpressing GluN3A was around 14-fold higher than wild type, although the voltage was not stated (Tong et al., 2007). The changes in IC_{50} were small similar to what was found in the present study, and the difference with the current

recombinant study may be due to the differing GluN2 subunits present in neurones (Kuner and Schoepfer, 1996).

Sensitivity to Mg^{2+} is dependent on the GluN2 subunit that is expressed. GluN2A and GluN2B are the most sensitive, and GluN2C and GluN2D containing receptors are the least (Kuner and Schoepfer, 1996). It is currently unknown if the different GluN2 subunits alter the Mg^{2+} sensitivity of GluN3 containing receptors. It may be that if the binding site is moved to the threonine ring then the differing GluN2 subunits may lose their ability to influence block, and no difference may be found. But as the GluN2 subunits have the same residues at the N and N+1 site they must not mediate differences in Mg^{2+} block by changes in the selectivity filter. Chimeras of the transmembrane domains, the linkers to the ligand binding domains, linkers to the N-terminal domain and the N-terminal domain itself have all been shown to be involved in various aspects of channel gating and Mg^{2+} sensitivity (Wrighton et al., 2007, Yuan et al., 2009). These regions could similarly be transferred incorporating the GluN3 subunits to determine if they play a role, although it must be noted that transferring the M2 region of GluN3A to GluN1-1a did not produce functional channels (Villmann et al., 1999).

4.3.2 Memantine

Memantine showed a similar pattern to Mg^{2+} as there was a significant increase in IC_{50} for GluN1-1a/2A/3A and GluN1-1a/2A/3B compared with GluN1-1a/2A, and GluN1-1a/2A/3B was significantly higher than GluN1-1a/2A/3A. The amine head group is thought to bind to the N-site of GluN1-1a (Chen and Lipton, 2005). If GluN1-1a was replaced by a GluN3 subunit then it would account for the increase in IC_{50} found with GluN1-1a/2A/3A and GluN1-1a/2A/3B, as well as the partial recovery with the GluN1-1a/2A/3A N mutations. But from the EC_{50} data it seems less likely that a GluN2

subunit was replaced. The number electrostatic interactions within the pore would be reduced as GluN2 has been shown to mediate these (Chen and Lipton, 2005). However, the Woodhull model has shown that suggest that the presence of GluN3A subunit had a higher δ than GluN1-1a/2A alone. Further positions that have previously been shown to be involved in memantine block are altered with the GluN3 subunits (Figure 94). Changes at +29 (A-S) led to the loss of hydrophobic side chain and the loss of the aromatic residue at -8 (W-N) and the may have led to the increased IC_{50} values found, but are the same for the GluN3A and GluN3B subunits (Kashiwagi et al., 2002).

The Woodhull model showed that the GluN1-1a/2A/3A^{R704N} mutated receptor had an increased δ even beyond the level of GluN1-1a/2A/3A, while a complete change of charge with GluN1-1a/2A/3A^{R704D} caused a dramatic reduction in δ below the level of GluN1-1a/2A receptors. Memantine interaction with GluN2 subunit is thought to involve the externally pointing carbonyl oxygen of position 704 (Chen and Lipton, 2005). Therefore, GluN3A wild-type which has a full positive charge (R) and GluN3A^{R704D} which has a full negative at this position may be interfering with binding, as the GluN3A^{R704N} mutation was shown to have the highest δ. Interpreting the δ values is also further complicated as it has been proposed that two memantine molecules bind in the channel, and that would produce an average δ of around 0.45 which is the value found for GluN3A^{G704N} (Sobolevsky and Koshelev, 1998, Kashiwagi et al., 2002).

The on-rate for memantine seemed unaffected by at GluN1-1a/2A/3A and GluN1-1a/2A/3B as no significant differences were found at any voltage, or with the GluN3A mutations. However, with GluN1-1a/2A/3A the off-rate had a τ that was generally significantly slower than GluN1-1a/2A and GluN1-1a/2A/3B. All the GluN3A mutations restored the speed of τ, but an effect was only found at -75 and -50 mV. The

slower off-rate of GluN1-1a/2A/3A may be related to the number of electrical interactions between GluN1-1a/2A/3A and memantine, as it had an increased δ compared with GluN1-1a/2A. By this reasoning GluN1-1a/2A/3A^{R704N} should have had the slowest rate, but it was not found.

Block by memantine at GluN1-1a/2A/3B containing receptors was not voltage-dependent and a large decrease in δ was found. It may be that amino acid differences, or constrictions in the pore, caused the compound to bind at the superficial site, which has been indirectly estimated to have an IC_{50} of 79.1 μM at -66 mV (Kotermanski et al., 2009). The current study found that memantine had an IC_{50} at GluN1-1a/2A/3B of 17.54 μM at -75 mV, and may be a better measure. The superficial site IC_{50} was calculated using a double-pulse protocol hoping that the second pulse left the superficial site free, and may not have been sufficiently accurate. At -50 mV the IC_{50} for memantine was not significantly different between GluN1-1a/2A/3A and GluN1-1a/2A/3B indicating that binding at GluN1-1a/2A/3A may have shifted to the superficial site, which has been shown to occur at voltages more positive than -60 mV (Antonov et al., 1998). Block at the GluN1-1a/2A/3A^{R704D} mutation was also shown to not be voltage-dependent and it also had a δ that was lower than GluN1-1a/2A. However, it may not represent binding at the superficial site as the IC_{50} for memantine was not similar to that of GluN1-1a/2A/3B, and remained potent. The superficial site is located at position +35 and could be mutated in order to determine if block at GluN1-1a/2A/3B or GluN1-1a/2A/3A^{R704D} was impaired.

4.3.3 MK-801

Compared to the other compounds tested MK-801 was the most potent at all receptor subunit combinations at all voltages. When comparing the IC_{50} of the various subunits at -100 mV MK-801 showed a significant increase in IC_{50} with GluN1-1a/2A/3A and GluN1-1a/2A/3B (around 3-fold), but no significant difference was found between the GluN3 subunits. However, the effect of GluN1-1a/2A/3A was dependent on voltage as when it was increased no difference was found, while GluN1-1a/2A/3B continued to have an increased IC_{50}. MK-801 is thought to bind with high affinity to the N-site in such a way that agonist can dissociate and the channel can close while it is still bound in the pore, and the restoration of activity found with the GluN3A N mutations support the claim that binding occurs in this region (Kashiwagi et al., 2002). It has also been shown that there are many further residues that influence MK-801 binding across the channel (Figure 94). It is unlikely that the compound can bind to M1, M3 and the N-site simultaneously, unless more than one molecule can block the receptor. The wide range of residues may represent a pathway into the N-site.

The aromatic groups of MK-801 are more likely to make hydrophobic interactions that possibly encourage entry into the pore similar manner to the DRPEER motif that attracts Ca^{2+}. Changes could due to increased aromatic residues such at W (+8), F (+26) and Y (+45) for GluN3A and F (+45) for GluN3B. However, few residues that have been directly implicated in MK-801 block are different between the GluN3 subunits (Figure 94) (Kashiwagi et al., 2002). It may be that the voltage-dependent differences in IC_{50} for MK-801 are representative of structural changes within the M3 region restricting access to the N-site, such as the threonine ring. It could also be due to an altered M3 region as the P at position +11 may have introduced kinks or flexibility into the α-helix (Cordes et

al., 2002). Such a change may explain the Woodhull analysis which showed that GluN1-1a/2A/3B containing receptors had the most electrostatic interactions with MK-801, even though GluN1-1a/2A/3A had the most additional aromatic groups. If the GluN1-1a/2A/3B N-site mutation showed no effect then that would support the conclusion that the structure of M3 was impairing access.

The presence of GluN3A in a GluN1-1a/2A/3A receptor assembly led to a faster on-rate for MK-801 while the mutations GluN1-1a/2A/3A^{G703N} and GluN1-1a/2A/3A^{R704N} were shown to slow the rate back down. The off-rate showed a similar pattern, with GluN1-1a/2A/3A generally being significantly faster than the other subunit combinations, while the GluN1-1a/2A/3A^{R704N} mutation slowed the rate. Woodhull analysis has shown that GluN1-1a/2A/3A had the lowest δ for MK-801 block and the faster rate may represent easier access, even though the GluN3A has more additional aromatic residues in the pore compared to GluN3B.

4.3.4 PhTX

PhTX-343 had an IC_{50} that was not significantly different to MK-801 at GluN1-1a/2A or GluN1-1a/2A/3B at -100 mV, meaning that at low voltages it can be considered a particularly potent compound. GluN1-1a/2A/3A and GluN1-1a/2A/3B were both shown to significantly increase IC_{50} for PhTX-343 by the same magnitude (~10-fold), but only at -100 mV. The subunit differences may be related to the ability for the terminal amine group to reach a deep site at -100 mV which was impaired by the presence of the GluN3 subunits or by increased voltage. For polyamines to have maximum potency at AMPA receptors they require two amine groups; whereas for block of the NMDA receptor they require three (Mellor et al., 2003, Nelson et al., 2009). The additional charge is thought to bind to the N-site of NMDA receptors which is not implicated in some

models of AMPA receptor binding, which show two amines binding to G at +2 while the head group binds in the M3 vestibule (Andersen et al., 2006). At NMDA receptors the head group of the anthraquinone toxins has been shown to bind in M3 region, with the tail binding to the negatively charged E at position +5 of GluN1, located beyond the selectivity filter (Figure 94) (Jin et al., 2007). At GluN3A +5 is I and at GluN3B it is S, so at -100 mV the binding may be impaired, leading to the increased IC_{50} values that were found. As the voltage was increased then it may not have been possible for the terminal amine to reach the site at any receptor combination, as no differences were found for PhTX-343 block at any subunit combinations.

PhTX-343 was the most voltage-dependent of the compounds tested supporting the conclusion that deeper binding site was only accessible as the voltage was made more negative. The Woodhull model found a reduction in δ with GluN1-1a/2A/3A compared with GluN1-1a/2A indicating that there may have been reduced interactions possibly related to position +5. The GluN1-1a/2A/3A^{R704N} mutation also had an increased δ and may represent an additional binding site for the compound when the positive charge was removed and replaced with N. The increased δ may also represent deeper binding as the R residue was removed. GluN1-1a/2A/3B had the highest δ of all the subunit combinations tested which may be a result of further binding of the head group within the M3 region similar to the anthraquinone toxins and MK-801 (Kashiwagi et al., 2007). However, the Woodhull model may again have limitations as it is unable to describe multiple complex binding properties in a non-uniform electrical field, properties that are characteristic of the polyamines.

For PhTX-343 the presence of the GluN3A and GluN3B subunits generally led to a faster on-rate and off-rate at all voltages. The amine groups of PhTX-343 may bind to

less residues on GluN3A and GluN3B leading to faster kinetics. There could be the loss of interaction at deep position +5 which may have led to an increased off-rate, but is not supported by the continued increased rates as the voltage was increased. It could be that the interaction with the N-site was lost; however, it was shown that the GluN3A mutations did not restore the binding kinetics, which would have been expected.

For the anthraquinone toxins the mutation at the N-site of GluN1 to G reduced the potency of AQ343 and AQ444 (Kashiwagi et al., 2002). At the same site on GluN2B the G mutation increased the potency of AQ343 (Kashiwagi et al., 2007). Therefore, the G at the N-site of the GluN3 subunits could have been expected to not interfere with PhTX-343 binding. But this was not found as all the mutations partially restored block at -100 mV. One explanation is that the positively charged R at position 703 could have been blocking the terminal amine group from reaching the deep binding site. Therefore, the N and D mutations at position 704 removed the barrier increasing potency, but only partially as the N-site was not also restored.

The selectivity filter has been shown to be important for the activity of polyamine toxins. An R at the Q/R site on the GluA2 subunit of the AMPA receptor results in receptors that are not blocked by polyamines (Isaac et al., 2007). However, the same was not found with the R at the N+1 site of the GluN3 subunits, as the loss of activity by PhTX-343 was less dramatic. It may be that the residue is not exposed in the pore, or the charge is not located at a critical position. Mutating the G to R at the N-site of the GluN3 subunits may result in NMDA receptors that are not blocked by polyamines, but if so it may mean that no PhTX will have the same discriminative effect that is found with AMPA receptors (Andersen et al., 2006).

The presence of GluN3A showed a different pattern with PhTX-12 than the other blockers. A significant decrease in IC_{50} compared to 1-1a/2A at -100 mV and -75 mV was found, with no difference between GluN1-1a/2A and GluN1-1a/2A/3B containing receptors. PhTX-343 requires three charges to optimally block the NMDA receptor; therefore, the loss of two charges with PhTX-12 impaired potency consistent with previous reports (Mellor et al., 2003). However, at GluN3A there is a G at the N-site so the loss of charge with PhTX-12 means that it was not interacting at this site even at GluN1-1a/2A receptors therefore amino acid changes did not impair block. The G may expand the channel and allow deeper binding, letting terminal amine group interact with G+2 similar to AMPA receptor (Andersen et al., 2006). Such an interaction could be further explored using PhTX-74 or PhTX-84 which could possibly have increased potency compared with PhTX-12 due to the increased charge at the end of the tail group. PhTX compounds with two amines on the tail group may also stop it from folding back on itself, which may be what occurs with PhTX-12 (Tikhonov et al., 2004). Therefore, these compounds may retain a shape that is accommodated better in the pore region than PhTX-12, increasing potency.

The IC_{50} for PhTX-12 also shows again that the R at +1 does not have the same effect as the Q/R switch in GluA2. But the data shows that changes in the pore led to increased potency of PhTX-12 at GluN1-1a/2A/3A containing receptors. But as the GluN3A and GluN3B subunits are similar in this region it does not explain why there was no similar decrease in IC_{50} for GluN3B. The Woodhull analysis found that GluN1-1a/2A and GluN1-1a/2A/3A receptors had the same δ value while there was a reduction for GluN1-1a/2A/3B. Potency and δ may not be not tightly correlated, and changes to the on-rate and off rates may have helped explain this, but only limited quantities were available.

PhTX-12 was the least potent of all the blockers tested and its activity may just be unspecific in nature. Block was not voltage-dependent at GluN1-1a/2A/3A and GluN1-1a/2A/3B containing NMDA receptors, although the results may be due to the poor fits of the Hill equation masking statistical significance when the IC_{50} values were compared. Lack of voltage-dependence can indicate that open channel block is not occurring; however, it is not the case that all open channel blockers are voltage-dependent. Picrotoxin blocks GABA receptors in a manner that cannot be voltage-dependent as it does not have a charge (Bali and Akabas, 2007). It has also been shown that block of NMDA receptors by bicuculline is not voltage-dependent, even though it is thought to bind in the pore (Li, 1999). Block of muscle nAChR by PhTX-12 was shown to not be voltage-dependent and may be due to the chain/head group structure becoming radically distorted (Mellor et al., 2003). It has been shown that if the tail section of the PhTX-12 molecule folds back on itself it would have a diameter around 10–14 Å which would be larger than the pore, therefore block may be occurring in extracellular regions of the NMDA receptor (Tikhonov et al., 2004). The current study found that the IC_{50} for PhTX-12 was 293 μM at -75 mV whereas NMDA responses to whole rat brain RNA have been previously shown to have an IC_{50} of 7 μM at -80 mV (Mellor et al., 2003). The latter expressed the whole range of GluN1 splice variants, GluN2 and GluN3 subunits so the reduced potency found in the current study may be due to inhibition at the N1 cassette or due to a differing activity at regions of the GluN2 subunit, possibly the NTD similar to spermine.

4.3.5 Methoctramine

The study also reports for the first time the ability of methoctramine to inhibit recombinant NMDA receptors, and was shown to be a potent compound with an IC_{50} in the μM range. Similar to MK-801, there was a significant increase in the IC_{50} with GluN1-1a/2A/3A and GluN1-1a/2A/3B containing receptors at -100 mV, but when the voltage was increased the difference with GluN1-1a/2A/3A was lost while GluN1-1a/2A/3B continued to impair block. However, unlike MK-801 the presence of the GluN3B subunit had no effect at -50 mV. Results from the Woodhull model suggest that methoctramine had a low δ for all subunit combinations tested, particularly GluN1-1a/2A/3B. Such a finding is surprising for a compound with the largest number of amine groups tested (4), and may mean that it does not interact with the same residues that the extended polyamine PhTX-343 tail does.

Methoctramine is large compound with two aromatic groups at either end of a chain that may orientate itself in a V shape (Rosini et al., 2002). It may be that the aromatic rings interact with the same residues that interact with MK-801 in the M3 region, as it has a similar pattern of activity. The amines in the linker region could then interact with the selectivity filter as the GluN3A N mutations were shown to partially restore block at -100 mV. Methoctramine has been shown to be less potent than PhTX-343 at -100 mV, so the increase in amines did not lead to increased potency. However, as the voltage was increased methoctramine retained potency as the deep site E at position +5 implicated in PhTX-343 block may not be involved.

The on-rate for methoctramine was significantly faster for GluN1-1a/2A/3A but only at -75 and -50 mV and was unaltered by the GluN1-1a/2A/3A mutations. The presence of

GluN1-1a/2A/3A and GluN1-1a/2A/3B significantly slowed the off-rates, but were not restored by the GluN3A mutations. In fact, the GluN1-1a/2A/3A^{G703N} mutation further slowed the off-rate. They generally had the same δ so must be unrelated to electrical interactions. The changes in rate may again represent binding of the aromatic resides in methoctramine to aromatic residues in the pore.

4.4 Channel Properties

The I/V relationship showed that GluN1-1a/2A had a reversal potential of +12.15 mV which was reduced to -2.646 mV for GluN1-1a/2A/3A, indicating reduced Ca^{2+} current, similar to previous reports (Sasaki et al., 2002). Both receptor types also showed negative slope conductance at voltages less than -100 mV that is unrelated to Mg^{2+} block, similar to previous reports (Soloviev et al., 1996). GluN1/3A glycine activated receptors have been shown to be have the same negative slope at voltages lower than -50 mV, and it is thought that it is due to inhibition by Ca^{2+} (Madry et al., 2010). The negative slope region may have been pushed to more negative voltages in the current study by the presence of the GluN2 subunit.

The current study also found that there was a significant reduction in steady state current through the NMDA receptor after activation by NMDA/glycine when the GluN3A and GluN3B subunits were present. Flux may have been reduced due to the threonine ring and as the current measured for GluN1-1a/2A/3A and GluN1-1a/2A/3B was not significantly different to each other indicating that the ring was present in GluN1-1a/2A/3B as well as GluN1-1a/2A/3A. Reduced current could also be due to the DRPEER motif which is not present on the GluN2A, GluN3A or GluN3B and is important for mediating Ca^{2+} permeability (Watanabe et al., 2002). If a GluN3 subunit

replaced a GluN1-1a subunit then it would lead to reduced Ca^{2+} current through the channel.

NMDA receptors are known to be susceptible to Ca^{2+} dependent desensitisation/inactivation over the region of 10 to 50 s (Medina et al., 1995). In Xenopus oocytes, the initial peak transient component of the NMDA response was previously shown to be reduced in GluN1/GluN3B glycine activated channels indicating reduced Ca^{2+} entry through the receptor (Chatterton et al., 2002). The current study has shown that there was a significant decrease in the peak to plateau ratio, indicating reduced Ca^{2+} permeability through GluN1-1a/2A/3A and GluN1-1a/2A/3B containing channels, by suffering less from Ca^{2+} induced desensitisation.

4.5 Glycine Gated NMDA Receptors

It was previously thought that GluN1 expressed alone in Xenopus oocytes produced functional glycine activated channels; however, this has been shown to be due to the presence of an endogenous *Xen*GluN2 subunits (Schmidt and Hollmann, 2008). The same study also showed that there was a full set of homologous GluN2 mRNA in oocytes, while GluN2B protein was also found. It has also been shown that low concentrations of Zn^{2+} potentiate, rather than inhibit, responses for *Xen*GluN1-1/*Xen*GluN2B receptors, and the same effect was also thought to occur with the apparent homomeric GluN1 current (Traynelis et al., 1998, Schmidt and Hollmann, 2008).

Any study which relies on the absence of a subunit which has a homologous protein present in the expression system may be being misinterpreted. Early attempts to express glycine gated receptors failed, but if such an assembly was robust then these should have

consistently produced receptors since it was first attempted (Ciabarra et al., 1995, Sucher et al., 1995, Smothers and Woodward, 2009). During the course of the study they could not be obtained. But as *Xen*GluN2B levels have been shown to be highly variable it would explain the difficulties found when they were originally expressed (Smothers and Woodward, 2009). Interpreting the nature of these receptors would be further complicated when considering the opposite effect Zn^{2+} can have on these channels. When considering *Xen*GluN2B it would change the claims of Madry et al., 2008 and Madry et al., 2010 where glycine activated receptors with Zn^{2+} potentiation were found. In fact, NTD deletions of GluN1 and GluN3A did not alter the potentiation, possibly indicating a different subunit was involved (Madry et al., 2008).

Homomeric GluN1 currents and GluN1/3 receptors were never found with HEK-293 cells possibly ruling out the existence of an endogenous GluN2 subunit in this system (Nishi et al., 2001, Perez-Otano et al., 2001). But these cells require both GluN3A and GluN3B to produce functional glycine activated receptors, and may represent a folding requirement where GluN3B is allowed to take the position taken by the endogenous *Xen*GluN2B subunit. If GluN3B was acting as a GluN2 then it may explain why it is thought that GluN1/3A/3B glycine gated receptors are preferentially formed in Xenopus oocytes (Ulbrich and Isacoff, 2008).

When the *Xen*GluN2B is present it may mean that gating is altered so it can be activated by glycine alone. In glycine gated receptors it has been shown that glycine binding to the GluN1 subunit causes fast desensitisation rather than activation, and that glycine binding to GluN3 alone will open the channel (Awobuluyi et al., 2007, Madry et al., 2007). Now that the *Xen*GluN2B subunit has been cloned these gating properties can be tested.

Glycine has been previously shown to activate oocytes injected with GluN1-1a/2A and again may represent the influence of *Xen*GluN2B (Meguro et al., 1992).

GluN1-3b/GluN3B receptors expressed in Xenopus oocytes have also been shown to be activated by glutamate alone (Cavara et al., 2009). They state that batch-batch differences in *Xen*GluN2B expression could influence results, and that such recordings had to be manually eliminated. The same study showed that GluN1-4a/2A/3A produced channels in HEK-293 cells that were opened by glutamate or glycine alone (Smothers and Woodward, 2009). However, it was previously shown that glutamate or NMDA alone did not activate GluN1-1a/2A/3A, but in that study they did not state which GluN1 splice variant was used (Chatterton et al., 2002). Although it is known that NMDA receptors require both agonists for the pore to open, it has been shown in single channel studies that AMPA receptors show subunit specific opening depending on agonist occupancy (Rosenmund et al., 1998). The GluN3 and *Xen*2B subunit may allow altered gating to occur where only either agonist is required for channel opening, rather than both.

Altered gating may be dependent on which position the subunits take in the receptor. Those in the proximal position (A, C) have an extended M3 region that would be constricted at P +45, and they move less than those in the distal position (B, D) (Figure 95) (Sobolevsky et al., 2009). The proximal subunits were shown to be GluN1 and therefore have a lesser role in gating. The GluN3 subunits may lead to the loss of the proline at +45 which could widen the channel at the gate, allowing it to open under different circumstances.

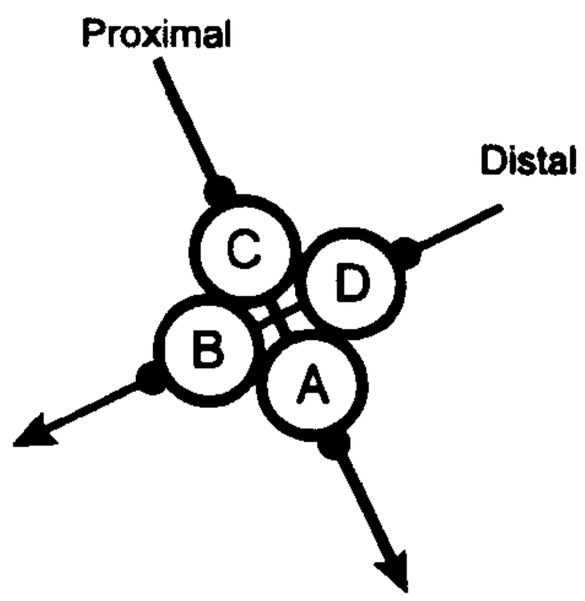

Figure 95: AMPA receptor composition showing stoichometry of subunits. A/C are termed proximal, and B/D are termed the distal, to the overall two-fold axis of symmetry.

The current study has shown that glycine alone did not lead to channel opening. Rat GluN2A does not have the same properties as *Xen*GluN2B and it therefore may have retained the original gating properties. The fact that glycine alone did not open the channel also questions the conclusions of Ulbrich and Isacoff (2008) which suggested that two separate populations of receptor would be formed, GluN1/2 and GluN1/3. If this was occurring then glycine alone or with Zn^{2+} would have activated the glycine activated component, but it was not found. In the Ulbrich and Isacoff study only GluN2 (green) and GluN3 (red) subunits were tagged. The receptors that contained the endogenous subunit could be interpreted as being GluN1/3, as only the GluN3 would have been detected. The authors also freely admitted that that they found receptors with both red and green spots. They used a Monte Carlo method to confirm it was possible with their interpretation, rather than admit their conclusions may have some shortcomings. They also did not determine if functional channels were produced. Even if their interpretation was correct then it does not explain why some studies have shown that channels could be activated by glutamate alone, as the GluN1-1a/2A component would still need both agonists for activation (Cavara et al., 2009, Smothers and Woodward, 2009).

If the glycine activated receptors are not just a phenomenon resulting from the combination of exogenous and endogenous subunits in ways that have not evolved in nature, the lack of convincing evidence *in vivo* is problematic. It would be expected that transgenic animals overexpressing GluN3 subunits would lead to an abundance of glycine activated currents, but currents mediated by glycine alone were not found (Tong et al., 2007). Excitatory glycine currents in the presence of strychnine were however found in cerebrocortical neurones (Chatterton et al., 2002). These were inhibited by D-serine rather than potentiated which would have been expected with GluN1-1a/2A, but the experiment has never been repeated. Therefore, the remaining evidence *in vivo* is patches that have two different conductance levels with no direct transitions, although no superimpositions were found (Perez-Otano et al., 2001, Sasaki et al., 2002). Furthermore, these studies did not check if glycine activated the lower conductance alone. If glycine activated receptors were abundant in the nervous system then it would be expected to have been found, waiting for the glycine gated receptors to be identified. Then there is the lack of subsequent convincing evidence even when researchers were actively looking for the receptors, tending to support the conclusion that they are merely a quirk of the expression systems used (Das et al., 1998, Chatterton et al., 2002, Sasaki et al., 2002, Tong et al., 2007).

As the GluN3 subunits are known to be rapidly incorporated into endogenous NMDA receptors, as well as to undergo rapid endocytosis throughout development, it may be that the two conductance states merely represent such a process (Perez-Otano et al., 2001, Tong et al., 2007). If expression is not uniform throughout the membrane, and GluN3 was being incorporated and removed dynamically, then the system would by produce a GluN1-1a/2A channel and another containing GluN3. By increasing the ratio

of GluN3 it has been shown that the larger GluN1-1a/2a conductance is reduced and may represent a larger proportion of GluN3 being incorporated into NMDA receptors (Das et al., 1998). However, biphasic dose response curves were not found and the inhibition curves tended toward zero in the current study. Therefore it is suggested that uniform expression of GluN1/2/3 was obtained.

4.6 Resolving GluN3 Receptor Assemblies

To solve the glycine gated story their gating properties could be explored by expressing a range of rat GluN1 and GluN3 together with *Xen*GluN2B. Furthermore, inhibition by ifenprodil is retained with the *Xen*GluN2B subunit but, as stated they are potentiated by Zn^{2+} (Schmidt and Hollmann, 2009). The combination of these modulators provides a pharmacological tool for establishing the presence of *Xen*GluN2B in glycine activated receptor studies, which would be confirmed if they were inhibited by ifenprodil and potentiated by Zn^{2+}.

Glycine activated receptors are known to be difficult to express and were not found during the course of the work reported in this thesis (Sucher et al., 1995, Ciabarra et al., 1995). A possible way to gain more robust expression would be to mutate the ligand binding domain of GluN1, which causes fast desensitisation, so it cannot bind glycine or block the binding site pharmacologically using MDL-29951, L689560 or 5,7-DCKA (Yao and Mayer, 2006, Awobuluyi et al., 2007, Madry et al., 2007). If consistent expression of a glycine gated component occurred then an siRNA could be injected to block *Xen*GluN2B expression. If there were then no fucntional channels then it would show that the endogenous *Xen*GluN2B subunit was required to produce them.

An additional way to determine the stoichometry of GluN3 containing receptors is to exploit the positioning of residues found with the AMPA crystal (Sobolevsky et al., 2009). It was found that position P at +45 (part of the DRPEER motif) on the GluN1-1a subunits in the proximal position were positioned close together. When they were mutated to a cysteine they cross-linked and this effect was detected by western blotting. The GluN3 subunit is thought to replace the GluN1 subunit in a GluN1/2 dimer (Perez-Otano et al., 2001). By producing the C mutants at P +45 on GluN1 which is I at the same position on GluN3A their proximity could be determined. If these mutations resulted in crosslinking then it would show that there were GluN1 and GluN3 subunits in the proximal position.

4.7 Alzheimer's Disease and Multi-target Ligands

4.7.1 Carbacrine Series

It was found that of the carbacrine compounds, carbacrine(3) was the most potent with an IC_{50} around 0.74 μM at -100 mV. Due to its potency it was promisingly shown to have an IC_{50} that was not significantly different to memantine at all the voltages tested. The potency of carbacrine(3) must be unrelated to charge as all members of the group had the same number of amines. Increasing the chain length was shown to impair block, therefore alkyl chains of three or less may have been required for potency. It may be that those with alkyl chains of less than three carbons would have an increased potency, but no smaller compounds were produced. For other classes of NMDA receptor antagonist chain length has been shown to produce non-systematic effects on potency. For none, one and two carbons between the phenylcyclohexyl and the terminal amino group of a range of compounds tested, the smallest (IEM-1921) and largest chains (IEM-2044) were shown to be 10-fold more potent than the compound with the intermediate length (IEM-

2014) (Bolshakov et al., 2005). Chain length has been shown to alter block by competitive antagonists of the GluN2 binding site. With a heptyl chain (*(R)*-CPP) it was found that there was a 50-fold difference in affinity across the GluN2 subunits, whereas those compounds which had pentyl chain showed a 5-fold difference (Feng et al., 2005). Therefore, carbacrine(3) with its propyl linker may have a potency that was already optimal, and no improvements can be made by reducing its size.

It was found that block by carbacrine(3) and carbacrine(5) was voltage-dependent suggesting that they may be open channel blockers, possibly at the N-site typical of most compounds of this type. However, Woodhull analysis resulted in a δ value of 0.2 which does not support block at the N-site if δ is taken as a measure of distance, so it may represent limited electrostatic interactions with the receptor (Zhu and Auerbach, 2001). It may be that these compounds were blocking in an area similar to the superficial memantine site; however, the δ value was greater than that for GluN3B containing receptors from the first chapter. Block at the superficial site could be tested with the $GluN1^{N616D}$ mutation which has been shown to allow block at different sites with 200 μM and 2 mM memantine (Chen and Lipton, 2005). Carbacrine(3) and carbacrine(5) were shown to be voltage-dependent, it is not a property of the superficial site limiting the interpretation (Kotermanski et al., 2009).

On the contrary, block by carbacrine(4) and carbacrine(6) was not voltage-dependent and Woodhull analysis showed these to have a low δ similar to that found with GluN3B containing receptors. These are more likely to indicate block at the superficial memantine site as they were not voltage-dependent. However, the changes in the δ values indicated by the Woodhull model may also be explained by less electrical interactions between the compounds and the receptor. Carbacrine is a large molecule that has two

pharmacophores that can both interact with the pore and may have interactions that were impaired with chain lengths of four and six.

The carbacrine compounds were numbered according to their alkyl chain length, but it was shown that extending of the chain from propyl to pentyl gave voltage-dependent properties that may indicate binding at the N-site. Although it is a competitive antagonist, a similar alternating chain effect has been shown with AP5, where increasing the alkyl chain by one carbon reduced potency, but was restored with a subsequent additional group (Evans et al., 1982). Determining where these compounds block would depend on their promise as MTDL drugs, and due to the low activity of carbacrine(4), carbacrine(5) and carbacrine(6) at the NMDA receptor it would only be worthwhile to determine these properties for carbacrine(3).

The carbacrine compounds were combinations of the pharmacophores derived from the β-blocker carvedilol and the AChEI tacrine. However, carvedilol has been shown to be competitive for MK-801 binding indicating open-channel block (Lysko et al., 1992). There is also evidence that tacrine can act as an open-channel blocker, but increasing the size of the molecule with the bis(7)-tacrine form resulted in a compound that was not thought to bind in the pore of the NMDA receptor as it lacked voltage-dependence (Liu et al., 2008). Therefore it may be that for carbacrine(3) and carbacrine(4) the carvedilol moiety of the MTDL was interacting with the channel, as block was voltage-dependent. The chain-dependent effects of the propyl and pentyl chains may have oriented the moieties in a similar way leading to similar properties. However, the potency of carvedilol is low and is not consistent with what was found for carbacrine(3), but it is possible it changes when it is placed within a larger backbone (Lysko et al., 1992).

For carbacrine(5) and carbacrine(6) it may have been that the tacrine moiety was preferentially interacting with the receptor as the compound would possibly have taken the properties of the non voltage-dependent bis(7) form due to its placement within the larger sized MTDL backbone. The carbacrine compounds could also have had a mixed mode of action which would depend on the orientation of the molecule as it docks with the receptor. Regardless, a threshold was reached with a propyl chain, and the decrease in IC_{50} may have been due to the constraint of the two functional moieties within the linker.

These data formed part of an ongoing study measuring the ability of these compounds to show potential therapeutic effects when tested using *in vitro* assays for AD. The carbacrine compounds were shown to retain AChEI activity, as would be expected due to its tacrine moiety (Rosini et al., 2008). Carbacrine had an IC_{50} for AChE in the nanomolar range and this effect was not altered through increasing chain length. Rather surprisingly the carbacrine compounds were shown to be a more potent than tacrine or the 6-chloro derivative alone when inhibiting AChE (Camps et al., 2008, Rosini et al., 2008). The property may be due to their increased size compared to the originator molecules allowing them to inhibit both the catalytic and peripheral anionic site of AChE. Donepezil is similar, as when it was crystallised it was shown to inhibit both regions of AChE (Kryger et al., 1999). Binding at both sites has also been shown to allow donepezil to inhibit AChE induced aggregation of Aβ (Bartolini et al., 2003). Bis-(7)-tacrine was also shown to bind to both sites with a minimum of five methylene groups linking the tacrine moieties (Carlier et al., 1999). Docking studies showed that carbacrine(3) could bind to both sites of AChE, with the tacrine moiety shown to interact with the catalytic pocket, while the carbazole interacted with the peripheral anionic site (Rosini et al., 2008). Such an ability may affect AChE induced $A\beta_{1\text{-}40}$ aggregation as the carbacrine compounds were shown to inhibit it in a manner that was not altered by chain

length. The same study did however also find that they were able to inhibit self-induced aggregation of Aβ. Chain length influenced this as carbacrine(3) resulted in 36% inhibition, whereas carbacrine(6) only led to 23.7% inhibition of aggregation (Rosini et al., 2008). Furthermore, the same study also showed that the carbacrine compounds had an increased IC_{50} at BChE compared with AChE, possibly giving the group a favourable side effect profile.

4.7.2 Donepezil Derived Compounds 1 and 2

2b and **2a** have a similar structure to each other, with the methoxy group of the phenyl group located on the same carbon. The potency of these compounds was low, with inhibition of the control response being minimal at the highest concentrations tested. When the Hill equation was fitted to the data, it was either not possible, or the parameters obtained were not meaningful due to a poor fit. There was no effect of the linker region, as the pentyl linker of **2a** and the hexyl linker of **2b** had no effect on potency.

Compounds **1a-e** moved the methoxy group to a different carbon on the phenyl region which generally led to increased potency at the NMDA receptor, indicating it may have been involved in impairing block when it was in its previous position. However, a compound was not produced with an equivalently sized alkyl chain so the change in structure cannot be directly compared. The group had IC_{50} values around 50-100 μM which would limit their use as therapeutics. That with a butyl chain (**1b**) and that which had the largest (**1e**, nonyl) had the lowest IC_{50} values. The octyl chain of **1d** seriously impaired the ability of the group to block the NMDA receptor. From **1d**, which had eight carbons, the loss or gain of one carbon was shown to restore block similar to previous compounds that have been discussed. The voltage-dependence of the series was

not measured due to the limited quantities available. IC_{50} values were calculated only at -100 mV and if these were acting as open channel blockers it would be expected to increase with an increase in voltage. The potential as therapeutics would be further reduced by the voltage-dependence as the membrane potential of neurones *in vivo* would not be as low.

The low potency of **1** and **2** can be compared to that of carbacrine as both have the same carbazole pharmacophore derived from carvedilol. For the carbacrine compounds the tacrine moiety may have represented the region of the compound that interacted with the pore region with high affinity, as this group is lost with **1** and **2** possibly explaining their low potency. It may be that the carbacrine compound became constrained in such a way with a propyl linker that the tacrine moiety was the predominant area in which the compound interacted with the receptor, leaving a mixed mode of action with the larger chains. **1** and **2** also contain a group derived from donepezil (the methoxyphenyl and a piperazine group), but it is unknown if the small region added to the MTDL is that which is involved mediating its NMDA receptor activity, so may have been lost (Wang et al., 1999).

4.7.3 Dimebon Derived Compounds

Compounds **3**, **4** and **5** took dimebon, removed the pyridine group and linked two dimebons producing a series that explored the effect of differing linker regions on potency. Of these, **4** had a 3, 6 – dioxa octyl chain and was found to be the most potent of the series at all voltages tested. However, modifications to PhTX-343 that included oxygen within the polyamine chain were shown to reduce potency at the NMDA receptor (Mellor et al., 2003). Such an effect may have been due to the electronegative oxygen of the modified PhTX-343 not being accommodated well within the negatively

charged pore region, and the IC_{50} of **4** found in the current study was similar to that of the PhTX-343 analogues with oxygen groups in the chain (Mellor et al., 2003).

The remaining compounds had an alkyl chain (**3a-c**) or an aniline group within the chain (**5**), and these had similar potencies. Differing sizes of alkyl chain (**3a-c**) also had little effect on potency, apart from a small increase in IC_{50} with the hexyl chain (**3b**). These data indicates that these substitutions within the chain region may not have been important for block, which as it acts mainly as a linker region would be desired.

Antagonism by the dimebon derived compounds was found to be voltage-dependent, indicating open channel block of the NMDA receptor. When the alkyl chain length, the methoxy and the alinine substitutions were introduced in the linker region it did not alter voltage-dependence. Woodhull analysis suggests that block by these molecules was more extracellular than the N-site asparagine and the same comments can be made regarding the superficial memantine site that were discussed for the carbacrine series. Compound **5** was shown to have a δ value that was larger than the other compounds. The Woodhull results may indicate that the aniline substitution within the chain allowed block to occur deeper within the pore, or that the addition of the nitrogen atom within the chain caused more electrostatic interactions with other aromatic side chains within the pore.

Compared to memantine dimebon was shown to be a weak blocker of NMDA receptor currents with an IC_{50} around 13 μM. Furthermore, the IC_{50} showed a non-linear voltage-dependence on a log-scale, which meant Woodhull analysis could not be carried out. It was shown that only when the voltage was increased to -50 mV could an increase in IC_{50} be measured.

The compound has numerous targets in the nervous system; therefore a working hypothesis explaining why it could be beneficial in AD is difficult to produce. The current study has shown that this is probably unrelated to any memantine like effects, as the potency is too low to be considered a good therapeutic through similar mechanisms. The potency at NMDA receptors is what has previously described; however, NMDA activity is just one of the many targets of the compound and the current study has confirmed that most of its probable CNS targets (adrenergic, dopamine, histamine, imidazoline and 5-HT) have a much higher affinity to dimebon (Wu et al., 2008). Only L-type Ca^{2+} channels and CYP450 and 2C19 were in the same range. But it must be considered that taken as a whole low level activity at NMDA receptors is not undesirable from a drug-design perspective. Therefore blockers with low potency described in this chapter may still have potential as therapeutics, as the NMDA receptor is but one of their targets.

4.7.4 Lipocrine

Lipocrine took the 6-chloro tacrine AChEI moiety and combined it with the anti-oxidant lipoic acid within a chain containing an amide group. It was the most potent MTDL tested, as it had an IC_{50} that was significantly lower than memantine at all voltages tested. Woodhull analysis found that the compound blocked at 0.6 through the membrane which would suggest binding to the N-site of the NMDA receptor (Zhu and Auerbach, 2001). The binding site could be confirmed by a mutation at the N-site. Comparing it to carbacrine(3), it may be that the smaller lipoic acid group or the amide in the chain allowed the tacrine moiety to bind within the pore deeper, increasing potency. Furthermore, it is not thought that lipocrine is fully-trapping as responses were obtained after wash-out (data not shown). If it can be shown to have a fast off-rate then the compound may have future use as a therapeutic.

Lipocrine has also been shown to act as an AChEI and was shown to be 10-fold more potent at doing so than the carbacrine compounds (Rosini et al., 2005). It also has around a 10-fold higher IC_{50} at BChE meaning the compound may have a more favourable side effect profile. Both cholinesterase effects were shown to be more potent than tacrine, possibly indicating binding to both sites due to its increased size within the MTDL backbone. The same study also showed it was a potent inhibitor of AChE induced Aβ aggregation, even though lipoic acid and tacrine do not posses this ability. Furthermore, as would be expected from its lipoic acid moiety it can block oxidative damage in SH-SY5Y cells, and may have a beneficial role in AD (Rosini et al., 2005).

Compound **6** took the opposite approach to lipocrine, taking the carvedilol carbazole pharmacophore and adding to lipoic acid. The potency was severely impaired as it was shown to be a weak inhibitor of NMDA receptor current. It would therefore be mainly the tacrine moiety that allows the MTDL compounds to be potent NMDA receptor blockers, providing further evidence that it is this region that is involved in block by carbacrine(3). It may be that future MTDL combinations should use tacrine to retain the effect.

Lipocrine and **6** contain anti-oxidant pharmacophores in order to target the proposed role that free radicals have in AD covered in the introduction. However, although diseases that seem to demand treatment with anti-oxidants remain plausible, they have proved disappointing in practice. In most cases systematic reviews have either found that there are no effects (e.g. gastrointestinal cancer (Bjelakovic et al., 2008b), pre-eclampsia (Rumbold et al., 2008) and aging (Bjelakovic et al., 2008a)) or that studies have been so poorly executed that no meaningful conclusion can be made. It is to the latter category

which lipoic acid (Klugman et al., 2004) and vitamin E (Isaac et al., 2008) belong for dementia and AD. Until a rigorous study is carried out, no meaningful conclusion can be made regarding antioxidant activity in AD. Although the argument for the involvement of biometals and the production of ROS seems to lend plausibility, by the measure of previous disappointments it may be unlikely antioxidants have any real effect.

4.7.5 Memantine-like Properties

Memantine is the only currently approved drug for AD whose receptor target is the NMDA receptor. Its tolerability is due to a fast unblocking rates and its partial-trapping mechanism that means it does not have the same side effects that are found with high-affinity, fully-trapping blockers such as MK-801 (Chen and Lipton, 2006). Memantine was originally determined to have fast kinetics meaning that it did not accumulate in the channel like MK-801 (Chen et al., 1992). On and off-rates could be calculated for the MTDL compounds in order to determine if these properties were retained by lipocrine and carbacrine(3). Another important property of memantine was that there was increasing inhibition with increasing concentrations of agonist (Chen et al., 1992). Such a property was desirable as it meant that in excitotoxic conditions the potency of memantine was increased which would leave normal transmission less affected. Such an experiment could be carried out using the MTDL compounds by determining the level of inhibition with increasing concentrations of NMDA. Another property of memantine is that it is more potent at GluN2A containing receptors than those containing GluN2D and the MTDL compounds could be tested to see if it is retained (Wrighton et al., 2007). Although this effect has not been directly implicated in AD it may represent a further mechanism that means memantine has a favourable side effect profile.

4.7.6 Neuroprotection

In order to determine that there is not just block of recombinant NMDA receptors but that it led to neuroprotection, an excitotoxicity assay could be carried out. Neuronal cultures would be exposed to excitotoxic doses of L-glutamate, and the ability of these compounds to block cell death is measured using the trypan blue exclusion method. Memantine has been shown to block excitotoxicity in primary cultures of rat hippocampal neurones and would be desirable in the MTDL compounds (Krieglstein et al., 1996).

However, clinical trials for NMDA receptor antagonists for use in stroke have failed, and the evidence for 'slow excitotoxicity' in AD remains poor (Ikonomidou and Turski, 2002). There are many possible reasons why memantine failed in stroke trials, one of which may be that downstream signalling proteins may in fact up-regulate the survival genes such as brain derived neurotrophic factor (BDNF), vasoactive intestinal peptide (VIP), bcl-2 and mcl-1 (Ikonomidou and Turski, 2002). In rat models of stroke there is a 10 to 100-fold rapid increase in extracellular glutamate levels, but it only lasts 30 mins after insult (Benveniste et al., 1984). In humans, there seems to be a small but sustained increase in glutamate levels that lasts days. It may be that immediately following injury NMDA receptors are involved in apoptosis, but that in the long-term increased activation of these channels may actually form part of a survival mechanism. Therefore, application of NMDA antagonists such as memantine could be beneficial if applied before, and for a short time after stroke, which for an essentially random event is impossible. In relation to AD, BDNF is decreased in the hippocampus and parietal cortex of those with AD and $A\beta_{1-42}$ down regulates bcl-2 in neuronal primary cultures (Phillips et al., 1991, Paradis et al., 1996, Holsinger et al., 2000). Therefore, as AD is a

progressive disease unrelated to an unpredictable event, blocking NMDA receptors may still have undesirable effects on neuronal survival.

4.7.7 Modelling Alzheimer's Disease

In vitro models of AD are used in the drug development process but these have been shown to have major limitations (see Bryan, 2009). It is possible to mimic Aβ expression without neuronal loss or impairment in some behavioural tasks. These transgenic animals produce Aβ activity but may not be correctly modelling the disease. By this measure, it would appear that these animals are only acting as an expression system that also has the ability to measure behaviour. Transgenic invertebrates that produce Aβ can now be produced and these also allow for pharmacological intervention in order to measure changes in behaviour and may be just as relevant to human disease as models using small mammals (see Link, 2005).

Suitable human biomarkers for AD may be a better way to test new drugs rather than continuing to use flawed animal models. In humans treated with donepezil the cerebrospinal fluid showed an increase in the G_4 from of AChE compared with controls (Amici et al., 2001). It has been shown that low levels of $A\beta_{1\text{-}42}$ and high levels of tau in the cerebrospinal fluid (CSF) could predict post-mortem severity of AD (Tapiola et al., 2009). The future of biomarkers will probably take into consideration the protein products from the newly associated genes in humans in CSF or blood of AD patients (Harold et al., 2009). If a group of biomarkers can be found then it is likely that combinations of these may accurately predict AD. The activity of these proteins could be a signature that could be measured in clinical trials directly in humans to determine drug efficacy. Moving into human subjects must be the next step for AD research due to the poor validity of animal models.

The pharmaceutical industry is close to producing viable biologics (e.g. bapineuzumab) that are human antibodies that can remove amyloid *in vivo* (Black et al., 2010). But another study that immunised patients against Aβ formation to stop its free production found that patients had no plaques in the nervous post-mortem, but no improvement in the actual dementia was observed (Gilman et al., 2005). The fact that Aβ can be removed without improving cognition has led researchers to believe that the disease causing process is not fully understood. By having a poorly understood mechanism it may mean that any biomarkers may not accurately represent the disease process, or be able to measure the efficacy of any drugs developed to treat it. There is a fear that Aβ may not have anything to do with the disease, and if a drug was approved on the basis of a biomarker related to a mechanism that is not fully understood, then it would take years to become apparent due to the timescales involved. Furthermore, another disincentive to the pharmaceutical industry is the patent protection may be lost if compounds efficacy was determined at endpoint due to the timescales involved.

5

General Discussion

The current study has shown that the presence of GluN3A and GluN3B subunits of the NMDA receptor in a receptor assembly that originally contained GluN1-1a and GluN2A generally caused a significant increase in the IC_{50} for open channel blockers tested. The N-site and N+1 site asparagines are known to play a role in the binding of these compounds, but the N mutations of GluN3A did not completely restore block. It may be that that the constricted threonine ring of the GluN1/3 dimer becomes a more superficial binding site with lower affinity, or it may be restricting flux which has also been shown to affect affinity (Wada et al., 2006, Yang et al., 2009). When the N-site was restored partial recovery was found, but the ring was unaltered so flux may not have been restored. It may also be that the deep binding site and the threonine ring led to a situation where block was mediated by the mixed properties of both sites if the relative affinities were not far apart, leading to partial recovery (Chen and Lipton, 2005). Or it could be that the double N mutant at N and N+1 was required to fully restore block. The study has also shown that the increased IC_{50} found with PhTX-343 may be due to an inability to bind at a deep site at position +5 in the pore when GluN3A and GluN3B were present. It has also been claimed that the differences found with MK-801 and methoctramine may be due to the aromatic groups interacting with the pore region in different ways, blocking entry to the N-site.

The functional role of the GluN3 subunits *in vivo* is currently unclear. GluN3A expression peaks during the right period to suggest that it is related to synapse maturation in rat, but it is unknown if it acts as a brake by increasing threshold for activity, protects against excitotoxicity or as a tag for synapse removal (see Henson et al., 2010). The brake

theory is supported by the reduction in Ca^{2+} permeability found, but the reduced block by Mg^{2+} found in the current study tends to suggest that there would be more NMDA receptor mediated current at lower voltages. However, increasing the Mg^{2+} IC_{50} may encourage increased LTP and mature synapse development at a lower threshold, which may be required during development. It also may be that GluN3 acts as a tag for receptor removal from the membrane. Strong synaptic activity could drive GluN3 containing receptors out of the synapse, and the weak synapses would retain GluN3 and would be 'tagged' for removal. These could then be removed by the PACSIN1/syndapin1 complex which has been shown to interact with the C-terminus of GluN3A and occurs at extrasynaptic regions (Perez-Otano et al., 2006).

The current study has shown that there is a further significant increase in Mg^{2+} IC_{50} with GluN3B, but no difference in current through the channel. GluN3B is expressed throughout development in adult rat and humans (Bendel et al., 2005). During development, GluN2B and GluN2D are predominantly expressed; while in adulthood there is GluN2A and GluN2C (see Henson et al., 2010). GluN3B may play the same role as GluN3A in adulthood, but due to the presence of mature NMDA receptor subunits, to have the same function it may require an increased loss of Mg^{2+} affinity, where only a lower level was required in the developing brain. It is currently unknown if GluN3B interacts with PACSIN1/syndapin1 in the same way so these receptors may not undergo endocytosis, and any postulated role for the subunit in adults is further complicated by its common null allele in humans (Niemann et al., 2007).

Determining the pharmacology of GluN3 containing receptors is also not helped by conflicting *in vitro* studies, with some advocating glycine gated NMDA receptors and some advocating triheteromeric receptors (Madry et al., 2006, Tong et al., 2007). Until the

debate is solved it makes determining their physiological relevance difficult. The current study has shown that glycine did not open the channels alone, which is what would be expected if there was a glycine activated component (Ulbrich and Isacoff, 2008). By carrying out some of the experiments outlined in the discussion section, it is likely to be shown that these channels are being produced in oocytes with an endogenous *Xen*GluN2B subunit, leading altered gating properties. If so, then it is unlikely these glycine gated channels have any relevance.

The NMDA receptor is a fundamental ionotropic receptor of the nervous system and it is unsurprising that is has been linked to AD (see Chen and Lipton, 2006). The current study has shown that carbacrine(3) and lipocrine are potentially useful compounds that, not only have similar or better potency than memantine, have the ability to treat other aspects of the disease due to their MTDL composition. However, drugs cannot be designed without toxicity being considered thought the planning stage. One of the main reasons for candidates being refused a licence or being withdrawn is the prolongation of the QT interval, which can provoke torsade de pointes leading to fatal ventricular arrhythmias (van Noord et al., 2010). It is caused by block of the inwardly rectifying K^+ channel encoded by the human Ether-à-go-go Related Gene (hERG) in cardiomyocytes. If there is prolonged repolarisation, there can be early after depolarisations caused by the blocking of the rapid component responsible for repolarisation. The channel is very promiscuous in relation to binding small compounds, meaning that the production of new chemical entities has to include hERG activity profiling at the outset. Excessive hERG activity has stopped selective GluN2B blockers from being used clinically (Kew and Kemp, 2005). The IC_{50} for hERG channel activity should at an absolute minimum be 30-fold greater than the maximum plasma concentration of the drug (C_{max}), but the safety

margin would also have to consider the possible benefits given to the severity of the disease (Redfern et al., 2003).

Therefore, when designing drugs for use in humans it would be useful to screen for hERG activity early on in the drug design process. If a compound could be shown to have a very high IC_{50} at these channels then it would immediately give the compound hope of being developed further, regardless of large swathes of data on efficacy. It may be that the hugely reductionist approach to drug design is being tripped up by cardiac arrhythmias and regulation; therefore, it may be better to look at what drugs are *safe* and then determine if they are suitable for treating a disease. The effects of small compounds on hERG and other voltage gated channels is fast becoming a very important area of research in drug development as the brakes can be applied at a very early stage when the results from cheap *in-vitro* studies are known.

6

Appendix

A

Compound	Memantine	PhTX-343	Methoctramine	MK-801	PhTX-12
Mg^{2+}	**P<0.001**	**P<0.001**	P=0.323	**P<0.001**	**P<0.001**
Memantine		**P<0.001**	**P=0.010**	**P<0.001**	**P<0.001**
PhTX-343			**P<0.001**	P=0.133	**P<0.001**
Methoctramine				**P<0.001**	**P<0.001**
MK-801					**P<0.001**

B

Compound	Memantine	PhTX-343	Methoctramine	MK-801	PhTX-12
Mg^{2+}	**P<0.001**	P=0.243	**P=0.005**	**P<0.001**	**P<0.001**
Memantine		P=0.589	P=0.370	**P<0.001**	**P<0.001**
PhTX-343			P=0.270	**P<0.001**	**P<0.001**
Methoctramine				**P<0.001**	**P<0.001**
MK-801					**P<0.001**

C

Compound	Memantine	PhTX-343	Methoctramine	MK-801	PhTX-12
Mg^{2+}	**P<0.001**	P=0.817	**P<0.001**	**P<0.001**	**P<0.001**
Memantine		**P<0.001**	P=0.122	**P<0.001**	**P<0.001**
PhTX-343			**P<0.001**	**P<0.001**	**P<0.001**
Methoctramine				**P<0.001**	**P<0.001**
MK-801					**P<0.001**

Table 24: Comparison of fits for block of NMDA/glycine-evoked currents mediated by 1-1a/2A NMDA receptors. (A) -100 mV, (B) -75 mV and (C) -50 mV.

A

Compound	Memantine	PhTX-343	Methoctramine	MK-801	PhTX-12
Mg^{2+}	**P=0.003**	**P<0.001**	**P<0.001**	**P<0.001**	**P<0.001**
Memantine		P=0.783	P=0.677	**P<0.001**	**P<0.001**
PhTX-343			**P=0.023**	**P=0.0001**	**P<0.001**
Methoctramine				**P<0.0001**	**P<0.001**
MK-801					**P<0.001**

B

Compound	Memantine	PhTX-343	Methoctramine	MK-801	PhTX-12
Mg^{2+}	**P<0.001**	**P<0.001**	**P<0.001**	**P<0.001**	**P<0.001**
Memantine		**P=0.047**	**P<0.001**	**P<0.001**	**P<0.001**
PhTX-343			**P=0.037**	**P<0.001**	**P<0.001**
Methoctramine				**P<0.001**	**P<0.001**
MK-801					**P<0.001**

C

Compound	Memantine	PhTX-343	Methoctramine	MK-801	PhTX-12
Mg^{2+}	P=0.120	P=0.503	**P<0.001**	**P<0.001**	**P<0.001**
Memantine		P=0.815	**P<0.001**	**P<0.001**	**P<0.001**
PhTX-343			**P=0.002**	**P<0.001**	**P<0.001**
Methoctramine				**P<0.001**	**P<0.001**
MK-801					**P<0.001**

Table 25: Comparison of fits for block of NMDA/glycine-evoked currents mediated by 3A NMDA receptors. (A) -100 mV, (B) -75 mV and (C) -50 mV.

A

Compound	Memantine	PhTX-343	Methoctramine	MK-801	PhTX-12
Mg^{2+}	P=0.754	**P<0.001**	**P<0.001**	**P<0.001**	**P=0.001**
Memantine		**P<0.001**	**P<0.001**	**P<0.001**	**P=0.025**
PhTX-343			**P<0.001**	P=0.422	**P<0.001**
Methoctramine				**P<0.001**	**P<0.001**
MK-801					**P<0.001**

B

Compound	Memantine	PhTX-343	Methoctramine	MK-801	PhTX-12
Mg^{2+}	**P=0.002**	**P<0.001**	**P<0.001**	**P<0.001**	**P<0.001**
Memantine		**P<0.001**	**P<0.001**	**P<0.001**	**P<0.001**
PhTX-343			P=0.492	**P=0.031**	**P<0.001**
Methoctramine				P=0.056	**P<0.001**
MK-801					**P<0.001**

C

Compound	Memantine	PhTX-343	Methoctramine	MK-801	PhTX-12
Mg^{2+}	**P<0.001**	P=0.614	**P<0.001**	**P<0.001**	**P=0.002**
Memantine		**P=0.001**	**P<0.001**	**P<0.001**	**P<0.001**
PhTX-343			**P<0.001**	**P<0.001**	**P=0.006**
Methoctramine				P=0.294	**P<0.001**
MK-801					**P<0.001**

Table 26: Comparison of fits for block of NMDA/glycine-evoked currents mediated by 1-3B NMDA receptors. (A) -100 mV, (B) -75 mV and (C) -50 mV.

A

Compound	Memantine	PhTX-343	Methoctramine	MK-801
Mg^{2+}	**P<0.001**	**P<0.001**	**P=0.010**	**P<0.001**
Memantine		**P<0.001**	**P=0.042**	**P<0.001**
PhTX-343			**P<0.001**	**P<0.001**
Methoctramine				**P<0.001**

B

Compound	Memantine	PhTX-343	Methoctramine	MK-801
Mg^{2+}	P=0.051	P=0.170	**P<0.001**	**P<0.001**
Memantine		P=0.992	**P<0.001**	**P<0.001**
PhTX-343			**P<0.001**	**P<0.001**
Methoctramine				**P<0.001**

C

Compound	Memantine	PhTX-343	Methoctramine	MK-801
Mg^{2+}	**P<0.001**	**P<0.001**	**P<0.001**	**P<0.001**
Memantine		**P<0.001**	**P<0.001**	**P<0.001**
PhTX-343			**P<0.001**	**P<0.001**
Methoctramine				**P<0.001**

Table 27: Comparison of fits for block of NMDA/glycine-evoked currents mediated by 1-3A^{G703N} NMDA receptors. (A) -100 mV, (B) -75 mV and (C) -50 mV.

A

Compound	Memantine	PhTX-343	Methoctramine	MK-801
Mg^{2+}	**P=0.010**	**P<0.001**	P=0.201	**P<0.001**
Memantine		**P=0.002**	P=0.156	**P<0.001**
PhTX-343			**P<0.001**	**P<0.001**
Methoctramine				**P<0.001**

B

Compound	Memantine	PhTX-343	Methoctramine	MK-801
Mg^{2+}	**P=0.022**	**P=0.045**	P=0.084	**P<0.001**
Memantine		P=0.548	P=0.508	**P<0.001**
PhTX-343			P=0.873	**P<0.001**
Methoctramine				**P<0.001**

C

Compound	Memantine	PhTX-343	Methoctramine	MK-801
Mg^{2+}	**P<0.001**	P=0.781	**P<0.001**	**P<0.001**
Memantine		**P<0.001**	P=0.530	**P<0.001**
PhTX-343			**P<0.001**	**P<0.001**
Methoctramine				**P<0.001**

Table 28: Comparison of fits for block of NMDA/glycine-evoked currents mediated by $3A^{R704N}$ NMDA receptors. (A) -100 mV, (B) -75 mV and (C) -50 mV.

A

Compound	Memantine	PhTX-343
Mg^{2+}	**P<0.001**	**P<0.001**
Memantine		**P<0.001**

B

Compound	Memantine	PhTX-343
Mg^{2+}	**P<0.001**	**P<0.001**
Memantine		P=0.197

C

Compound	Memantine	PhTX-343
Mg^{2+}	**P<0.001**	**P<0.001**
Memantine		**P<0.001**

Figure 96: Comparison of fits for block of NMDA/glycine-evoked currents mediated by $3A^{R704D}$ NMDA receptors. (A) -100 mV, (B) -75 mV and (C) -50 mV.

Compound	1c	1b	1e	Memantine
1a	P=0.882	P=0.076	P=0.433	**P<0.001**
1c		P=0.004	P=0.123	**P<0.001**
1b			P=0.027	**P<0.001**
1e				**P<0.001**

Table 29: Comparison of fits for compound 1 block of NMDA/glycine-evoked currents mediated by 1-1a/2A NMDA receptors at -100 mV

A

Compound	Carbacrine(6)	Carbacrine(4)	Carbacrine(5)	Memantine
Carbacrine(3)	**P<0.001**	**P<0.001**	**P<0.001**	P=0.773
Carbacrine(6)		**P=0.043**	P=0.549	**P<0.001**
Carbacrine(4)			P=0.255	**P<0.001**
Carbacrine(5)				**P<0.001**

B

Compound	Carbacrine(6)	Carbacrine(4)	Carbacrine(5)	Memantine
Carbacrine(3)	**P<0.001**	**P<0.001**	**P<0.001**	P=0.737
Carbacrine(6)		P=0.301	**P=0.015**	**P<0.001**
Carbacrine(4)			**P=0.003**	**P<0.001**
Carbacrine(5)				**P<0.001**

C

Compound	Carbacrine(6)	Carbacrine(4)	Carbacrine(5)	Memantine
Carbacrine(3)	**P<0.001**	**P<0.001**	**P<0.001**	P=0.485
Carbacrine(6)		P=0.346	P=0.871	**P<0.001**
Carbacrine(4)			P=0.293	**P<0.001**
Carbacrine(5)				**P<0.001**

Figure 97: Comparison of fits for carbacrine block of NMDA/glycine-evoked currents mediated by 1-1a/2A NMDA receptors. (A) at -100 mV, (B), -80 mV and (C) -50 mV.

A

Compound	3b	3c	4	5	Memantine	Dimebon
3a	P=0.526	P=0.189	**P<0.001**	P=0.275	**P<0.001**	P=0.772
3b		P=0.479	**P<0.001**	P=0.484	**P<0.001**	P=0.436
3c			**P=0.001**	P=0.737	**P<0.001**	P=0.200
4				P=0.088	**P<0.001**	**P<0.001**
5					**P<0.001**	P=0.298
Memantine						**P<0.001**

B

Compound	3b	3c	4	5	Memantine	Dimebon
3a	**P=0.017**	**P=0.003**	**P<0.001**	**P=0.035**	**P<0.001**	P=0.023
3b		P=0.290	**P<0.001**	P=0.549	**P<0.001**	P=0.232
3c			**P=0.002**	P=0.915	**P<0.001**	P=0.552
4				**P=0.033**	**P<0.001**	P=0.258
5					**P<0.001**	P=0.595
Memantine						**P<0.001**

C

Compound	3b	3c	4	5	Memantine	Dimebon
3a	**P=0.004**	**P=0.037**	**P<0.001**	P=0.245	**P<0.001**	**P<0.001**
3b		P=0.147	**P=0.003**	P=0.238	**P<0.001**	**P<0.001**
3c			**P<0.001**	P=0.793	**P<0.001**	**P<0.001**
4				**P=0.001**	**P<0.001**	**P<0.001**
5					**P<0.001**	**P<0.001**
Memantine						**P<0.001**

Figure 98: Comparison of fits for dimebon derived series. (A) at -100 mV, (B), -80 mV and (C) -50 mV.

7

References

AL-HALLAQ, R. A., JARABEK, B. R., FU, Z., VICINI, S., WOLFE, B. B. & YASUDA, R. P. 2002. Association of NR3A with the N-methyl-D-aspartate receptor NR1 and NR2 subunits. *Mol Pharmacol,* 62, 1119-27.

ALBERDI, E., SANCHEZ-GOMEZ, M. V., CAVALIERE, F., PEREZ-SAMARTIN, A., ZUGAZA, J. L., TRULLAS, R., DOMERCQ, M. & MATUTE, C. 2010. Amyloid beta oligomers induce Ca2+ dysregulation and neuronal death through activation of ionotropic glutamate receptors. *Cell Calcium,* 47, 264-72.

AMICI, S., LANARI, A., ROMANI, R., ANTOGNELLI, C., GALLAI, V. & PARNETTI, L. 2001. Cerebrospinal fluid acetylcholinesterase activity after long-term treatment with donepezil and rivastigmina. *Mech Ageing Dev,* 122, 2057-62.

ANDERSEN, T. F., TIKHONOV, D. B., BOLCHO, U., BOLSHAKOV, K., NELSON, J. K., PLUTEANU, F., MELLOR, I. R., EGEBJERG, J. & STROMGAARD, K. 2006. Uncompetitive antagonism of AMPA receptors: Mechanistic insights from studies of polyamine toxin derivatives. *J Med Chem,* 49, 5414-23.

ANDERSSON, O., STENQVIST, A., ATTERSAND, A. & VON EULER, G. 2001. Nucleotide sequence, genomic organization, and chromosomal localization of genes encoding the human NMDA receptor subunits NR3A and NR3B. *Genomics,* 78, 178-84.

ANTONOV, S. M., GMIRO, V. E. & JOHNSON, J. W. 1998. Binding sites for permeant ions in the channel of NMDA receptors and their effects on channel block. *Nat Neurosci,* 1, 451-61.

AOKI, C., LEE, J., NEDELESCU, H., AHMED, T., HO, A. & SHEN, J. 2009. Increased levels of NMDA receptor NR2A subunits at pre- and postsynaptic sites of the hippocampal CA1: an early response to conditional double knockout of presenilin 1 and 2. *J Comp Neurol,* 517, 512-23.

ARANEDA, R. C., LAN, J. Y., ZHENG, X., ZUKIN, R. S. & BENNETT, M. V. 1999. Spermine and arcaine block and permeate N-methyl-D-aspartate receptor channels. *Biophys J,* 76, 2899-911.

AWOBULUYI, M., YANG, J., YE, Y., CHATTERTON, J. E., GODZIK, A., LIPTON, S. A. & ZHANG, D. 2007. Subunit-specific roles of glycine-binding domains in activation of NR1/NR3 N-methyl-D-aspartate receptors. *Mol Pharmacol,* 71, 112-22.

BACHURIN, S. O., SHEVTSOVA, E. P., KIREEVA, E. G., OXENKRUG, G. F. & SABLIN, S. O. 2003. Mitochondria as a target for neurotoxins and neuroprotective agents. *Ann N Y Acad Sci,* 993, 334-44; discussion 345-9.

BALI, M. & AKABAS, M. H. 2007. The location of a closed channel gate in the GABAA receptor channel. *J Gen Physiol,* 129, 145-59.

BANKE, T. G., DRAVID, S. M. & TRAYNELIS, S. F. 2005. Protons trap NR1/NR2B NMDA receptors in a nonconducting state. *J Neurosci,* 25, 42-51.

BAR-AM, O., WEINREB, O., AMIT, T. & YOUDIM, M. B. 2009. The novel cholinesterase-monoamine oxidase inhibitor and antioxidant, ladostigil, confers neuroprotection in neuroblastoma cells and aged rats. *J Mol Neurosci,* 37, 135-45.

BARTOLINI, M., BERTUCCI, C., CAVRINI, V. & ANDRISANO, V. 2003. beta-Amyloid aggregation induced by human acetylcholinesterase: inhibition studies. *Biochem Pharmacol,* 65, 407-16.

BENDEL, O., MEIJER, B., HURD, Y. & VON EULER, G. 2005. Cloning and expression of the human NMDA receptor subunit NR3B in the adult human hippocampus. *Neurosci Lett,* 377, 31-6.

BENVENISTE, H., DREJER, J., SCHOUSBOE, A. & DIEMER, N. H. 1984. Elevation of the extracellular concentrations of glutamate and aspartate in rat hippocampus during transient cerebral ischemia monitored by intracerebral microdialysis. *J Neurochem,* 43, 1369-74.

BENVENISTE, M. & MAYER, M. L. 1993. Multiple effects of spermine on N-methyl-D-aspartic acid receptor responses of rat cultured hippocampal neurones. *J Physiol,* 464, 131-63.

BENVENISTE, M. & MAYER, M. L. 1995. Trapping of glutamate and glycine during open channel block of rat hippocampal neuron NMDA receptors by 9-aminoacridine. *J Physiol,* 483 (Pt 2), 367-84.

BI, X., GALL, C. M., ZHOU, J. & LYNCH, G. 2002. Uptake and pathogenic effects of amyloid beta peptide 1-42 are enhanced by integrin antagonists and blocked by NMDA receptor antagonists. *Neuroscience,* 112, 827-40.

BIEWENGA, G. P., HAENEN, G. R. & BAST, A. 1997. The pharmacology of the antioxidant lipoic acid. *Gen Pharmacol,* 29, 315-31.

BIXEL, M. G., KRAUSS, M., LIU, Y., BOLOGNESI, M. L., ROSINI, M., MELLOR, I. S., USHERWOOD, P. N., MELCHIORRE, C., NAKANISHI, K. & HUCHO, F. 2000. Structure-activity relationship and site of binding of polyamine derivatives at the nicotinic acetylcholine receptor. *Eur J Biochem,* 267, 110-20.

BJELAKOVIC, G., NIKOLOVA, D., GLUUD, L. L., SIMONETTI, R. G. & GLUUD, C. 2008a. Antioxidant supplements for prevention of mortality in healthy participants and patients with various diseases. *Cochrane Database Syst Rev,* CD007176.

BJELAKOVIC, G., NIKOLOVA, D., SIMONETTI, R. G. & GLUUD, C. 2008b. Systematic review: primary and secondary prevention of gastrointestinal cancers with antioxidant supplements. *Aliment Pharmacol Ther,* 28, 689-703.

BLACK, R. S., SPERLING, R. A., SAFIRSTEIN, B., MOTTER, R. N., PALLAY, A., NICHOLS, A. & GRUNDMAN, M. 2010. A single ascending dose study of bapineuzumab in patients with Alzheimer disease. *Alzheimer Dis Assoc Disord,* 24, 198-203.

BLANPIED, T. A., BOECKMAN, F. A., AIZENMAN, E. & JOHNSON, J. W. 1997. Trapping channel block of NMDA-activated responses by amantadine and memantine. *J Neurophysiol,* 77, 309-23.

BOLOGNESI, M. L., CAVALLI, A. & MELCHIORRE, C. 2009a. Memoquin: a multi-target-directed ligand as an innovative therapeutic opportunity for Alzheimer's disease. *Neurotherapeutics,* 6, 152-62.

BOLOGNESI, M. L., MATERA, R., MINARINI, A., ROSINI, M. & MELCHIORRE, C. 2009b. Alzheimer's disease: new approaches to drug discovery. *Curr Opin Chem Biol,* 13, 303-8.

BOLSHAKOV, K. V., KIM, K. H., POTAPJEVA, N. N., GMIRO, V. E., TIKHONOV, D. B., USHERWOOD, P. N., MELLOR, I. R. & MAGAZANIK, L. G. 2005. Design of antagonists for NMDA and AMPA receptors. *Neuropharmacology,* 49, 144-55.

BOLSHAKOV, K. V., TIKHONOV, D. B., GMIRO, V. E. & MAGAZANIK, L. G. 2000. Different arrangement of hydrophobic and nucleophilic components of channel binding sites in N-methyl-D-aspartate and AMPA receptors of rat brain is revealed by channel blockade. *Neurosci Lett,* 291, 101-4.

BOULTER, J., HOLLMANN, M., O'SHEA-GREENFIELD, A., HARTLEY, M., DENERIS, E., MARON, C. & HEINEMANN, S. 1990. Molecular cloning and functional expression of glutamate receptor subunit genes. *Science,* 249, 1033-7.

BOURNE, Y., TAYLOR, P., BOUGIS, P. E. & MARCHOT, P. 1999. Crystal structure of mouse acetylcholinesterase. A peripheral site-occluding loop in a tetrameric assembly. *J Biol Chem,* 274, 2963-70.

BOWEN, D. M., SMITH, C. B., WHITE, P. & DAVISON, A. N. 1976. Neurotransmitter-related enzymes and indices of hypoxia in senile dementia and other abiotrophies. *Brain,* 99, 459-96.

BOWIE, D. & MAYER, M. L. 1995. Inward rectification of both AMPA and kainate subtype glutamate receptors generated by polyamine-mediated ion channel block. *Neuron,* 15, 453-62.

BRAMBLETT, G. T., GOEDERT, M., JAKES, R., MERRICK, S. E., TROJANOWSKI, J. Q. & LEE, V. M. 1993. Abnormal tau phosphorylation at Ser396 in Alzheimer's disease recapitulates development and contributes to reduced microtubule binding. *Neuron,* 10, 1089-99.

BRIER, T. J., MELLOR, I. R., TIKHONOV, D. B., NEAGOE, I., SHAO, Z., BRIERLEY, M. J., STROMGAARD, K., JAROSZEWSKI, J. W., KROGSGAARD-LARSEN, P. & USHERWOOD, P. N. 2003. Contrasting actions of philanthotoxin-343 and philanthotoxin-(12) on human muscle nicotinic acetylcholine receptors. *Mol Pharmacol,* 64, 954-64.

BRYAN, K. J., LEE, H., PERRY G., SMITH, M.A., CASADESUS, G. 2009. Transgenic Mouse Models of Alzheimer's Disease: Behavioral Testing and Considerations. *In:* BUCCAFUSCO, J. J. (ed.) *Methods of Behavior Analysis in Neuroscience*

CAI, S. X., KHER, S. M., ZHOU, Z. L., ILYIN, V., ESPITIA, S. A., TRAN, M., HAWKINSON, J. E., WOODWARD, R. M., WEBER, E. & KEANA, J. F. 1997. Structure-activity relationships of alkyl- and alkoxy-substituted 1,4-dihydroquinoxaline-2,3-diones: potent and systemically active antagonists for the glycine site of the NMDA receptor. *J Med Chem,* 40, 730-8.

CAMPS, P., FORMOSA, X., GALDEANO, C., GOMEZ, T., MUNOZ-TORRERO, D., SCARPELLINI, M., VIAYNA, E., BADIA, A., CLOS, M. V., CAMINS, A., PALLAS, M., BARTOLINI, M., MANCINI, F., ANDRISANO, V., ESTELRICH, J., LIZONDO, M., BIDON-CHANAL, A. & LUQUE, F. J. 2008. Novel donepezil-based inhibitors of acetyl- and butyrylcholinesterase and acetylcholinesterase-induced beta-amyloid aggregation. *J Med Chem,* 51, 3588-98.

CARLIER, P. R., HAN, Y. F., CHOW, E. S., LI, C. P., WANG, H., LIEU, T. X., WONG, H. S. & PANG, Y. P. 1999. Evaluation of short-tether bis-THA AChE inhibitors. A further test of the dual binding site hypothesis. *Bioorg Med Chem,* 7, 351-7.

CAVARA, N. A., ORTH, A. & HOLLMANN, M. 2009. Effects of NR1 splicing on NR1/NR3B-type excitatory glycine receptors. *BMC Neurosci,* 10, 32.
CHANG, H. R. & KUO, C. C. 2008. The activation gate and gating mechanism of the NMDA receptor. *J Neurosci,* 28, 1546-56.
CHAO, J., SEILER, N., RENAULT, J., KASHIWAGI, K., MASUKO, T., IGARASHI, K. & WILLIAMS, K. 1997. N1-dansyl-spermine and N1-(n-octanesulfonyl)-spermine, novel glutamate receptor antagonists: block and permeation of N-methyl-D-aspartate receptors. *Mol Pharmacol,* 51, 861-71.
CHATTERTON, J. E., AWOBULUYI, M., PREMKUMAR, L. S., TAKAHASHI, H., TALANTOVA, M., SHIN, Y., CUI, J., TU, S., SEVARINO, K. A., NAKANISHI, N., TONG, G., LIPTON, S. A. & ZHANG, D. 2002. Excitatory glycine receptors containing the NR3 family of NMDA receptor subunits. *Nature,* 415, 793-8.
CHEN, B. S. & ROCHE, K. W. 2007. Regulation of NMDA receptors by phosphorylation. *Neuropharmacology,* 53, 362-8.
CHEN, H. S. & LIPTON, S. A. 1997. Mechanism of memantine block of NMDA-activated channels in rat retinal ganglion cells: uncompetitive antagonism. *J Physiol,* 499 (Pt 1), 27-46.
CHEN, H. S. & LIPTON, S. A. 2005. Pharmacological implications of two distinct mechanisms of interaction of memantine with N-methyl-D-aspartate-gated channels. *J Pharmacol Exp Ther,* 314, 961-71.
CHEN, H. S. & LIPTON, S. A. 2006. The chemical biology of clinically tolerated NMDA receptor antagonists. *J Neurochem,* 97, 1611-26.
CHEN, H. S., PELLEGRINI, J. W., AGGARWAL, S. K., LEI, S. Z., WARACH, S., JENSEN, F. E. & LIPTON, S. A. 1992. Open-channel block of N-methyl-D-aspartate (NMDA) responses by memantine: therapeutic advantage against NMDA receptor-mediated neurotoxicity. *J Neurosci,* 12, 4427-36.
CHEN, H. S., WANG, Y. F., RAYUDU, P. V., EDGECOMB, P., NEILL, J. C., SEGAL, M. M., LIPTON, S. A. & JENSEN, F. E. 1998. Neuroprotective concentrations of the N-methyl-D-aspartate open-channel blocker memantine are effective without cytoplasmic vacuolation following post-ischemic administration and do not block maze learning or long-term potentiation. *Neuroscience,* 86, 1121-32.
CHEN, P. E., GEBALLE, M. T., KATZ, E., ERREGER, K., LIVESEY, M. R., O'TOOLE, K. K., LE, P., LEE, C. J., SNYDER, J. P., TRAYNELIS, S. F. & WYLLIE, D. J. 2008. Modulation of glycine potency in rat recombinant NMDA receptors containing chimeric NR2A/2D subunits expressed in Xenopus laevis oocytes. *J Physiol,* 586, 227-45.
CHILDS, A. C., MEHTA, D. J. & GERNER, E. W. 2003. Polyamine-dependent gene expression. *Cell Mol Life Sci,* 60, 1394-406.
CIABARRA, A. M. & SEVARINO, K. A. 1997. An anti-chi-1 antibody recognizes a heavily glycosylated protein in rat brain. *Brain Res Mol Brain Res,* 46, 85-90.
CIABARRA, A. M., SULLIVAN, J. M., GAHN, L. G., PECHT, G., HEINEMANN, S. & SEVARINO, K. A. 1995. Cloning and characterization of chi-1: a developmentally regulated member of a novel class of the ionotropic glutamate receptor family. *J Neurosci,* 15, 6498-508.
COLLINGRIDGE, G. L., OLSEN, R. W., PETERS, J. & SPEDDING, M. 2009. A nomenclature for ligand-gated ion channels. *Neuropharmacology,* 56, 2-5.
CORDES, F. S., BRIGHT, J. N. & SANSOM, M. S. 2002. Proline-induced distortions of transmembrane helices. *J Mol Biol,* 323, 951-60.

COURT, J., MARTIN-RUIZ, C., PIGGOTT, M., SPURDEN, D., GRIFFITHS, M. & PERRY, E. 2001. Nicotinic receptor abnormalities in Alzheimer's disease. *Biol Psychiatry,* 49, 175-84.

COWBURN, R. F., WIEHAGER, B., TRIEF, E., LI-LI, M. & SUNDSTROM, E. 1997. Effects of beta-amyloid-(25-35) peptides on radioligand binding to excitatory amino acid receptors and voltage-dependent calcium channels: evidence for a selective affinity for the glutamate and glycine recognition sites of the NMDA receptor. *Neurochem Res,* 22, 1437-42.

COYLE, J. T., PRICE, D. L. & DELONG, M. R. 1983. Alzheimer's disease: a disorder of cortical cholinergic innervation. *Science,* 219, 1184-90.

CULL-CANDY, S., BRICKLEY, S. & FARRANT, M. 2001. NMDA receptor subunits: diversity, development and disease. *Curr Opin Neurobiol,* 11, 327-35.

CULL-CANDY, S., KELLY, L. & FARRANT, M. 2006. Regulation of Ca2+-permeable AMPA receptors: synaptic plasticity and beyond. *Curr Opin Neurobiol,* 16, 288-97.

CULL-CANDY, S. G. & LESZKIEWICZ, D. N. 2004. Role of distinct NMDA receptor subtypes at central synapses. *Sci STKE,* 2004, re16.

CURTIS, D. R., PHILLIS, J. W. & WATKINS, J. C. 1959. Chemical excitation of spinal neurones. *Nature,* 183, 611-2.

CZAJKOWSKI, C. & KARLIN, A. 1995. Structure of the nicotinic receptor acetylcholine-binding site. Identification of acidic residues in the delta subunit within 0.9 nm of the 5 alpha subunit-binding. *J Biol Chem,* 270, 3160-4.

DANBOLT, N. C. 2001. Glutamate uptake. *Prog Neurobiol,* 65, 1-105.

DANTOINE, T., AURIACOMBE, S., SARAZIN, M., BECKER, H., PERE, J. J. & BOURDEIX, I. 2006. Rivastigmine monotherapy and combination therapy with memantine in patients with moderately severe Alzheimer's disease who failed to benefit from previous cholinesterase inhibitor treatment. *Int J Clin Pract,* 60, 110-8.

DANYSZ, W. & PARSONS, C. G. 2003. The NMDA receptor antagonist memantine as a symptomatological and neuroprotective treatment for Alzheimer's disease: preclinical evidence. *Int J Geriatr Psychiatry,* 18, S23-32.

DAS, S., SASAKI, Y. F., ROTHE, T., PREMKUMAR, L. S., TAKASU, M., CRANDALL, J. E., DIKKES, P., CONNER, D. A., RAYUDU, P. V., CHEUNG, W., CHEN, H. S., LIPTON, S. A. & NAKANISHI, N. 1998. Increased NMDA current and spine density in mice lacking the NMDA receptor subunit NR3A. *Nature,* 393, 377-81.

DE CARVALHO, L. P., BOCHET, P. & ROSSIER, J. 1996. The endogenous agonist quinolinic acid and the non endogenous homoquinolinic acid discriminate between NMDAR2 receptor subunits. *Neurochem Int,* 28, 445-52.

DEL VALLE-PINERO, A. Y., SUCKOW, S. K., ZHOU, Q., PEREZ, F. M., VERNE, G. N. & CAUDLE, R. M. 2007. Expression of the N-methyl-D-aspartate receptor NR1 splice variants and NR2 subunit subtypes in the rat colon. *Neuroscience,* 147, 164-73.

DI MARIA, E., BONVICINI, C., BONOMINI, C., ALBERICI, A., ZANETTI, O. & GENNARELLI, M. 2009. Genetic Variation in the G720/G30 Gene Locus (DAOA) Influences the Occurrence of Psychotic Symptoms in Patients with Alzheimer's Disease. *J Alzheimers Dis,* 18, 953-60.

DINGLEDINE, R., BORGES, K., BOWIE, D. & TRAYNELIS, S. F. 1999. The glutamate receptor ion channels. *Pharmacol Rev,* 51, 7-61.

DOODY, R. S., GAVRILOVA, S. I., SANO, M., THOMAS, R. G., AISEN, P. S., BACHURIN, S. O., SEELY, L. & HUNG, D. 2008. Effect of dimebon on cognition, activities of daily living, behaviour, and global function in patients with mild-to-moderate Alzheimer's disease: a randomised, double-blind, placebo-controlled study. *Lancet,* 372, 207-15.

DRAVID, S. M., PRAKASH, A. & TRAYNELIS, S. F. 2008. Activation of recombinant NR1/NR2C NMDA receptors. *J Physiol,* 586, 4425-39.

ELDEFRAWI, A. T., ELDEFRAWI, M. E., KONNO, K., MANSOUR, N. A., NAKANISHI, K., OLTZ, E. & USHERWOOD, P. N. 1988. Structure and synthesis of a potent glutamate receptor antagonist in wasp venom. *Proc Natl Acad Sci U S A,* 85, 4910-3.

ERIKSSON, M., NILSSON, A., FROELICH-FABRE, S., AKESSON, E., DUNKER, J., SEIGER, A., FOLKESSON, R., BENEDIKZ, E. & SUNDSTROM, E. 2002. Cloning and expression of the human N-methyl-D-aspartate receptor subunit NR3A. *Neurosci Lett,* 321, 177-81.

ERREGER, K., DRAVID, S. M., BANKE, T. G., WYLLIE, D. J. & TRAYNELIS, S. F. 2005a. Subunit-specific gating controls rat NR1/NR2A and NR1/NR2B NMDA channel kinetics and synaptic signalling profiles. *J Physiol,* 563, 345-58.

ERREGER, K., GEBALLE, M. T., DRAVID, S. M., SNYDER, J. P., WYLLIE, D. J. & TRAYNELIS, S. F. 2005b. Mechanism of partial agonism at NMDA receptors for a conformationally restricted glutamate analog. *J Neurosci,* 25, 7858-66.

ERREGER, K., GEBALLE, M. T., KRISTENSEN, A., CHEN, P. E., HANSEN, K. B., LEE, C. J., YUAN, H., LE, P., LYUBOSLAVSKY, P. N., MICALE, N., JORGENSEN, L., CLAUSEN, R. P., WYLLIE, D. J., SNYDER, J. P. & TRAYNELIS, S. F. 2007. Subunit-specific agonist activity at NR2A-, NR2B-, NR2C-, and NR2D-containing N-methyl-D-aspartate glutamate receptors. *Mol Pharmacol,* 72, 907-20.

ERREGER, K. & TRAYNELIS, S. F. 2008. Zinc inhibition of rat NR1/NR2A N-methyl-D-aspartate receptors. *J Physiol,* 586, 763-78.

EVANS, R. H., FRANCIS, A. A., HUNT, K., OAKES, D. J. & WATKINS, J. C. 1979. Antagonism of excitatory amino acid-induced responses and of synaptic excitation in the isolated spinal cord of the frog. *Br J Pharmacol,* 67, 591-603.

EVANS, R. H., FRANCIS, A. A., JONES, A. W., SMITH, D. A. & WATKINS, J. C. 1982. The effects of a series of omega-phosphonic alpha-carboxylic amino acids on electrically evoked and excitant amino acid-induced responses in isolated spinal cord preparations. *Br J Pharmacol,* 75, 65-75.

FARLOW, M. R. 2004. Utilizing combination therapy in the treatment of Alzheimer's disease. *Expert Rev Neurother,* 4, 799-808.

FENG, B., MORLEY, R. M., JANE, D. E. & MONAGHAN, D. T. 2005. The effect of competitive antagonist chain length on NMDA receptor subunit selectivity. *Neuropharmacology,* 48, 354-9.

FERRER-MONTIEL, A. V., MERINO, J. M., PLANELLS-CASES, R., SUN, W. & MONTAL, M. 1998. Structural determinants of the blocker binding site in glutamate and NMDA receptor channels. *Neuropharmacology,* 37, 139-47.

FERRI, C. P., PRINCE, M., BRAYNE, C., BRODATY, H., FRATIGLIONI, L., GANGULI, M., HALL, K., HASEGAWA, K., HENDRIE, H., HUANG, Y., JORM, A., MATHERS, C., MENEZES, P. R., RIMMER, E. & SCAZUFCA,

M. 2005. Global prevalence of dementia: a Delphi consensus study. *Lancet,* 366, 2112-7.
FONTE, J., MIKLOSSY, J., ATWOOD, C. & MARTINS, R. 2001. The severity of cortical Alzheimer's type changes is positively correlated with increased amyloid-beta Levels: Resolubilization of amyloid-beta with transition metal ion chelators. *J Alzheimers Dis,* 3, 209-219.
FRANCIS, P. T., PALMER, A. M., SNAPE, M. & WILCOCK, G. K. 1999. The cholinergic hypothesis of Alzheimer's disease: a review of progress. *J Neurol Neurosurg Psychiatry,* 66, 137-47.
FREDERICKSON, C. J., SUH, S. W., SILVA, D., FREDERICKSON, C. J. & THOMPSON, R. B. 2000. Importance of zinc in the central nervous system: the zinc-containing neuron. *J Nutr,* 130, 1471S-83S.
FURUKAWA, H. & GOUAUX, E. 2003. Mechanisms of activation, inhibition and specificity: crystal structures of the NMDA receptor NR1 ligand-binding core. *Embo J,* 22, 2873-85.
FURUKAWA, H., SINGH, S. K., MANCUSSO, R. & GOUAUX, E. 2005. Subunit arrangement and function in NMDA receptors. *Nature,* 438, 185-92.
GIELEN, M., SIEGLER RETCHLESS, B., MONY, L., JOHNSON, J. W. & PAOLETTI, P. 2009. Mechanism of differential control of NMDA receptor activity by NR2 subunits. *Nature,* 459, 703-7.
GILMAN, S., KOLLER, M., BLACK, R. S., JENKINS, L., GRIFFITH, S. G., FOX, N. C., EISNER, L., KIRBY, L., ROVIRA, M. B., FORETTE, F. & ORGOGOZO, J. M. 2005. Clinical effects of Abeta immunization (AN1792) in patients with AD in an interrupted trial. *Neurology,* 64, 1553-62.
GLENNER, G. G. & WONG, C. W. 1984. Alzheimer's disease: initial report of the purification and characterization of a novel cerebrovascular amyloid protein. *Biochem Biophys Res Commun,* 120, 885-90.
GLIEBUS, G. & LIPPA, C. F. 2007. The influence of beta-blockers on delayed memory function in people with cognitive impairment. *Am J Alzheimers Dis Other Demen,* 22, 57-61.
GOEDERT, M. & GHETTI, B. 2007. Alois Alzheimer: his life and times. *Brain Pathol,* 17, 57-62.
GOGAS, K. R. 2006. Glutamate-based therapeutic approaches: NR2B receptor antagonists. *Curr Opin Pharmacol,* 6, 68-74.
GOTO, Y., NIIDOME, T., AKAIKE, A., KIHARA, T. & SUGIMOTO, H. 2006. Amyloid beta-peptide preconditioning reduces glutamate-induced neurotoxicity by promoting endocytosis of NMDA receptor. *Biochem Biophys Res Commun,* 351, 259-65.
GRUNDKE-IQBAL, I., IQBAL, K., QUINLAN, M., TUNG, Y. C., ZAIDI, M. S. & WISNIEWSKI, H. M. 1986. Microtubule-associated protein tau. A component of Alzheimer paired helical filaments. *J Biol Chem,* 261, 6084-9.
GUTZMANN, H. & HADLER, D. 1998. Sustained efficacy and safety of idebenone in the treatment of Alzheimer's disease: update on a 2-year double-blind multicentre study. *J Neural Transm Suppl,* 54, 301-10.
HAGER, K., KENKLIES, M., MCAFOOSE, J., ENGEL, J. & MUNCH, G. 2007. Alpha-lipoic acid as a new treatment option for Alzheimer's disease--a 48 months follow-up analysis. *J Neural Transm Suppl,* 189-93.
HAN, X., TOMITORI, H., MIZUNO, S., HIGASHI, K., FULL, C., FUKIWAKE, T., TERUI, Y., LEEWANICH, P., NISHIMURA, K., TOIDA, T., WILLIAMS, K., KASHIWAGI, K. & IGARASHI, K. 2008. Binding of spermine and

ifenprodil to a purified, soluble regulatory domain of the N-methyl-D-aspartate receptor. *J Neurochem,* 107, 1566-77.

HAREL, A., WU, F., MATTSON, M. P., MORRIS, C. M. & YAO, P. J. 2008. Evidence for CALM in directing VAMP2 trafficking. *Traffic,* 9, 417-29.

HAROLD, D., ABRAHAM, R., HOLLINGWORTH, P., SIMS, R., GERRISH, A., HAMSHERE, M. L., PAHWA, J. S., MOSKVINA, V., DOWZELL, K., WILLIAMS, A., JONES, N., THOMAS, C., STRETTON, A., MORGAN, A. R., LOVESTONE, S., POWELL, J., PROITSI, P., LUPTON, M. K., BRAYNE, C., RUBINSZTEIN, D. C., GILL, M., LAWLOR, B., LYNCH, A., MORGAN, K., BROWN, K. S., PASSMORE, P. A., CRAIG, D., MCGUINNESS, B., TODD, S., HOLMES, C., MANN, D., SMITH, A. D., LOVE, S., KEHOE, P. G., HARDY, J., MEAD, S., FOX, N., ROSSOR, M., COLLINGE, J., MAIER, W., JESSEN, F., SCHURMANN, B., VAN DEN BUSSCHE, H., HEUSER, I., KORNHUBER, J., WILTFANG, J., DICHGANS, M., FROLICH, L., HAMPEL, H., HULL, M., RUJESCU, D., GOATE, A. M., KAUWE, J. S., CRUCHAGA, C., NOWOTNY, P., MORRIS, J. C., MAYO, K., SLEEGERS, K., BETTENS, K., ENGELBORGHS, S., DE DEYN, P. P., VAN BROECKHOVEN, C., LIVINGSTON, G., BASS, N. J., GURLING, H., MCQUILLIN, A., GWILLIAM, R., DELOUKAS, P., AL-CHALABI, A., SHAW, C. E., TSOLAKI, M., SINGLETON, A. B., GUERREIRO, R., MUHLEISEN, T. W., NOTHEN, M. M., MOEBUS, S., JOCKEL, K. H., KLOPP, N., WICHMANN, H. E., CARRASQUILLO, M. M., PANKRATZ, V. S., YOUNKIN, S. G., HOLMANS, P. A., O'DONOVAN, M., OWEN, M. J. & WILLIAMS, J. 2009. Genome-wide association study identifies variants at CLU and PICALM associated with Alzheimer's disease. *Nat Genet,* 41, 1088-93.

HATTON, C. J. & PAOLETTI, P. 2005. Modulation of triheteromeric NMDA receptors by N-terminal domain ligands. *Neuron,* 46, 261-74.

HAUGAARD, N. & LEVIN, R. M. 2002. Activation of choline acetyl transferase by dihydrolipoic acid. *Mol Cell Biochem,* 229, 103-6.

HAYASHI, T. 1954. Effects of sodium glutamate on the nervous system. *Keio J. Med,* 3, 192-193.

HAZELL, A. S. 2007. Excitotoxic mechanisms in stroke: an update of concepts and treatment strategies. *Neurochem Int,* 50, 941-53.

HENSON, M. A., ROBERTS, A. C., PEREZ-OTANO, I. & PHILPOT, B. D. 2010. Influence of the NR3A subunit on NMDA receptor functions. *Prog Neurobiol,* 91, 23-37.

HENSON, M. A., ROBERTS, A. C., SALIMI, K., VADLAMUDI, S., HAMER, R. M., GILMORE, J. H., JARSKOG, L. F. & PHILPOT, B. D. 2008. Developmental Regulation of the NMDA Receptor Subunits, NR3A and NR1, in Human Prefrontal Cortex. *Cereb Cortex.*

HOEY, S. E., WILLIAMS, R. J. & PERKINTON, M. S. 2009. Synaptic NMDA receptor activation stimulates alpha-secretase amyloid precursor protein processing and inhibits amyloid-beta production. *J Neurosci,* 29, 4442-60.

HOLLMANN, M., BOULTER, J., MARON, C., BEASLEY, L., SULLIVAN, J., PECHT, G. & HEINEMANN, S. 1993. Zinc potentiates agonist-induced currents at certain splice variants of the NMDA receptor. *Neuron,* 10, 943-54.

HOLMQUIST, L., STUCHBURY, G., BERBAUM, K., MUSCAT, S., YOUNG, S., HAGER, K., ENGEL, J. & MUNCH, G. 2007. Lipoic acid as a novel

treatment for Alzheimer's disease and related dementias. *Pharmacol Ther,* 113, 154-64.
HOLSINGER, R. M., SCHNARR, J., HENRY, P., CASTELO, V. T. & FAHNESTOCK, M. 2000. Quantitation of BDNF mRNA in human parietal cortex by competitive reverse transcription-polymerase chain reaction: decreased levels in Alzheimer's disease. *Brain Res Mol Brain Res,* 76, 347-54.
HOWLETT, D. R., GEORGE, A. R., OWEN, D. E., WARD, R. V. & MARKWELL, R. E. 1999. Common structural features determine the effectiveness of carvedilol, daunomycin and rolitetracycline as inhibitors of Alzheimer beta-amyloid fibril formation. *Biochem J,* 343 Pt 2, 419-23.
IKONOMIDOU, C. & TURSKI, L. 2002. Why did NMDA receptor antagonists fail clinical trials for stroke and traumatic brain injury? *Lancet Neurol,* 1, 383-6.
ISAAC, J. T., ASHBY, M. & MCBAIN, C. J. 2007. The role of the GluR2 subunit in AMPA receptor function and synaptic plasticity. *Neuron,* 54, 859-71.
ISAAC, M. G., QUINN, R. & TABET, N. 2008. Vitamin E for Alzheimer's disease and mild cognitive impairment. *Cochrane Database Syst Rev*, CD002854.
JACOB, C. P., KOUTSILIERI, E., BARTL, J., NEUEN-JACOB, E., ARZBERGER, T., ZANDER, N., RAVID, R., ROGGENDORF, W., RIEDERER, P. & GRUNBLATT, E. 2007. Alterations in expression of glutamatergic transporters and receptors in sporadic Alzheimer's disease. *J Alzheimers Dis,* 11, 97-116.
JESUDASON, E. P., MASILAMONI, J. G., ASHOK, B. S., BABEN, B., ARUL, V., JESUDOSS, K. S., JEBARAJ, W. C., DHANDAYUTHAPANI, S., VIGNESH, S. & JAYAKUMAR, R. 2008. Inhibitory effects of short-term administration of DL-alpha-lipoic acid on oxidative vulnerability induced by Abeta amyloid fibrils (25-35) in mice. *Mol Cell Biochem,* 311, 145-56.
JIANG, H. & JIA, J. 2009. Association between NR2B subunit gene (GRIN2B) promoter polymorphisms and sporadic Alzheimer's disease in the North Chinese population. *Neurosci Lett,* 450, 356-60.
JIN, L., SUGIYAMA, H., TAKIGAWA, M., KATAGIRI, D., TOMITORI, H., NISHIMURA, K., KAUR, N., PHANSTIEL, O. T., KITAJIMA, M., TAKAYAMA, H., OKAWARA, T., WILLIAMS, K., KASHIWAGI, K. & IGARASHI, K. 2007. Comparative studies of anthraquinone- and anthracene-tetraamines as blockers of N-methyl-D-aspartate receptors. *J Pharmacol Exp Ther,* 320, 47-55.
JOHANSSON, S., RADESATER, A. C., COWBURN, R. F., THYBERG, J. & LUTHMAN, J. 2006. Modelling of amyloid beta-peptide induced lesions using roller-drum incubation of hippocampal slice cultures from neonatal rats. *Exp Brain Res,* 168, 11-24.
KARAKAS, E., SIMOROWSKI, N. & FURUKAWA, H. 2009. Structure of the zinc-bound amino-terminal domain of the NMDA receptor NR2B subunit. *Embo J.*
KASHIWAGI, K., MASUKO, T., NGUYEN, C. D., KUNO, T., TANAKA, I., IGARASHI, K. & WILLIAMS, K. 2002. Channel blockers acting at N-methyl-D-aspartate receptors: differential effects of mutations in the vestibule and ion channel pore. *Mol Pharmacol,* 61, 533-45.
KASHIWAGI, K., PAHK, A. J., MASUKO, T., IGARASHI, K. & WILLIAMS, K. 1997. Block and modulation of N-methyl-D-aspartate receptors by polyamines and protons: role of amino acid residues in the transmembrane and pore-forming regions of NR1 and NR2 subunits. *Mol Pharmacol,* 52, 701-13.

KASHIWAGI, K., WILLIAMS, K. & IGARASHI, K. 2007. Anthraquinone polyamines: novel channel blockers of N-methyl-D-aspartate receptors. *Amino Acids,* 33, 299-304.

KESSELS, M. M. & QUALMANN, B. 2002. Syndapins integrate N-WASP in receptor-mediated endocytosis. *Embo J,* 21, 6083-94.

KEW, J. N. & KEMP, J. A. 2005. Ionotropic and metabotropic glutamate receptor structure and pharmacology. *Psychopharmacology (Berl),* 179, 4-29.

KIEBURTZ, K., MCDERMOTT, M. P., VOSS, T. S., COREY-BLOOM, J., DEUEL, L. M., DORSEY, E. R., FACTOR, S., GESCHWIND, M. D., HODGEMAN, K., KAYSON, E., NOONBERG, S., POURFAR, M., RABINOWITZ, K., RAVINA, B., SANCHEZ-RAMOS, J., SEELY, L., WALKER, F. & FEIGIN, A. 2010. A randomized, placebo-controlled trial of latrepirdine in huntington disease. *Arch Neurol,* 67, 154-60.

KLECKNER, N. W. & DINGLEDINE, R. 1988. Requirement for glycine in activation of NMDA-receptors expressed in Xenopus oocytes. *Science,* 241, 835-7.

KLUGMAN, A., SAUER, J., TABET, N. & HOWARD, R. 2004. Alpha lipoic acid for dementia. *Cochrane Database of Systematic Reviews.*

KONZACK, S., THIES, E., MARX, A., MANDELKOW, E. M. & MANDELKOW, E. 2007. Swimming against the tide: mobility of the microtubule-associated protein tau in neurons. *J Neurosci,* 27, 9916-27.

KOTERMANSKI, S. E., WOOD, J. T. & JOHNSON, J. W. 2009. Memantine binding to a superficial site on NMDA receptors contributes to partial trapping. *J Physiol,* 587, 4589-604.

KRIEGLSTEIN, J., LIPPERT, K. & POCH, G. 1996. Apparent independent action of nimodipine and glutamate antagonists to protect cultured neurons against glutamate-induced damage. *Neuropharmacology,* 35, 1737-42.

KROGSGAARD-LARSEN, P., HONORE, T., HANSEN, J. J., CURTIS, D. R. & LODGE, D. 1980. New class of glutamate agonist structurally related to ibotenic acid. *Nature,* 284, 64-6.

KRYGER, G., SILMAN, I. & SUSSMAN, J. L. 1999. Structure of acetylcholinesterase complexed with E2020 (Aricept): implications for the design of new anti-Alzheimer drugs. *Structure,* 7, 297-307.

KRYSTAL, J. H., D'SOUZA, D. C., MATHALON, D., PERRY, E., BELGER, A. & HOFFMAN, R. 2003. NMDA receptor antagonist effects, cortical glutamatergic function, and schizophrenia: toward a paradigm shift in medication development. *Psychopharmacology (Berl),* 169, 215-33.

KULAGOWSKI, J. J., BAKER, R., CURTIS, N. R., LEESON, P. D., MAWER, I. M., MOSELEY, A. M., RIDGILL, M. P., ROWLEY, M., STANSFIELD, I., FOSTER, A. C. & ET AL. 1994. 3'-(Arylmethyl)- and 3'-(aryloxy)-3-phenyl-4-hydroxyquinolin-2(1H)-ones: orally active antagonists of the glycine site on the NMDA receptor. *J Med Chem,* 37, 1402-5.

KUNER, T. & SCHOEPFER, R. 1996. Multiple structural elements determine subunit specificity of Mg2+ block in NMDA receptor channels. *J Neurosci,* 16, 3549-58.

KURYATOV, A., LAUBE, B., BETZ, H. & KUHSE, J. 1994. Mutational analysis of the glycine-binding site of the NMDA receptor: structural similarity with bacterial amino acid-binding proteins. *Neuron,* 12, 1291-300.

LAFERLA, F. M., GREEN, K. N. & ODDO, S. 2007. Intracellular amyloid-beta in Alzheimer's disease. *Nat Rev Neurosci,* 8, 499-509.

LEESON, P. D., BAKER, R., CARLING, R. W., CURTIS, N. R., MOORE, K. W., WILLIAMS, B. J., FOSTER, A. C., DONALD, A. E., KEMP, J. A. & MARSHALL, G. R. 1991. Kynurenic acid derivatives. Structure-activity relationships for excitatory amino acid antagonism and identification of potent and selective antagonists at the glycine site on the N-methyl-D-aspartate receptor. *J Med Chem,* 34, 1243-52.

LEESON, P. D., CARLING, R. W., MOORE, K. W., MOSELEY, A. M., SMITH, J. D., STEVENSON, G., CHAN, T., BAKER, R., FOSTER, A. C., GRIMWOOD, S. & ET AL. 1992. 4-Amido-2-carboxytetrahydroquinolines. Structure-activity relationships for antagonism at the glycine site of the NMDA receptor. *J Med Chem,* 35, 1954-68.

LERMONTOVA, N. N., REDKOZUBOV, A. E., SHEVTSOVA, E. F., SERKOVA, T. P., KIREEVA, E. G. & BACHURIN, S. O. 2001. Dimebon and tacrine inhibit neurotoxic action of beta-amyloid in culture and block L-type Ca(2+) channels. *Bull Exp Biol Med,* 132, 1079-83.

LESNE, S., ALI, C., GABRIEL, C., CROCI, N., MACKENZIE, E. T., GLABE, C. G., PLOTKINE, M., MARCHAND-VERRECCHIA, C., VIVIEN, D. & BUISSON, A. 2005. NMDA receptor activation inhibits alpha-secretase and promotes neuronal amyloid-beta production. *J Neurosci,* 25, 9367-77.

LI, M. (ed.) 1999. *NMDA Receptor Protocols*: Humana Press.

LINK, C. D. 2005. Invertebrate models of Alzheimer's disease. *Genes Brain Behav,* 4, 147-56.

LIPTON, S. A. & ROSENBERG, P. A. 1994. Excitatory amino acids as a final common pathway for neurologic disorders. *N Engl J Med,* 330, 613-22.

LIU, H. P., LIN, W. Y., LIU, S. H., WANG, W. F., TSAI, C. H., WU, B. T., WANG, C. K. & TSAI, F. J. 2009. Genetic Variation in N-Methyl-D-Aspartate Receptor Subunit NR3A but Not NR3B Influences Susceptibility to Alzheimer's Disease. *Dement Geriatr Cogn Disord,* 28, 521-527.

LIU, J., HEAD, E., GHARIB, A. M., YUAN, W., INGERSOLL, R. T., HAGEN, T. M., COTMAN, C. W. & AMES, B. N. 2002. Memory loss in old rats is associated with brain mitochondrial decay and RNA/DNA oxidation: partial reversal by feeding acetyl-L-carnitine and/or R-alpha -lipoic acid. *Proc Natl Acad Sci U S A,* 99, 2356-61.

LIU, L., WONG, T. P., POZZA, M. F., LINGENHOEHL, K., WANG, Y., SHENG, M., AUBERSON, Y. P. & WANG, Y. T. 2004. Role of NMDA receptor subtypes in governing the direction of hippocampal synaptic plasticity. *Science,* 304, 1021-4.

LIU, M., NAKAZAWA, K., INOUE, K. & OHNO, Y. 1997. Potent and voltage-dependent block by philanthotoxin-343 of neuronal nicotinic receptor/channels in PC12 cells. *Br J Pharmacol,* 122, 379-85.

LIU, Y. W., LUO, J. L., REN, H., PEOPLES, R. W., AI, Y. X., LIU, L. J., PANG, Y. P., LI, Z. W., HAN, Y. F. & LI, C. Y. 2008. Inhibition of NMDA-gated ion channels by bis(7)-tacrine: whole-cell and single-channel studies. *Neuropharmacology,* 54, 1086-94.

LOVELL, M. A., XIE, C., XIONG, S. & MARKESBERY, W. R. 2003. Protection against amyloid beta peptide and iron/hydrogen peroxide toxicity by alpha lipoic acid. *J Alzheimers Dis,* 5, 229-39.

LOW, C. M., LYUBOSLAVSKY, P., FRENCH, A., LE, P., WYATTE, K., THIEL, W. H., MARCHAN, E. M., IGARASHI, K., KASHIWAGI, K., GERNERT, K., WILLIAMS, K., TRAYNELIS, S. F. & ZHENG, F. 2003. Molecular

determinants of proton-sensitive N-methyl-D-aspartate receptor gating. *Mol Pharmacol,* 63, 1212-22.
LUCAS, D. R. & NEWHOUSE, J. P. 1957. The toxic effect of sodium L-glutamate on the inner layers of the retina. *AMA Arch Ophthalmol,* 58, 193-201.
LUO, J., LI, W., LIU, Y., ZHANG, W., FU, H., LEE, N. T., YU, H., PANG, Y., HUANG, P., XIA, J., LI, Z. W., LI, C. & HAN, Y. 2007. Novel dimeric bis(7)-tacrine proton-dependently inhibits NMDA-activated currents. *Biochem Biophys Res Commun,* 361, 505-9.
LYSKO, P. G., LYSKO, K. A., WEBB, C. L. & FEUERSTEIN, G. 1992. Neuroprotective effects of carvedilol, a new antihypertensive, at the N-methyl-D-aspartate receptor. *Neurosci Lett,* 148, 34-8.
LYSKO, P. G., LYSKO, K. A., WEBB, C. L., FEUERSTEIN, G., MASON, P. E., WALTER, M. F. & MASON, R. P. 1998. Neuroprotective activities of carvedilol and a hydroxylated derivative: role of membrane biophysical interactions. *Biochem Pharmacol,* 56, 1645-56.
LYSKO, P. G., WEBB, C. L. & FEUERSTEIN, G. 1994. Neuroprotective effects of carvedilol, a new antihypertensive, as a Na+ channel modulator and glutamate transport inhibitor. *Neurosci Lett,* 171, 77-80.
MADRY, C., BETZ, H., GEIGER, J. R. & LAUBE, B. 2008. Supralinear potentiation of NR1/NR3A excitatory glycine receptors by Zn2+ and NR1 antagonist. *Proc Natl Acad Sci U S A,* 105, 12563-8.
MADRY, C., BETZ, H., GEIGER, J. R. & LAUBE, B. 2010. Potentiation of Glycine-Gated NR1/NR3A NMDA Receptors Relieves Ca-Dependent Outward Rectification. *Front Mol Neurosci,* 3, 6.
MADRY, C., MESIC, I., BARTHOLOMAUS, I., NICKE, A., BETZ, H. & LAUBE, B. 2006. Principal role of NR3 subunits in NR1/NR3 excitatory glycine receptor function. *Biochem Biophys Res Commun.*
MADRY, C., MESIC, I., BARTHOLOMAUS, I., NICKE, A., BETZ, H. & LAUBE, B. 2007. Principal role of NR3 subunits in NR1/NR3 excitatory glycine receptor function. *Biochem Biophys Res Commun,* 354, 102-8.
MALENKA, R. C. & BEAR, M. F. 2004. LTP and LTD: an embarrassment of riches. *Neuron,* 44, 5-21.
MARCELLO, E., GARDONI, F., MAUCERI, D., ROMORINI, S., JEROMIN, A., EPIS, R., BORRONI, B., CATTABENI, F., SALA, C., PADOVANI, A. & DI LUCA, M. 2007. Synapse-associated protein-97 mediates alpha-secretase ADAM10 trafficking and promotes its activity. *J Neurosci,* 27, 1682-91.
MATSUDA, K., FLETCHER, M., KAMIYA, Y. & YUZAKI, M. 2003. Specific assembly with the NMDA receptor 3B subunit controls surface expression and calcium permeability of NMDA receptors. *J Neurosci,* 23, 10064-73.
MATSUDA, K., KAMIYA, Y., MATSUDA, S. & YUZAKI, M. 2002. Cloning and characterization of a novel NMDA receptor subunit NR3B: a dominant subunit that reduces calcium permeability. *Brain Res Mol Brain Res,* 100, 43-52.
MATVEEVA, I. A. 1983. [Action of dimebon on histamine receptors]. *Farmakol Toksikol,* 46, 27-9.
MAY, T. E. & PIEK, T. 1979. Neuromuscular block in locust skeletal muscle caused by a venom preparation made from the digger wasp Philanthus triangulum F. from Egypt. *J Insect Physiol,* 25, 685-91.
MAYER, M. L. 2006. Glutamate receptors at atomic resolution. *Nature,* 440, 456-62.

MAYER, M. L. & WESTBROOK, G. L. 1987. Permeation and block of N-methyl-D-aspartic acid receptor channels by divalent cations in mouse cultured central neurones. *J Physiol,* 394, 501-27.

MAYER, M. L., WESTBROOK, G. L. & GUTHRIE, P. B. 1984. Voltage-dependent block by Mg2+ of NMDA responses in spinal cord neurones. *Nature,* 309, 261-3.

MCCULLOCH, R. M., JOHNSTON, G. A., GAME, C. J. & CURTIS, D. R. 1974. The differential sensitivity of spinal interneurones and Renshaw cells to Kainate and N-methyl-D-aspartate. *Exp Brain Res,* 21, 515-8.

MEALING, G. A., LANTHORN, T. H., MURRAY, C. L., SMALL, D. L. & MORLEY, P. 1999. Differences in degree of trapping of low-affinity uncompetitive N-methyl-D-aspartic acid receptor antagonists with similar kinetics of block. *J Pharmacol Exp Ther,* 288, 204-10.

MEDINA, I., FILIPPOVA, N., CHARTON, G., ROUGEOLE, S., BEN-ARI, Y., KHRESTCHATISKY, M. & BREGESTOVSKI, P. 1995. Calcium-dependent inactivation of heteromeric NMDA receptor-channels expressed in human embryonic kidney cells. *J Physiol,* 482 (Pt 3), 567-73.

MEGURO, H., MORI, H., ARAKI, K., KUSHIYA, E., KUTSUWADA, T., YAMAZAKI, M., KUMANISHI, T., ARAKAWA, M., SAKIMURA, K. & MISHINA, M. 1992. Functional characterization of a heteromeric NMDA receptor channel expressed from cloned cDNAs. *Nature,* 357, 70-4.

MELCHIORRE, C., ANTONELLO, A., BANZI, R., BOLOGNESI, M. L., MINARINI, A., ROSINI, M. & TUMIATTI, V. 2003. Polymethylene tetraamine backbone as template for the development of biologically active polyamines. *Med Res Rev,* 23, 200-33.

MELLOR, I. R., BRIER, T. J., PLUTEANU, F., STROMGAARD, K., SAGHYAN, A., ELDURSI, N., BRIERLEY, M. J., ANDERSEN, K., JAROSZEWSKI, J. W., KROGSGAARD-LARSEN, P. & USHERWOOD, P. N. 2003. Modification of the philanthotoxin-343 polyamine moiety results in different structure-activity profiles at muscle nicotinic ACh, NMDA and AMPA receptors. *Neuropharmacology,* 44, 70-80.

MELLOR, I. R., OGILVIE, J., PLUTEANU, F., CLOTHIER, R. H., PARKER, T. L., ROSINI, M., MINARINI, A., TUMIATTI, V. & MELCHIORRE, C. 2004. Methoctramine analogues inhibit responses to capsaicin and protons in rat dorsal root ganglion neurons. *Eur J Pharmacol,* 505, 37-50.

MELLOR, I. R. & USHERWOOD, P. N. 2004. Targeting ionotropic receptors with polyamine-containing toxins. *Toxicon,* 43, 493-508.

MIRSHAHI, T. & WOODWARD, J. J. 1995. Ethanol sensitivity of heteromeric NMDA receptors: effects of subunit assembly, glycine and NMDAR1 Mg(2+)-insensitive mutants. *Neuropharmacology,* 34, 347-55.

MOE, S. T., SMITH, D. L., CHIEN, Y., RASZKIEWICZ, J. L., ARTMAN, L. D. & MUELLER, A. L. 1998. Design, synthesis, and biological evaluation of spider toxin (argiotoxin-636) analogs as NMDA receptor antagonists. *Pharm Res,* 15, 31-8.

MONAGHAN, D. T. & JANE, D. E. 2009. Pharmacology of NMDA Receptors. *In:* VANDONGEN, A. M. (ed.) *Biology of the NMDA receptor.* Boca Ranton: CRC Press.

MONY, L., KEW, J. N., GUNTHORPE, M. J. & PAOLETTI, P. 2009a. Allosteric modulators of NR2B-containing NMDA receptors: molecular mechanisms and therapeutic potential. *Br J Pharmacol,* 157, 1301-17.

MONY, L., KRZACZKOWSKI, L., LEONETTI, M., LE GOFF, A., ALARCON, K., NEYTON, J., BERTRAND, H. O., ACHER, F. & PAOLETTI, P. 2009b. Structural basis of NR2B-selective antagonist recognition by N-methyl-D-aspartate receptors. *Mol Pharmacol,* 75, 60-74.

MONYER, H., BURNASHEV, N., LAURIE, D. J., SAKMANN, B. & SEEBURG, P. H. 1994. Developmental and regional expression in the rat brain and functional properties of four NMDA receptors. *Neuron,* 12, 529-40.

MORIGUCHI, S., ZHAO, X., MARSZALEC, W., YEH, J. Z. & NARAHASHI, T. 2005. Modulation of N-methyl-D-aspartate receptors by donepezil in rat cortical neurons. *J Pharmacol Exp Ther,* 315, 125-35.

MORIYOSHI, K., MASU, M., ISHII, T., SHIGEMOTO, R., MIZUNO, N. & NAKANISHI, S. 1991. Molecular cloning and characterization of the rat NMDA receptor. *Nature,* 354, 31-7.

MULLER, U. & KRIEGLSTEIN, J. 1995. Prolonged pretreatment with alpha-lipoic acid protects cultured neurons against hypoxic, glutamate-, or iron-induced injury. *J Cereb Blood Flow Metab,* 15, 624-30.

NELSON, J. K., FROLUND, S. U., TIKHONOV, D. B., KRISTENSEN, A. S. & STROMGAARD, K. 2009. Synthesis and biological activity of argiotoxin 636 and analogues: selective antagonists for ionotropic glutamate receptors. *Angew Chem Int Ed Engl,* 48, 3087-91.

NEYTON, J. & PAOLETTI, P. 2006. Relating NMDA receptor function to receptor subunit composition: limitations of the pharmacological approach. *J Neurosci,* 26, 1331-3.

NIEMANN, S., LANDERS, J. E., CHURCHILL, M. J., HOSLER, B., SAPP, P., SPEED, W. C., LAHN, B. T., KIDD, K. K., BROWN, R. H., JR. & HAYASHI, Y. 2007. Motoneuron-specific NR3B gene. No association with ALS and evidence for a common null allele. *Neurology*.

NILSEN, A. & ENGLAND, P. M. 2007. A subtype-selective, use-dependent inhibitor of native AMPA receptors. *J Am Chem Soc,* 129, 4902-3.

NILSSON, A., ERIKSSON, M., MULY, E. C., AKESSON, E., SAMUELSSON, E. B., BOGDANOVIC, N., BENEDIKZ, E. & SUNDSTROM, E. 2007. Analysis of NR3A receptor subunits in human native NMDA receptors. *Brain Res*.

NISHI, M., HINDS, H., LU, H. P., KAWATA, M. & HAYASHI, Y. 2001. Motoneuron-specific expression of NR3B, a novel NMDA-type glutamate receptor subunit that works in a dominant-negative manner. *J Neurosci,* 21, RC185.

NOWAK, L., BREGESTOVSKI, P., ASCHER, P., HERBET, A. & PROCHIANTZ, A. 1984. Magnesium gates glutamate-activated channels in mouse central neurones. *Nature,* 307, 462-5.

NUNOMURA, A., PERRY, G., ALIEV, G., HIRAI, K., TAKEDA, A., BALRAJ, E. K., JONES, P. K., GHANBARI, H., WATAYA, T., SHIMOHAMA, S., CHIBA, S., ATWOOD, C. S., PETERSEN, R. B. & SMITH, M. A. 2001. Oxidative damage is the earliest event in Alzheimer disease. *J Neuropathol Exp Neurol,* 60, 759-67.

OHYAGI, Y., YAMADA, T., NISHIOKA, K., CLARKE, N. J., TOMLINSON, A. J., NAYLOR, S., NAKABEPPU, Y., KIRA, J. & YOUNKIN, S. G. 2000. Selective increase in cellular A beta 42 is related to apoptosis but not necrosis. *Neuroreport,* 11, 167-71.

OKABE, S., MIWA, A. & OKADO, H. 1999. Alternative splicing of the C-terminal domain regulates cell surface expression of the NMDA receptor NR1 subunit. *J Neurosci,* 19, 7781-92.

OKADA, T., WAKABAYASHI, M., IKEDA, K. & MATSUZAKI, K. 2007. Formation of toxic fibrils of Alzheimer's amyloid beta-protein-(1-40) by monosialoganglioside GM1, a neuronal membrane component. *J Mol Biol,* 371, 481-9.

OLNEY, J. W. & HO, O. L. 1970. Brain damage in infant mice following oral intake of glutamate, aspartate or cysteine. *Nature,* 227, 609-11.

OLNEY, J. W., LABRUYERE, J. & PRICE, M. T. 1989. Pathological changes induced in cerebrocortical neurons by phencyclidine and related drugs. *Science,* 244, 1360-2.

OPAZO, C., HUANG, X., CHERNY, R. A., MOIR, R. D., ROHER, A. E., WHITE, A. R., CAPPAI, R., MASTERS, C. L., TANZI, R. E., INESTROSA, N. C. & BUSH, A. I. 2002. Metalloenzyme-like activity of Alzheimer's disease beta-amyloid. Cu-dependent catalytic conversion of dopamine, cholesterol, and biological reducing agents to neurotoxic H(2)O(2). *J Biol Chem,* 277, 40302-8.

PAOLETTI, P. & NEYTON, J. 2006. NMDA receptor subunits: function and pharmacology. *Curr Opin Pharmacol.*

PARADIS, E., DOUILLARD, H., KOUTROUMANIS, M., GOODYER, C. & LEBLANC, A. 1996. Amyloid beta peptide of Alzheimer's disease downregulates Bcl-2 and upregulates bax expression in human neurons. *J Neurosci,* 16, 7533-9.

PEREZ-OTANO, I., LUJAN, R., TAVALIN, S. J., PLOMANN, M., MODREGGER, J., LIU, X. B., JONES, E. G., HEINEMANN, S. F., LO, D. C. & EHLERS, M. D. 2006. Endocytosis and synaptic removal of NR3A-containing NMDA receptors by PACSIN1/syndapin1. *Nat Neurosci,* 9, 611-21.

PEREZ-OTANO, I., SCHULTEIS, C. T., CONTRACTOR, A., LIPTON, S. A., TRIMMER, J. S., SUCHER, N. J. & HEINEMANN, S. F. 2001. Assembly with the NR1 subunit is required for surface expression of NR3A-containing NMDA receptors. *J Neurosci,* 21, 1228-37.

PERIN-DUREAU, F., RACHLINE, J., NEYTON, J. & PAOLETTI, P. 2002. Mapping the binding site of the neuroprotectant ifenprodil on NMDA receptors. *J Neurosci,* 22, 5955-65.

PETRENKO, A. B., YAMAKURA, T., BABA, H. & SHIMOJI, K. 2003. The role of N-methyl-D-aspartate (NMDA) receptors in pain: a review. *Anesth Analg,* 97, 1108-16.

PHILLIPS, H. S., HAINS, J. M., ARMANINI, M., LARAMEE, G. R., JOHNSON, S. A. & WINSLOW, J. W. 1991. BDNF mRNA is decreased in the hippocampus of individuals with Alzheimer's disease. *Neuron,* 7, 695-702.

PIEK, T. (ed.) 1986. *Venoms of the Hymenoptera,* London: Academic Press.

PINHEIRO, P. & MULLE, C. 2006. Kainate receptors. *Cell Tissue Res,* 326, 457-82.

POULSEN, M., LUCAS, S., STRØMGAARD, K. & KRISTENSEN, K. S. Year. Characterisation of Philanthotoxin Analogues in Subtype-Selective AMPA receptive antagonists. *In:* BRØSEN, K., ed. 16th World Congress on Basic and Clinical Pharmacology 2010 Denmark. NordicPharmacologicalSociety, 530-531.

PRAKASH, A. K. & KUMAR, A. 2009. Effect of chronic treatment of carvedilol on oxidative stress in an intracerebroventricular streptozotocin induced model of dementia in rats. *J Pharm Pharmacol,* 61, 1665-72.

PRATICO, D., URYU, K., LEIGHT, S., TROJANOSWKI, J. Q. & LEE, V. M. 2001. Increased lipid peroxidation precedes amyloid plaque formation in an animal model of Alzheimer amyloidosis. *J Neurosci,* 21, 4183-7.

QIAN, A. & JOHNSON, J. W. 2002. Channel gating of NMDA receptors. *Physiol Behav,* 77, 577-82.

QUINN, J. F., BUSSIERE, J. R., HAMMOND, R. S., MONTINE, T. J., HENSON, E., JONES, R. E. & STACKMAN, R. W., JR. 2007. Chronic dietary alpha-lipoic acid reduces deficits in hippocampal memory of aged Tg2576 mice. *Neurobiol Aging,* 28, 213-25.

RACHLINE, J., PERIN-DUREAU, F., LE GOFF, A., NEYTON, J. & PAOLETTI, P. 2005. The micromolar zinc-binding domain on the NMDA receptor subunit NR2B. *J Neurosci,* 25, 308-17.

RADITSCH, M., GEYER, M., KALBITZER, H. R., JAHN, W., RUPPERSBERG, J. P. & WITZEMANN, V. 1996. Polyamine spider toxins and mammalian N-methyl-D-aspartate receptors. Structural basis for channel blocking and binding of argiotoxin636. *Eur J Biochem,* 240, 416-26.

RADITSCH, M., RUPPERSBERG, J. P., KUNER, T., GUNTHER, W., SCHOEPFER, R., SEEBURG, P. H., JAHN, W. & WITZEMANN, V. 1993. Subunit-specific block of cloned NMDA receptors by argiotoxin636. *FEBS Lett,* 324, 63-6.

RAFIKI, A., BERNARD, A., MEDINA, I., GOZLAN, H. & KHRESTCHATISKY, M. 2000. Characterization in cultured cerebellar granule cells and in the developing rat brain of mRNA variants for the NMDA receptor 2C subunit. *J Neurochem,* 74, 1798-808.

RANG, H. P., DALE, M. M., RITTER, J. M. & FLOWER, R. J. 2007. *Rang and Dale's Pharmacology*, CHURCHILL LIVINGSTONE ELSEVIER.

RAYMOND, C. R., IRELAND, D. R. & ABRAHAM, W. C. 2003. NMDA receptor regulation by amyloid-beta does not account for its inhibition of LTP in rat hippocampus. *Brain Res,* 968, 263-72.

REDFERN, W. S., CARLSSON, L., DAVIS, A. S., LYNCH, W. G., MACKENZIE, I., PALETHORPE, S., SIEGL, P. K., STRANG, I., SULLIVAN, A. T., WALLIS, R., CAMM, A. J. & HAMMOND, T. G. 2003. Relationships between preclinical cardiac electrophysiology, clinical QT interval prolongation and torsade de pointes for a broad range of drugs: evidence for a provisional safety margin in drug development. *Cardiovasc Res,* 58, 32-45.

REISBERG, B., DOODY, R., STOFFLER, A., SCHMITT, F., FERRIS, S. & MOBIUS, H. J. 2003. Memantine in moderate-to-severe Alzheimer's disease. *N Engl J Med,* 348, 1333-41.

RIEPE, M. W., ADLER, G., IBACH, B., WEINKAUF, B., GUNAY, I. & TRACIK, F. 2006. Adding Memantine to Rivastigmine Therapy in Patients With Mild-to-Moderate Alzheimer's Disease: Results of a 12-Week, Open-Label Pilot Study. *Prim Care Companion J Clin Psychiatry,* 8, 258-263.

ROBERTS, A. C., DIEZ-GARCIA, J., RODRIGUIZ, R. M., LOPEZ, I. P., LUJAN, R., MARTINEZ-TURRILLAS, R., PICO, E., HENSON, M. A., BERNARDO, D. R., JARRETT, T. M., CLENDENINN, D. J., LOPEZ-MASCARAQUE, L., FENG, G., LO, D. C., WESSELING, J. F., WETSEL, W. C., PHILPOT, B. D. & PEREZ-OTANO, I. 2009. Downregulation of NR3A-containing NMDARs is required for synapse maturation and memory consolidation. *Neuron,* 63, 342-56.

ROSENMUND, C., STERN-BACH, Y. & STEVENS, C. F. 1998. The tetrameric structure of a glutamate receptor channel. *Science,* 280, 1596-9.

ROSINI, M., ANDRISANO, V., BARTOLINI, M., BOLOGNESI, M. L., HRELIA, P., MINARINI, A., TAROZZI, A. & MELCHIORRE, C. 2005. Rational approach to discover multipotent anti-Alzheimer drugs. *J Med Chem,* 48, 360-3.

ROSINI, M., BIXEL, M. G., MARUCCI, G., BUDRIESI, R., KRAUSS, M., BOLOGNESI, M. L., MINARINI, A., TUMIATTI, V., HUCHO, F. & MELCHIORRE, C. 2002. Structure-activity relationships of methoctramine-related polyamines as muscular nicotinic receptor noncompetitive antagonists. 2. Role of polymethylene chain lengths separating amine functions and of substituents on the terminal nitrogen atoms. *J Med Chem,* 45, 1860-78.

ROSINI, M., BUDRIESI, R., BIXEL, M. G., BOLOGNESI, M. L., CHIARINI, A., HUCHO, F., KROGSGAARD-LARSEN, P., MELLOR, I. R., MINARINI, A., TUMIATTI, V., USHERWOOD, P. N. & MELCHIORRE, C. 1999. Design, synthesis, and biological evaluation of symmetrically and unsymmetrically substituted methoctramine-related polyamines as muscular nicotinic receptor noncompetitive antagonists. *J Med Chem,* 42, 5212-23.

ROSINI, M., SIMONI, E., BARTOLINI, M., CAVALLI, A., CECCARINI, L., PASCU, N., MCCLYMONT, D. W., TAROZZI, A., BOLOGNESI, M. L., MINARINI, A., TUMIATTI, V., ANDRISANO, V., MELLOR, I. R. & MELCHIORRE, C. 2008. Inhibition of acetylcholinesterase, beta-amyloid aggregation, and NMDA receptors in Alzheimer's disease: a promising direction for the multi-target-directed ligands gold rush. *J Med Chem,* 51, 4381-4.

RUMBOLD, A., DULEY, L., CROWTHER, C. A. & HASLAM, R. R. 2008. Antioxidants for preventing pre-eclampsia. *Cochrane Database Syst Rev,* CD004227.

SAKURADA, K., MASU, M. & NAKANISHI, S. 1993. Alteration of Ca2+ permeability and sensitivity to Mg2+ and channel blockers by a single amino acid substitution in the N-methyl-D-aspartate receptor. *J Biol Chem,* 268, 410-5.

SALITURO, F. G., HARRISON, B. L., BARON, B. M., NYCE, P. L., STEWART, K. T., KEHNE, J. H., WHITE, H. S. & MCDONALD, I. A. 1992. 3-(2-Carboxyindol-3-yl)propionic acid-based antagonists of the N-methyl-D-aspartic acid receptor associated glycine binding site. *J Med Chem,* 35, 1791-9.

SAS, K., ROBOTKA, H., TOLDI, J. & VECSEI, L. 2007. Mitochondria, metabolic disturbances, oxidative stress and the kynurenine system, with focus on neurodegenerative disorders. *J Neurol Sci,* 257, 221-39.

SASAKI, Y. F., ROTHE, T., PREMKUMAR, L. S., DAS, S., CUI, J., TALANTOVA, M. V., WONG, H. K., GONG, X., CHAN, S. F., ZHANG, D., NAKANISHI, N., SUCHER, N. J. & LIPTON, S. A. 2002. Characterization and comparison of the NR3A subunit of the NMDA receptor in recombinant systems and primary cortical neurons. *J Neurophysiol,* 87, 2052-63.

SCHAFFHAUSER, H., MATHIASEN, J. R., DICAMILLO, A., HUFFMAN, M. J., LU, L. D., MCKENNA, B. A., QIAN, J. & MARINO, M. J. 2009. Dimebolin is a 5-HT6 antagonist with acute cognition enhancing activities. *Biochem Pharmacol,* 78, 1035-42.

SCHMIDT, C. & HOLLMANN, M. 2008. Apparent homomeric NR1 currents observed in Xenopus oocytes are caused by an endogenous NR2 subunit. *J Mol Biol,* 376, 658-70.
SCHMIDT, C. & HOLLMANN, M. 2009. Molecular and functional characterization of Xenopus laevis N-methyl-d-aspartate receptors. *Mol Cell Neurosci,* 42, 116-27.
SCHORGE, S. & COLQUHOUN, D. 2003. Studies of NMDA receptor function and stoichiometry with truncated and tandem subunits. *J Neurosci,* 23, 1151-8.
SCHULER, T., MESIC, I., MADRY, C., BARTHOLOMAUS, I. & LAUBE, B. 2008. Formation of NR1/NR2 and NR1/NR3 heterodimers constitutes the initial step in N-methyl-D-aspartate receptor assembly. *J Biol Chem,* 283, 37-46.
SHINOZAKI, H. & SHIBUYA, I. 1974a. A new potent excitant, quisqualic acid: effects on crayfish neuromuscular junction. *Neuropharmacology,* 13, 665-72.
SHINOZAKI, H. & SHIBUYA, I. 1974b. Potentiation of glutamate-induced depolarization by kainic acid in the crayfish opener muscle. *Neuropharmacology,* 13, 1057-65.
SIEDLAK, S. L., CASADESUS, G., WEBBER, K. M., PAPPOLLA, M. A., ATWOOD, C. S., SMITH, M. A. & PERRY, G. 2009. Chronic antioxidant therapy reduces oxidative stress in a mouse model of Alzheimer's disease. *Free Radic Res,* 43, 156-64.
SMOTHERS, C. T. & WOODWARD, J. J. 2003. Effect of the NR3 subunit on ethanol inhibition of recombinant NMDA receptors. *Brain Res,* 987, 117-21.
SMOTHERS, C. T. & WOODWARD, J. J. 2007. Pharmacological Characterization of Glycine-Activated Currents in HEK 293 Cells Expressing NMDA NR1 and NR3 Subunits. *J Pharmacol Exp Ther.*
SMOTHERS, C. T. & WOODWARD, J. J. 2009. Expression of glycine-activated diheteromeric NR1/NR3 receptors in human embryonic kidney 293 cells Is NR1 splice variant-dependent. *J Pharmacol Exp Ther,* 331, 975-84.
SNYDER, E. M., NONG, Y., ALMEIDA, C. G., PAUL, S., MORAN, T., CHOI, E. Y., NAIRN, A. C., SALTER, M. W., LOMBROSO, P. J., GOURAS, G. K. & GREENGARD, P. 2005. Regulation of NMDA receptor trafficking by amyloid-beta. *Nat Neurosci,* 8, 1051-8.
SOBOLEVSKY, A. & KOSHELEV, S. 1998. Two blocking sites of amino-adamantane derivatives in open N-methyl-D-aspartate channels. *Biophys J,* 74, 1305-19.
SOBOLEVSKY, A. I., BECK, C. & WOLLMUTH, L. P. 2002a. Molecular rearrangements of the extracellular vestibule in NMDAR channels during gating. *Neuron,* 33, 75-85.
SOBOLEVSKY, A. I., ROONEY, L. & WOLLMUTH, L. P. 2002b. Staggering of subunits in NMDAR channels. *Biophys J,* 83, 3304-14.
SOBOLEVSKY, A. I., ROSCONI, M. P. & GOUAUX, E. 2009. X-ray structure, symmetry and mechanism of an AMPA-subtype glutamate receptor. *Nature,* 462, 745-756.
SOLOVIEV, M. M., BRIERLEY, M. J., SHAO, Z. Y., MELLOR, I. R., VOLKOVA, T. M., KAMBOJ, R., ISHIMARU, H., SUDAN, H., HARRIS, J., FOLDES, R. L., GRISHIN, E. V., USHERWOOD, P. N. & BARNARD, E. A. 1996. Functional expression of a recombinant unitary glutamate receptor from Xenopus, which contains N-methyl-D-aspartate (NMDA) and non-NMDA receptor subunits. *J Biol Chem,* 271, 32572-9.

STEELE, J. W., KIM, S. H., CIRRITO, J. R., VERGES, D. K., RESTIVO, J. L., WESTAWAY, D., FRASER, P., HYSLOP, P. S., SANO, M., BEZPROZVANNY, I., EHRLICH, M. E., HOLTZMAN, D. M. & GANDY, S. 2009. Acute dosing of latrepirdine (Dimebon), a possible Alzheimer therapeutic, elevates extracellular amyloid-beta levels in vitro and in vivo. *Mol Neurodegener,* 4, 51.

STERN, P., BEHE, P., SCHOEPFER, R. & COLQUHOUN, D. 1992. Single-channel conductances of NMDA receptors expressed from cloned cDNAs: comparison with native receptors. *Proc Biol Sci,* 250, 271-7.

STOLL, L., HALL, J., VAN BUREN, N., HALL, A., KNIGHT, L., MORGAN, A., ZUGER, S., VAN DEUSEN, H. & GENTILE, L. 2007. Differential regulation of ionotropic glutamate receptors. *Biophys J,* 92, 1343-9.

SUCHER, N. J., AKBARIAN, S., CHI, C. L., LECLERC, C. L., AWOBULUYI, M., DEITCHER, D. L., WU, M. K., YUAN, J. P., JONES, E. G. & LIPTON, S. A. 1995. Developmental and regional expression pattern of a novel NMDA receptor-like subunit (NMDAR-L) in the rodent brain. *J Neurosci,* 15, 6509-20.

SUGIHARA, H., MORIYOSHI, K., ISHII, T., MASU, M. & NAKANISHI, S. 1992. Structures and properties of seven isoforms of the NMDA receptor generated by alternative splicing. *Biochem Biophys Res Commun,* 185, 826-32.

SUN, L., MARGOLIS, F. L., SHIPLEY, M. T. & LIDOW, M. S. 1998. Identification of a long variant of mRNA encoding the NR3 subunit of the NMDA receptor: its regional distribution and developmental expression in the rat brain. *FEBS Lett,* 441, 392-6.

TANZI, R. E. & BERTRAM, L. 2005. Twenty years of the Alzheimer's disease amyloid hypothesis: a genetic perspective. *Cell,* 120, 545-55.

TAPIOLA, T., ALAFUZOFF, I., HERUKKA, S. K., PARKKINEN, L., HARTIKAINEN, P., SOININEN, H. & PIRTTILA, T. 2009. Cerebrospinal fluid {beta}-amyloid 42 and tau proteins as biomarkers of Alzheimer-type pathologic changes in the brain. *Arch Neurol,* 66, 382-9.

TARIOT, P. N., FARLOW, M. R., GROSSBERG, G. T., GRAHAM, S. M., MCDONALD, S. & GERGEL, I. 2004. Memantine treatment in patients with moderate to severe Alzheimer disease already receiving donepezil: a randomized controlled trial. *JAMA,* 291, 317-24.

THAL, L. J., GRUNDMAN, M., BERG, J., ERNSTROM, K., MARGOLIN, R., PFEIFFER, E., WEINER, M. F., ZAMRINI, E. & THOMAS, R. G. 2003. Idebenone treatment fails to slow cognitive decline in Alzheimer's disease. *Neurology,* 61, 1498-502.

TIKHONOV, D. B., MELLOR, I. R. & USHERWOOD, P. N. 2004. Modeling noncompetitive antagonism of a nicotinic acetylcholine receptor. *Biophys J,* 87, 159-70.

TIKHONOV, D. B., MELLOR, J. R., USHERWOOD, P. N. & MAGAZANIK, L. G. 2002. Modeling of the pore domain of the GLUR1 channel: homology with K+ channel and binding of channel blockers. *Biophys J,* 82, 1884-93.

TONG, G., TAKAHASHI, H., TU, S., SHIN, Y., TALANTOVA, M., ZAGO, W., XIA, P., NIE, Z., GOETZ, T., ZHANG, D., LIPTON, S. A. & NAKANISHI, N. 2007. Modulation of NMDA receptor properties and synaptic transmission by the NR3A subunit in mouse hippocampal and cerebrocortical neurons. *J Neurophysiol.*

TRAYNELIS, S. F., BURGESS, M. F., ZHENG, F., LYUBOSLAVSKY, P. & POWERS, J. L. 1998. Control of voltage-independent zinc inhibition of NMDA receptors by the NR1 subunit. *J Neurosci,* 18, 6163-75.

TRAYNELIS, S. F., HARTLEY, M. & HEINEMANN, S. F. 1995. Control of proton sensitivity of the NMDA receptor by RNA splicing and polyamines. *Science,* 268, 873-6.

TRINH, N. H., HOBLYN, J., MOHANTY, S. & YAFFE, K. 2003. Efficacy of cholinesterase inhibitors in the treatment of neuropsychiatric symptoms and functional impairment in Alzheimer disease: a meta-analysis. *JAMA,* 289, 210-6.

TU, S., SHIN, Y., ZAGO, W. M., STATES, B. A., EROSHKIN, A., LIPTON, S. A., TONG, G. G. & NAKANISHI, N. 2007. Takusan: a large gene family that regulates synaptic activity. *Neuron,* 55, 69-85.

ULBRICH, M. H. & ISACOFF, E. Y. 2008. Rules of engagement for NMDA receptor subunits. *Proc Natl Acad Sci U S A.*

VAN NOORD, C., STURKENBOOM, M. C., STRAUS, S. M., WITTEMAN, J. C. & STRICKER, B. H. 2010. Non-cardiovascular drugs that inhibit hERG-encoded potassium channels and risk of sudden cardiac death. *Heart.*

VEPSALAINEN, S., HILTUNEN, M., HELISALMI, S., WANG, J., VAN GROEN, T., TANILA, H. & SOININEN, H. 2008. Increased expression of Abeta degrading enzyme IDE in the cortex of transgenic mice with Alzheimer's disease-like neuropathology. *Neurosci Lett,* 438, 216-20.

VILLMANN, C., STRUTZ, N., MORTH, T. & HOLLMANN, M. 1999. Investigation by ion channel domain transplantation of rat glutamate receptor subunits, orphan receptors and a putative NMDA receptor subunit. *Eur J Neurosci,* 11, 1765-78.

WADA, A., TAKAHASHI, H., LIPTON, S. A. & CHEN, H. S. 2006. NR3A modulates the outer vestibule of the "NMDA" receptor channel. *J Neurosci,* 26, 13156-66.

WANG, X. D., CHEN, X. Q., YANG, H. H. & HU, G. Y. 1999. Comparison of the effects of cholinesterase inhibitors on [3H]MK-801 binding in rat cerebral cortex. *Neurosci Lett,* 272, 21-4.

WATANABE, J., BECK, C., KUNER, T., PREMKUMAR, L. S. & WOLLMUTH, L. P. 2002. DRPEER: a motif in the extracellular vestibule conferring high Ca2+ flux rates in NMDA receptor channels. *J Neurosci,* 22, 10209-16.

WATKINS, J. C. & JANE, D. E. 2006. The glutamate story. *Br J Pharmacol,* 147 Suppl 1, S100-8.

WEE, K. S., WEE, Z. N., CHOW, N. B. & LOW, C. M. 2010. The distal carboxyl terminal of rat NR3B subunit regulates NR1-1a/NR3B and NR1-2a/NR3B surface trafficking. *Neurochem Int,* 57, 97-101.

WEE, K. S., ZHANG, Y., KHANNA, S. & LOW, C. M. 2008. Immunolocalization of NMDA receptor subunit NR3B in selected structures in the rat forebrain, cerebellum, and lumbar spinal cord. *J Comp Neurol,* 509, 118-35.

WILLIAMS, K. 1993. Ifenprodil discriminates subtypes of the N-methyl-D-aspartate receptor: selectivity and mechanisms at recombinant heteromeric receptors. *Mol Pharmacol,* 44, 851-9.

WILLIAMS, K. 1995. Pharmacological properties of recombinant N-methyl-D-aspartate (NMDA) receptors containing the epsilon 4 (NR2D) subunit. *Neurosci Lett,* 184, 181-4.

WILLIAMS, K. 1997. Interactions of polyamines with ion channels. *Biochem J,* 325 (Pt 2), 289-97.
WILLIAMS, K., PAHK, A. J., KASHIWAGI, K., MASUKO, T., NGUYEN, N. D. & IGARASHI, K. 1998. The selectivity filter of the N-methyl-D-aspartate receptor: a tryptophan residue controls block and permeation of Mg2+. *Mol Pharmacol,* 53, 933-41.
WILLIAMS, K., ZAPPIA, A. M., PRITCHETT, D. B., SHEN, Y. M. & MOLINOFF, P. B. 1994. Sensitivity of the N-methyl-D-aspartate receptor to polyamines is controlled by NR2 subunits. *Mol Pharmacol,* 45, 803-9.
WOLLMUTH, L. P., KUNER, T. & SAKMANN, B. 1998a. Adjacent asparagines in the NR2-subunit of the NMDA receptor channel control the voltage-dependent block by extracellular Mg2+. *J Physiol,* 506 (Pt 1), 13-32.
WOLLMUTH, L. P., KUNER, T. & SAKMANN, B. 1998b. Intracellular Mg2+ interacts with structural determinants of the narrow constriction contributed by the NR1-subunit in the NMDA receptor channel. *J Physiol,* 506 (Pt 1), 33-52.
WONG, H. K., LIU, X. B., MATOS, M. F., CHAN, S. F., PEREZ-OTANO, I., BOYSEN, M., CUI, J., NAKANISHI, N., TRIMMER, J. S., JONES, E. G., LIPTON, S. A. & SUCHER, N. J. 2002. Temporal and regional expression of NMDA receptor subunit NR3A in the mammalian brain. *J Comp Neurol,* 450, 303-17.
WOODHULL, A. M. 1973. Ionic blockage of sodium channels in nerve. *J Gen Physiol,* 61, 687-708.
WRIGHTON, D. C., BAKER, E. J., CHEN, P. E. & WYLLIE, D. J. 2007. Mg2+ and memantine block of rat recombinant NMDA receptors containing chimeric NR2A/2D subunits expressed in Xenopus laevis oocytes. *J Physiol.*
WU, J., LI, Q. & BEZPROZVANNY, I. 2008. Evaluation of Dimebon in cellular model of Huntington's disease. *Mol Neurodegener,* 3, 15.
WYLLIE, D. J., BEHE, P. & COLQUHOUN, D. 1998. Single-channel activations and concentration jumps: comparison of recombinant NR1a/NR2A and NR1a/NR2D NMDA receptors. *J Physiol,* 510 (Pt 1), 1-18.
WYLLIE, D. J., BEHE, P., NASSAR, M., SCHOEPFER, R. & COLQUHOUN, D. 1996. Single-channel currents from recombinant NMDA NR1a/NR2D receptors expressed in Xenopus oocytes. *Proc Biol Sci,* 263, 1079-86.
YAMAKURA, T., ASKALANY, A. R., PETRENKO, A. B., KOHNO, T., BABA, H. & SAKIMURA, K. 2005. The NR3B subunit does not alter the anesthetic sensitivities of recombinant N-methyl-D-aspartate receptors. *Anesth Analg,* 100, 1687-92.
YAMAKURA, T. & SHIMOJI, K. 1999. Subunit- and site-specific pharmacology of the NMDA receptor channel. *Prog Neurobiol,* 59, 279-98.
YANG, Y. C., LEE, C. H. & KUO, C. C. 2009. Ionic flow enhances low-affinity binding: a revised mechanistic view into Mg2+ block of NMDA receptors. *J Physiol,* 588, 633-50.
YAO, P. J., PETRALIA, R. S., BUSHLIN, I., WANG, Y. & FURUKAWA, K. 2005. Synaptic distribution of the endocytic accessory proteins AP180 and CALM. *J Comp Neurol,* 481, 58-69.
YAO, Y., HARRISON, C. B., FREDDOLINO, P. L., SCHULTEN, K. & MAYER, M. L. 2008. Molecular mechanism of ligand recognition by NR3 subtype glutamate receptors. *Embo J,* 27, 2158-70.

YAO, Y. & MAYER, M. L. 2006. Characterization of a soluble ligand binding domain of the NMDA receptor regulatory subunit NR3A. *J Neurosci,* 26, 4559-66.

YUAN, H., HANSEN, K. B., VANCE, K. M., OGDEN, K. K. & TRAYNELIS, S. F. 2009. Control of NMDA receptor function by the NR2 subunit amino-terminal domain. *J Neurosci,* 29, 12045-58.

ZARAIN-HERZBERG, A., LEE-RIVERA, I., RODRIGUEZ, G. & LOPEZ-COLOME, A. M. 2005. Cloning and characterization of the chick NMDA receptor subunit-1 gene. *Brain Res Mol Brain Res,* 137, 235-51.

ZHU, Y. & AUERBACH, A. 2001. Na(+) occupancy and Mg(2+) block of the n-methyl-d-aspartate receptor channel. *J Gen Physiol,* 117, 275-86.

ZIMMER, M., FINK, T. M., FRANKE, Y., LICHTER, P. & SPIESS, J. 1995. Cloning and structure of the gene encoding the human N-methyl-D-aspartate receptor (NMDAR1). *Gene,* 159, 219-23.

ZLOKOVIC, B. V., MARTEL, C. L., MACKIC, J. B., MATSUBARA, E., WISNIEWSKI, T., MCCOMB, J. G., FRANGIONE, B. & GHISO, J. 1994. Brain uptake of circulating apolipoproteins J and E complexed to Alzheimer's amyloid beta. *Biochem Biophys Res Commun,* 205, 1431-7.